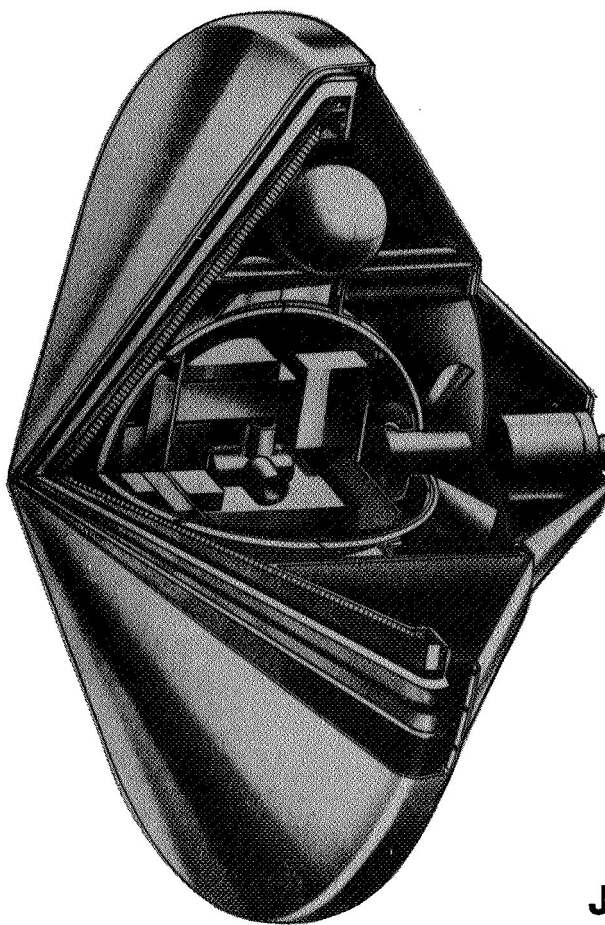# A STUDY OF A JUPITER ATMOSPHERIC ENTRY PROBE MISSION

FINAL REPORT
TECHNICAL SUMMARY

1971 AUGUST 13

PREPARED FOR
JET PROPULSION LABORATORY
PASADENA, CALIFORNIA

PREPARED BY

AVCO SYSTEMS DIVISION
201 LOWELL ST. WILMINGTON, MASSACHUSETTS 01887

A STUDY OF A JUPITER
ATMOSPHERIC ENTRY PROBE MISSION

FINAL REPORT
VOLUME II
TECHNICAL SUMMARY

Prepared by

AVCO GOVERNMENT PRODUCTS GROUP
AVCO SYSTEMS DIVISION
Wilmington, Massachusetts 01887

AVSD-0372-71-RR

1971 August 13

STUDY LEADER: HOWARD B. WINKLER

Approved by: _Ronald J. Massa_

Ronald J. Massa
Director
Space Systems Development Office

Prepared for

JET PROPULSION LABORATORY
Pasadena, California 91103

Contract NAS7-100   JPL 952897

FOREWORD

This report contains the results of a study of a Jupiter atmospheric entry probe mission. The purpose of the study was: 1) to screen a large number of Jupiter entry probe missions, 2) generate configuration descriptions, and 3) identify both missions studies and technology developments that are worthwhile to enhance the feasibility and improve the success of the mission.

This Management Summary Volume of the Final Report, was prepared to provide a technical specialist with an in-depth description of the study results, and with sufficient supporting analysis to allow for a high level of traceability of the decision making processes. A companion document, the Management Summary Volume of the Final Report was prepared to provide a technical generalist or technical manager with a concise document that reports the major background, scope, and results of the study.

ACKNOWLEDGEMENTS

TABLE OF CONTENTS

LIST OF FIGURES

xiv

LIST OF TABLES

1.0 SCOPE OF SYSTEM AND SUBSYSTEM PARAMETRIC TRADEOFFS

A study was conducted to satisfy the following set of objectives: (1) to screen a large number of Jupiter entry probe missions, (2) to generate configuration descriptions, and (3) to identify both mission studies and technology developments that are worthwhile to enhance the feasibility and improve the success of the mission. A principal groundrule for this study has been entry probe survival to the base of the cloud layer with remote sensing to provide information at greater atmospheric depths. This approach to the study of a Jupiter atmospheric entry probe is significantly different than the equally valid approach of entry probe survival to great depths with an in situ sensing. For example, in the nominal Jovian atmosphere the base of the clouds occur at a pressure of 17 atm and the ambient temperature of this level is 425 deg. K. Deep descent is considered to be the 1000 atm level and the corresponding ambient temperature is 1425 deg. K.

1.1 OVERALL STUDY APPROACH

The approach taken to this study was to first identify missions with good science return characteristics with respect to their ability to achieve the science objectives and to identify missions that tend to minimize engineering development. System level tradeoffs were conducted between these favorable science missions and favorable engineering missions, and many feasible and attractive missions were sifted out. A single mission was selected and served to define entry probe system and subsystem configurations. Description of the system and subsystem configurations and their requirements were used to identify the technology requirements that should be pursued to enhance the realization of a Jupiter entry probe mission. A flow diagram which illustrates this overall study approach is shown in Figure 1-1.

1.2 STUDY GUIDELINES

The following system and environmental guidelines were provided by JPL to ensure that (1) the broad scope and range of necessary tradeoffs of this study were understood, (2) the most up-to-date Jovian environmental data was available, and (3) the most up-to-date information on parallel programs that would support the entry probe mission was also available.

FIGURE 1-1

STUDY APPROACH

IDENTIFICATION OF MISSIONS WITH GOOD SCIENCE RETURN CHARACTERISTICS

IDENTIFICATION OF MISSIONS THAT TEND TO MINIMIZE ENGINEERING DEVELOPMENT

MISSION TRADEOFFS

DEFINITION OF ENTRY PROBE SYSTEM AND SUBSYSTEM CONFIGURATIONS

IDENTIFICATION OF TECHNOLOGY REQUIREMENTS

31 - 0113P
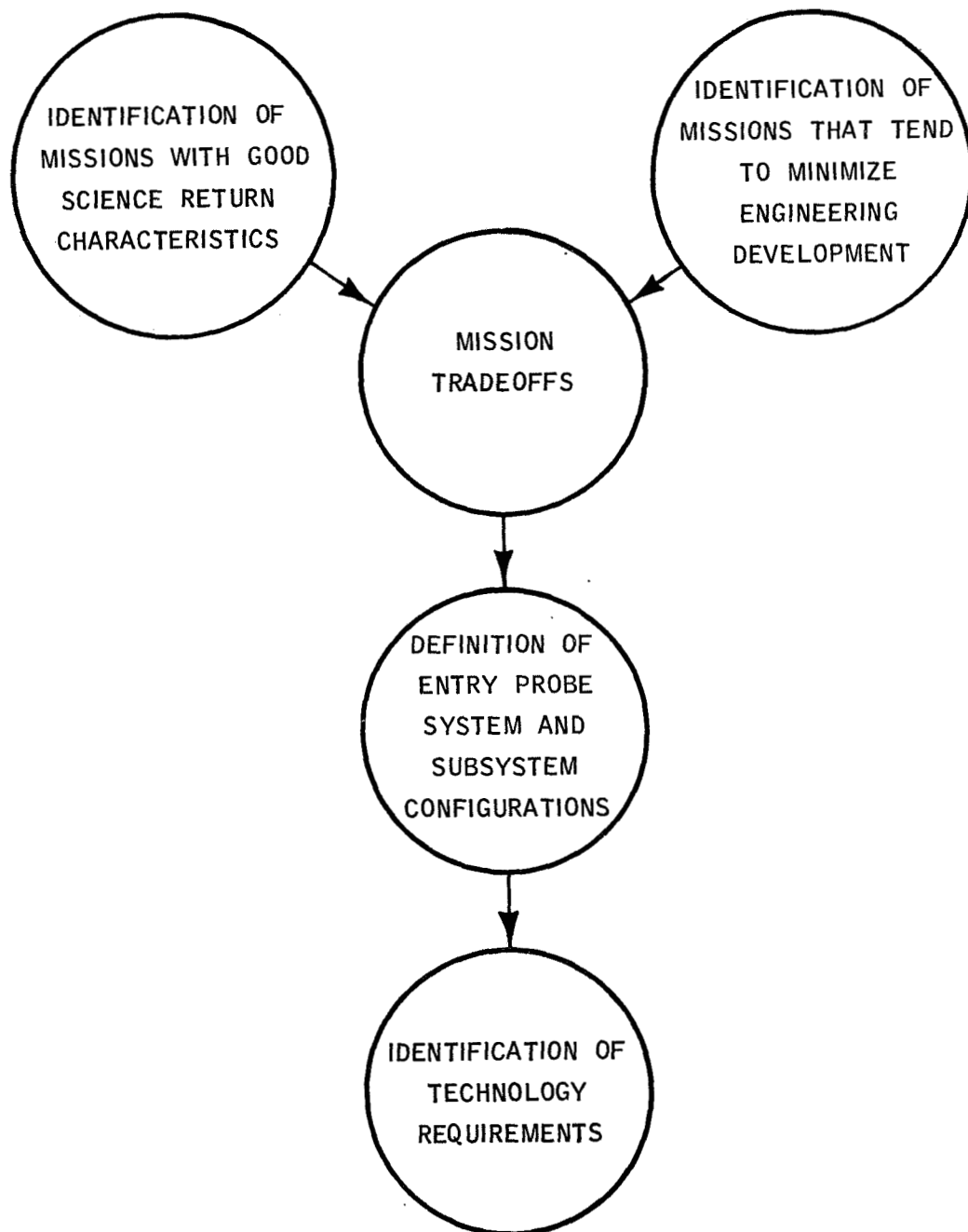
(a) Depth of Atmospheric Descent

The entry probe shall be instrumented and designed so that the science objectives can be achieved by in situ sensing during descent through the cloud layers, and by remote sensing during and immediately following emergence from the base of the clouds.

(b) Science Criteria

The five Jovian scientific objectives[1] for an entry probe mission were provided. These objectives include determination of: (1) the chemical and isotopic composition of the atmosphere, (2) thermal structure of the atmosphere, (3) composition and structure of the clouds, (4) existence of complex organic matter, and (5) nature of coloring matter in the clouds. A science payload, termed for this study, the baseline payload[1] was also provided. The instrument complement for this payload was selected based on a probe that can conduct in situ measurements during descent to 1000 atm pressure.

(c) Mission Opportunities

Both 1978 and 1980 launch opportunities with a flyby trajectory tailored to enhance the mission success and data return of an entry probe, and a 1979 launch opportunity with a flyby trajectory that has been tailored to satisfy the interplanetary guidance requirements of a Grand Tour Mission were studied. JPL generated interplanetary trajectory data,[2] and astrodynamic and planetary physical constants[3] were provided.

(d) Jovian Environment

A Jovian environmental handbook was provided.[4] The principal environmental factors which were of concern for this study were the model atmospheres, the magnetic field model, the trapped radiation belt models, and the electromagnetic radiation model.

The model atmospheres were the most important environmental constraints. Three models were provided: a warm/expanded model atmosphere, a nominal model atmosphere, and a cool/dense model atmosphere. The nominal model atmosphere was used as the basis of comparison for the influence on design of the bounding extremes.

(e) Forebody Heatshield Weight

The variation of forebody heatshield weight for a 60-deg. half-angle sharp cone was provided as a function of entry angle and ballistic parameter. Also

provided were tables that would permit estimates of heatshield thickness at four different stations. A chart was also given that showed the heatshield loss (normalized to the initial heatshield mass) as a function of the deceleration velocity profile (normalized to the initial velocity).[5]

(f) Interplanetary Bus Spacecraft Descriptions

Preliminary descriptions of both the thermoelectric outer planet spacecraft (TOPS) and the Pioneer F/G spacecraft were provided.[6] The TOPS is a three-axis stabilized, 1450 lb. spacecraft that uses a radioisotope thermoelectric generator (RTG) power source. The Pioneer F/G is a spin-stabilized, 550 lb. spacecraft that also uses an RTG. Both spacecraft have been designed for outer planet missions but have to be modified to also serve as a bus for an entry probe.

(g) Launch Vehicle

The Titan IIID family of launch vehicles[7] was used for this study. The first stage and second stage of the launch vehicle correspond to the two stages of Titan IIID. Two solid rocket motors of either five or seven segments serve as a zeroth stage. A Centaur, or higher performance stretched Centaur, or Agena serve as the third stage, and the Burner II or very high performance Versatile Upper Stage is the fourth and last stage. Two launch vehicle shrouds have been considered, i.e. a 12.5 ft. diameter dynamic shroud envelope, that is termed the Viking shroud, and a 10 ft. diameter dynamic shroud envelope. The payload injection capability of the launch vehicle is based on the use of the heavier Viking shroud. If the smaller 10 ft. diameter shroud is used, then a small increase in launch vehicle payload injection weight can be realized.

(h) Deep Space Net Capability

DSN capability was provided for three different modes of operation. From the point of view of greatest direct communication link performance, a probe-only mission which would require only an S-band receive mode at DSN would result in the greatest performance for a direct link mission. For a Pioneer F/G mission, the DSN must not only receive at S-band but must also transmit at S-band. This results in a reduction in performance of the receive S-band in comparison with a receive S-band only mission. For a TOPS mission, the DSN must receive S-band and X-band and transmit S-band. The receive S-band performance is further reduced in comparison to that for the Pioneer F/G mission.[8,9]

(i) System and Subsystem Performance Criterion

State-of-the-art as of 1975 was used in defining performance of the entry probe subsystem and spacecraft support subsystems.

(j) Planetary Quarantine

Planetary quarantine was not considered in this conceptual design study. However, NASA Document NHB 8020.12, "Planetary Quarantine Provision for Unmanned Planetary Mission," dated April, 1969 is expected to apply to a specific mission, and should be used in preparation of a preliminary design.

(k) Magnetic Cleanliness

Magnetic cleanliness requirements were not provided for this study. It is recognized that in an entry probe preliminary design study, the question of magnetic cleanliness is important. This is due to the presence of spacecraft magnetometers that are used to measure the interplanetary magnetic field and also entry probe magnetometers that are used to measure near-Jovian magnetic fields. The same technology that is developed to achieve spacecraft magnetic cleanliness can be applied to the elimination of the sources of entry probe magnetic fields.

(l) Reliability

A quantitative reliability assessment of the entry probe mission was not considered in the study. Reliability was factored into the study in a qualitative manner. Subsystem selection was made with the knowledge that the anticipated shelf life could range from two to five years. At present, hardware lists are, or have been prepared for three classes of long-lived spacecraft: (1) Mariner reliability for lifetimes up to two years, (2) Pioneer F/G reliability for lifetimes from two to five years, and (3) TOPS reliability for lifetimes from five to twelve years.

1.3 PARAMETRIC TRADEOFF AND MISSION SELECTION APPROACH

Identification of favorable missions and insight into Jovian mission limitations was gained by study of nine key mission tradeoffs. Four of these key tradeoffs are associated with good science return and include: (1) degree of comprehensiveness of science payload packages, (2) probe targeting to dayside or nightside sites, (3) model atmosphere influence, and (4) depth of atmospheric descent. Five of these key tradeoffs are associated with minimization of engineering development and include: (1) launch

opportunity: 1978, 1979, or 1980, (2) trajectory targeting, either fast Type I or slow Type II, (3) probe entry angle, steep to shallow, (4) communication link either direct from entry probe to DSN, or relay via the spacecraft from entry probe to DSN, and (5) spacecraft bus, either TOPS or Pioneer F/G.

Performance of the study was based on delegation of tasks into four groups each of which was assigned to a task leader. These groups are shown in the study flow chart of Figure 1-2. The initial point for the study was the system and subsystem descriptions that was provided in the Avco proposal in response to a request by JPL for a proposal to study a Jupiter atmospheric entry probe mission. This study was of six month duration, and after the first three months Avco made a mid-term oral progress report. The purpose of the study never changed, but the parametric studies were a dynamic changing set of tasks that continually reflected an improvement in the understanding of the interaction of the parameters.

The mission analysis tasks shown in Figure 1-2 include trajectory type, entry angle, entry longitude, deflection velocity and dispersions, entry deceleration profile, relay link communication range and communication angle, direct link communication range and communication angle, and launch vehicle selection. Communication analysis includes relay link and direct link frequency and modulation selection, selection of periapsis altitude and lead time, description of telemetry and data handling subsystem, and relay equipment subsystems. Science analysis includes depth of atmospheric descent, descent time to the base of the cloud layers, and science payload selections. Finally system design includes all: TOPS and Pioneer F/G integration, description of structure and heatshield subsystems, propulsion subsystem, payload container subsystem (which includes pressure vessel structure and thermal protection), parachute subsystem, integration of subsystems in an entry probe system, TOPS and Pioneer F/G subsystem modifications, and TOPS and Pioneer F/G flight article configuration.

1.4 REFERENCES

1. Science Criteria for Jupiter Entry Missions, Statement of Work, JPL Contract No. 952897, 1970 July 1.

2. JPL-generated trajectory data, informal communication.

3. JPL TR-32-1306, Constants and Related Information for Astrodynamic Calculations, 1968 July 15.

FIGURE 1-2

FLOW CHART OF THE GENERATION OF ENTRY PROBE SYSTEM AND SUBSYSTEM CONFIGURATION
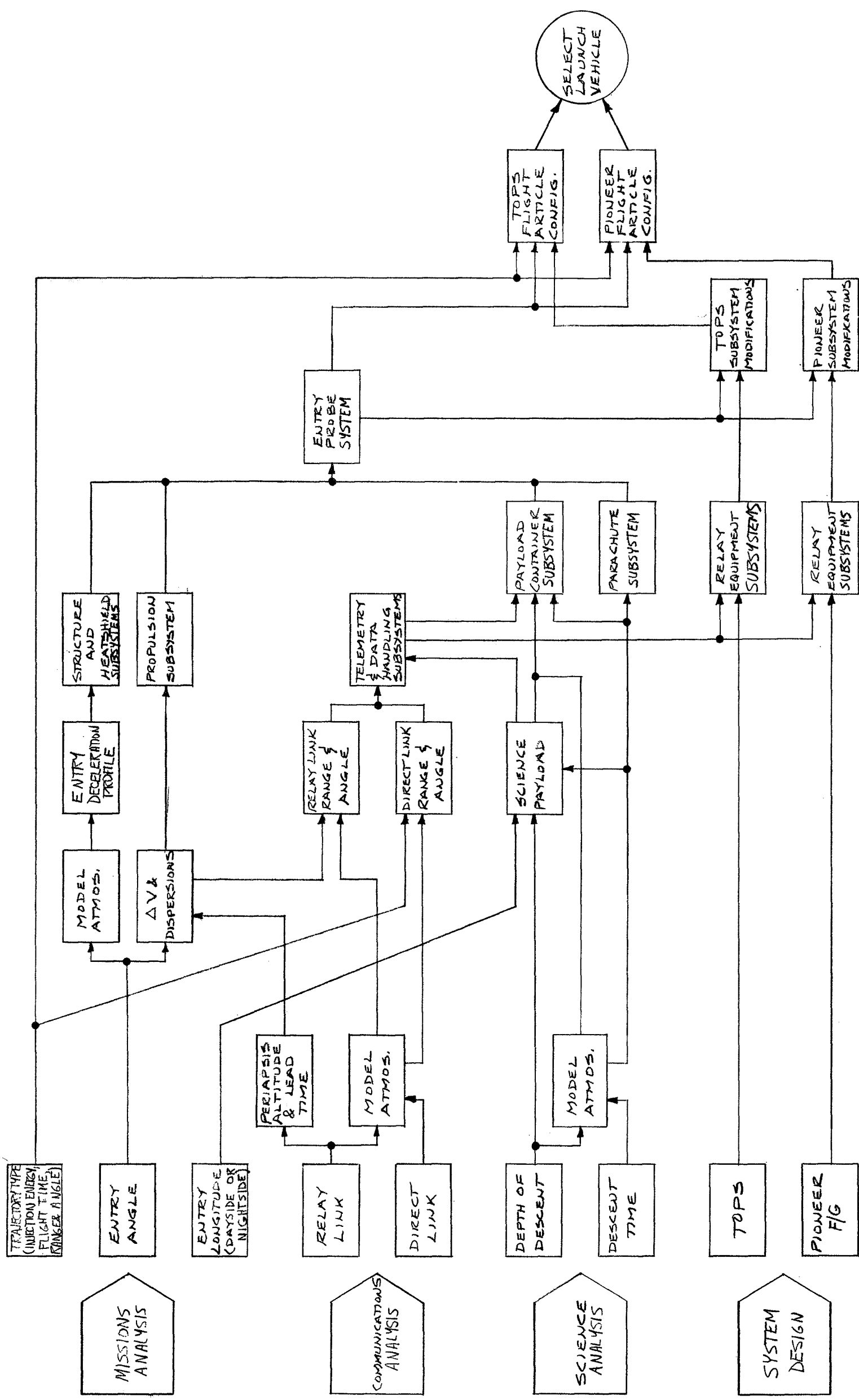
NASA Space Vehicle Design Criteria (Environment), The Planet Jupiter (1970), prepared by JPL, to be released.

Forebody Heatshield Weight Estimates for Jupiter Entry, Statement of Work, JPL Contract No. 952897; 1970 July 1.

Outer Planet Spacecraft System Descriptions, Statement of Work, JPL Contract No. 952897, 1970 July 1.

Titan III/Centaur Family Launch Vehicle Definition for a Jupiter Entry Mission Study, Statement of Work, JPL Contract No. 952897, 1970 July I.

Summary of DSN Capabilities for Jupiter Atmospheric Probe Mission, Statement of Work, JPL Contract No. 952897, 1970 July 1.

Telecon from M. Koerner of JPL, Telecommunication Division, 1970 December.

2.0 DESIGN REQUIREMENTS IMPOSED BY THE PHYSICAL ENVIRONMENTAL MODELS

An investigation was made of the various physical environments to which the entry probe would be exposed, from Earth launch to descent to the base of the Jovian cloud layers. Throughout the mission, the probe is either immersed in or impinged on by: high energy particles, fields, electromagnetic radiation, temperature, pressure, and an atmosphere. The approach that was followed utilized a qualitative evaluation to sort significant environments from the less significant. Once a significant environment was identified, a quantitative evaluation was made of its influence on the design of the entry probe.

There are four entry probe flight regimes. These are (1) near-Earth cruise while attached to the spacecraft, (2) interplanetary cruise while attached to the spacecraft, (3) near-Jupiter cruise, and (4) atmospheric descent of the probe alone. From launch to the orbit of Mars, the physical environment is understood to sufficient depth to permit successful operation of a spacecraft. Mariners IV, VI, and VII have had successful flights to Mars, and Mariner IV had a long post-encounter operational life. In the flight regime beyond Mars, the only new environment that has been identified in this study is the greater flux density of meteoroids that have resulted from the comminution of asteroids. In Section 2.1 there is reported the influence of these meteoroids on entry probe design. Near Jupiter, the entry probe and spacecraft will be immersed in strong decimeter radiation. This is a unique environment which has an important influence on the performance of a relay communication link. This microwave radiation will greatly increase the noise figure of the relay receiver on board the spacecraft. The presence of decimeter radiation has led to several postulations of its origin. The postulations have resulted in prediction of magnetic fields that are considerably stronger, and trapped radiation belts that are considerably more energetic than those near Earth. The influence of decimeter radiation is reported in Section 2.2, the magnetic fields in Section 2.3, and the influence of the trapped radiation belts is reported in Section 2.4. The entry probe is decelerated by the atmosphere and descends to the cloud base. In Section 2.5 there is reported the influence of the atmospheric environment on the design requirements for: deceleration loads, payload container, aerodynamic heating, radio frequency attenuation, and descent time.

2-1

2.1 INTERPLANETARY METEOROIDS

The entry probe requires protection from meteoroids during the inter-
planetary flight to protect the heatshield from pitting and cracking. Since
the spacecraft will spend most of its mission time between the orbits of
Mars and Jupiter, the asteroid belt flux levels will provide the limiting
environment. Meteoroids of asteroidal origin are more dense and more
abundant than cometary meteoroids. For a typical Type I trajectory, the
spacecraft will spend 580 days between the orbits of Mars and Jupiter, the
nominal bounds of the asteroidal belt. The transit time required for a
Type II trajectory will be about 1340 days. The probe design includes a
bumper shield designed to provide a 95% probability of zero puncture during
transit of the asteroid belt. The bumper shield which protects the probe
heatshield, is separated prior to planetary entry. This shield is estima-
ted to weigh 22 pounds for a Type I trajectory, and 32 pounds for a Type II
trajectory. A bumper shield, consisting of two aluminum sheets separa-
ted by two inches of polyurethane foam is estimated to require only 10%
of the weight of a single plate armor shield for the same degree of pro-
tection. The weight estimates are conservative because an isotopic mete-
oroid flux was assumed and meteoroid penetration was assumed to be inde-
pendent of impact angle. A preferred orientation of the probe during the
flight could reduce meteoroid shield weight requirements by at least 20%.

The method of Reference 1 was followed to estimate the thickness of a
single armor plate required for 95% probability of zero puncture. The
required armor plate thickness is given by:

$$t_a = 4.34 \, m_c^{\frac{1}{3}} \, \rho_m^{-\frac{1}{3}} \left(\frac{\rho_m}{\rho_t}\right)^{\frac{1}{2}} \left(\frac{V}{C}\right)^{\frac{2}{3}} \tag{1}$$

where:

t_a = required armor plate thickness in cm,
m_c = critical mass of meteoroids in gram,
ρ_m = average density of meteoroid (3.0 gm/cm^3 for stone)
ρ_t = density of the armor plate (2.8 gm/cm^3 for aluminum)
V = average velocity of meteoroids relative to probe (15 Km/Sec)
C = velocity of sound in the armor (5 Km/Sec for aluminum)

so that:

$$t_a = 6.52 \, m_c^{\frac{1}{3}} \tag{2}$$

The cumulative flux of meteoroids as a function of meteoroid mass is given as:

$$\phi = \alpha \, m^{-\beta} \tag{3}$$

where:

ϕ = number of meteoroids of mass, M, or greater per square meter per second,

m = Meteoroid mass in grams, and

α, β are constants

The average number of impacts, N, on area A, in mission time, Υ, by particles of critical mass m_c, or larger is then given by:

$$N = A\Upsilon\phi = A\Upsilon\alpha \, m_c^{-\beta} \tag{4}$$

Since the probability of occurrence of exactly n events when the average number of events is N, is defined by a Poisson distribution as:

$$P(n) = N^n e^{-N}/n!$$

the mission design probability of zero puncture is found to be:

$$P(0) = e^{-N} \tag{5}$$

Substituting (5) into (4), the critical mass becomes:

$$m_c = \left[\frac{\alpha A \Upsilon}{-\log_e P(0)} \right]^{\frac{1}{\beta}} \tag{6}$$

The required armor thickness then becomes:

$$t_a = 6.52 \left[\frac{\alpha A \Upsilon}{-\log_e P(0)} \right]^{\frac{1}{3\beta}} \tag{7}$$

The meteoroid flux model, in the form of (3), was taken from Reference 2 and 3 and assumed to be constant between the orbits of Mars and Jupiter:

$$\alpha = 10^{-10}, \text{ and}$$

$$\beta = 0.77$$

The heatshield is a 60 degree half angle cone with a diameter of 4 feet so that the area, $A = 1.35$ m^2. The transit time, γ, between the orbits of Mars and Jupiter which is 5×10^7 seconds (580 days) for a Type I trajectory, and 11.6×10^7 seconds (1340 days) for a Type II trajectory.

For a 95% probability of zero puncture ($P(o) = .95$), the armor plate (single aluminum plate) thickness required is, from (7), 2.72 cm for a Type I trajectory, or 3.9 cm for a Type II trajectory. The weight per unit area is then 15.4 pounds per square foot of surface area or 22.1 pounds per square foot of surface area for Types I or II trajectories, respectively.

The use of sandwich construction for the shield can result in a shield weight that is one-tenth the weight of a monolithic shield. The structural layer that is exposed to the environment serves as a bumper that causes the meteoroid particle to be shattered. A polyurethane foam serves to disperse and absorb the energy of the fragments, and the backup plate serves as the final barrier for retardation of fragments.

One-fifth of the total aluminum thickness is contained in the bumper, and the remaining four-fifths is in the backup plate. About 2 in. of 2 lb/ft^3 polyurethane foam separate the plates. The thickness of aluminum is given by:

$$(\rho t)_{BUMPER} = \frac{\rho_f}{6} + 14.4 \, t_T \tag{8}$$

$$t_T = t_F + t_B, \text{ and} \tag{9}$$

$$t_F = 0.2 \, t_T \tag{10}$$

where
  ρ_f = density of filler = 2 lbs/ft^3
  t_F = thickness of aluminum bumper plate in inches, and
  t_B = thickness of aluminum backup plate in inches

For a Type I trajectory: t_F = .0168 inch, and t_B = .0627 inch.
For a Type II trajectory: t_F = .0261 inch, and t_B = .1044 inch.

Meteoroid containers with the above dimensions will provide a 95% proba-
bility of zero puncture during transit of the asteroid belt. The number of
impacts per square meter is estimated, from (4), at 0.038 per square
meter. The critical meteoroid mass for a Type I trajectory is, from (6),
.072 gm, and for a Type II trajectory is 0.214 gram.

If the 22 pound meteoroid container is used for a Type II trajectory, the
probability of zero puncture by particles of mass greater than .072 gm
would be 88.8%, and if the 32 pound container were used for a Type I
trajectory, the probability of zero puncture by particles of mass greater
than 0.214 grams would be 97.8%.

Based on this calculation which is considered to be conservative in nature,
it was determined that the meteoroid environment would lead to the re-
quirement for a protective container. This container which weighs from
22 to 32 lb. represents about 8% of the entry probe separated weight.

2.2 DECIMETER RADIATION

Communicating near Jupiter in the decimeter wavelength bands can be
seriously affected by non-thermal RF noise emissions originating in the
Jovian radiation belts. For wavelengths longer than 3 cm, non-thermal
sources of radiation contribute an ever increasing fraction of the total
energy. The importance of this noise source from a communications
viewpoint is significant since above 30 cm wavelength, the noise tempera-
ture become prohibitive.

A curve of equivalent brightness temperature is shown plotted as a func-
tion of wavelength in Figure 2-1 (see Reference 4). The relationship shown
in this figure is the basis for establishing the frequency related losses
associated with the Jovian RF noise factor. The design of the communi-
cation system as constrained by this environmental factor tends to restrict
link frequencies to above L-band; also it can be said that link frequencies
at S-band and above are not measurably affected by this phenomenon (see
Reference 5).

2.3 MAGNETIC FIELD

Jupiter's UHF radiation gives evidence of a strong dipole magnetic field.
The measurements indicate that the center of the dipole may be displaced

FIGURE 2-1

JOVIAN NOISE TEMPERATURE PROFILE

EQUIVALENT BLACKBODY DISK TEMPERATURE (T), °K

WAVELENGTH (λ), cm
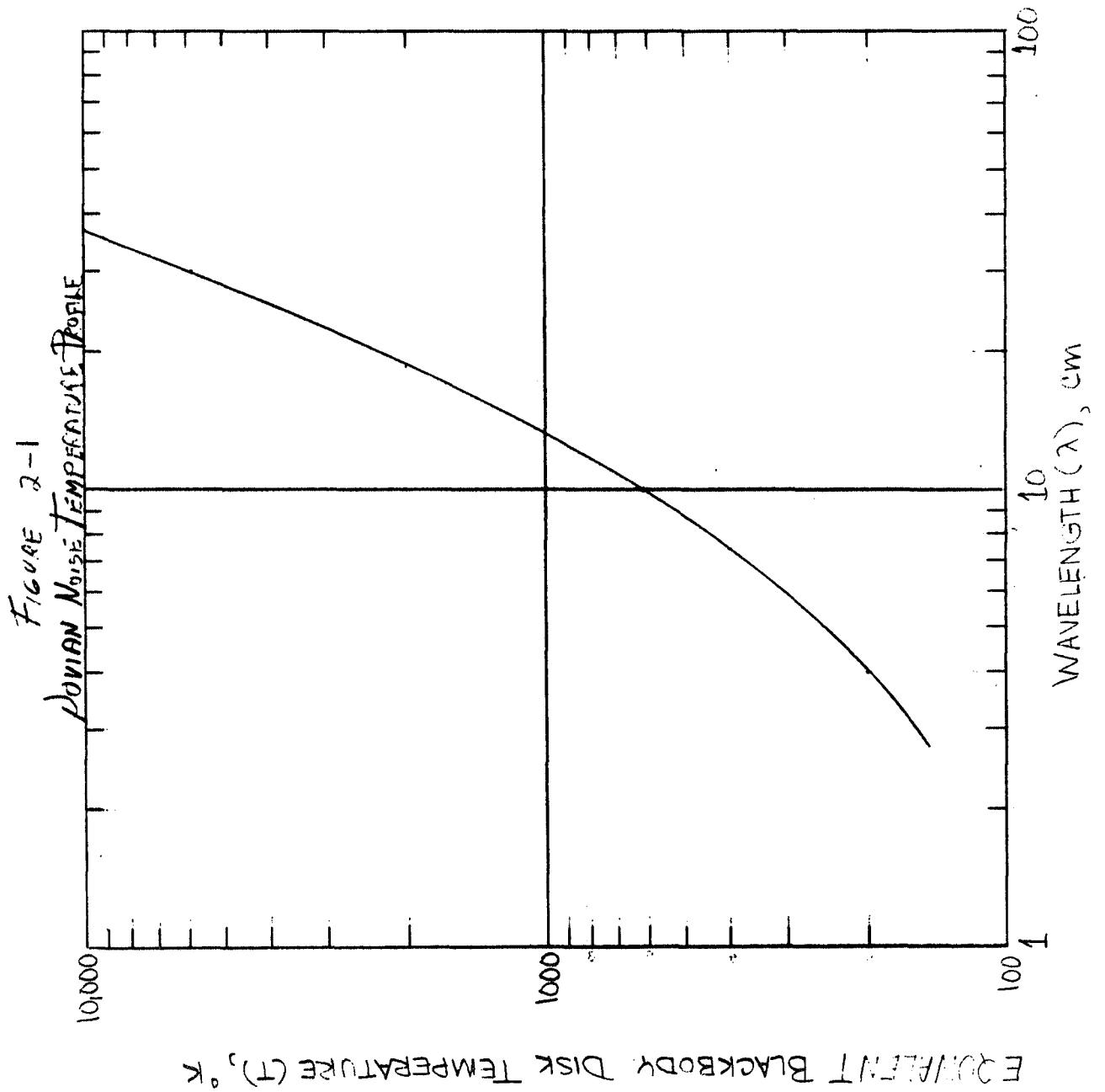
from the center of the planet by 70 to 1/3 to 3/4 of the planetary radius, and the dipole axis is tilted with respect to Jupiter's rotational axis by about 7 to 10 degrees. The magnitude of the magnetic dipole moment has been estimated as (2.1 to 8.4) x 10^{30} gauss-cm^3. The magnetic field at 1 RJ on the magnetic equator is estimated to be 6 to 24 gauss with a nominal value of 12 gauss, and varies as the inverse cube of the distance from the planet.

Intense magnetic fields can degrade the performance of subsystems which contain magnetic material, and depend on controlled magnetic fields for operation. Measurements indicate that data stored in magnetic core memories can be obliterated in a magnetic field of 11 gauss (see Reference 6). Components susceptible to degradation in fields of 11 gauss will have to be selectively shielded with high permeability material. It has been calculated that the Ni-Co shield requirements to reduce a magnetic field of 24 gauss to 10 gauss for a 80 cubic inch volume will weigh less than one pound. Spurious voltages induced in cables moving in the magnetic field can be minimized by: shielded cable, twisted pair leads, and balanced differential amplifiers to provide cancellation of common mode signals.

The probe can experience attitude perturbations and spin rate alteration as a result of traveling through the magnetic field. Precession torques can be produced by the interaction of the ambient field with (1) eddy currents generated in the spinning probe, and with (2) residual and stray magnetic fields or magnetic fields induced by the ambient field.

Spin rate decay is caused by eddy currents and by hysteresis losses as a result of the field induced in permeable materials. These effects can be minimized by careful spacecraft design such as avoiding magnetic material to the extent possible, and cable harness designs which tend to cancel stray fields. Design procedures which minimize attitude precession and despin torques have been published (see Reference 7) and the tradeoffs are well known. Attitude precession and despin, due to eddy currents and a probe magnetic moment, anticipated for the probe design and trajectory considered for this study are estimated in the following paragraphs.

For this analysis, it will be assumed that the probe approaches the planet on a Type II trajectory in the equatorial plane. A shallow entry angle of 15 degrees below the local horizontal and an entry velocity of 50 km/sec will also be assumed. For a probe trajectory in the equatorial plane, the magnetic field is essentially perpendicular to the spin axis and can be given by:

$$B_\perp(\rho) = B_\perp \, \rho^{-3}, \tag{1}$$

where $B_\perp = 1.2 \cdot 10^{-3} \ wb/m^2$ (nominal surface field),
and $\rho = \dfrac{R}{R_J}$ = relative radial distance to the center of the planet. The magnetic field component along the spin axis will be bounded by:

$$|B_s(\rho)| \leq |B_\perp(\rho)| \sin 10° = 0.175 \, |B_\perp(\rho)| \tag{2}$$

based on 10 deg. angle between the Jovian dipole axis and the Jovian spin axis.

Eddy Current Effects

Eddy currents generated in the probe structure as a result of spinning in a magnetic field can cause attitude precession and despin torques. The despin is given by the following equation:

$$\frac{d\omega_s}{dt} = -\frac{Ke \, B_\perp^2(\rho)}{I_s} \, \omega_s \tag{3}$$

where

$\dfrac{d\omega_s}{dt}$ = change in spin rate in rad/sec^2

$B_\perp(\rho)$ = magnetic field component perpendicular to the spin axis in wb/m^2

ω_s = spin rate in rad/sec,

I_s = probe spin-axis moment of inertia in kg-m^2, and

Ke = a constant which depends on the geometry and conductivity of the spinning probe in m^4/ohm.

Since the predominant effect occurs close to the planet, and the probe is assumed to be on a trajectory leading to a shallow entry angle, the radial velocity of the probe close to the planet can be approximated by:

$$dt = -\frac{R_o}{V_o \sin \gamma_o} \, \rho^{\frac{1}{2}} \, d\rho \tag{4}$$

where:

$\frac{d\rho}{dt}$ = radial velocity in 1/sec,

R_o = entry radius,

V_o = entry velocity, and

γ_o = entry angle relative to the local horizontal

Combining equations (1), (3), and (4) and integrating, the despin is computed as follows:

$$\frac{\omega_{s_2}}{\omega_{s_1}} = EXP\left[-\frac{2 K_e B_\perp^2 R_o}{9 I_s V_o \sin\gamma_o}\right] \tag{5}$$

The k_e factor depends on the geometry and electrical conductivity of probe parts which can provide closed paths for induced currents. Since the main probe parts which can provide closed circuits (aeroshell, heatshield, pressure vessel) can be approximated by thin spherical shells,

$$K_e = \frac{2\pi}{3} r^4 \sigma d \tag{6}$$

where

r = radius of the sphere in meters,

d = the shell thickness in meters, and

σ = electrical conductivity in mho/meter.

taking

$B_\perp$ = 1.2 to 2.4 x 10^{-3} wb/m^2 as the nominal to maximum magnetic field,

I_s = 9.4 slug-ft^2 = 12.8 kg-m^2

R_o = 7 x 10^7 meters,

V_o = 5 x 10^4 meters/sec, and

γ_o = 15 degrees,

the nominal to maximum despin becomes:

$$\frac{\omega_{s_2}}{\omega_{s_1}} = EXP\left[-(1.36 \text{ to } 5.42) K_e \times 10^{-4}\right] \tag{7}$$

The major conducting parts of the probe are the aeroshell and heatshield. The aeroshell will consist of titanium or beryllium with a thickness of .08 inches and a graphite ablator with a thickness of one-half inch. Since the shape of the probe can be approximated by a sphere with a radius of 2 ft. or .61 meters, the k_e factors, from equation (6), are as follows: $(.29 \, \sigma \, d)$

Component	Thickness (meters)	Conductivity (mho/meter)	k_e (m^4/ohm
Titanium Aeroshell	2.032×10^{-3}	2.09×10^{6}	1.23×10^{3}
Beryllium Aeroshell	2.032×10^{-3}	2.185×10^{7}	1.29×10^{4}
Graphite Ablator	1.27×10^{-2}	7.15×10^{4}	2.64×10^{2}

The despin, $\omega_{s_a}/\omega_{s_1}$, is, therefore

Component	Nominal	Maximum
Titanium Aeroshell	.847	.514
Beryllium Aeroshell	.174	$<.001$
Graphite Ablator	.965	.87

The probe with titanium aeroshell will, therefore, lose about 15 to 50% of its initial spin rate due to eddy currents in the aeroshell. About 3.5 to 13% will be lost due to eddy currents in the heatshield. The effect of conductivity is evident in that a beryllium aeroshell with a conductivity roughly ten times that of titanium would cause the probe to lose at least 83% of its initial spin rate.

Consideration of the pressure vessel within the probe which has a diameter of 10 inches and a thickness of .07 inches indicates a maximum spin rate decay of 2% for titanium and 18% for beryllium.

There are three ways in which to minimize or compensate for the eddy current effects. The first technique involves probe design. Material of the lowest possible conductivity should be utilized if other criteria can be satisfied, particularly with structural members of appreciable area located at the greatest distance from the spin axis. In addition, closed circuit current paths in structural sections can be opened by the insertion of insulating material, but this approach will require a tradeoff between structural integrity and spin decay.

The second approach is to increase the initial spin rate to compensate for the spin decay so as to maintain stabilization at entry. This approach involves consideration of experiment sensor sampling rates and the additional weight and/or power required for the initial spin-up.

The third approach is to provide an active spin rate control system. Again, weight and/or power tradeoffs need to be considered.

Additional spin rate decay may be expected due to hysteresis damping. This effect can be minimized by controlling the amount, location, and shape of magnetic material in the probe.

The precession torque due to eddy currents gives rise to a precession rate given by:

$$\frac{d\Theta_E}{dt} = \frac{K_e}{I_s} B_\perp(\rho) B_s(\rho) \tag{8}$$

Substitution of equation (4) and integration and comparison with equation (5) leads to the following bound on $\Delta\Theta_E$,

$$\Delta\Theta_E \leq \sin 10° \left(-\log_e \frac{\omega_{s_2}}{\omega_{s_1}}\right) \tag{9}$$

Using a titanium aeroshell and graphite ablator, the shift in attitude angle is bounded by

$$\Delta\Theta_E \leq 8°$$

In this case, techniques to reduce eddy currents must be traded off with the weight and power requirements of an active attitude control system.

Precession due to Permanent Magnetic Material in the Probe

The precession rate due to the interaction of a transverse magnetic field with a possible spin axis component of probe magnetic moment is given by

$$\frac{d\Theta_{MT}}{dt} = \frac{m_s B_\perp \rho^{-3}}{I_s \omega_s} \tag{10}$$

where

$\dfrac{d\Theta_{MT}}{dt}$ = precession rate in rad/sec and,

m_s = spin axis component of magnetic moment in A-m^2.

Substituting equation (4), neglecting spin decay, and integrating, the precession angle becomes:

$$\Delta\Theta_{MT} \doteq \frac{2 m_s \, B_\perp \, R_o}{3 \, I_s \, \omega_s \, V_o \sin \gamma_o} \tag{11}$$

For a 349 pound (158 kg) vehicle, the magnetic moment may be estimated (see Reference 7) to be $|m_s| \approx (0.1 \text{ to } 1.0) \times 0.63 \ \text{A-m}^2$ and substituting previous numerical values, the precession angle can be bounded as follows:

$$\frac{(0.1 \text{ to } 1.0) 12.2}{\omega_{s_1}} < \Theta_{MT} < \frac{(0.1 \text{ to } 1.0) 24.4}{\omega_{s_2}} \tag{12}$$

where Θ_{MT} is in deg.

For an initial spin rate on the order of 30 rpm, and assuming a 50% spin rate decay due to eddy current effects, the precession angle is bounded as

$$0.39 \ \text{Deg} < \Delta\Theta_{MT} < 15.5 \ \text{Deg}$$

Again, there is a tradeoff between the required weight and/or power requirements of an active attitude control system and the implications of increasing the initial spin rate or implementing procedures and techniques to reduce eddy current effects and the probe residual and stray magnetic fields.

In Section 8.5, an estimate is made of the attitude control system weight that can null out the effects of the despin and attitude perturbations. Due to the anticipated extreme environment of entry, the mission profile will be tailored to optimize the probe attitude and body rates prior to entry. The desirable quantitative entry conditions for the probe are low spin rates, near zero transverse rates, and near zero angle of attack. Magnetic fields effects can cause significant despin that could result in loss of gyrodynamic stability, and a significant non-zero angle of attack.

2.4 CHARGED PARTICLE RADIATION

The major sources of charged particle radiation consist of electrons and protons trapped in the Jovian radiation belts and solar and cosmic protons.

The most severe environment is posed by the trapped radiation belts and hence, the design requirements for the Jupiter probe must be based on estimates of the number, density, flux, and energy of trapped particles.

2.4.1 Jupiter Trapped Radiation Belt Model

The charged particles trapped in Jupiter's radiation belts present the most severe radiation environment for the probe since for near equatorial entry it must travel directly through the radiation belts to encounter the planet's outer atmosphere. Although the estimated particle densities, flux and energy levels are considerably higher than experienced in the Earth's Van Allen belts, the transit time of the probe through the Jovian radiation belts is short enough so that the effects of integrated exposures are more dependent on the model uncertainties than on peak flux levels. The anticipated time from 50 R_J is on the order of 60 hours while the time through the peak of the radiation belts (from 2 R_J) is about 45 minutes.

Although large uncertainties exist regarding the charged particle environment in the vicinity of Jupiter, a number of radiation models are available which are suitable for estimating minimum and maximum particle density, flux, and energy. The electron component is inferred from the radio emissions emanating from Jupiter which are interpreted as synchroton radiation from these particles trapped in the dipole magnetic field. There are no positive data from which proton fluxes have been inferred. The lower limit of flux is set at zero while energy dependent upper limits are established on the basis of trapping by the magnetic field, but it is thought that the resulting upper limits are not approached. The nominal number density is estimated to be equal to that of the electrons and the energy spectra are also estimated to be identical. Peak levels are believed to exist in the vicinity of 2 Jupiter radii from the center of the planet and extend, with decreasing flux and energy and increasing uncertainty to the vicinity of 50 Jupiter radii which is the estimated limit of the Jovian magnetosphere. The charged particle flux, integrated exposure, and energy range for a probe approaching Jupiter close to the equatorial plane, and hence, through the peak of the radiation belts, are summarized in Table 2-1.

This table has been adapted from NASA space vehicle design criteria (see Reference 8) which contains the latest models for the Jovian radiation belts. The minimum, nominal, and maximum models presented in the design criteria result from mathematically tractable functions encompassing most of the theoretical, measured, and extrapolated data published on the Jovian radiation belts. The table assumes probe approach through

TABLE 2-1

SUMMARY CHARGED PARTICLES - JOVIAN RADIATION BELTS

Probe entry close to equatorial plane

Particle Type	Distance from center of planet and (Probe transit time)	Particle Flux $(cm^{-2} - sec^{-1})$	Integrated Exposure (cm^{-2})	Peak Energy Range (MeV) of Particles > 1 MeV	Maximum Energy of Particle Stopped in .07 Inch Titanium
Electrons	$\leq 2\ R_J$ (45 Minutes)	6.3×10^6 Min. 5.67×10^7 Max.	1.7×10^{10} Min. 1.53×10^{11} Max.	30 MeV 300 MeV	1.3 MeV
	$2 - 50\ R_J$ (60 Hours)	$\sim \left[\dfrac{1}{R_J}\right]^{4 \pm 2}$	5.67×10^9 Min. 3.2×10^{11} Max.	$\sim \left[\dfrac{1}{R_J}\right]^{3 \pm 2}$	
Protons	$\leq 2\ R_J$ (45 Minutes)	Min. $= 0$ 6.3×10^6 Nom. 6.3×10^7 Max.	Min. $= 0$ 1.7×10^{10} Nom. 1.7×10^{11} Max.	300 MeV 3000 MeV	23 MeV
	$2 - 50\ R_J$ (60 Hours)	Min. $= 0$ $\sim \left[\dfrac{1}{R_J}\right]^{4 \pm 4}$	Min. $= 0$ 1×10^{10} Nom. 1.3×10^{13} Max.	$\sim \left[\dfrac{1}{R_J}\right]^{3 \pm 3}$	

Probe entry close to equatorial plane

the peak of the radiation belts and represents an upper bound on charged
particles since the planned approach is close to the equatorial plane of
the planet. Although the peak levels, along the magnetic equator, are
inclined by about 10 degrees from the planet's mass equator, the planet
will make over 120 revolutions while the probe is approaching from 50 R_J
and the variation due to approach geometry is much less than the uncertain-
ties which exist in the models.

Peak fluxes are expected to occur at 2 R_J or less from the center of the
planet. The proton fluxes were estimated by assuming an average particle
speed of 10^{10} centimeters per second in order to simplify the table. For
energies ranging from 3 to 3000 MeV the tabulated proton flux can be high
or low by a factor of three. The integrated exposure was obtained by
assuming that the probe would be exposed to the peak flux from 2 R_J to
atmospheric entry (45 minutes).

As the distance from the planet increases out to the limit of the magneto-
sphere (50 R_J), the flux levels decrease and the ranges of uncertainty
increase as shown in the table. The integrated exposure from 2 to 50 R_J
was obtained by integrating the flux as a function of R_J over the time the
probe takes to travel from 50 R_J to 2 R_J. For the Type II trajectory
(longest transit time), the incremental time is related to range by

$$dt = 1710 \; R_T^{0.316} \; dR_J$$

where t is the exposure time, and
       R_J Jovian Planetary radii

The radiation model also accounts for the energy spectra of trapped par-
ticles. The energy distribution is given as $N_E = N_0 (1 + E/E_0)$ exp
$(-E/E_0)$, where N_E is the number of particles per cubic centimeter
with energy greater than E, N_0 is the total number of particles per cubic
centimeter, and E_0 is the local characteristic energy. Both N_0 and E_0
decrease with increasing distance from the planet as shown in the table. An
upper bound is established for the peak energy at about 10 E_0 since only
0.1% of the particles will have energies greater than 9 E_0. At 50 R_J the
peak electron energy will be about 8 MeV while the nominal model for pro-
tons suggests about 11 MeV. The maximum model for protons assumes
constant energy and density with increasing R_J suggesting peak energies
to about 3000 MeV. The radiation belt model indicates that the probe will
be subjected to increasing flux and energy as it approaches the planet.

Solid state and organic materials are particularly susceptible to damage from charged particle radiation (see Reference 9). Radiation effects can be minimized by careful selection of components and materials (particularly semiconductors and thermal control material), radiation resistant circuit design, and shielding. A certain amount of shielding is provided by component cases, location and the outer shell of the probe. As indicated in the table, the titanium pressure vessel, which has a thickness of .07 inches, will shield electrons with energies below about 1.3 MeV and protons below about 23 MeV (see Reference 10). In addition, some energy is lost when a particle passes through the shell and component cases so that the flux levels reaching susceptible components will be less than those impinging on the spacecraft. The meteoroid shield will provide additional shielding until a couple of hours before atmospheric entry.

Table 2-1 is not meant to convey a negative prognosis of success, but only that the problem requires more effort and should be considered in the early design stages.

Experience with satellites orbiting Earth suggests that spacecraft can be designed to survive charged particle radiation although the flux, integrated dose, and energy levels near Earth are lower than those suggested by the Jovian model. Certain satellites in the ISIS and Alouette series in polar orbits around Earth, are still operating successfully after two to five years in orbit. Satellites in polar orbits can be expected to experience annual doses of 10^{11} to 10^{15} electrons/cm^2 with peak energies in the range of five to ten MeV and trapped proton doses in the range of 10^8 to 10^{12} protons/cm^2 with energies extending to something in excess of 50 MeV. Satellites in polar Earth orbits can also be expected to experience high energy cosmic protons with annual doses of 10^6 to 10^7 per cm^2 and solar flare protons with annual doses of 10^8 to 10^9 per cm^2 with energies greater than 30 MeV and extending to about 200 MeV (see Reference 10).

Radiation data from specific satellites have not been examined during the study period. This data should be searched to determine if such data can be used to establish the survivability of current design techniques at high particle energies. The susceptibility of components to damage by charged particle radiation depends on how much energy is absorbed. At very high energies, the likelihood increases that a particle will pass completely through the component and hence, the absorbed energy should not increase indefinitely with particle energy. For protons, the energy absorbed per unit distance decreases with increasing energy. For electrons, the absorbed energy per unit distance is less susceptible to energy level, but as the energy level increases, more energy is lost due to X-radiation as a result of stopping electrons. The bremstrahlung radiation is important

in considering the effects of shielding in that the device being shielded may be more or less susceptible to X-radiation than particle collision.

Although the trapped radiation environment will influence the probe design, careful circuit design and selection of materials and components, along with selective shielding can minimize the radiation effects. Confidence in the ultimate probe design will have to be balanced against the confidence in the radiation model used to establish design criteria. More detailed study of the radiation effects on satellites and subsystems experiencing high energy charged particles should provide more or less confidence in the survivability of existing design techniques while a narrowing of the uncertainties associated with current radiation models can provide more specific design criteria.

2.4.2   Nuclear Radiation

The electronics and scientific payload on board the probe will be subjected to nuclear radiation from the large RTG power supply on the flight space-craft and possibly from a small RTG heater unit in the probe. In both cases, the isotope fuel will be Pu-238 in the form of $Pu-O_2$.

The radiation emanating from the Pu-238 isotope source arises mainly from interactions of the emitted alpha particles and spontaneous fission. The primary heat source of Pu-238 is the alpha particle emission during radioactive decay. These alpha particles, which are stopped in the fuel form, can undergo interactions with the plutonium, oxygen, or other fuel impurities. The principal neutron source of Pu-238 comes from the neutrons generated by alpha particle interactions with oxygen isotopes O^{17} and O^{18}, which are 18 times greater than the spontaneous fission neutron source. The alpha particle interactions also produce low yield gamma rays. The spontaneous fission of Pu-238 gives rise to neutrons and gamma rays. The gamma ray source is the prompt fission, and fission product decay gamma rays.

The TOPS spacecraft will carry an RTG, utilizing Pu-238, to generate 400 to 500 watts of electrical power and will be located on a boom, and removed from the payload compartment (see Reference 11). The radiation at the probe is expected to consist of neutrons with a peak flux on the order of 3.5×10^3 neutrons per cm^2 per second with a 10-year integrated flux of 1.4×10^{12} neutrons per cm^2. Gamma rays are anticipated at a peak rate of 10^{-1} rads per hours, with a 10-year integrated dose of 10^4 rads. Energy levels of both types of radiation will span the range of less

than 0.5 MeV to greater than 3 MeV. It should be stressed that, for TOPS, these dose rates and integrated fluxes are for a 10-year mission, whereas the probe lifetime will be on the order of 2 to 4 years depending on the trajectory chosen.

In addition to the radiation source associated with alpha particles, neutrons and fission reactions, the impurity level of the Pu-236 isotope in production grade Pu-238 is of prime importance. The Pu-236 which is obtained as a trace impurity in Pu-238 can seriously affect the radiation levels at long post-separation time of the Pu-238 fuel. The Pu-236 decays by alpha and beta emission to the ground state Pb-208. In the decay scheme, the thallium 208 isotope emits a 2.62 MeV gamma ray. This energetic emission will increase in the Pu-238 fuel until, at periods of greater than one year, the radiation level from the Pu-236 impurity will become a principal gamma ray contributor to shielded and unshielded gamma ray radiation levels.

The isotope source that could be designed for the probe will utilize Pu-238 to generate about 20 to 40 watts of heat for thermal control. Although such a small RTG in the probe will be closer to the probe electronics by a factor of five, the flux should be considerably reduced since the fuel volume would be approximately 500 times less than that required for the TOPS RTG.

The predicated Pu-238 age for this mission, which depends on the initial age of the source from separation, should be at least one-half the age of the TOPS fuel (assuming at least an 8-year flight time for TOPS) thereby resulting in a substantial reduction in the gamma radiation from the Tl-208 buildup from the Pu-236 impurity.

Although the nuclear radiation will be a significant factor in the development of the probe design, careful attention to type and location of electronic components, and provision of local shielding for radiation sensitive sensors should minimize its overall impact on the final probe design performance.

2.5 ATMOSPHERE

The design requirements that were imposed by use of the Jovian model atmospheres constituted the main trade-off areas of this study. Five key tradeoffs were identified as being very sensitive to the atmospheric environment. These tradeoffs included:

Deceleration Loads - The scale height (see Reference 12) of the atmosphere combined with the entry conditions of velocity and entry angle determine the G-loading on the entry probe. A large scale height provides a longer distance over which deceleration can occur, and so results in reduced loads. It is interesting to note that the scale height of Jupiter is about three times greater (in the Jovian nominal model atmosphere) than that of Earth, but the enormous entry velocities into Jupiter offset the advantage to be gained by entry into a large scale height atmosphere.

The variation of scale height between the model atmospheres is quite significant, and so the G-loading has a large variation with model atmosphere. As the G loads increase, the aeroshell structural weight increases and also the stress levels in all subsystem components. A more complete discussion is given in Section 5.1.

Aerodynamic Heating - The scale height and the atmospheric composition (see Reference 12) are the two physical parameters that characterize the heating during entry. These parameters control the physical mechanisms for transporting the energy in the hot gas between the shock layer and entry probe to the heatshield. The heatshield performance (see Reference 13) was provided to Avco in the form of heatshield fraction and the variation of this fraction with entry probe ballistic parameter and flight path angle. For this conceptual design study it was assumed that the heatshield performance was independent of the model atmosphere.

Payload Container - The physical parameters of the temperature and pressure govern the design of the payload container. This design requirement for a container arises out the necessity to penetrate to great depths where the temperature and pressure is high. It is possible to trade-off deep descent with types of instruments and/or with data return. A description of the thermal protection subsystems for the payload container is given in Section 8.3.

Descent Time - The time to descend through a constant lapse rate atmosphere is a function of the ratio of the local pressure divided by the square root of the local density. Descent time requirements can be controlled through selection of probe ballistic parameter. For this study the dynamic ballistic parameter afforded by the payload container alone and payload container with chute of 25 ft. in diameter was sufficient for all missions. (see Section 9.2)

RF Propagation Losses - The temperature, pressure, and atmospheric composition were the controlling factors in the attenuation of RF energy. It was determined that the ammonia constituent of the atmosphere was the principal absorber. For deep entry, the mass of ammonia that had to be penetrated increased and so did the losses. A summary of the variation of RF losses from the bottom of the cloud layers and the variation of the loss with wavelength is presented in Section 5.1.

2.6   REFERENCES

1. I. J. Loeffler, S. Lieblein, and N. Clough, Meteoroid Protection for Space Radiators, American Rocket Society Space Power Systems Conference, Sept. 25 - 28, 1962; Santa Monica, California

2. Data provided by JPL from Advanced Planetary Probe, Jupiter Flyby Application, JPL Report EPD-358, 1966 May 2.

3. Jupiter Orbiting Vehicle for Exploration, Volume II, prepared by Auburn University, NASA Report No. CR-61180; August, 1967.

4. Handbook of the Physical Properties of Jupiter NASA SP-3031, 1967

5. Receiver Noise Figure Analysis, Memo 10-VI, Jupiter Atmospheric Entry Probe Study.

6. Study of Pioneer Missions to Jupiter, Final Report Contract NAS 2-4900, TRW Systems, Oct. 25, 1968, Appendix 6

7. Spacecraft Magnetic Torques, NASA SP-8018, 1969

8. The Planet Jupiter (1970), NASA Space Vehicle Design Criteria (Environment), July, 1970 (to be published) as modified by Neil Divine, Jupiter Trapped Radiation Material, JPL Interoffice Memo 2947-660, 8 October 1970.

9. J. B. Rittenhouse and J. B. Singletary, Space Materials Handbook, NASA

10. W. H. Barkas and M. J. Berger, Tables of Energy Losses and Ranges of Heavy Charged Particles, NASA SP-3013, 1964, and M. J. Berger and S. M. Seltzer, Tables of Energy Losses and Ranges of Electrons and Positions, NASA SP-3012, 1964.

11. TOPS Spacecraft and Missions, Aeronautics and Astronautics, September, 1970

12. "Preliminary Model Atmosphere for Jupiter," Statement of Work, JPL Contract No. 952897, 1970

13. "Forebody Heatshield Weight Estimate for Jupiter Entry," dated June 5, 1970.

3.0 SCIENCE EXPERIMENT SELECTION

The basic underlying mission concept that was employed in this study was achievement of science objectives by a probe that enters the atmosphere and survives descent to the base of the cloud layers. An alternative approach is to enter the atmosphere and survive descent to very deep penetration of the atmosphere. The former concept used in this study is based on a combination of in situ measurements and remote measurements. This approach of survival to the cloud base had a significant influence on the scientific instrument selection, and on the resulting entry probe subsystem configurations. The latter, alternative, concept that employs direct measurement also has significant influence on the scientific instrument selection and on the resulting entry probe subsystem configurations. For example, the pressure and temperature of the atmosphere at the base of the clouds in the nominal model atmosphere is 17 atm and 425 deg K, respectively; and the total mass per unit area of gas above the probe along a radial line from the center of Jupiter is 6.7 Kg/cm^2. For deep descent like 1000 atm, the corresponding temperature in the nominal model atmosphere is 1425 deg K and the mass per unit area of gas is 396 Kg/cm^2. The pressure and temperature is a measure of the local environment in which the probe must be designed to operate, and the mass per unit area is an indicator of the radio frequency attenuation.

3.1 SCIENCE OBJECTIVES

The science objectives of this first-generation entry probe designed to enter the atmosphere, descend through the clouds, and survive to the base of the cloud layer will provide both in situ and remote measurements of physical parameters and phenomena well below the visible cloud tops. These measurements below the cloud tops are unique to an entry probe, and cannot be obtained by Earth-based observation, flyby, or orbiter observation. Jupiter atmospheric entry probe science objectives have been specified for this study in terms of a set of questions. These questions that appear in Table 3-1 were provided in Reference 1.

3.2 ABILITY OF ENTRY PROBE TO ACHIEVE SCIENCE OBJECTIVES

The five science questions of Table 3-1 represent the mission science objectives. These questions have been rewritten as science objectives and it is required

TABLE 3-1

SCIENCE QUESTIONS FOR
A JUPITER ATMOSPHERIC ENTRY PROBE MISSION

1. What are the relative abundances of hydrogen, deuterium, helium,
    neon, and other elements, and what are their isotopic compositions?

2. What are the present-day atmospheric composition and altitude
    profiles of pressure, temperature, and density, and what effect
    do they have on the radiation balance?

3. What are the chemical composition and vertical distribution of the
    clouds?

4. Do complex molecules exist in the atmosphere of Jupiter?

5. What are the nature and origin of the colors observed in Jupiter's
    atmosphere?

for a successful mission that a set of measurements be conducted that will
permit a determination of:

1) the chemical and isotopic composition of the atmosphere,
2) the thermal structure of the atmosphere,
3) the composition and structure of the clouds,
4) the presence or absence of complex organic matter,
5) the nature of the coloring matter present in the clouds.

The ensuing discussion is based on the atmospheric model atmospheres
provided in Reference 2, and supplementary data available on cloud models
appearing in more recent studies (References 3 to 10). This study is based
on achievement of the above enumerated objectives by a probe that descends
to the base of the cloud layers. The three model atmospheres considered
are termed the cool/dense model atmosphere, nominal model atmosphere,
and warm/expanded model atmosphere. All of the model atmospheres
indicate a presence of discrete, massive cloud layers above the 490 deg K,
425 deg K, and 387 deg K level in the cool/dense, nominal, and warm/
expanded model atmospheres, respectively. Below the cloud base there is
a substantially clear atmosphere extending downward to below the 1000 deg K
level. In the cool/dense model atmosphere the cloud base occurs at a pressure
of 490 deg K and 525 atm, in the nominal at 425 and 17, and in the warm/
expanded at 387 and 3.5. The discussion that follows is based on descent
into the nominal model atmosphere.

3.2.1 Chemical Isotopic Composition of the Atmosphere

It is not as obvious that science objective 1 can be satisfied by a probe that
is designed to survive to the base of the cloud layers. In essence a
strategy is employed in which the natural chemical stratification of the
atmosphere brought about by vapor-pressure fractionation of the constituents
effects a separation of elements and compounds which might otherwise
seriously interfere with each other in a mass spectral analysis. This
stratification is independent of the Jovian cloud models, and is a useful
technique for data reduction that is independent of the simplicity or com-
plexity of the mass composition instrumentation complement.

High above the cloud tops on Jupiter only H_2, He, Ne, Ar, and CH_4 are found,
and it is possible to conduct a mass spectral and chemical analysis of these
components. At temperatures near 148 deg K ammonia will also be present,
and the overlap of the NH_3 mass spectrum with that of CH_4 can be easily

interpreted using earlier determination of the CH_4 mass spectrum.
Similarly, near 210 deg K H_2S will be present, and its mass spectrum can
be determined by subtracting out the already known Ar mass spectrum.
Below the 274 deg K level, H_2O may be similarly investigated, and below
425 deg K HCl and the heavier hydrogen halides will be present. If a small
Pd getter is employed to remove H_2 from one sample, the mass spectrum of
He may also be determined unambiguously. In this way it may be possible
to obtain the isotopic composition and chemical composition of the atmosphere
for the elements H, He, C, N, O, Ne, S, Cl, and Ar from as few as four
mass spectra, as conducted at a temperature of less than 425 deg K. The
other reasonably abundant elements like Si, Mg, and Fe, and so involatile
that they cannot plausibly be expected to be present in the atmosphere above
the $\sim$ 1500 deg K level or even the 2000 deg K level. Thus no further
evidence on the elemental and isotopic composition of Jupiter's atmosphere
could be obtained even by penetration to levels where the pressure is greater
than 1000 atm. This strategy is doubly useful in that it obviates the necessity
for carrying out complete fractionations of atmospheric gases on board the
entry vehicle. Instead, the natural vapor-pressure fractionation of the
atmosphere can be seen to suffice.

It is concluded that objective 1 is met fully and without compromise by a
probe that descends to the cloud base. If the isotopic composition of Cl is
considered unimportant, all other objectives could be met simply by a probe
that descends to the base of the water clouds (temperature of 374 deg K).

3.2.2 Thermal Structure of the Atmosphere

The achievement of science objective 2 can be viewed as two distinct
objectives. Firstly, it is required that the detailed thermal structure of the
clouds be determined. The heat of condensation in the formation of clouds
may have an appreciable effect on the temperature gradient. Plainly, any
probe which traverses the clouds slowly may be instrumented to answer
this question. Secondly, it is required that an assessment of the tempera-
ture gradient to great depths be made. To determine the value of the
temperature gradient, it is necessary to understand the relationship between
the heat balance and the thermal structure. It is then indicated how electro-
magnetic measurements of energy arising from great depths within the
atmosphere, and detected by sensors located at the base of the clouds, can
be used to infer a temperature gradient and provide information about the
thermal structure.

3.2.2.1 Heat Balance and Thermal Structure

The fundamental distinction which must be made for Jupiter (and for each of the outer planets in turn) is whether the planet emits an amount of heat greater than the heat absorbed from the incident sunlight. The easiest way to make this measurement is to observe the total radiant flux emerging from Jupiter over the thermal wavelength region, that is, the wavelength range in which the radiated power, calculated from the Planck function for a black body at about 140 deg K is largest. This requires either a wide-band radiometric measurement or numerous high-resolution measurements at wavelengths covering this region, roughly from 10 to several hundred microns. Ideally the measurements should span all phase angles, so that a possible anisotropy in the radiation field could be detected and allowed for. There is no overwhelming reason why the thermal emission from Jupiter has to be isotropic; it is a simple matter to postulate that a modest increase in cloud mass occurs on the night side of the planet due to the absence of sunlight capable of "burning away" a thin haze. This may suffice to increase the opacity of the atmosphere at thermal wavelengths sufficiently to reduce radiative loss from the nightside of the planet to negligible levels. It is, of course, impossible to resolve this question experimentally from Earth; the semi-major axis of Earth's orbit is five times smaller than that of Jupiter's orbit; the phase angle of Jupiter for an earth bound observer never exceeds about 12°.

The weight of existing evidence strongly suggests that the sunlit side of Jupiter by itself radiates more energy than it receives from the sun, but proof of the phase-independence of this measurement is lacking. Clearly, the crucial measurement is whole-disk radiometry of Jupiter over a wide range of phase angles, sufficient to establish the effective temperature of the dark side of the planet. This will permit a direct calculation of the total radiant flux emerging from Jupiter and comparison with the already known incident solar flux. It is clear that this experiment is ideally suited for a flyby vehicle.

Once the question of the existence of an internal heat source has been resolved with certainty, then a more subtle point must be raised; is the observed heat flux (which shall presently be assumed to exist) sufficiently large to require convective heat transport to deliver the observed amount of energy from the deep interior of the planet up to the top of its clouds? The answer to this question requires a quantitative knowledge of the thermal conductivity and infrared-microwave opacity of the atmosphere. If there exists an altitude range deep within the atmosphere of Jupiter inside which

the opacity of the gas at thermal wavelengths vanishes, then thermal radiation from below this clear region will interact strongly and directly with the absorbing species above the clear region. As a result there will be a net upward energy flux proportional to the difference between the fourth powers of the temperatures of these two layers, and the temperature gradient in the clear region will swiftly vanish. Therefore, the heat flux will be transported upward without the initiation of convection. In contrast, if there exists an altitude range within which the opacity at thermal wavelengths is abnormally high, as a result either of the presence of an additional gaseous absorber or a dense cloud layer, then radiative transfer of energy through this opaque layer will be much less effective than elsewhere in the atmosphere, and the temperature gradient in this layer will increase. Therefore, this opaque layer is acting like a layer of insulation. However, this is not a simple model in which any arbitrary temperature gradient can be borne by the insulator without breakdown. In fact since the system is gaseous, whenever the temperature gradient infinitesimally exceeds the adiabatic lapse rate, given by $-Mg/C_p$, the lower portion of the superadiabatic layer begins to rise and the upper portion begins to sink. The resulting mass motions of the atmosphere transport huge quantities of heat upward. This is precisely the familiar phenomenon of convection.

It should now be clear that a simple knowledge of the net upward heat flux, while essential for any study of the thermal structure of the atmosphere, does not by itself suffice to define a unique thermal model. One must also know enough about the opacity of the atmosphere as a function of wavelength and of depth to determine whether radiative transport is adequate to deliver the observed heat flux. At extremely great depths within the planet, hydrogen itself is sufficiently opaque at thermal wavelengths to require convection if the current estimates of the magnitude of the internal heat source are correct. It is equally clear that the stratosphere of Jupiter is optically thin at thermal wavelengths, and thus nearly isothermal. The complications arise in the upper troposphere, where abrupt changes in opacity occur within small altitude ranges, due to the removal of condensible gases from the atmosphere and the formation of cloud layers. Thus two different types of information are required to settle this question. First, an accurate measurement of the net heat flux as a function of phase and latitude is needed, and could be supplied by a flyby or an orbiter. Because of the strong correlations between convective activity and heat transport, it would be most informative to combine visual imaging of the cloud tops with low-resolution thermal imaging for a prolonged period of time. This combination of experiments and mission requirements points strongly to an orbiter as the ideal

platform. Second, the atmospheric composition and cloud density must be determined as functions of altitude. To do this with adequate precision and depth of penetration requires the use of an entry probe. Direct opacity measurements at selected wavelengths made by an entry probe would be most helpful. Such an experiment is discussed in the next section.

Finally, there is the important but difficult question of local meteorology. It would plainly be of great interest to determine whether convective heat transport was occurring at the entry site of an atmospheric probe mission. The simple process of measuring the temperature and pressure during a traverse of the upper troposphere suffices to establish whether the temperature gradient is adiabatic or markedly subadiabatic

3.2.2.2 Infrared and Microwave Radiometry

The point has been made previously, that the understanding of the thermal structure of the Jovian atmosphere requires: 1) the existence or absence of a thermal heat source within the planet, and 2) the mechanism for transport of energy from the interior to the cloud layers, i.e. either radiation, conduction, or convection. Existence of an internal heat source can best be determined from a flyby or orbiter, whereas the heat transport mechanism must be determined from a probe that descends beneath the cloud tops. Remote microwave radiometry is used to determine the thermal gradients below the clouds to great depths, and in situ infrared radiometry is used to determine the opacity of the atmosphere as a function of altitude, to provide data on heat transport within the cloud layers.

One of the crucial problems in understanding the thermal structure of the atmosphere of Jupiter is determination of the opacity as a function of both wavelength (in the microwave and in the infrared) and altitude. Because of the important contribution to the thermal opacity due to the cloud layers, a low-resolution infrared photometer aboard an entry probe could be used to locate and measure the temperatures of the cloud layers either above or below the entry vehicle. Further, should there be an extensive "clear" region below the clouds, the infrared radiometer would permit the approximate measurement of the temperature at great atmospheric depths. The microwave radiometer would always allow measurement to great depths whether or not the base of the cloud layer is reached and a clear region is found since the scattering of energy at microwave frequency from clouds is small due to the large wavelength in comparison to the anticipated dimensions

of cloud particles. At infrared frequencies, the wavelength is comparable to the cloud particle dimension. Although the center of the thermal wavelength region is near 15μ, absorption due to methane and ammonia block the spectral region at wavelengths much beyond 5μ. Earth based observations of Jupiter at 5μ suggest that opacity at this wavelength is due to clouds not gas, and hence 5μ radiometry conducted below the cloud base may permit remote sensing of the lower atmosphere. It would also be useful to include a microwave detector sensitive at wavelengths beyond 3 cm, where the atmosphere is appreciably more transparent and the opacity is largely independent of light scattering by cloud particles. These two instruments would probe the atmosphere to different depths, and would be deployed so as to cover the upward and downward directions (fields of view of 60° would suffice). Three to five sideward looking infrared photometers could supply data on horizontal inhomogeneties within a cloud layer and on the horizontal and vertical scale size of such structure.

As an illustration of such instrumentation in establishing the thermal structure of the deep atmosphere, two cases are proposed. In the first case the temperature gradient decreases to a distinctly subadiabatic value just below the bottom of the water clouds or lowest cloud layer, and in the second case the temperature gradient increases to a distinctly adiabatic or superadiabatic value.

The first case of a subadiabatic temperature gradient is examined. There are two radically different ways of looking at the cause of this phenomenon, and the resolution requires quantitative test. The first possibility is the existence of an isothermal atmosphere. Since clouds are present in the upper troposphere, an upward circulation is needed to support these clouds, and the temperature gradient which creates the circulation could be maintained by a greenhouse effect, using trapped solar radiation. The second possibility is that the interior of the planet is extremely hot, and that the planet does, indeed, emit more heat than it receives from the sun. The subadiabatic region is simply a layer which, for some reason such as the absence of aerosols, is so transparent at thermal wavelengths that convective heat transport is not required to transport energy, and that this transport is accomplished by radiative processes. For the first possibility, the presence of an isothermal atmosphere, the brightness temperature looking downward at microwave frequency would be essentially the same as the local temperature measured by the temperature sensor aboard the probe. For the second possibility, the brightness temperature looking downward at microwave frequency would be greater than the local temperature. This comparison of remote brightness temperature and local in situ temperature is used to define the phenomenon that could cause a subadiabatic temperature gradient measurement by the entry probe.

For the second case, if the temperature gradient, as measured by the probe temperature gauge is adiabatic or superadiabatic, then an increase in microwave brightness relative to the local temperature measurement would indicate that energy is transported by convection, and that no isothermal layer is present. To whatever depth the entry probe penetrates (even if failure occurs above the base of the clouds), the microwave radiometer experiment adds considerable downward reach.

Note that the data reduction from a downward looking radiometer alone in the absence of a simultaneously upward looking microwave radiometer could result in an underestimation of the temperature gradient, i.e. opacity must be accounted for. The upward-looking microwave radiometer reports on the brightness temperature of a portion of the atmosphere whose thermal structure is already measured, and an increase in the opacity of the atmosphere would be easily deducible from the fact that the upward-directed microwave radiometer would also indicate a decreased temperature difference, i.e., due to the opacity it would be measuring the brightness temperature of atmospheric gas closer to the entry probe, which should be closer in value to the direct temperature measurement. For example, if the temperature differential between the upward brightness temperature and temperature gauge, and the downward brightness temperature and temperature gauge is comparable, then the atmosphere is opaque. Thus, variations in temperature gradient and in opacity can be separated whatever their cause because of the independent methods of measurement.

In the upper troposphere, the dominant form of thermal opacity may well prove to be the clouds. In this case, the infrared radiometry will report the approximate temperature of the next cloud layer as soon as it emerges from the base of the preceeding layer. Due to the large scattering by the cloud particles, the infrared brightness temperature will remain nearly constant until the entry probe begins to break through the bottom of the layer. If it is found that the rate of change of the infrared brightness temperature is nearly the same as the directly measured temperature gradient, then it can be concluded that the entry probe is falling through an extensive cloud free region in which the temperature gradient is constant and the opacity is governed by molecular processes at the base. Under these circumstances, the opacity may be calculated from the known atmospheric composition as derived from the mass spectrometer analyses.

Infrared radiometry allows for the possibility of 1) detailed description of the cloud structure, 2) unique data for depths of descent at which the solar flux is nearly extinct, and 3) data to support a dark side entry mission.

3.2.2.3 Calculation of Lapse Rate Based on Brightness Temperature Information

A temperature gradient or lapse rate based on a microwave brightness temperature is determined in the following manner. At a given instant of time, the following entry probe data is available: the microwave brightness temperature of the downward looking radiometer, the microwave brightness temperature of the upward looking radiometer, the local pressure, the local temperature, and the local atmospheric composition. With this data, it is possible to calculate a lapse rate. An assessment of the atmospheric opacity can be gained from reduction in data of the outputs of the upward and downward looking radiometers, and the atmospheric composition. The local temperature and pressure is known from the outputs of the gauges aboard the probe, and with composition data, and also an assumption of a constant lapse rate, the downward atmospheric profile can be constructed. There is a unique brightness temperature for a given atmospheric structure model and opacity model. The assumed lapse rate is varied until the calculated microwave brightness temperature agrees with the measured microwave brightness temperature.

3.2.3 Composition and Structure of Clouds

It is clear that this objective can be achieved by a probe that is designed to survive to the base of the cloud layers. Rate of descent through the clouds is the important design criteria, and the limiting descent rate is imposed by the long sample ingestion to data output time of the gas chromatograph. For polar gases like ammonia, water, and hydrogen cyanide the sample time is like five minutes; for non-polar gases like argon, helium, neon, methane, and hydrogen, the sample time is two minutes.

3.2.4 Complex Organic Matter

Production of complex organic matter requires the presence of an energy source, and a low temperature and low pressure environment to allow for the existence of the organic matter. Within the upper cloud layers, solar energy can support ultraviolet photolysis which can lead to the production of organic matter. Also the presence of lightning within the cloud layers can provide the necessary energy. At ambient conditions of 1000 deg K and pressures near 1000 atm analytical searches for traces or organic matter which is in fact a disequilibrium material may be wholly superfluous. At elevated temperature and pressure, complete chemical equilibration is extremely rapid. It is concluded that if organic matter is present it is not likely to exist within the cloud layers.

3.2.5 Coloring Matter Present in Clouds

The detection of coloring matter in clouds is clearly available to a probe that descends through the clouds.

3.3 ENTRY SITE SELECTION

The principal targeting requirement for a first, and single entry probe is the selection of an area that is typical of the planet. Such an approach will permit return of data generally representative of the entire planet. A subsidiary requirement is a constraint on the solar elevation angle imposed by the presence of certain sun-sensing photometer instruments.

The dominant features of the visual appearance of Jupiter define the main parameters which relate to the choice of a landing site. Most of the visible disc of the planet is covered most of the time with alternating light and dark-colored bands. These bands are frequently punctuated with small, dark or light spots with short lifetimes (a few weeks or months). The basic band structure is not constant, but over years or decades the relative widths and color intensities of the bands may vary considerably. The polar regions are covered by two relatively featureless and fairly bright "polar caps" which clearly are a cloud phenomenon. Occasionally, photographs of the planet taken within the wavelength coverage of a fairly strong methane absorption band show anomalously bright small caps over the extreme polar regions, extending roughly ten degrees from the poles of rotation. The most interesting quasi-permanent feature on the planet is the Great Red Spot (GRS), a pinkish, orange, or reddish brown ellipse. The dimensions, color, and longitude of the GRS all are subject to erratic and unpredictable changes. The size and stability (persistence) of the GRS are unique; the color changes and erratic drifting are typical of other areas of the planet.

There are many lines of evidence regarding the nature of Jupiter's magnetic field. Suffice it to say that a grossly dipolar field aligned fairly well with the rotation axis of the planet is indicated by the data. The magnetic field observations can be characterized as implying that Jupiter has an intense dipole field which may conceivably be dynamically coupled with the lower atmosphere, and that measurement of atmospheric properties in the immediate vicinity of the magnetic poles would not produce representative data on the planet. Also at high latitudes, "polar caps" are noted. The area covered by these "caps" at high latitude is small as compared with the Jovian surface area at low latitudes.

Finally, it should be noted that the exact rotational equator is unique from a meteorological point of view. The dynamics of the atmosphere are dominated over almost all of the planet by the great Coriolis forces produced by the planet's rapid rotation. These forces vanish at the equator. In addition, there is a phenomenon of the equatorial jet, a high-velocity narrow current of uncertain origin.

The above discussion provides, in general, the latitude restriction on targeting. Illumination considerations provide longitude restrictions. It has been pointed out that photometer requirements necessitate dayside entry. Due to cloud top irregularities, the angle between the negative velocity vector (assuming vertical descent) and the sun line, should not be greater than 70 deg to avoid the solar flux obscuring problems of cloud top irregularities. At shallow entry angles, irregularities in cloud tops could make clouds look considerably thicker, and this would give rise to a spurious interpretation of the photometer outputs.

With these discinctions in mind, the following targeting strategy for entry probes can be considered. If only a single entry probe is to be landed on the planet, or if a first entry probe mission is intended to provide in situ baseline data to assist in the design of later entry probes, then it is essential that the probe be targeted in what can best be described an an innocuous region. This can be achieved by landing within about 20 or 25 degrees of the equator (but not within about 5 degrees of the equator) at arbitrary longitude. The probe will then land in either a "typical" light band or a "typical" dark band.

If more than one entry probe can be planned, then the order in which they should be targeted towards the distinctive regions of Jupiter is:

1) A "typical" region as above;
2) The Great Red Spot;
3) The immediate vicinity of the magnetic and rotational pole; and
4) A "typical" region as above, but one of opposite color (light vs dark) to the one probed by the first entry vehicle.

There is some question as to the advantages of targeting to a light region or a dark region. The text that follows investigates the significance of this targeting tradeoff. Because of the high 5μ brightness temperature measurements which have been reported for the dark-brown North Equatorial Belt (NEB), it seems likely that the highest cloud layer, presumably composed of

solid ammonia, is either broken or abnormally diffuse in this region. If this interpretation is not correct, then there is no reason to prefer either dark or light regions as landing sites except for the possibility that the coloring matter in the darker regions might be analyzed by the GC/MS package. Thus, if observations of Jupiter over the next few years fail to turn up any evidence for elevation differences between the dark and light cloud bands, there would be some slight reason to prefer entry into the dark bands.

On the other hand, there is a substantial probability that there is indeed an important difference in cloud structure between the NEB and a typical light region such as the North Equatorial Zone (NEqZ). If the top-most cloud layer is indeed partially transparent in the NEB, then it would be possible to conduct photometer or spectrometer measurements down to temperature levels possibly as high as 300 deg K. At wavelengths beyond the ammonia UV cutoff principal sources of opacity are gaseous H_2S absorption and scattering by cloud particles. The possible absence of the NH_3 cloud cover over the NEB makes it impossible to determine the level of the NH_3 cloud deck directly by a light-scattering (nephelometer) experiment, but permits measurements of the optical properties of the gaseous medium down to depths not otherwise obtainable. Therefore, it is necessary to carefully consider the relative importance of the two alternatives: first, entry into the NEqZ, in which detailed nephelometer data is returned on the structure of the cloud layer about which the most is already known, and UV data is truncated at the same level point; second, entry into the NEB, in which no structural data on the NH_3 clouds can be assumed, but UV data and analysis of the coloring matter in the clouds would both be more extensive. In the NEB one may also collect light-scattering data on the structure of a lower cloud layer composed of something besides NH_3.

Based on our current ideas about the cloud structure on Jupiter, entry into a dark band may be slightly more productive than a similar mission into a light band. The principal conclusion, however, must be that there is no reason why this decision has to be made for several years, within which time the issue may be sufficiently well resolved.

3.4 SCIENCE DESCRIPTION

The nominal dayside science payload contains five instruments that have not been incorporated into the JPL baseline payloads (See Figure 3-1). These include: 1) an R.F. click detector to provide a coincidence check for the optical flash (or lightning) detector to improve the certainty that the recorder flash was of electromagnetic origin; 2) five infrared radiometers to provide

FIGURE 3-1 SCIENCE PAYLOADS

PAYLOAD / INSTRUMENT	JPL BASELINE	SMALL	NOMINAL		EXPANDED	
			DAYSIDE	NIGHTSIDE	DAYSIDE	NIGHTSIDE
TEMPERATURE GAUGE	▓	▓	▓	▓	▓	▓
PRESSURE GAUGE	▓	▓	▓	▓	▓	▓
ION MASS SPEC	▓	▓	▓	▓	▓	▓
GAS/CHROM & N. MASS SPEC	▓	▓	▓		▓	▓
ACCELEROMETERS	▓		▓	▓	▓	▓
P H O T O M E T E R S — CLOUD TOP DETECTOR	▓		▓		▓	
AEROSOL PARTICLES	▓		▓		▓	▓
LIGHTNING DETECTOR	▓		▓	▓	▓	▓
H/D DETERMINATION	▓				▓	▓
METHANE ABUNDANCE	▓					
AMMONIA ABUNDANCE	▓					
R. F. CLICK DETECTOR			▓	▓	▓	▓
NEPHELOMETER				▓	▓	▓
IR RADIOMETER			▓		▓	▓
MICROWAVE RADIOMETER					▓	▓
EVAPORIMETER/CONDENSIMETER						
UV SPECTROMETER			▓		▓	▓
MAGNETOMETER					▓	▓
TURBULENCE INDICATOR						▓

31-0113P

3-14

data on the infrared brightness temperature and cloud opacity in both
horizontal and vertical directions; 3) two microwave radiometers for
measurement of microwave brightness temperature at great depths and
for measurement of microwave opacity; 4) a magnetometer to operate
following probe separation from the bus to entry, and a magnetometer to
operate during descent through the clouds; and 5) an accelerometer which
serves as a turbulence indicator to measure the atmospheric gustiness.
For the nominal nightside science payload (See Figure 3-1) all solar flux
sensing, photometers are removed, and a nephelometer (an instrument
which provides its own light source) is added. The solar sensing photo-
meters are functionally redundant to the neutral particle mass spectro-
meter and gas chromatograph instruments, and if they are removed, then
an independent measurement of atmospheric composition is lost.

An expanded science payload was generated, based on the philosophy that
instruments would be added to increase the functional redundancy of the
measurements that are made by the nominal science payload. The expanded
dayside science payload is shown in Figure 3-1. There are two instru-
mentation changes. Firstly, the infrared photometers that measure
methane and ammonia abundance are removed and a UV spectrometer is
added. Secondly, an evaporimeter-condensimeter is added to provide more
data on cloud structure. For the nightside mission, all solar sensing
photometer instruments are removed, and a nephelometer is added.

The selection of the instrumentation complement for the small payload is
premised on the philosophy of inclusion of a minimum number of instruments
that conduct measurements that are unique to a probe that descends below
the cloud tops. The small science payload is also shown in Figure 3-1.
Since no solar sensing instrument is included, there is no distinction
between dayside and nightside operation. An ion mass spectrometer is
added to allow the possibility of data return from the upper thresholds of
the atmosphere. In the event the probe does not survive entry, return of
information on the composition of the upper atmosphere is of cosmological
importance. This data, albeit limited, provides an important failure mode
return. Note that in this small payload, the thermal structure of the
atmosphere can only be determined to the cloud base since no radiometers
are included. Therefore, a candidate additional instrument for the small
science payload is a microwave radiometer to provide data on temperature
gradients and thermal structure of the atmosphere below the clouds.

The methane and ammonia abundance measurement photometers operate in
the infrared region in the JPL baseline payload. For all the payloads that

use photometers, the infrared photometers have been removed and ultra-violet photometers added in their place. Use of ultraviolet sensors greatly reduce the need to guide on the sun. An ultraviolet sensor with a field of view of one steradian could derive useful data on the decrease of intensity of Rayleigh-scattered light with depth even at landing sites, quite close to the terminator. Monitoring the extinction of solar red and infrared light at shallow viewing angles, requires accurate tracking of the solar disc. In addition, the path lengths through the atmosphere are so great at low solar elevation angles that interpretation of this data could be greatly complicated by horizontal inhomogeneities in the atmosphere. This would remain true even if several additional photometer channels clear of important absorption bands could be added to monitor baseline fluctuations. For these reasons, selective ultraviolet photometry can be a more flexible technique than infrared photometry. In Table 3-2 there are presented a list of instruments that correspond to the list in Figure 3-1. and the usefulness of the instrument in achieving the science objective is indicated. Note that in the JPL baseline payload both an aerosol photometer and cloud top detector is included. In the Avco payloads, the aerosol photometer also serves as a cloud top detector.

The most important type of data which can be returned by an entry probe is a detailed chemical analysis of the atmosphere, including isotopic composition. This type of information has direct relevance to the composition, cloud, organic matter, and coloring matter objectives. The fundamental structural data concerning the upper atmosphere requires returning accelerometer data during entry, and the thermal structure within the troposphere requires knowledge of the temperature and pressure as a function of altitude. Cloud profiles require, in addition to adequate chemical analyses, careful measurement of the thermal profile, and a measurement of the cloud particle number density. Direct measurement of the temperature gradient during a traverse of the upper portion of the troposphere may be very usefully supplemented by measurement of the radiometric brightness temperature at the point of deepest penetration. Perhaps the least important objectives for an early entry probe mission are determination of organic matter and coloring matter. These are also experimentally the most demanding. Since both of these problems are intimately associated with disequilibrium energy inputs into the atmosphere, it would be helpful to monitor the depth of penetration of solar UV light at selected wavelengths and to search for electrical discharge activity. Any simple measurements which can contribute to the meteorological problems should be conducted, but the inclusion of elaborate special instrumentation for such purposes would be unquestionably premature.

TABLE 3-2

INSTRUMENT SELECTION FOR ACHIEVEMENT OF SCIENCE OBJECTIVES

INSTRUMENT \ SCIENCE OBJECTIVE	ABUNDANCE	STRUCTURE	CLOUDS	ORGANIC MATTER	COLORING MATTER
TEMPERATURE GAUGES	-	D	D	-	-
ACCELEROMETERS	-	D	-	-	-
PRESSURE GAUGES	-	D	-	-	-
UV PHOTOMETER	D	D	-	-	-
UV SPECTROMETER	D	D	-	-	-
NEUTRAL PART. MASS SPEC. AND GAS CHROMATOGRAPH	D	-	D	D	D
H:D PHOTOMETER	D	-	-	-	-
AEROSOL PHOTOMETER	-	-	D	-	-
NEPHELOMETER	-	-	D	-	-
EVAPORIMETER-CONDENSIMETER	-	-	D	-	-
OPTICAL FLASH DETECTOR	-	-	-	D	D
R. F. CLICK DETECTOR	-	-	-	D	D
IR RADIOMETER	-	D	-	-	-
MICROWAVE RADIOMETER	-	D	-	-	-
ION MASS SPEC.	D	-	-	-	-

D - DIRECT MEASUREMENT
I - INDIRECT MEASUREMENT

Tables 3-3 through 3-19 summarize the performance, design characteristics, and integration requirements of the instruments used in this study to achieve the science objectives.

The value of incorporation of an imaging device on the entry probe was evaluated. It was determined that the only truly effective imaging experiment which could confidently be proposed based on our present level of knowledge would be relevant to the fundamental nature of Jovian planetary circulation. For these purposes, spatial resolution not greater than about one-half mile would be sufficient. This figure corresponds to the resolution of the Nimbus weather satellite. The most useful data return would require watching the global movements of cloud formations over a period of several weeks. To obtain this one-half mile resolution, a 600 line miniature vidicon camera system with a focal length of 28 mm, image format of 6.4 mm, that weighs 2 lbs was assumed. Use of this device would require that the image be recorded about 1200 Km above the cloud tops. The dimension of the corresponding ground image is 266 Km, or one picture is obtained at one instant of time that covers one, one-millionth of the Jovian surface area. This is hardly a global picture over several weeks. In addition, based on a 6 bit gray scale, some 2 million bits per picture must be transmitted. The data content of this instrument is many orders of magnitude greater than the data content of a nominal dayside science payload which is 27,000 bits. Global imaging over a period of several weeks is best suited to an orbiter.

3.5 <u>ASSEMBLY OF SCIENCE PAYLOADS</u>

The characteristics of the nominal dayside, nominal nightside, expanded dayside, expanded nightside, and small science payloads are presented in Table 3-20. This table is based on the use of the instruments developed in Figure 3-1, and the instrument performance described in Tables 3-3 to 3-19. The total bit content is about 27,000 bits for the nominal dayside science payload. This bit content is based on use of science sampling requirements which, in general, are not linear functions of time. It is possible to consider use of time varying sampling requirements, but it may not be practical if a simple data handling system is desired. Therefore, in general, if the science sampling requirements are selected as the design goal, and a constant sampling rate with time is also selected, then the total bit content of a given mission will increase; or if the total bits are held at 27,000, then the constant incremental sampling time will not result in satisfaction of the science sampling requirements.

In Table 3-20 there is also indicated for comparison the JPL baseline payload. Note that the bit content is 45,000. The large bit generators are the temperature and pressure measurements. In the baseline payload,

TABLE 3-3

TEMPERATURE GAUGE

WEIGHT:	1.0 lb.
POWER:	0.2 w
VOLUME:	15 in^3
SAMPLING RATE:	1 sample/km
BIT/SAMPLE:	9
INTEGRATION	Sensor must be located beyond boundary layer of descending probe and must be shielded from thermal radiation from probe. Two gauge units are included. Electronics within payload container.
USAGE:	All dayside and nightside payloads from 0.7M to cloud base.
DESCRIPTION:	Chromel-alumel thermocouple range switched. Temperature range of operation: 113 deg. K to 425 deg. K. Two sensors are for redundancy, but data output from only one sensor is telemetered. Design goals for temperature measurements should be for an absolute accuracy of $\pm$ 1 deg. K and a relative accuracy of $\pm$ 0.2 deg. K, up to 350 deg. K with allowable errors twice as high above this temperature. The sampling rate should be one sample per kilometer of fall to ensure that lapse rate changes can be detected.
REFERENCE:	• Rosemont Engineering Co. • Science Criteria for Jupiter Entry Missions, Statement of Work, JPL Contract No. 952897, 1970 July 1.

TABLE 3-4

ACCELEROMETER

WEIGHT: 1. 0 lb.

POWER: 1. 0 w

VOLUME: 6 in^3

SAMPLING RATE: 0. 1 sec

BIT /SAMPLE: 7

INTEGRATION: Triad of accelerometers located at c. g. of entry probe, plus redundant longitudinal accelerometer. Total of four accelerometer units are included. Located within payload container.

USAGE: For dayside and nightside payloads from entry to 0. 7M.

DESCRIPTION: Permit determination of scale height to 1%. Pendulous force mass balance type of sensor. Output of all accelerometers is telemetered. Includes all accelerometer and constraint electronics. Range of deceleration 0. 1G to 525G (for -15 deg entry angle). Data collected from entry to chute deployment and playout is interleaved with real time data. The crucial measurement is the axial component of acceleration.

REFERENCE: • Bell Aerosystems DVM VII
                 • Science Criteria for Jupiter Entry Missions, Statement of Work, JPL Contract No. 952897.

TABLE 3-5

PRESSURE GAUGE

WEIGHT: 2.0 lb.

POWER: 0.1 w

VOLUME: 10 in^3

SAMPLING RATE: 1 sample/km

BIT/SAMPLE: 7

INTEGRATION: Entrance port near forward point on subsonic configuration. Two units are included. Electronics located within payload container.

USAGE: All dayside and nightside payloads from 0.7M to cloud base.

DESCRIPTION: Deployed at 0.7 Mach. No. Three of five sensors are used to cover range from 0.05 to 17 atm and are range switched. Pressure measurements should be made to an accuracy of ± 1% at all levels, and should be made coincidentally with the temperature measurements.

REFERENCE: · Edcliff Instruments
                     · Science Criteria for Jupiter Entry Missions, Statement of Work, JPL Contract No. 952897, 1970 July 1.

TABLE 3-6

UV PHOTOMETER

WEIGHT:	1. 3 lb.
POWER:	. 8 w
VOLUME:	24 (four 1 x 1 x 6 units) in^3
SAMPLING RATE:	Once above clouds, then once every 10% increase in pressure
BIT/SAMPLE:	40
INTEGRATION:	One unit located within payload container with a field of view of 90 deg. Can share window with aerosol photometer.
USAGE:	For dayside payload only from 0.7M to cloud base.
DESCRIPTION:	Five spectral channels of 200 angstrom width and centered on wavelengths 400, 700, 1200, 1900, and 2500 angstroms. A sampling rate of once every 10% increase in pressure ensures that a sample is obtained within every cloud layer. Field of view should enclose a very wide expanse of sky, and for best sensitivity the field of view should include the sun. Ten bits per channel. The multichannel UV photometer permits independent determination of the abundances of H_2, CH_4, NH_3, and H_2S as functions of altitude. Multiple channels contribute valuable direct data on the depth of penetration of ultraviolet light as a function of wavelength.
REFERENCE:	· NASA SP-3028 Instruments and Spacecraft · Science Criteria for Jupiter Entry Missions, Statement of Work, JPL Contract No. 952897, 1970 July 1.

TABLE 3-7

UV SPECTROMETER

WEIGHT:	12 lb.
POWER:	4 w
VOLUME:	400 in^3
SAMPLING RATE:	Once above clouds, then once every 10% increase in pressure
BIT/SAMPLE:	160
INTEGRATION:	One unit located within payload container, with a field of view of 90 deg.
USAGE:	For dayside payload only from 0.7M to cloud base.
DESCRIPTION:	Eighteen spectral channels 100 angstrom width from 800 to 2500 angstrom. Field of view should enclose a wide expanse of sky, and for best sensitivity should include the sun. Ten bits per channel. If data rate is available, then 76 channels of 20 angstrom width should be considered.
REFERENCE:	· NASA SP-3028 Instruments and Spacecraft · Science Criteria for Jupiter Entry Missions, Statement of Work, JPL Contract No. 952897, 1970 July 1.

TABLE 3-8

GAS CHROMATOGRAPH/NEUTRAL PARTICLE MASS SPECTROMETER

WEIGHT:	7 lb.
POWER:	12 w
VOLUME:	320 (4 x 8 x 10) in^3
SAMPLING RATE:	1 sample above, within, and below each cloud layer.
BIT/SAMPLE:	290 bit/scan
INTEGRATION:	Located within payload container.
USAGE:	Simple gas chromatograph for dayside science payload; more elaborate gas chromatograph for nightside payload from 0.7M to cloud base.
DESCRIPTION:	Mass spectrometer scans from 1 to 4, 12 to 22, 24 to 30, and 34 to 40 m/e. The dynamic range is 10^6 and the measurement accuracy, 1%. For dayside entry, it is assumed that the gas chromatograph bit output is 10% that of the neutral particle mass spectrometer output, for a total output of the GC/MS of 290 bit/sample. For nightside entry the gas chromatograph bit output is comparable to that of the neutral particle mass spectrometer, for a total output of 520 bit/sample. A more elaborate gas chromatograph provides a substitute to the photometers for determination of the vertical distribution of gases. A sampling rate of above, within, and below each cloud layer requires a sophisticated adaptive system to sense a cloud. This can be accomplished in a closed loop fashion based on onboard temperature and pressure outputs. A minimum sample mission could be based on one sample per 100 deg K of ambient temperature change. In all instruments, the sampling time is small. In the gas chromatograph, a processing time of two minutes is required for non-polar gases, and a sampling time of five minutes is required for polar gases.
REFERENCE:	• NASA SP-3028 Instruments and Spacecraft • Science Criteria for Jupiter Entry Missions, Statement of Work, JPL Contract No. 952897, 1970 July 1.

TABLE 3-9

H:D PHOTOMETER

WEIGHT: 0.35 lb.

POWER: 0.2 w

VOLUME: 6 (1 x 1 x 6) in^3

SAMPLING RATE: Once above clouds, then every 10% increase in pressure.

BIT/SAMPLE: 10

INTEGRATION: One unit located within payload container. Sun must be within field of view of the detector. The detector can share a window with the optical flash detector.

USAGE: For dayside science payload only, from 0.7M to cloud base.

DESCRIPTION: One channel at 4.55μ. The output provides the only source of information on the deuterium abundance. Unlike the ultraviolet detectors which are more sensitive when the sun is within the field of view, this experiment will not work unless the sun is within the field of view.

REFERENCE: · NASA SP-3028 Instruments and Spacecraft
                  · Science Criteria for Jupiter Entry Missions, Statement of Work, JPL Contract No. 952897, 1970 July 1.

TABLE 3-10

AEROSOL PHOTOMETER

WEIGHT: 0. 65 lb.

POWER: 0. 4 w

VOLUME: 12 (two 1 x 1 x 6 units) in^3

SAMPLING RATE: Once above clouds, then every 10% increase in pressure.

BIT/SAMPLE: 20

INTEGRATION: One unit located within payload container. The field
                    of view of ninety deg should enclose sun. Shares
                    window with ultraviolet photometers.

USAGE: For dayside payload only, from 0. 7M to cloud base.

DESCRIPTION: Two channels near 1 μ. This photometer can monitor
                    extinction of total sunlight over the red end of the visible
                    spectrum, or search for scattered light at large angles
                    to the sun-probe line. The first mode of operation is
                    preferred since it is somewhat more sensitive and
                    permits instrument placement and orientation in the
                    same manner as the photometer experiments at shorter
                    wavelengths.

REFERENCE: • NASA SP-3028 Instruments and Spacecraft
                    • Science Criteria for Jupiter Entry Missions, Statement
                    of Work, JPL Contract No. 952897, 1970 July 1.

TABLE 3-11

NEPHELOMETER

WEIGHT: 4 lb.

POWER: 3 w

VOLUME: 100 in^3

SAMPLING RATE: 10 sample/km

BIT/SAMPLE: 10

INTEGRATION: One unit located within payload container. Two ports
                  must be provided.

USAGE: For nightside payload only, from 0.7M to cloud base.

DESCRIPTION: Clouds are detected and estimates made of cloud particle
                  density by measuring the backscattering of light from
                  clouds. This instrument provides a substitute for the
                  photometers, and is used to obtain data on the cloud
                  structure. An intense collimated light beam is directed
                  outward through a port and a detector "telescope"
                  looking through a second port a few inches away from
                  this beam is directed so that the field of view of the
                  detector intersects the illuminated cylinder at a dis-
                  tance of about one foot from the probe surface. The
                  axis of the light port is normal to the probe longitudinal
                  axis; the axis of the detector port is inclined to inter-
                  cept the light beam about one foot from the probe.

REFERENCES: A Venus Multiple-Entry Probe Direct-Impact Mission,
                  NASA Goddard.

TABLE 3-12 .

EVAPORIMETER-CONDENSIMETER

WEIGHT: 2 lb.

POWER: 10 w

VOLUME: 70 in^3

SAMPLE RATE: 1 sample/km

BIT/SAMPLE: 9

INTEGRATION: One unit: electronics, detector, and light source are
                   located within payload container. A reflector is
                   located external to the container where atmosphere gas
                   flow exists.

USAGE: For dayside and nightside science payloads, from 0.7M
                   to cloud base.

DESCRIPTION: A light source illuminates a reflector which is located
                   external to the container, and which is cycled over a
                   wide temperature range. At a pressure and tempera-
                   ture characteristic of the particular condensible, con-
                   densation or evaporation occurs depending upon
                   whether the reflector temperature is decreasing, or
                   increasing. The change in reflected light intensity is
                   sensed by the phototube. Will require two optical ports.

REFERENCES: A Venus Multiple-Entry Probe Direct-Impact Mission,
                   NASA Goddard.

TABLE 3-13

OPTICAL FLASH DETECTOR

WEIGHT:	.65 lb.
POWER:	.4 w
VOLUME:	70 in^3
SAMPLING RATE:	1 sample/km
BIT/SAMPLE	16
INTEGRATION:	One unit looks at upward hemisphere with a ninety degree field of view and can share window with H:D photometer.
USAGE:	For dayside and nightside science payloads from, 0.7M to cloud base.
DESCRIPTION:	Coincidence of measurement with RF Click Detector should be indicated. Records number and intensity of flashes.
REFERENCES:	Science Criteria for Jupiter Entry Missions, Statement of Work, JPL Contract No. 952897, 1970 July 1.

TABLE 3-14

RF CLICK DETECTOR

WEIGHT: 2. 0 lb.

POWER: 1. 0 w

VOLUME: 100 in^3

SAMPLING RATE: 1 sample/km

BIT/SAMPLE: 16

INTEGRATION: One unit, stub antenna located near optical flash detector.

USAGE: For dayside and nightside science payloads, from 0. 7M to cloud base.

DESCRIPTION: Coincidence of measurement with optical flash detector should be indicated. Records number and intensity of flashes.

REFERENCES: Orbital Imagery for Planetary Exploration, Imaging Sensor System Scaling Laws, Volume IV, ITT Research Institute, Contract No. NAS 2-4494, July 1969.

TABLE 3-15

IR RADIOMETER

WEIGHT:	1.0 lb.
POWER:	1.5 w
VOLUME:	25 (3D x 3.5) in^3
SAMPLING RATE:	1 sample above, within, and below each cloud layer.
BIT/SAMPLE:	10
INTEGRATION:	Five radiometer units are located on a meridianal line about external subsonic configuration. Each sensor has a 45 deg field of view. The optical axes measuring from the forward point are located at 0, 45, 90, 135, and 180 deg. The sampling rate chosen is equivalent to that of the GC/MS package since the instrument is used to provide data on the thermal structure of clouds.
DESCRIPTION:	Sensitive to wide wavelength range near 5μ, and should have a wide field of view.
USAGE:	For dayside and nightside science payloads from 0.7M to cloud base.
REFERENCES:	Science Criteria for Jupiter Entry Missions, Statement of Work, JPL Contract No. 952897, 1970 July 1.

TABLE 3-16

MICROWAVE RADIOMETER

WEIGHT:	2.5 lb.
POWER:	1.0 w
VOLUME:	200 in^3
SAMPLING RATE:	1 sample above, within, and below each cloud layer.
BIT/SAMPLE:	10
INTEGRATION:	Two radiometer units are used with a wide field of view. One unit is located at the forward point of the descent probe and looks down into the atmosphere while the other unit, located at the trailing point, looks up.
USAGE:	For dayside and nightside science payloads, from 0.7M to cloud base.
DESCRIPTION:	The detector is sensitive to wavelengths beyond 3 cm.
REFERENCES:	Orbital Imagery for Planetary Exploration, Imaging Sensor System Scaling Laws, Volume IV, ITT Research Institute, Contract No. NAS 2-4494, July 1969.

TABLE 3-17

MAGNETOMETER

WEIGHT:	**3. 2 lb.**
POWER:	0. 3 w
VOLUME:	50 in^3
SAMPLING RATE:	1 sample/km
BIT/SAMPLE:	16
INTEGRATION:	Two unit sensors are located about one body radius away from probe, where the estimated probe induced field is about 2 gamma.
USAGE:	For dayside and nightside science payloads. One instrument is deployed following entry probe separation from the spacecraft. Sensor and boom is separated near the top of the atmosphere when meteoroid container is separated from entry probe. Second sensor and boom is deployed after descent to 0. 7M and provides data to the cloud base.
DESCRIPTION:	Two axis saturable core magnetometer. Provides magnetic field data in the regime from periapsis passage of the spacecraft to the top of the atmosphere. Based on a planetary radius periapsis passage of two, the excursion of the field is 8:1. During descent the field is changing about 100 gamma/km. Descent magnetic field measurements are valuable to assess the existence of coupling between the magnetic field and the atmosphere.
REFERENCES:	NASA SP-3028 Instruments and Spacecraft

TABLE 3-18

ION MASS SPECTROMETER

WEIGHT:	3 lb.
POWER:	1 w
VOLUME:	80 (2.5 x 4 x 8) in^3
SAMPLING RATE:	2 sec (for last minute prior to blackout)
BIT/SAMPLE:	180 bit/scan
INTEGRATION:	One unit since operation is required prior to entry, instrument can be mounted to hypersonic configuration. Entrance port should be roughly parallel to velocity vector.
USAGE:	All dayside and nightside science payloads, for one minute prior to probe entry.
DESCRIPTION:	Could also provide data within regime from periapsis passage to entry. Instrument should scan from 1 to 20 m/e. Almost without exception, the only data will be for m/e 1 to 4. At the very base of the exosphere some contribution from CH_4 and N_e may be seen from m/e 12 to 20, and traces of HeH^+ may be present under some conditions.
REFERENCE:	Science Criteria for Jupiter Entry Missions, Statement of Work, JPL Contract No. 952897, 1970 July 1.

TABLE 3-19

TURBULENCE INDICATOR

WEIGHT: 2.0 lb.

POWER: 2 w

VOLUME: 10 (2 x 2 x 2) in^3

SAMPLING RATE: 1 sample/km

BIT/SAMPLE: 18

INTEGRATION: One accelerometer unit located within payload con-
                  tinaer, and with sensitive axis along probe longitudinal
                  axis.

DESCRIPTION: Turbulent structure is determined by measuring the
                  vertical component of acceleration. This vertical
                  acceleration during descent is caused by small scale
                  updrafts and downdrafts and can be used to determine
                  the gustiness or turbulence of the atmosphere. Data
                  processor provides magnitude/frequency rms output
                  per km of descent.

REFERENCES: Bell Aerosystems DVM VII

TABLE 3-20

SCIENCE PAYLOAD CHARACTERISTICS

PAYLOAD CHARACTERISTIC	JPL BASELINE	SMALL	NOMINAL		EXPANDED	
			DAYSIDE	NIGHTSIDE	DAYSIDE	NIGHTSIDE
WEIGHT, LB	19	16	43	45	56	47
POWER, W	18	15	34	36	48	46
VOLUME, IN^3	485	450	1321	1379	1767	1449
TOTAL BITS	45,000*	5200	27,700	25,900	43,000	38,600

* TO 1000 BARS

temperature and pressure is sampled once every 300 m of descent to a
pressure of 1000 atm, whereas in the Avco payloads the temperature and
pressure is sampled once every kilometer to a pressure of 17 atm.

3.6 SCIENCE EFFECTIVENESS

A qualitative assessment was made of the five science payloads. The results
of these assessments are shown in Tables 3-21 to 3-25. These tables show
the ability of the instrument to provide data for achievement of a particular
science objective. Both direct and indirect measurement of a science
objective by a particular instrument is indicated. The payloads can be
compared by summation of direct and indirect measurements available for
each science objective.

A qualitative comparison of the payloads is shown in Table 3-26. Note that
there does not appear to be a great difference between a nominal dayside
science mission and an expanded nightside mission. This has resulted in
part due to the approach taken. Instruments that are added to an expanded
payload must provide functional redundancy. For example, block redundancy
could be considered, and more than one instrument of each type could be
included in the payload. This block redundancy approach was not pursued
because it did not contribute to the solution of ambiguities, although the
approach would increase the numerical value in Table 3-26 for example,
two GC/MS instruments could be counted as two direct measurements. It
was difficult to find additional simple experiments for the expanded payload.
For example, it would be valuable to find an instrument for the expanded
nightside science payload that would replace the solar sensing photometers
in measuring the vertical distribution of CH_4, NH_3, H_2O, and H_2S. An
ultraviolet absorption spectroscopic instrument could provide this distribu-
tion. It would entail incorporation of a continuous ultraviolet source, a
long-path cell of the order of one meter and an appropriate detector. Such
an instrument would satisfy the requirement of functional redundancy, but
would probably be difficult to integrate into the Jupiter probe payload
container.

3.7 INFLUENCE OF MISSION PROFILE FAILURE MODES ON SCIENCE RETURN

From a failure mode point of view, the most critical part of the flight
regime of a Jupiter entry probe is the atmospheric entry with the attendant
simultaneous severe heating and inertial loading. Immediately prior to
entry, the probe has survived a 450 to 1450 day flight in a reasonably well

TABLE 3-21

INSTRUMENT SELECTION FOR ACHIEVEMENT OF SCIENCE OBJECTIVES

NOMINAL SCIENCE/DAYSIDE DESCENT PAYLOAD

INSTRUMENT \ SCIENCE OBJECTIVE	ABUN-DANCE	STRUC-TURE	CLOUDS	ORGANIC MATTER	COLORING MATTER
ION MASS SPECTROMETER	D	I	I	I	I
NEUTRAL PART. MASS SPEC.	D	I	D	D	D
GAS CHROMATOGRAPH	D	I	D	D	D
UV PHOTOMETER	D	D	I	I	I
H₂O PHOTOMETER	D	I	I	I	I
AEROSOL PHOTOMETER	I	I	D	I	I
ACCELEROMETERS	I	D	I	I	I
PRESSURE TRANSDUCERS	I	D	I	I	I
TEMPERATURE GAUGES	I	D	D	I	I
IR DETECTOR	I	D	I	I	I
MICROWAVE RADIOMETER	I	D	I	I	I
OPTICAL FLASH DETECTOR	I	I	I	D	D
R. F. CLICK DETECTOR	I	I	I	D	D
MAGNETOMETER	METEOROLOGICAL IMPORTANCE				
TURBULENCE INDICATOR					

D ~ DIRECT MEASUREMENT

I ~ INDIRECT MEASUREMENT

TABLE 3-22

INSTRUMENT SELECTION FOR ACHIEVEMENT OF SCIENCE OBJECTIVES

NOMINAL SCIENCE/NIGHTSIDE DESCENT PAYLOAD

SCIENCE OBJECTIVE / INSTRUMENT	ABUN-DANCE	STRUC-TURE	CLOUDS	ORGANIC MATTER	COLORING MATTER
ION MASS SPECTROMETER	D	I	I	I	I
NEUTRAL PART. MASS SPEC.	D	I	D	D	D
GAS CHROMATOGRAPH	D	I	D	D	D
NEPHELOMETER	I	I	D	I	I
ACCELEROMETERS	I	D	I	I	I
PRESSURE TRANSDUCERS	I	D	I	I	I
TEMPERATURE GAUGES	I	D	D	I	I
IR DETECTOR	I	D	I	I	I
MICROWAVE RADIOMETER	I	D	I	I	I
OPTICAL FLASH DETECTOR	I	I	I	D	D
R.F. CLICK DETECTOR	I	I	I	D	D
MAGNETOMETER	METEOROLOGICAL IMPORTANCE				
TURBULENCE INDICATOR					

D ~ DIRECT MEASUREMENT

I ~ INDIRECT MEASUREMENT

TABLE 3-23

INSTRUMENT SELECTION FOR ACHIEVEMENT OF SCIENCE OBJECTIVES

EXPANDED SCIENCE/DAYSIDE DESCENT PAYLOAD

SCIENCE OBJECTIVE / INSTRUMENT	ABUN-DANCE	STRUC-TURE	CLOUDS	ORGANIC MATTER	COLORING MATTER
ION MASS SPECTROMETER	D	-	-	-	-
NEUTRAL PART. MASS SPEC.	D	-	D	D	D
GAS CHROMATOGRAPH PKG.	D	-	D	D	D
UV SPECTROMETER	D	D	I	I	I
CONDENSIMETER-EVAP.	-	I	D	I	-
H₂O PHOTOMETER	D	-	-	-	-
AEROSOL PHOTOMETER	-	-	D	-	-
ACCELEROMETERS	-	D	-	-	-
PRESSURE TRANSDUCERS	-	D	-	-	-
TEMPERATURE GAUGES	-	D	D	-	-
IR DETECTOR	-	D	-	-	-
MICROWAVE RADIOMETER	-	D	-	-	-
OPTICAL FLASH DETECTOR	-	-	-	D	D
R. F. CLICK DETECTOR	-	-	-	D	D
MAGNETOMETER	METEOROLOGICAL IMPORTANCE				
TURBULENCE INDICATOR					

D ～ DIRECT MEASUREMENT
I ～ INDIRECT MEASUREMENT

TABLE 3-24

INSTRUMENT SELECTION FOR ACHIEVEMENT OF SCIENCE OBJECTIVES

EXPANDED SCIENCE/NIGHTSIDE DESCENT PAYLOAD

SCIENCE OBJECTIVE / INSTRUMENT	ABUN-DANCE	STRUC-TURE	CLOUDS	ORGANIC MATTER	COLORING MATTER
ION MASS SPECTROMETER	D	I	I	I	I
NEUTRAL PART. MASS SPEC.	D	I	D	D	D
GAS CHROMATOGRAPH PKG.	D	I	D	D	D
CONDENSIMETER-EVAP.	I	I	D	I	I
NEPHELOMETER	I	I	D	I	I
ACCELEROMETERS	I	D	I	I	I
PRESSURE TRANSDUCERS	I	D	I	I	I
TEMPERATURE GAUGES	I	D	D	I	I
IR DETECTOR	I	D	I	I	I
MICROWAVE RADIOMETER	I	D	I	I	I
OPTICAL FLASH DETECTOR	I	I	I	D	D
R. F. CLICK DETECTOR	I	I	I	D	D
MAGNETOMETER	METEOROLOGICAL IMPORTANCE				
TURBULENCE INDICATOR					

D ~ DIRECT MEASUREMENT

I ~ INDIRECT MEASUREMENT

TABLE 3-25

INSTRUMENT SELECTION FOR ACHIEVEMENT OF SCIENCE OBJECTIVES

SMALL SCIENCE/DAYSIDE AND NIGHTSIDE DESCENT PAYLOAD

SCIENCE OBJECTIVE / INSTRUMENT	ABUN-DANCE	STRUC-TURE	CLOUDS	ORGANIC MATTER	COLORING MATTER
ION MASS SPECTROMETER	D	-	-	-	-
NEUTRAL PART. MASS SPEC.	D	I	D	D	D
GAS CHROMATOGRAPH	D	I	D	D	D
PRESSURE TRANSDUCERS	-	D	I	-	-
TEMPERATURE GAUGES	-	D	D	-	-

D ~ DIRECT MEASUREMENT

I ~ INDIRECT MEASUREMENT

TABLE 3-26

QUALITATIVE COMPARISON OF PAYLOADS TO ACHIEVE
SCIENCE OBJECTIVES

PAYLOAD SCIENCE OBJECTIVE	ABUNDANCE	STRUCTURE	CLOUDS	ORGANIC MATTER	COLORING MATTER
NOMINAL DAYSIDE	5 D	6 D	4 D	4 D	4 D
	-	3 I	4 I	1 I	1 I
NOMINAL NIGHTSIDE	3 D	5 D	4 D	4 D	4 D
	-	3 I	3 I	-	-
EXPANDED DAYSIDE	5 D	6 D	5 D	4 D	4 D
	-	4 I	4 I	1 I	1 I
EXPANDED NIGHTSIDE	3 D	5 D	5 D	4 D	4 D
	-	4 I	3 I	-	-
SMALL	3 D	2 D	3 D	2 D	2 D
	-	1 I	1 I	-	-

D - DIRECT MEASUREMENT

I - INDIRECT MEASUREMENT

defined environment except for the meteoroid hazard, and is in close proximity to the top of the atmosphere. It would be valuable to record and transmit unique upper atmosphere data immediately prior to entry. The ion mass spectrometer has been included in all science payloads, because the data output will permit the assessment of the composition of atmospheric gases in the Jovian exosphere. By extending the inlet port of the ion mass spectrometer beyond the heat shield it probably is possible to make an uncontaminated measurement during the initial heating phase. Communication blackout will probably occur before inlet port burnup, and the hydrogen to helium ratio data must be stored for subsequent playout after emergence from blackout.

This upper atmospheric measurement is most valuable if the probe can descend to, make a measurement, and transmit below the turbopause. The turbopause is the region that marks the interface between turbulent mixing of the atmospheric constituents and diffusive separation of the constituent gases. The hydrogen to helium ratio measured below the turbopause can be presumed to exist to great depths within the atmosphere. For a Jupiter entry probe mission, it was determined that S-band is mandatory for a direct communication link, and that L-band for a relay link with a Pioneer F/G, and S-band for a relay link with TOPS yields the greatest performance. For the relay link the frequency selection is strongly influenced by the large change in probe to spacecraft communication angles during the one-hour descent. Consideration of X-band relay link operation yielded poorer performance for the Jupiter probe relay communication link. However, study of a turbopause mission (Reference 11) has indicated that high frequency of operation like X-band or K-band is required to avoid entry probe communication blackout and transmission of composition ratio prior to entry. A turbopause relay communication link can consider use of higher frequencies due to the fact that the mission is over in about 10 sec, and the probe and spacecraft (for the mandatory relay link) can be considered as fixed in space. It is concluded that the relay link frequency for an efficient turbopause probe mission is not compatible with the relay link frequency for an efficient entry probe mission. Dual transmitter and antenna subsystems is one obvious design approach.

If the probe survives entry, and is extracted by the parachute from the hypersonic configuration, then it must descend into an atmosphere in which the temperature and pressure is increasing, and in which there could be significant turbulence. From a failure mode point of view, high data rates are valuable in that the data storage is kept to a minimum. For this phase of the mission, data rates that permit real time transmission of data is

desirable. The only data that must be stored is the last one minute of output from the ion mass spectrometer prior to entry, and the outputs of the accelerometers that are generated during entry probe deceleration.

3.8 REFERENCES

1. Science Criteria for Jupiter Entry Missions, Statement of Work, JPL Contract No. 952897, 1970 July 1.

2. JPL Interoffice Memo 2947-617, Jupiter Model Atmospheres by Neil Devine, 1970 May 8.

3. J. S. Lewis and R. G. Prinn, Science, 169, 472, (1970).

4. F. C. Gillett, F. J. Low, and W. A. Stein, Astrophys. J., 157, 925, (1969).

5. J. A. Westphal, Astrophys. J. 159, L63 (1969).

6. J. R. McNesby, J. Atmos. Sci. 26, 59 (1969).

7. D. M. Hunter, J. Atmos. Sci. 26, 826 (1969).

8. D. F. Strobel, J. Atmos. Sci. 26, 906 (1969).

9. R. G. Prinn, Icarus in press (1970).

10. J. S. Lewis and R. G. Prinn, "Chemistry and Photochemistry of the Atmosphere of Jupiter" to appear in Theory and Experiment in Exobiology, A. W. Schwartz, ed. (1970).

11. The Jovian Turbopause Probe, Part II, an analysis of critical problems associated with the feasibility of a Jovian Turbopause Probe, George M. Levin, GSFC X-110-70-443, December 1970.

4.0 ENGINEERING EXPERIMENT SELECTION

There exists a quandary in the design of a first atmospheric entry probe mission. The science objectives of the mission, if met, will result in knowledge about the physical characteristics of the planet, but the knowledge of these physical characteristics are necessary for the design of the entry probe. In addition, knowledge of the physical characteristics is important in the specification of the dynamic measurement range for the scientific instrumentation. The approach to the problem has been, and is for this study, to choose a range of environments, and base the design of all systems and subsystems on this range. There exists two limiting approaches that have conflicting program aspects. The first extreme approach is to choose a narrow range of possible environments. This approach tends to 1) maximize the scientific payload that can be carried, 2) increase the risk of the effects of environmental uncertainties on probe survival, and 3) minimize the allocation of resources necessary to develop entry probe systems and subsystems. The second and diametrically opposed extreme approach is to choose a wide range of possible environments. This approach tends to 1) minimize the scientific payload that can be carried, 2) decrease the risk of the effects of environmental uncertainties on probe survival, and 3) maximize the allocation of the resources necessary to develop entry probe system and subsystems.

It is obvious that neither limiting approach is pursued, but that a compromise approach is selected that trades off the achievement of the science objectives with an acceptable value of entry probe survival. A possible criteria for measurement of mission success (which includes achievement of science objectives and entry probe survival) is the value of the returned data in the improvement of the design of a subsequent mission.

This criteria could be used to trade off the science objectives with entry probe survival objectives. It is possible to conceive of an instrument complement for a first entry probe mission that is designed to provide engineering support data for future missions. This data would, of course, also be of scientific value.

The identification of engineering experiments for this first mission to support subsequent missions is considered to be as important as the selection of the scientific instrumentation. A set of engineering experiments can be defined by first determining the critical engineering subsystems and the physical characteristics of Jupiter that will influence their performance.

4-1

This identification of physical characteristics that influence the performance of engineering subsystems is then matched against the data that will be returned by the science payload. The difference between the physical data needed for engineering development, and the physical data needed to satisfy the science objectives represents the additional data that must be returned to support the development of entry probes for subsequent missions. In the following sections, the engineering instruments necessary to reduce risk and enhance performance of later entry probe missions, have been catagorized according to entry probe flight regime.

4.1 FLYBY FLIGHT REGIME

For a relay communication link mission the decimeter radiation from Jupiter is important. The relay link antenna which is on board the spacecraft is directed towards Jupiter, and the decimeter radiation fills the antenna beamwidth. For a direct communication link mission, the DSN antenna is also directed towards Jupiter, but the planet and the decimeter radiation covers only a small fraction of the total beamwidth of the antenna. Based on the science objectives of Section 1.2, the decimeter radiation will not be measured by the entry probe. There is a possibility that a microwave radiation experiment could be included in spacecraft science payload.

The non thermal RF noise emission from the Jovian radiation belts (see description of environment Section 2.2) cause a severe restriction in the design of a relay link receiving system by: 1) limiting the lowest frequency of link operation to L-band, and 2) degrading link performance up through X-band frequencies by raising the level of the noise threshold. The impact of this environmental effect is shown in Figure 4-1. Note that X-band operating frequency is the zero point of the comparison. It can be seen that as the telemetry operating frequency decreases, the systems losses due to decimeter radiation increase. This factor is the single most important consideration in restricting relay link frequencies for the entry probe mission to 1 GHz or lower.

The instrumentation requirements to monitor the levels of decimeter radiation about the planet are centered about four areas; these are: 1) antenna system, 2) RF spectrum analyzer, 3) signal scanning and classification, and 4) data processing techniques.

Antenna system concepts to provide wide bandwidth capability might include one or more specific frequency band elements, wide-band log periodic types, or other frequency scanning techniques.

FIGURE 4-1

FIGURE 4-1

Effect of Decimeter Radiation on Receiving System
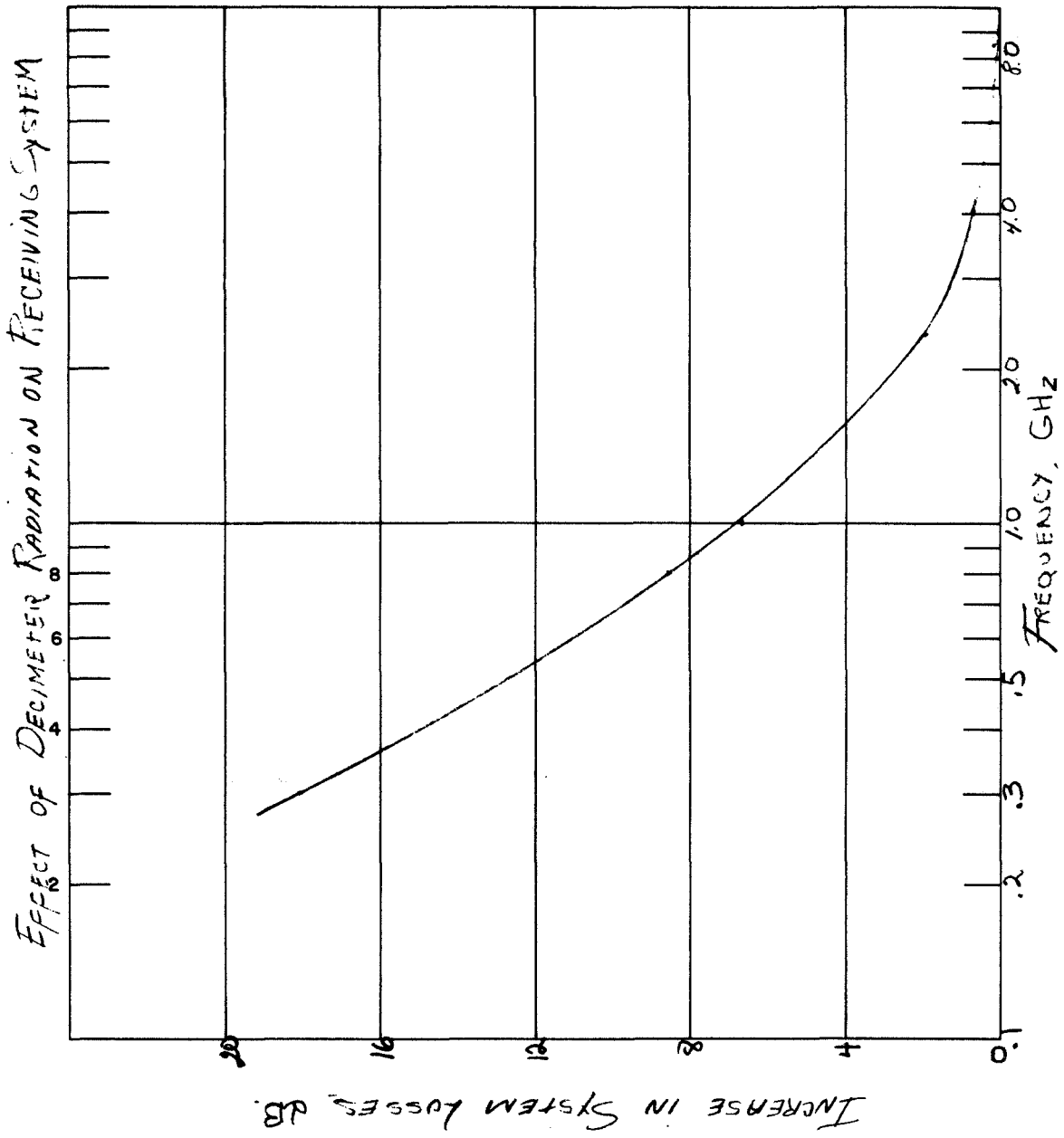
The spectrum analyzer requirements and performance will be based on the RF spectrum measurement range, the decimeter radiation signal levels, and receiver noise bandwidths.

Signal scanning techniques and classification can probably be integrated with existing TOPS or Pioneer F/G instrumentation that must be provided for orientation of other electromagnetic sensors. The data could also be keyed to the spacecraft range code for timing and classification purposes.

To minimize data storage and spacecraft link transmission requirements, the on board processing of the measured data could be performed by data compression techniques such as: a) adaptive sampling, b) redundancy data reduction, and c) parameter keyed sampling. Techniques to classify the characteristic nature of the environment effect would be the prime consideration in any data processing scheme. A sample block diagram of the experiment to obtain data on the decimeter radiation is indicated in Figure 4-2.

FIGURE 4-2

BLOCK DIAGRAM OF DECIMETER NOISE MEASUREMENT EXPERIMENT
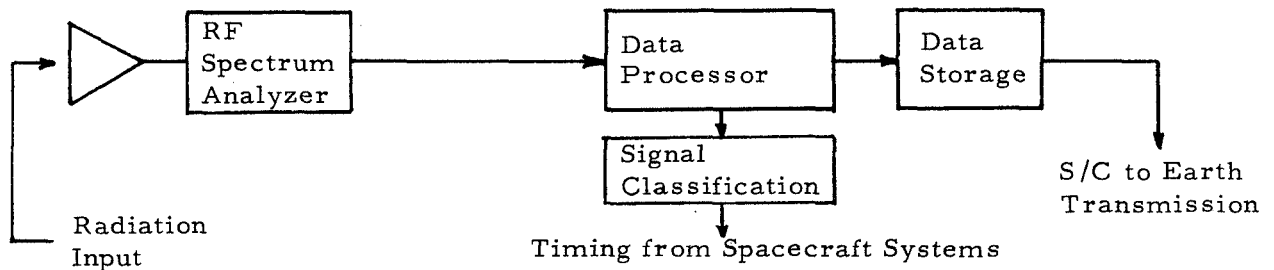
4.2 POST SEPARATION FLIGHT REGIME

Following separation from the spacecraft the entry probe will be exposed to an environment like that experienced by the spacecraft, i.e., solar flux, cosmic radiation, solar proton flux, and interplanetary meteoroids. The solar flux is well defined, and the cosmic radiation, and solar proton flux are not expected to create any design problems. As the entry probe approaches Jupiter the post separation environment is altered and near-Jovian meteoroids, charged particle radiation, and magnetic fields become

important. The exoatmospheric flight regime that extends from the periapsis passing distance of the spacecraft to the top of the Jovian atmosphere represents a science measurement gap. Measurement of the meteoroid flux, charged radiation flux, and magnetic field strength in this regime is of scientific value, and also of engineering value. Passage through the cis - Jovian environment will offer a unique opportunity to conduct direct measurements. Direct measurement of these environments are not possible by observation from Earth. Estimates can only be inferred from other phenomena. The influence of the meteoroid flux charged radiation flux, and magnetic field strength on entry probe design is reported in Sections 2. 1, 2. 4, and 2. 3 respectively.

The main problem connected with addition of instruments that must operate in this flight regime is the provision of power for the instruments, as well as power for the communication and data handling subsystems. During the 30 to 60 day post separation flight the entry probe has limited power capability. The addition of instruments are the need for telemetry of data impose greater requirements, and a simple entry probe tends to become more complex.

Charged particle detectors and meteoroid detectors are well understood types of instrumentation that will probably be part of the spacecraft science payload. These detectors can be modified if necessary for use on board an entry probe. A magnetometer was added to the nominal and expanded science payloads, and its characteristics are reported in Table 3-17.

It has been pointed out that the addition of engineering experiments can provide useful design information for subsequent missions. There is a corollary to this point. Incorporation of environmental sensors can also help in the understanding of a subsystem failure. For example, if the level of charged particle radiation is observed to increase continuously and precipitously and if a malfunction occurs, it becomes possible to deduce the cause of the malfunction.

4. 3 HYPERSONIC ENTRY FLIGHT REGIME

Entry at 49 Km/sec is the outstanding feasibility question for the Jupiter entry probe mission. The instrumentation that is carried to support the science mission will provide all the data needed to describe the physical environment in which the entry probe is being retarded. The ion mass spectrometer can provide the composition and scale height in the vicinity of the turbopause; the triad of accelerometers can be used to infer the scale

height and density where the probe is decelerating; and the gas chromato-graph neutral particle mass spectrometer, and temperature, and pressure measurements will provide the mass composition and structure of the atmosphere immediately below the hypersonic flight regime.

It would appear then that there is not any need for further instrumentation. However, since the problem of simultaneous simulation of the convective heating environment, radiative heating environment, and pressure loads are impractical in ground based facilities, and can only be approximated in an earth entry flight test (due to differences in atmospheric composition), it is of great practical value to instrument the entry probe so that the performance of the heat shield can be evaluated. During the period of atmospheric retardation (about 75 sec for shallow angle entry) the probe will be enveloped in a plasma of electrons that have been created by the intense heating of the atmospheric gases. Real time communication from instrumentation will not be possible, and so data storage with transmission following emergence from blackout will be mandatory. Thus, if failure should occur, the only conclusion that can be drawn is that the heat shield subsystem (or aeroshell structure subsystem with less likelihood) was under designed. If the entry probe survives, then valuable design data can be obtained.

Two types of instrumentation are valuable for this regime of operation. The first type measures the thermal performance of the heat shield material and would include ablation sensors, and thermocouples that would be imbedded in the heat shield. The second type measures the entry probe dynamics and would give some indication of the symmetry with which the heat shield was removed, and would include a minimum of one rate gyro to record the spin history or three rate gyros to record induced body rates about all entry probe axes. Due to the severity of the heating environment, radiometers to measure preselected spectra would not be recommended. Such devices would require holes through the heat shield for emplacement of windows. The problem of window and seal survival seems like an unreasonable additional complexity to an existing difficult design problem.

4.4 SUBSONIC DESCENT FLIGHT REGIME

During subsonic descent the principal uncertainty in the system perform-ance is associated with the communication subsystem. The environmental factors that are associated with the design of the communication link are: 1) the attenuation of the RF signal by the constituent gases and cloud layers,

2) the dynamic motions of the entry probe that result from atmospheric turbulence, and lead to the requirement for an increase in the beamwidth of the entry probe antenna, and 3) the turbulence induced fluctuations in refractive index of the atmosphere; these fluctuations are spatially inhomogeneous and will result in the scattering of RF energy and lead to signal fading and attenuation.

Another important subsystem that is influenced by the environment is the payload container which is an insulated-pressure vessel that isolates the payload from the increasing temperature and pressure associated with descent into the Jovian atmosphere. The environmental factors that influence the design of the payload container subsystem are the temperature, pressure, and composition of the atmosphere.

The instrumentation that has been proposed to satisfy the science objectives of this entry probe mission will also yield the environmental information needed to enhance the engineering design of the atmospheric attenuation contribution to the telecommunications loss stack-up, and also the information needed for the design of the payload container.

The simulation of the environment in which the payload container is immersed can be accomplished in Earth based test facilities. At present a combined pressure and thermal facility in which to test a payload container is not available. This is due to the lack of requirements of other technology programs, rather than a test facility feasibility problem. During descent, however, it would be of value to instrument the pressure vessel with strain gauges and the insulation system with thermocouples to record the actual performance and compare with predicted performance.

The dynamic motions of the probe induced by turbulence can be inferred by the addition of a turbulence indicator. This turbulence indicator is a longitudinal accelerometer which is used to measure the local up-drafts and down-drafts which should correlate with local wind shears and wind gusts. A turbulence indicator was included in the nominal and expanded science payload packages, and is reported in Table 3-19. Dynamic motions caused by the local turbulence can be observed directly by the addition of a rate gyro package(s). The rate gyro package that is used during hypersonic descent might also serve as the rate measuring instrument for subsonic descent. The main problem with dual function is the design of a sensor that is sufficiently rugged and sensitive to satisfy the design requirements of two significantly different environments.

There also exist a class of engineering experiments that are of value in providing status reports on the various subsystems that comprise the entry probe system. These sensors are simple and measure: local temperature at various locations about the entry probe, the internal pressure of the payload container, and voltages of various instruments and components. This data does not necessarily provide information about the physical environment in which the probe is immersed, but does provide data on the performance of the subsystems. In the event of a malfunction, the availability of these status reports would be invaluable in understanding the cause of the malfunction and its influence on subsequent performance.

5.0 MISSION PERFORMANCE BOUNDARIES

A total of nine key mission tradeoffs have been identified. These include:
1) science payload, 2) probe targeting, 3) model atmosphere, 4) depth of
atmospheric descent, 5) launch opportunity, 6) interplanetary trajectory,
7) probe entry angle, 8) communication link, and 9) spacecraft. This
section provides a description of the important interactions between these
key tradeoffs. The resulting mission performance boundaries and penalties
have been grouped into three categories: a) entry probe/spacecraft system
and subsystem design, b) Earth departure and Jupiter arrival charcateristics
of transfer trajectories, and c) communication performance. These
boundaries are presented in Sections 5.1, 5.2, and 5.3 respectively.

5.1 DESIGN PERFORMANCE BOUNDARIES

This section describes the boundaries imposed by entry angle, model
atmosphere, science payload size, depth of atmospheric descent, and
spacecraft selection. Descent time through the atmosphere was not key
tradeoff area for this study. However, also included in this section is a
brief discussion of the descent times used and the reason for selection.

5.1.1 Influence of Entry Angle on Entry Probe Design

The flight path angle at entry has a direct influence on the entry probe weight.
Entry probe weight increases quite rapidly as the entry angle is increased.
In Figure 5-1, there is shown the variation of entry probe weight with flight
path angle. It has been assumed that the science payload, and electrical
supporting subsystem weights are independent of entry angle. This
assumption is based on the following argument. As the G-load increases,
the stresses within the many elements comprising the subsystem also
increase. These stresses can be reduced by providing more structural
material which will result in an increase in weight of the elements, or by
miniaturization which tends to reduce the mass of material that must be
supported, and hence the weight of the elements. Reduction of the character-
istic dimension of the element in the direction of the deceleration diminishes
the stress, and the structural fraction of the weight. The technology con-
tinually moves towards greater miniaturization. From Figure 5-1, it can
be seen that the aeroshell structure and heat shield subsystem weights
represent about 43% of the total entry weight at -15 deg entry angle and this
grows to 64% for a -45 deg entry angle. The heat shield weight increases
from 119 lb at the shallow angle to 235 lb at the steep angle while the aero-

FIGURE 5-1

PROBE SEPARATION WEIGHT

NOMINAL PAYLOAD
NOMINAL ATMOSPHERE
DESCENT TO BASE
OF CLOUDS

HEAT
SHIELD

AEROSHELL

AUXILARY STRUCTURE

SEPARATION

ENVIRONMENTAL

ELECTRICAL

SCIENCE

SUBSYSTEM WEIGHT −LB

RELATIVE FLIGHT PATH ANGLE AT ENTRY −DEG

31−0123

5−2
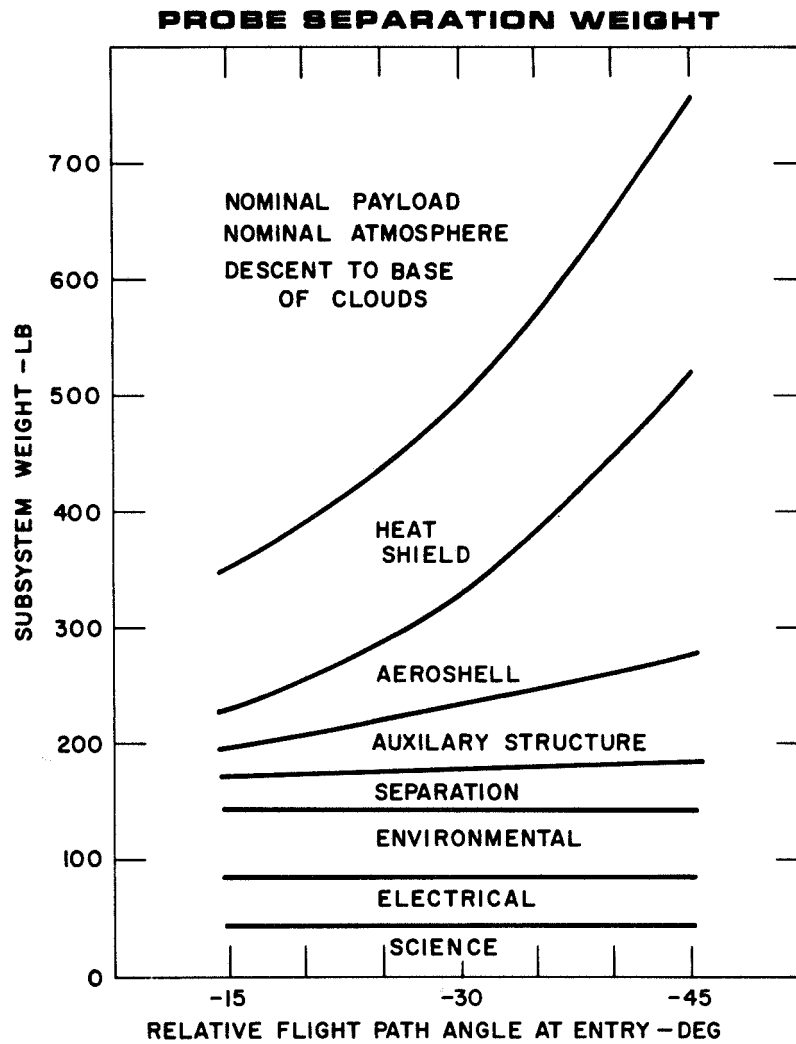
shell structural weight grows from 32 lb to 239 lb. Note that the weight data presented in Figure 5-1 is based on packaging of the nominal payload into a spherical payload container, and designing the probe, based on entry into the nominal model atmosphere, and descent to the base of the ammonium chloride clouds. It was determined that the resulting spherical payload container could be packaged into a 4 ft diameter, 60 deg blunt cone, and that static stability would be satisfied. This 4 ft diameter aeroshell was used in the calculation of all the aeroshell structure and heatshield subsystem weights. It was determined that based on the titanium honeycomb construction used for the aeroshell, that entry in the vicinity of -70 to -90 deg would not be feasible. At these high entry angles, the aeroshell structure weight is increasing at a faster rate than the weight that is available for structure. This phenonenon is based on the following argument.

The aeroshell structural weight can be approximated by:

$$W_{A/S} = K_1 D^3 \frac{M_E}{C_D A} \frac{\sin \gamma_E}{C} \tag{1}$$

where $W_{A/S}$ is the aeroshell structural weight

K_1 constant

D entry probe diameter

M_E entry probe mass

C_D drag coefficient

A drag area based on D

γ_E flight path angle at entry

C scale height of atmosphere

The mass of the entry probe can be expressed as:

$$M_E = M_{PAY} + M_{A/S} + M_{H/S} \tag{2}$$

5-3

where M_E is the mass of the entry probe

M_{PAY} is the mass of the payload; constant with entry angle

$M_{A/s}$ is the mass of the aeroshell structure

$M_{H/s}$ is the mass of the heat shield

Since the heat shield weight grows slowly with entry angle as compared with the aeroshell structure, it can be considered constant. The reason for this can be realized by combining equations (1) and (2) and yields:

$$W_{A/s} = K_2 \; \frac{\sin \gamma_E (M_{PAY} + M_{H/s})}{1 - K_2 \sin \gamma_E}$$

$$K_2 = \frac{K_1 g D^2}{C_D A_C}$$

(3)

When the term, $1 - K_2 \sin \gamma_E$ goes to zero, then aeroshell structure weight goes to infinity. This occurs somewhere between -70 to -90 deg entry angle. At slightly shallower entry angles, the entry probe weights are so great and the payload weight to entry weight ratio, so small, that the mission is undesirable. For this study, the entry angle was not allowed to exceed -50 deg.

The JPL supplied heat shield data (see Section 8.4) shows that the heat shield mass fraction, that is the weight of heat shield to weight of the entry probe increases as entry angle increases, and decreases as ballistic parameter increases. The net effect as indicated in Figure 5-1 is a slow growth of heat shield weight with entry angle due to the fact that the ballistic parameter of the entry probe is also growing with entry angle. Increasing ballistic parameter with entry angle is a result of holding the entry probe diameter constant. Note that in equation (1) that the aeroshell structural weight increases as ballistic parameter and entry angle increases.

Shallow entry angle is associated with reduced heating rates. The achievement of a heat shield environmental simulation for qualification test is more easily achieved in a ground test facility or flight test if the heating rates are low. Therefore, shallow entry angle is preferred because it results in a more benign environment. The G loads are lower, and this eases the

5-4

development and test of the subsystems; the heating rates are lower, and this eases the heat shield development problem. The aeroshell structural weight and heat shield weights are also lower and so result in a more favorable payload fraction.

5.1.2 Influence of Model Atmosphere on Entry Probe Design

Three model atmospheres were provided as a guideline for the mission study, and are termed the nominal model atmosphere, the cool/dense model atmosphere, and the warm/expanded model atmosphere. The temperature and pressure profiles and atmospheric constituents were used to construct cloud models. The cloud models are shown in Figure 5-2. It is important to note that the base of the cloud layers occurs at a pressure of 17 atm in the nominal model atmosphere. Therefore, the entry probe must survive to a relatively benign temperature of 425 deg K at 17 atm in comparison with descent to 1000 atm and a corresponding temperature of 1425 deg K. In the cool/dense model atmosphere the base of the clouds occur at a pressure of 525 atm and a pressure of 490 deg K in comparison to descent to 1000 atm where the temperature is 572 deg K. In the warm/expanded model atmosphere, the base of the clouds occur at a pressure of 3.5 atm and a temperature of 387 deg K whereas the temperature at the 1000 atm level is 3771 deg K. In the atmosphere with the higher temperature gradient, the condensation temperatures of different gases are reached within a narrower altitude interval; therefore, the cloud layers lie closer together. The cool/dense model atmosphere has the lowest lapse rate of the three models considered.

The influence of the model atmosphere on an entry probe packaged to contain the nominal dayside science payload is shown in Table 5-1. The maximum G loads indicated in the table are based on a shallow entry angle of -15 deg. It can be seen that the G loads are greatest for entry into the cool/dense model atmosphere. This is a direct result of the small scale height associated with the cool/dense model atmosphere. A small scale height results in entry probe deceleration over a short path length with the attendant large deceleration loads. As the model atmosphere varies from warm/expanded to nominal to cool/dense, the entry probe weight increases as a result of 1) increases in aeroshell structural weight and auxiliary structural weight due to decrease in scale height, and 2) increase in pressure vessel weight due to increased pressure at the cloud base. Note that the heat shield data as supplied by JPL does not distinguish between model atmospheres. For this study the heat shield weight is independent of the model atmosphere.

Figure 5-2

JUPITER CLOUD MODELS

COOL/DENSE   NOMINAL   WARM/EXPANDED
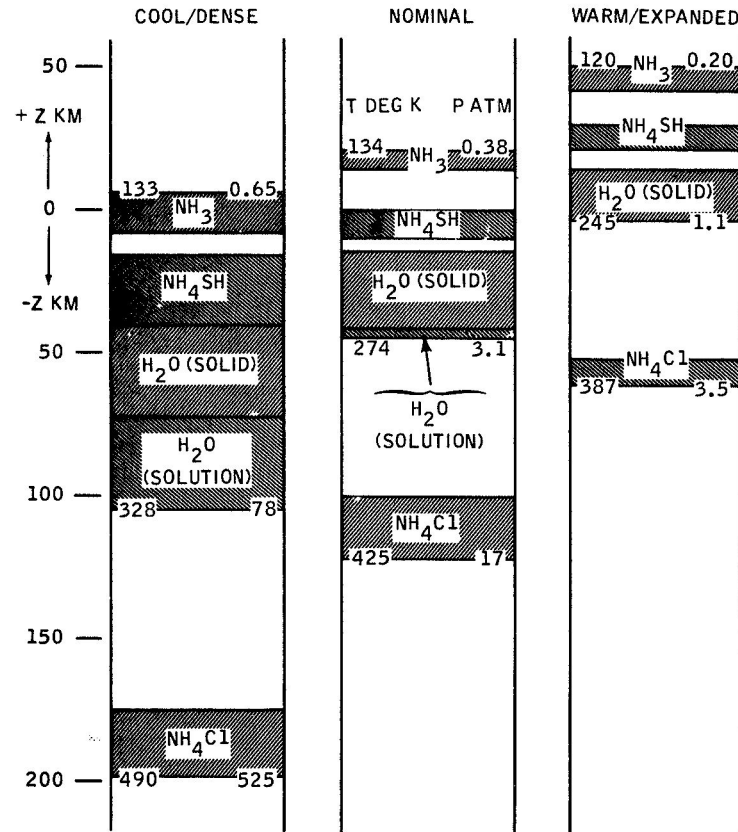
30-2159

Table 5-1

INFLUENCE OF ATMOSPHERIC MODEL
ON ENTRY PROBE DESIGN

RELAY LINK, SHALLOW ENTRY ANGLE, NOMINAL DAYSIDE PAYLOAD

ATMOSPHERE CHARACTERISTICS	COOL/DENSE	NOMINAL	WARM/ EXPANDED
MAXIMUM G	1250	525	260
PROBE ENTRY WEIGHT, LB	630	356	316
RELAY LINK FREQUENCY	UHF	S	S
TRANSMITTER OUTPUT POWER, W	32	25	16
TOTAL BITS	34,000	28,000	24,000

31-0113P

In the cool/dense model atmosphere, the telemetry frequency must be in the vicinity of UHF if R.F. transmission losses are not to be severe. Thus, direct communication link operation is precluded for entry into the cool/ dense model atmosphere (unless DSN can be modified to receive at this lower frequency) and a relay link mission must be considered. It was determined that at S-band, the R.F. losses associated with vertical propagation through the cool/dense model atmosphere is 55 dB; for the nominal, model atmosphere is 3 dB, and for the warm/expanded model atmosphere is 0.1 dB. The R.F. propagation losses from below the Jupiter cloud layers, have been assessed over a range of transmission frequencies from 10^8 to 10^{10} Hz. The results are shown plotted in Figure 5-3 for three model atmospheres. Loss composite profiles for vertical transmission shown in this figure are based on the sum of the following loss mechanisms: 1) ionospheric attenuation, 2) gaseous (NH_3, H_2O) absorption, 3) refractive losses (all gaseous constituents), and 4) cloud absorption and scattering. At the high frequencies the principal loss mechanism results from ammonia absorption, and at low frequency, from ionospheric attenuation, thus giving rise to a distinct minimum as shown in Figure 5-3.

The influence of the model atmosphere on the entry probe weight is shown in Figure 5-4. It can be seen that the weight penalty for entry and descent to the base of the clouds for an entry probe is strongly influenced by the model atmosphere over the range of entry angles. The weight differential between a probe designed to enter and descend to the base of the clouds in the cool/ dense model atmosphere and a probe designed to enter and descend to the base of the clouds in the nominal model atmosphere, increases as the entry angle increases.

It was determined that the warm/expanded model atmosphere does not provide any significant entry probe design constraint, and that the cool/dense model atmosphere sets the design requirements for most entry probe systems and subsystems.

5.1.3 Influence of Science Payload Size on Entry Probe Design

In Section 3.4, there is described the five payloads that have been assembled for this study. These payloads are the: nominal dayside science payload, nominal nightside science payload, expanded dayside science payload and small science payload. An increase or decrease in the weight, volume, and power requirements of the payload will cause a corresponding increase or decrease in the total separated probe weight. In Figure 5-5 there is presented the variation in probe separated weight with payload weight. The payload weight in Figure 5-5 is defined to be the sum of the science, cabling,

Figure 5-3

R.F. PROPAGATION LOSSES
FROM BOTTOM OF JUPITER CLOUDS

Figure 5-4

INFLUENCE OF ATMOSPHERE ON
PROBE SEPARATION WEIGHT

Figure 5-5

INFLUENCE OF PAYLOAD WEIGHT
ON PROBE SEPARATION WEIGHT
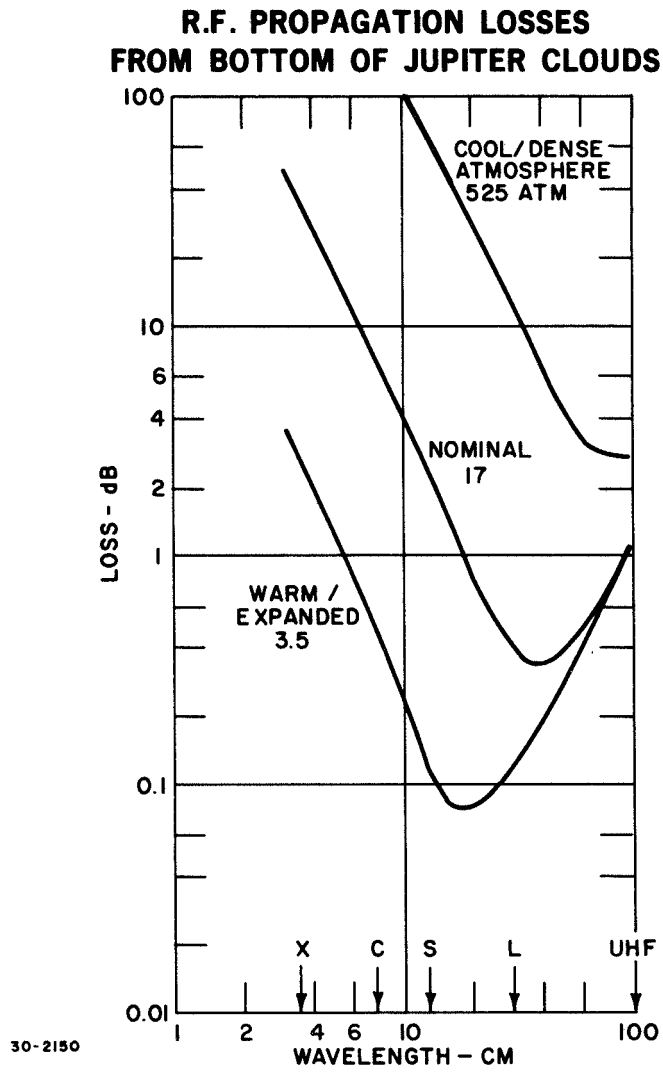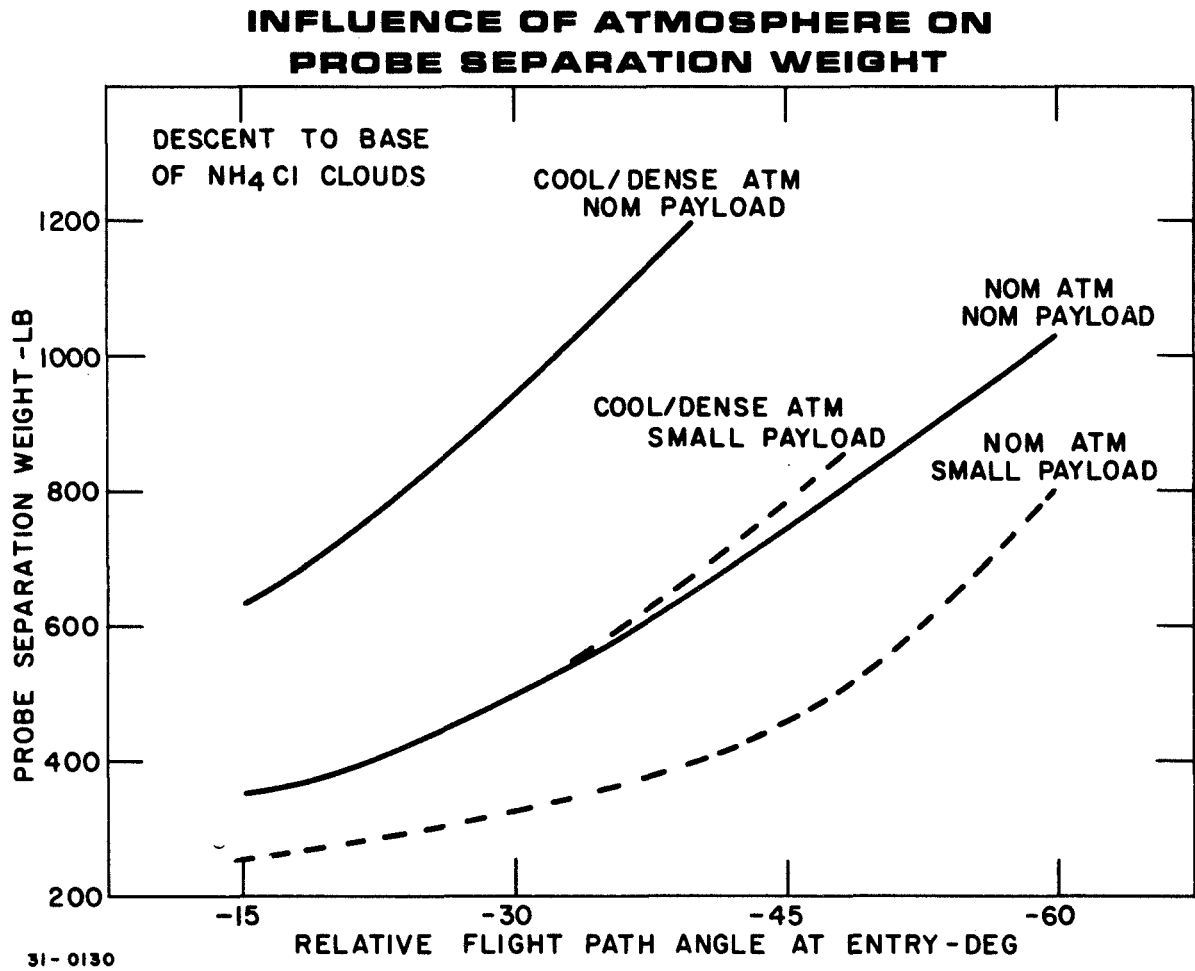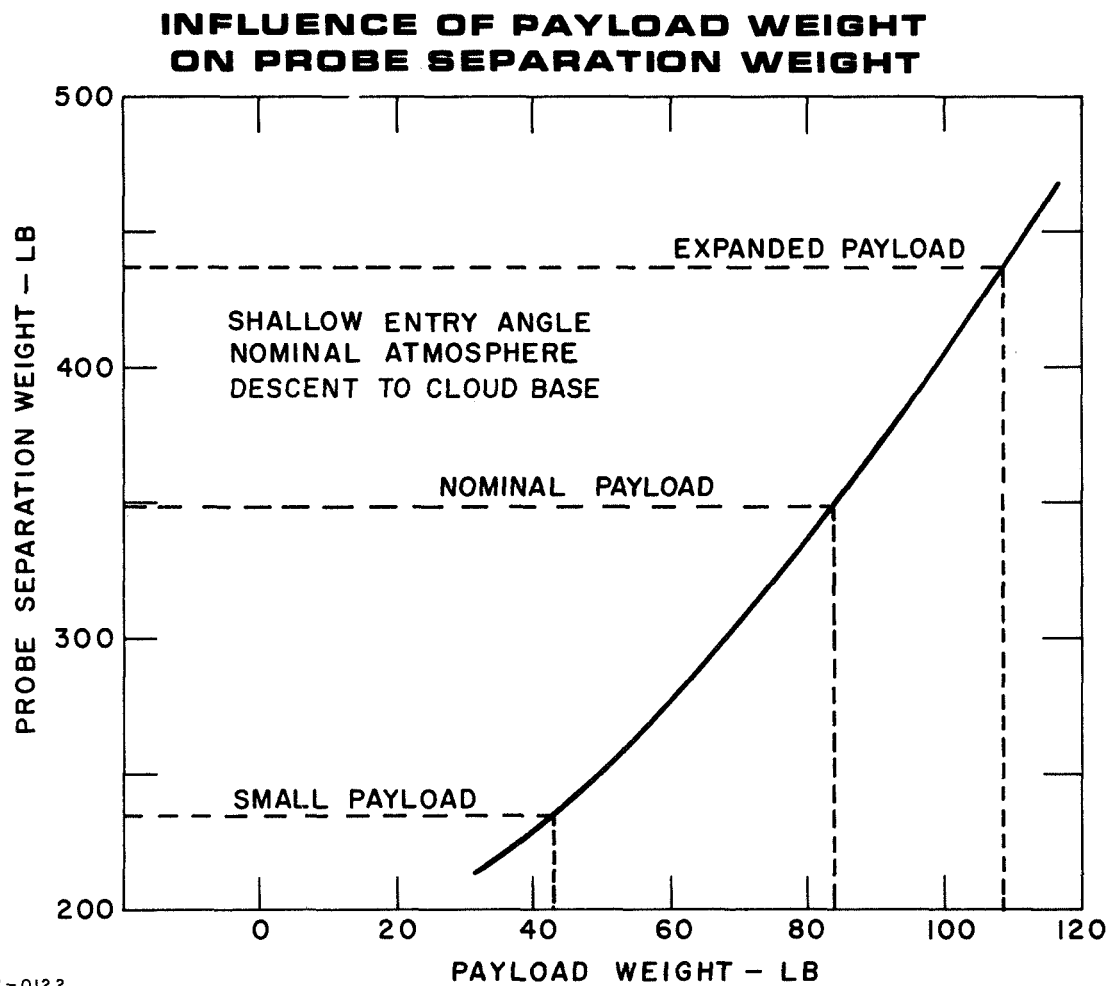
31-0122

programmer, data handling, communication, and power subsystems weights. This broader definition of payload weight in comparison to a narrower definition that is based solely on science payload provides a more realistic measure of the sensitivity of separated weight to changes in payload. For example, it is possible to alter the science payload by addition or substitution of an instrument and then alter the transmitter power or descent time (and power requirements) without changing the probe separation weight. There is a secondary effect, but small effect that arises through changes in the internal power profile, i. e. , a change in the thermal control subsystem requirement. This secondary effect is not accounted for.

From Figure 5-5, it can be shown that for every one pound change in payload weight the probe separation weight is changed by 3. 1 lb. A summary of the probe separated weight for the small, nominal dayside, and expanded dayside science payloads is provided in Table 5-2.

In Figure 5-4, there is also indicated the comparison between the small science payload and nominal dayside science payload missions as a function of the flight path angle, for entry into the nominal model atmosphere and cool/dense model atmosphere. It appears that the magnification factor of 3. 1 lb separated weight to payload weight will increase as the entry angle becomes steeper. The same trend holds for the cool/dense model atmosphere.

5. 1. 4 Influence of Depth of Atmospheric Descent on Entry Probe Design

The influence of depth of atmospheric descent on entry probe design was evaluated, and limited to consideration of only the cool/dense model atmosphere. A comparison was made between descent to the base of the water clouds and descent to the base of the cloud layers, i. e. , the ammonium chloride clouds. The water clouds were chosen because about ninety-eight percent of the total cloud mass lies above the base of the clouds, and descent to their base would allow for achievement of most of the science objectives. Descent to the base of the clouds, the ammonium chloride clouds would permit an unobstructed view of the lower atmosphere by the radiometers. It would be valuable if the brightness temperature of the lower atmosphere could be measured without the necessity of having to account for the influence of attenuation by this lowest layer.

A reduction in the depth of atmospheric descent does not influence the G loads experienced by the probe, and so does not directly influence the aeroshell structure and heat shield subsystems. Since the atmospheric tempera-

TABLE 5-2

SUMMARY WEIGHT BREAKDOWN OF PROBE SEPARATION WEIGHT[1]

Payload Subsystem	Small	Nominal	Expanded
Science	15 lb	42 lb	55 lb
Electrical[2]	28	35	54
Environmental[3]	45	71	75
Separation[4]	23	25	40
Auxiliary Structure	13	25	34
Aeroshell Structure	24	34	39
Heatshield	88	120	140
TOTAL	236 lb	352	437

1   Shallow entry angle (-15 deg), dayside science payload, nominal atmosphere, and descent to cloud base.

2   Includes communication, programming and data handling, cabling, and battery power subsystems.

3   Includes thermal control (& RTG), pressure vessel, and meteoroid container subsystems.

4 Includes separation, propulsion, and parachute subsystems.

ture and pressure is lower, if the depth of descent is reduced, then the pressure vessel weight and insulation weight requirements are also reduced. For the same aeroshell diameter, the entry probe ballistic parameter will be reduced as a result of the lower pressure vessel and insulation weights and so, in turn, result in a reduction of the aeroshell loads and subsequent aeroshell structural weight. The influence of depth of descent on entry probe separated weight is shown in Figure 5-6. It can be seen that the reduction in weight varies from 50 lb for shallow entry to about 100 lb for steep angle entry. A comparison with Figure 5-4 shows that the separated probe weight for descent to the base of the water clouds in the cool/dense model atmosphere is significantly greater than separated probe weight designed for entry into the nominal model atmosphere and descent to the base of the ammonium chloride clouds.

The R.F. attenuation loss for descent to the base of the water clouds and the base of the ammonium chloride clouds for the three model atmospheres is shown in Table 5-3. The increase in R.F. loss in the cool/dense model atmosphere is caused by the higher pressure at which the clouds are located. At the greater pressure there exists more ammonia, the principal absorber, along the communication line of sight. Note that the S-band R.F. loss in the cool/dense model atmosphere is reduced from a non-feasible 55 dB to a very large loss of 20 dB. For descent into the cool/dense model atmosphere, a lower radio frequency must be considered.

TABLE 5-3

R. F. LOSS FOR VERTICAL TRANSMISSION AT S-BAND

MODEL ATM LEVEL	COOL/DENSE	NOMINAL	WARM/EXPANDED
BASE OF WATER CLOUDS	20 dB	0.2	0
BASE OF AMMONIUM CHLORIDE CLOUDS	55 dB	3	0.1

If the cool/dense model atmosphere is realistic, then descent to the base of the water clouds can offer substantial reduction in design problems. If the nominal model atmosphere is realistic, then descent to the base of the cloud layers, the ammonium chloride cloud will not result in undue engineering design penalties

5.1.5 Selection of Entry Probe Descent Time

For all 1978 and 1980 relay communication link missions a descent time of one hour was chosen. Descent time is defined as the time from 0.7 Mach

Figure 5-6

INFLUENCE OF DEPTH OF DESCENT
ON PROBE SEPARATION WEIGHT
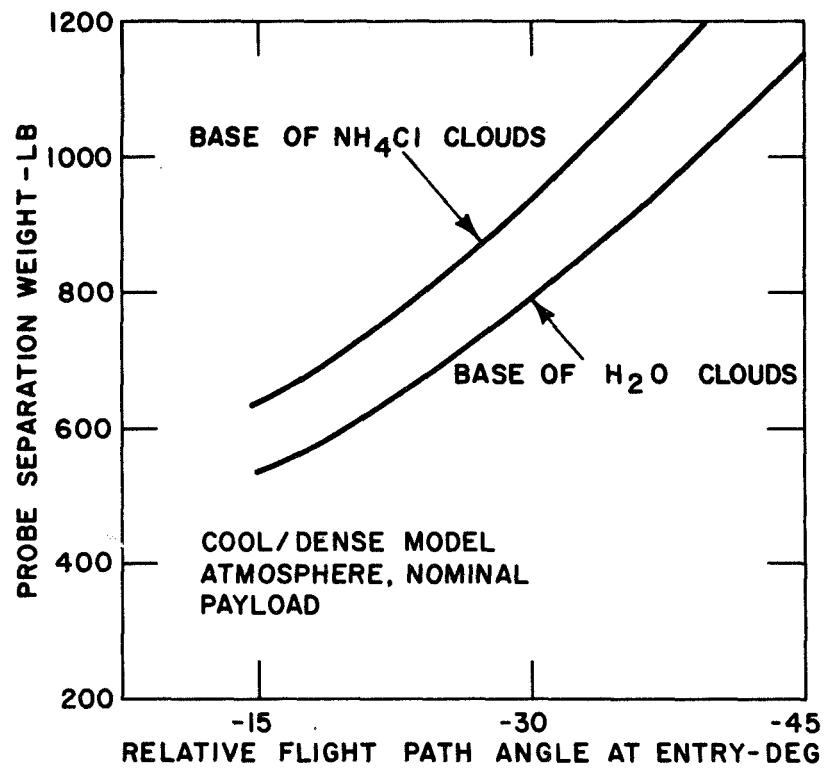
to the base of the clouds. The sampling requirements imposed by science
objectives and the instrument process time of the gas chromatograph served
to provide the minimum allowable descent time constraint. It is desirable
to conduct a gas chromatograph measurement above, within, and below each
cloud layer. There are nine such measurements required in the warm/
expanded and cool/dense model atmospheres, and ten measurements in the
nominal model atmosphere. A total sampling process time for a polar gas
through the gas chromatograph column is five minutes. This results in a
total absolute minimum descent time of 50 min., which was rounded off to
one hour. With a descent time of one hour it will be possible to playout all
of the gas chromatograph data (except the last measurement) before the
entry probe reaches the base of the clouds. The last measurement is
played out from below the base of the clouds. This approach will result in
a minimum data rate requirement. To implement this approach it is necessary
to 1) size the parachute large enough to allow for low descent rates in the
upper clouds where there are many layers, and 2) in the vicinity of the base
of the water clouds jettison the chute to increase the descent rate so that
the total time does not exceed one hour. It will be necessary to consider
the use of two gas chromatograph columns so that the samples can be pro-
cessed in parallel. The sequencing will be quite complex, since the sample
times cannot be preprogrammed. It will be necessary to provide adaptive
programming. Local atmospheric temperature can be used as the environ-
mental input that is used to sequence the gas chromatograph/mass spectro-
meter. It may be necessary to use a joint temperature and pressure indicator
if there remains a large uncertainty in the Jovian temperature and pressure
profiles prior to launch.

For all direct link missions, and the 1979 flyby mission (JUN Grand Tour),
a descent time of 0.5 hr was used. It is difficult to obtain a one hour
descent time for a direct link mission without resorting to steep entry angles,
a steerable entry probe antenna, or transmitter output power in excess of
50 w. Descent time for direct link missions varied from 0.28 hr (1000 sec)
to 0.445 hr (1600 sec). All entry probe configurations considered in this
study use simple, fixed antennas. For a relay link to a JUN Grand Tour
flyby a steerable antenna and/or more than 50 w of transmitter power would
be required to increase the descent time beyond 0.5 hr.

Although it is desirable to sample the gas chromatograph above, within, and
below each cloud layer, it is possible to consider a reduced sampling mode
of once per 100 deg K increase in atmospheric temperature. This will
result in the requirement of four gas chromatograph measurements in each
of the three model atmospheres, and based on a five minute process time,

a minimum descent time of 0. 33 hr. It can be seen that for the same direct link mission that either a double gas chromatograph column must be used or gas chromatograph samples be relaxed to three (900 sec descent time).

5. 1. 6 Entry Probe/Spacecraft Integration

This study has considered two spacecraft, the TOPS and Pioneer F/G, as a possible interplanetary bus for a Jupiter entry probe. Each of these space-craft configurations have been investigated from the viewpoint of: equipment relocation, and modification to structural, attitude control, propulsion communication, power, and thermal control subsystems.

5. 1. 6. 1 TOPS/Entry Probe Integration

The entry probe is mounted on TOPS in apparently the only space available that will not result in a major modification to the spacecraft. It is mounted to the equipment compartment as shown in Figure 5-7, just below the high gain antenna. Either side of the equipment compartment could be used. The entry probe is mounted to the spacecraft with a truss adapter connected at three points on the probe and several hard points on the spacecraft equipment compartment as shown in Figure 5-8. Separation of the probe occurs at the probe three point interface, and the adapter section remains attached to the spacecraft.

The entry probe axis is canted to the TOPS longitudinal axis by an angle of about 52 deg. This permits the line of action of the spring force that separates the entry probe from the spacecraft to pass through the common center of gravity of the entry probe/spacecraft system, hence minimizing the separation impulse perturbation. It may be necessary, however, to move the magnetometers and radio emission detectors because of the field distrubances created by the entry probe. It can be seen in Figure 5-8 that the entry probe and relay link antenna can be integrated into both the 10 ft or 12. 5 ft diameter shroud.

To accommodate an entry probe on TOPS, several modifications must be made to the spacecraft subsystems.

Scientific Equipment: Deployment of the magnetometers and radio emission detectors is not hindered by the mounting of the entry probe. However, the magnetometer must be located, such that when fully deployed, the magnetic field background is less than 0. 01 gamma. The entry probe may also have

FIGURE 5-7

CRUISE MODE CONFIGURATION OF TOPS

PLASMA WAVE DETECTOR

14 FT. DIA. HIGH GAIN ANTENNA

RTG

EQUIPMENT
COMPARTMENT

MAGNETOMETER

THERMAL CONTROL
LOUVERS

48 IN. DIA. ENTRY PROBE

RELAY ANTENNA/
MEDIUM GAIN ANTENNA
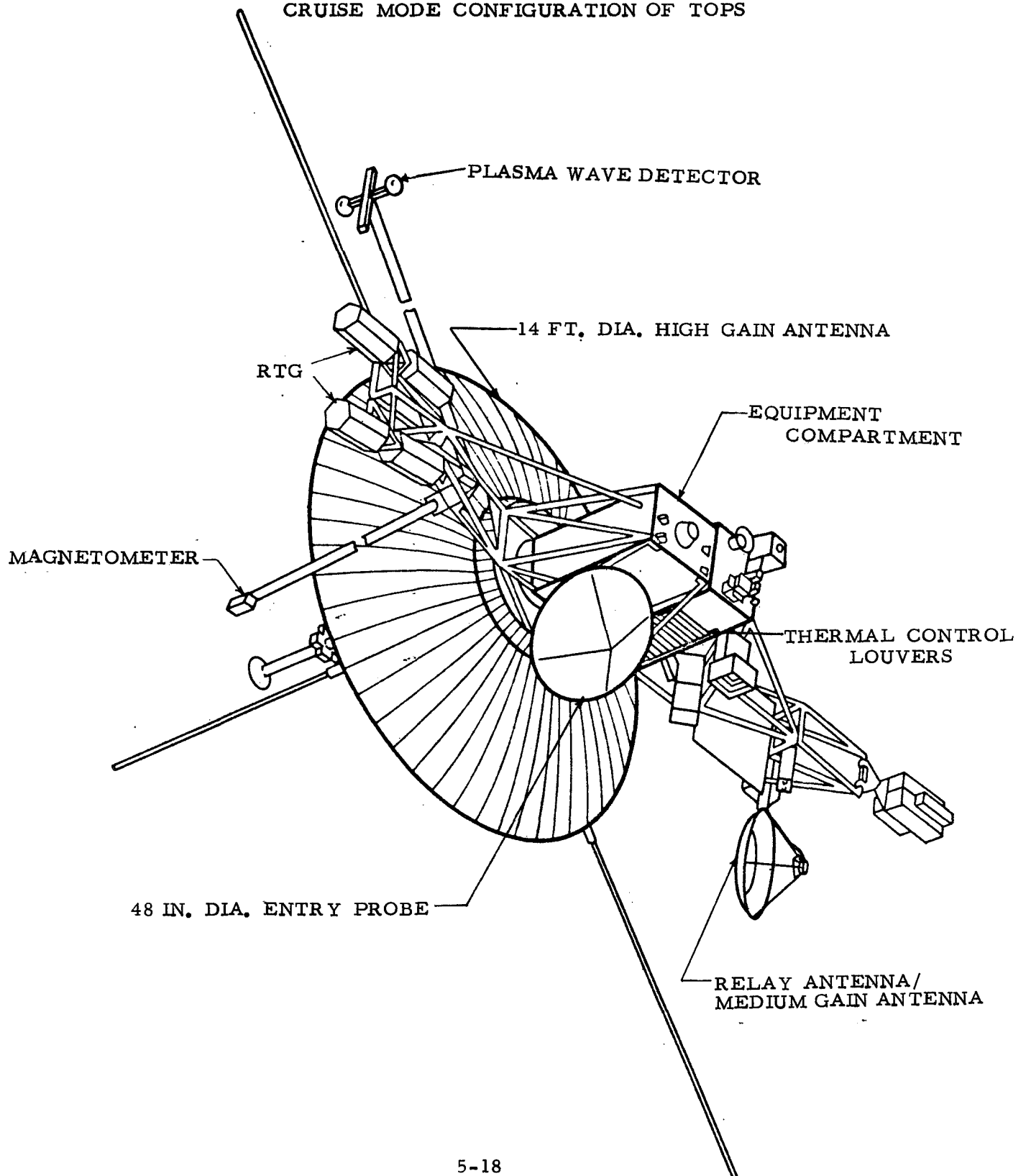
FIGURE 5-8
LAUNCH CONFIGURATION OF TOPS SPACECRAFT

12.5 FT DIA SHROUD

10 FT DIA
SHROUD

ENTRY PROBE

BURNER II

ELLIPTICAL
RELAY ANTENNA

31-0143
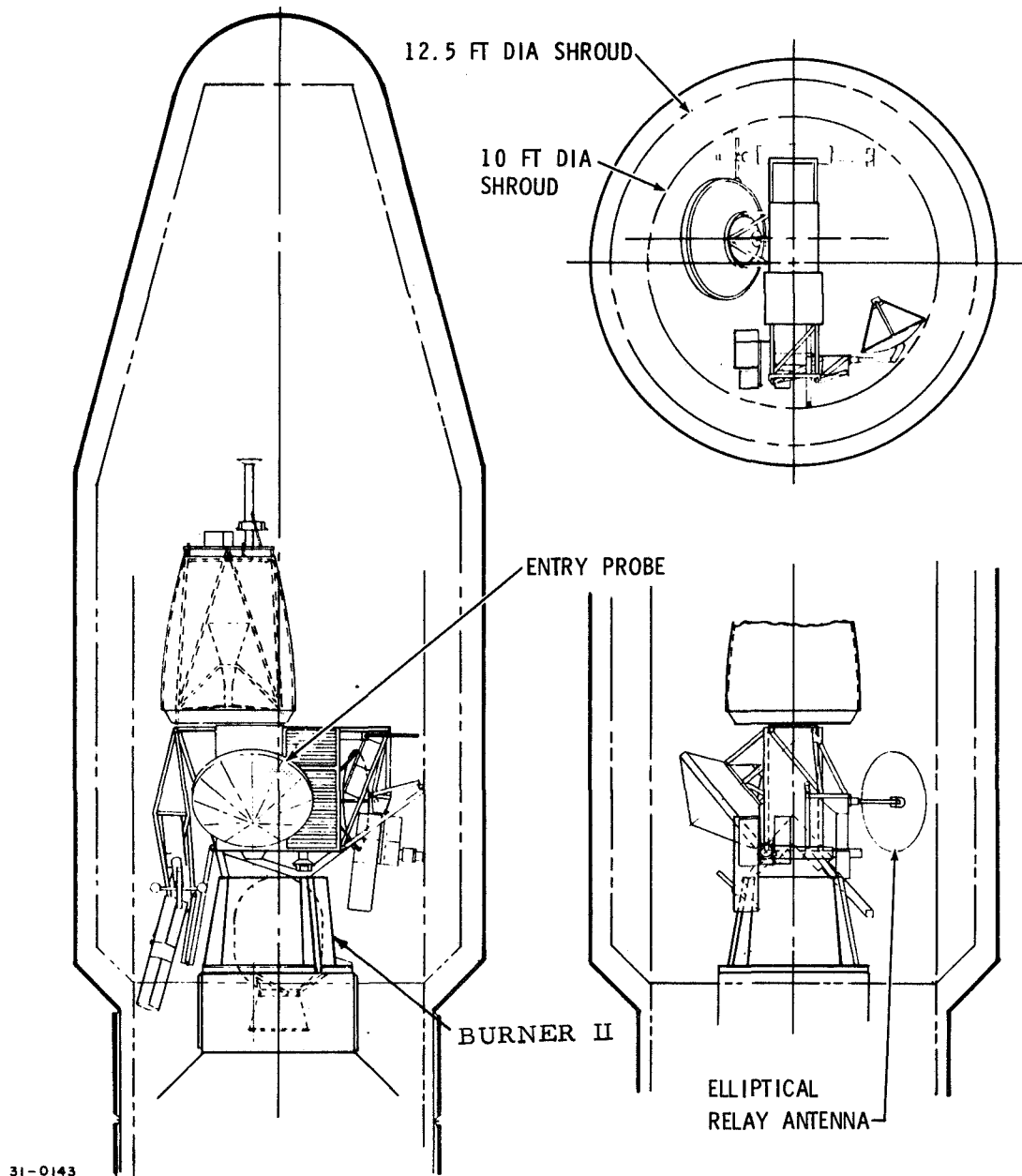
an RTG. The background from this power source could result in displacement of other spacecraft particle and field instruments.

Structures: Modifications of the spacecraft structure subsystem fall into three major areas: 1) probe to spacecraft adapter, 2) strengthening the basic spacecraft structure, and 3) strengthening the launch vehicle adapter. The probe-spacecraft adapter is a simple truss structure that supports the probe during launch and interplanetary cruise. It is designed to react the launch vehicle loads imposed on the probe which is cantilevered off the spacecraft by the adapter. It is constructed of aluminum tubing forming a three point interface at the probe and a three point connection to the spacecraft. The adapter weighs approximately 7 pounds.

Due to the additional hard point loads imposed on the spacecraft from the probe adapter, the TOPS equipment compartment structure will require some modifications and strengthening. Since little is known of the internal makeup of the TOPS spacecraft structure, a true assessment of these modifications cannot be evaluated, but only conjectured as approximately equivalent to the weight and complexity of the probe-spacecraft adapter (i. e., approximately 7 pounds).

The additional weight of the probe (400 lbs) on the TOPS (1450 lbs) will require strengthening of the launch vehicle adapter, with no modification to the existing adapter configuration. It is anticipated that this added strengthening will result in an 11 pound weight increase in the adapter.

ACS: The most significant modification to this subsystem will be the relocation of the ACS roll and pitch attitude thrusters located on the equipment compartment directly below the recommended probe mount position. Since it is not clear as to the internal arrangement of the equipment compartment, an assessment of this modification cannot be made at this time.

With the addition of the 400 pound probe, the spacecraft center of gravity will shift and the difference in the moment of inertia will increase, causing cross coupling in the control system. To reduce this effect, a second set of attitude thrusters located about the spacecraft/entry probe center of gravity may be required. Similarly, new limit cycling rates and ACS operation may be necessary to accommodate this change. The weight increase of thrusters and propellant, and the extent of modification to the ACS should be minimal, likely not to exceed a few pounds with no change in the basic system.

Propulsion: Due to the increased weight on the TOPS, the propulsion propellant must be increased to perform necessary interplanetary trajectory corrections. This propellant weight increase is expected to be less than 12 pounds.

Communications: The TOPS communication subsystem can provide two functions for the probe. First, it can provide a relay data link after probe separation and during Jupiter entry for the relay link class of missions; secondly, it must provide a hard line link to the probe while it is attached to the spacecraft for system checkout and separation. To accomplish the first function, a relay antenna and receiver must be added to the existing spacecraft. The 16 in. diameter single axis medium gain X-band antenna is removed. In its place is added an elliptical antenna with a two axis gimbal that is programmed to track the center of Jupiter during entry probe to TOPS relay communication contact. The elliptical antenna is a dual function antenna. It serves as: 1) a high gain receiving antenna for the relay link, and 2) with the addition of an offset feed that illuminates a quarter portion of the dish, it can also be used as an X-band antenna in a medium gain mode for the TOPS to DSN downlink. The antenna dimensions are 31 x 41 inches, and the peak gain is 25 dB.

These modifications to the antenna system will result in approximately 15 pounds of additional weight. The S-band receiver required for probe relay links will weigh about 8 pounds and require about 6 watts of spacecraft power. It is not expected that any modification will be required in the space-craft data storage, since only 27,000 bits of data will be received from the probe during entry, which is far less than the TOPS data storage capacity of 10^9 bits.

The spacecraft will be required to process, store and transmit probe data for: a) in-flight system checkout, b) engineering diagnostics, and c) separation verification. These data link requirements are minimal, requiring approximately 10 bit/sec over approximately a 15 minute period with a maximum of 2000 total bits of data. In-flight system checkout and engineering diagnostic data requirements will probably occur simultaneously once every month during the flight history. To verify separation, the spacecraft must transmit data acquired from the probe and separation mechanism prior to, during, and after probe ejection. This data may also be acquired and trans-mitted along with the final system checkout and engineering diagnostic data. These modifications to the TOPS communication and data handling subsystem will probably result in a couple of pounds of cabling and added circuitry in the data handling subsystem.

Power: Spacecraft power will br required for: 1) thermal control, 2) checkout of the entry probe subsystem, and 3) operation of spacecraft receiver for a relay link. During cruise near Jupiter, the power requirements for thermal control could rise as high as 60w. This figure of 60w is based on the total absence of an insulation system. With the addition of an insulation blanket around the probe, the thermal requirement could be reduced to a few watts. Checkout at full power will require the expenditure of 230w for a period of about 15 min or a total energy expenditure of 57 whr. Near entry probe separation, and after the probe batteries are activated by the addition of electrolyte, the probe system will be checked out using probe power. It is assumed that this checkout will occur at least one day before separation. Based on a recharge time of 24 hours about 3w of continuous power will be required. It should be pointed out that during cruise, the spacecraft power requirements will be small due to the inoperation of the encounter science. During this phase there should be sufficient power to support the entry probe. Following probe separation during the encounter period spacecraft power consumption will be maximum. Support of relay link will require about 6w. During the encounter period the TOPS should have an excess power capacity of 60w that could be used for support of a relay link mission. It is estimated that 1 lb will be required to provide the necessary spacecraft to probe power cabling.

Thermal Control: The significant modification to the spacecraft thermal control subsystem will be to maintain, as near as possible, an adiabatic thermal interface between the probe and spacecraft. By providing this type of interface, both the probe and spacecraft thermal control subsystem can be simplified, in that both subsystems can be thermally designed essentially independent of each other. To provide this interface, TOPS spacecraft will require some thermal control coating modification and addition of blankets directly under the probe, and possibly reorientation of the thermal control louvers in the adjacent equipment compartment.

5. 1. 6. 2 Pioneer F/G/Entry Probe Integration

The most desirable mounting location for the Jupiter Probe on Pioneer F/G is at the base of the equipment compartment between the Burner II and Pioneer F/G spacecraft. The Pioneer F/G is shown pictorially in Figure 5-9, in the interplanetary cruise configuration, and in Figure 5-10 in the launch configuration.

Since the Pioneer F/G is a spin stabilized spacecraft, mounting the probe on this axis minimizes both the spacecraft and probe interface requirements.

FIGURE 5-9

CRUISE MODE CONFIGURATION OF PIONEER F/G

RTG

9 FT. DIA. HIGH GAIN ANTENNA

CIRCUMFERENTIAL ARRAY RELAY ANTENNA

THERMAL CONTROL LOUVERS

48 IN. DIA. PROBE

LOW GAIN ANTENNA

EQUIPMENT COMPARTMENT
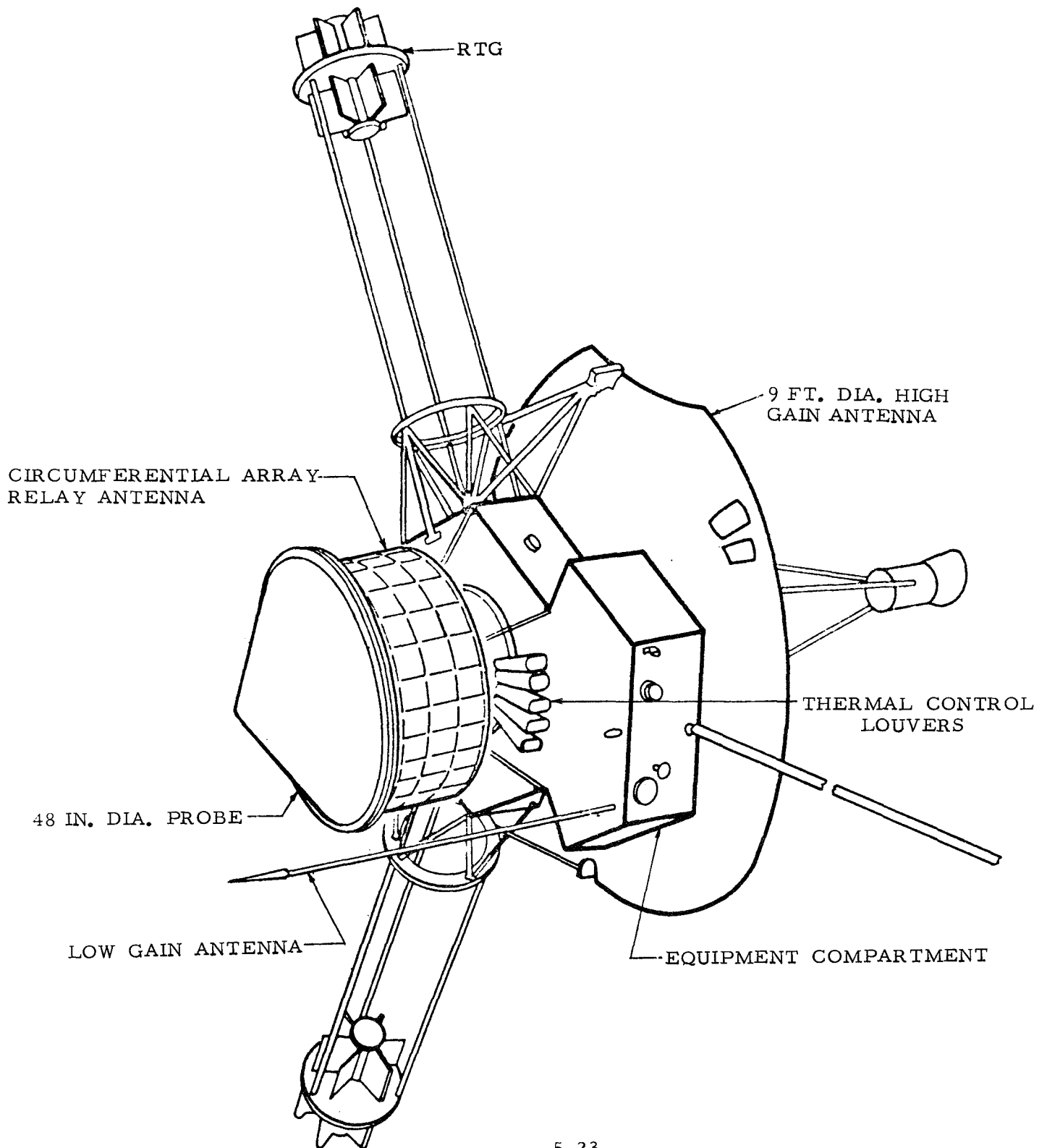
FIGURE 5-10
LAUNCH CONFIGURATION OF PIONEER F/G SPACECRAFT

12.5 FT DIA SHROUD

10 FT DIA SHROUD

CIRCUMFERENTIAL
RELAY ANTENNA

ENTRY PROBE

BURNER II

31-0142
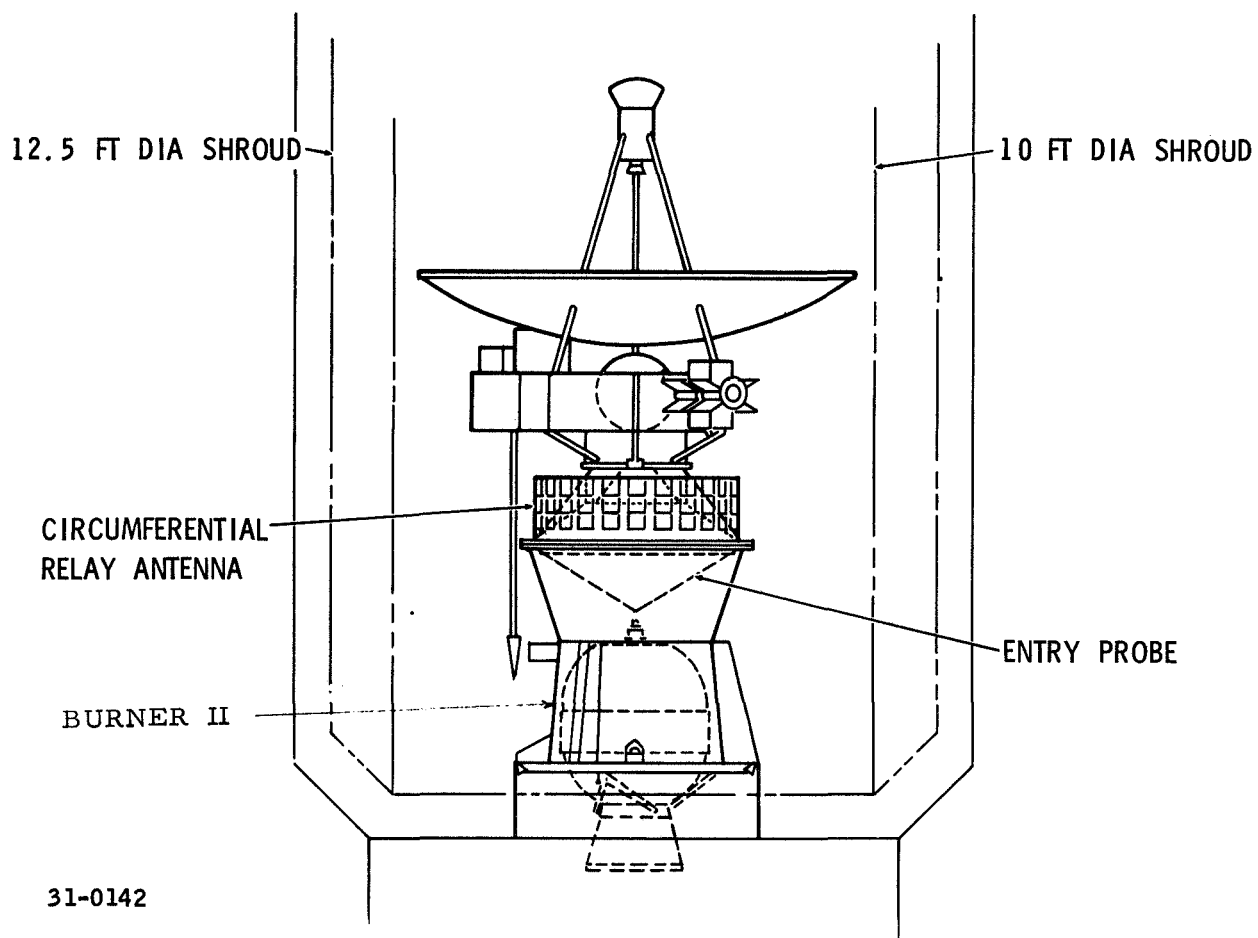
The spin-to-pitch mass moment of inertia ratio of the spacecraft is reduced with this mounting arrangement, however, spacecraft symmetry is maintained after probe separation. A major change is required in the launch vehicle adapter, since now the adapter must go around the probe and carry the launch loads for the spacecraft to the Burner II, as illustrated in Figure 5-10.

The launch vehicle adapter utilizes the present spacecraft and Burner II interfaces and is constructed of two conical shells which completely enclose the probe. Launch vehicle separation occurs at the maximum diameter location leaving the probe clear for separation. The probe is mounted to the spacecraft at the base of the conical shell by a simple truss structure that attaches to the probe at the three interface separation points. It can be seen in Figure 5-10 that the entry probe and relay link can be integrated into both the 10 ft or 12.5 ft diameter shroud.

To accommodate the probe throughout its mission, certain Pioneer F/G spacecraft subsystems must be modified. These modifications are outlined in the following discussion for each spacecraft subsystem affected.

Scientific Equipment: Attachment of the entry probe should not disturb the physical location of Pioneer F/G science. However, the presence of a probe could require greater displacement of magnetometer sensors or a requirement for greater probe magnetic cleanliness.

Structure: Modification to the Pioneer F/G structure will involve a new launch vehicle adapter and a probe adapter. Since the spacecraft is raised in the shroud, to allow the probe to be mounted between the spacecraft and Burner II last stage, a new launch adapter will be required. It is anticipated that this adapter will be two truncated conical aluminum shells with the launch vehicle separation interface at the maximum diameter. The complete adapter, with the separation mechanism should weigh about 49 pounds to carry launch loads.

The probe adapter is a truss connected to the probe and spacecraft at three hard points. Separation of the probe from the spacecraft occurs at the three points on the probe, thus leaving the adapter with spacecraft. This adapter, which is designed for axial launch loads, is constructed of aluminum tubing and weighs approximately 5 pounds.

Another area on the spacecraft that may require modification is the basic spacecraft structures. Since the spacecraft is raised higher on the launch

vehicle the launch loads will increase slightly, particularly in bending moment and vibration, which may mean that the structure will require some additional stiffening.

Propulsion and ACS: Since spin stability is employed as the primary attitude control mechanism on Pioneer F/G, a common propulsion subsystem is utilized for despinning, trajectory corrections, maintaining spin rate and precession torquing. The propulsion subsystem is a set of gas jets located on the periphery of the high gain antenna support structures. Due to the increased weight on the spacecraft (400 pound probe compared to a 547 pound spacecraft) the amount of propellant must be greatly increased. In addition, the spin moment of inertia is also increased while the probe is attached, which will increase the spin (and despin) and precession torquing propellant requirements. Using scaling factors with the available information on the Pioneer F/G propulsion subsystem, an estimated 44 pound increase in propellant will be required.

Communication: The Pioneer communication and data handling subsystem must provide: 1) hard line data link to the probe during interplanetary cruise for system checkout and transfer of ground station commands and 2) relay link communication after probe separation and during entry. To provide the hard line data link, certain cabling and circuitry will be required to process,format, and transfer ground station commands, and return necessary probe data. The cabling required should not exceed a couple of pounds, however, the internal circuitry in the data handling subsystem necessary to interface with the probe is difficult to assess without full knowledge of the spacecraft data handling design.

For the relay link communication the spacecraft must provide an S-band receiver and antenna as well as process, format and possible store probe data. The receiver will weigh 8 pounds and require 6 watts of power during relay. It is anticipated another 3 pounds will be required for cabling, circuitry and additional data storage (Pioneer has a total data storage capacity of 49, 152 bits, the probe will send approximately 27,000 along during entry).

The relay antenna required on the spacecraft for probe communication is a circumferential array, 50 inches in diameter and 14 inches long, located around the launch vehicle adapter and next to the probe/spacecraft interface, as shown in Figure 5-9. The complete antenna weighs approximately 24 pounds, and has a peak gain 13 dB.

Another modification required in the spacecraft communication subsystem is the relocation of the low gain antenna located near the probe-launch vehicle interface (see Figure 5-10). Because of added length due to the probe extending below the spacecraft interface, this antenna must be moved outboard and extend below the probe to allow a full field of view past the probe for near Earth operation.

Thermal Control: The major modification to the spacecraft thermal control subsystem is the possible relocation of louvers located around the base of the equipment compartment. With the recommended mounting position of the probe, the enlargement of the launch vehicle adapter and the use of a circumferential relay antenna, the present position of the louvers are obstructed from viewing space.

It will be desirable from both the spacecraft and probe thermal control standpoint to provide, as near as possible, an adiabatic thermal interface. In view of this, the complete thermal control design of the spacecraft must be re-evaluated with possible changes in thermal control coating on the spacecraft.

5.1.6.3 Summary of Spacecraft Modifications

A summary of the modifications that must be made to the TOPS and Pioneer F/G is indicated in Table 5-4. It can be seen that the integration weight requirement of mounting entry probe to Pioneer F/G is more than a factor of two greater than that for a TOPS. This large penalty only slightly offsets the weight advantage of the Pioneer F/G. A Pioneer F/G weighs 550 lb and a TOPS 1450 lb, or a difference of 900 lb in favor of Pioneer F/G. Assuming a 352 lb entry probe and the integration weight penalties as shown in Table 5-4, the Pioneer F/G and entry probe configuration weighs 1047 lb and a TOPS and entry probe configuration weighs 1874 lb, and the weight differential of Pioneer F/G relative to TOPS is reduced to 827 lb.

Based on the work that has been accomplished it is concluded that both spacecraft can serve as a bus for an entry probe. It has been tacitly assumed that the total angular error in the attitude of the entry probe during the deflection maneuver that alters the probe trajectory from flyby to impact is the same for both spacecraft. This assumption is based on the premise that the necessary modifications in the spacecraft attitude determination and attitude control subsystems will result in only minor design perturbations. This angular error is composed of the uncertainty in the spacecraft attitude and the uncertainty in the entry probe deflection maneuver. The angular error

TABLE 5-4

SUMMARY SPACECRAFT MODIFICATION - JUPITER PROBE INTEGRATION

SPACECRAFT SUBSYSTEM	TOPS		PIONEER F/G	
	MODIFICATION	WEIGHT, LB.	MODIFICATION	WEIGHT, LB.
Scientific Equipment	Possible relocation of magnetometer and radio emission detector due to probe magnetic field.	--	None	--
Structure	Add probe/spacecraft adapter Strengthen spacecraft structure Strengthen launch vehicle adapter	7 7 11	Add probe/spacecraft adapter Strengthen spacecraft structure Provide new launch vehicle adapter	5 2 49
Propulsion and ACS	Add second set of thrusters about new center of gravity Increase propulsion propellant	2 12	Increase propulsion propellant	44
Communication	Add hard line cabling and circuitry Add relay S-band receiver (6 watt) Enlarge medium gain antenna and add two axis gimbal control	2 8 15	Add hard line cabling and circuitry Add relay S-band receiver (6 watt) Add circumferential antenna Add additional data storage Move low gain antenna	2 8 24 3 --
Power (assuming RTG aboard probe)	Provide minimum of 230 for 15 minutes periodically Add power cabling to prove	-- 1	Provide minimum of 230 watts for 15 minutes periodically Add power cabling to probe	-- 1
Thermal Control	Provide adiabatic interface Possibly modify thermal control louvers	--	Provide adiabatic interface Relocate louvers in equipment compartment	--
Probe Separation	New subsystem	7	New subsystem	7

Total Modification Weight   72 lb.   145 lb.

in spacecraft attitude is an important contributor to the dispersion in entry angle, and the dispersion in probe to spacecraft communication range, and probe to spacecraft communication angle.

It is concluded that both a 10 ft or 12.5 ft diameter shroud is compatible with either a TOPS with 48 inch diameter probe or Pioneer F/G with a 48 inch diameter probe.

A mass properties summary was prepared and is indicated in Table 5-5. The difference in the (I_x-I_y) and (I_x-I_z) moments increase and the difference in the (I_y-I_z) decrease for TOPS, and the spin moment of inertia increases for Pioneer F/G. These mass property alterations result in greater expenditure of propellants for attitude maneuvers of both TOPS and Pioneer F/G and greater expenditure for changes in body rates.

5.2 TRAJECTORY PERFORMANCE CONSTRAINTS

During any given planetary launch opportunity there are essentially an infinite number of interplanetary transfer trajectories, uniquely defined by the launch and arrival dates, that could be employed. The process of selecting an optimum launch period from this almost limitless number of trajectories involves consideration of many factors; e.g. the launch vehicle payload/energy relationship; trajectory constraints during launch, injection and interplanetary flight; science objectives and requirements; mission configuration and post encounter mission objectives; and subsystem requirements. The following sections describe the procedure used in establishing the launch period parameters for these Jupiter missions during the 1978, 1979, and 1980 launch opportunities.

5.2.1 Launch Constraints

The launch or mission independent constraints used in this analysis and that are applicable, in part or total to any interplanetary flight, are listed in Table 5-6. These constraints include: 1) restriction on the launch azimuth by virtue of range safety considerations; 2) launch window duration and parking orbit coast-time limitations; 3) restrictions on DLA and interplanetary transfer trajectory inclination imposed by tracking and orbit determination requirements, and 4) launch vehicle considerations concerning launch period duration and the injection energy/payload relationship.

The launch vehicle payload/energy relationship is unique for each launch vehicle and is one of the primary factors that can be utilized to limit the number of potential interplanetary trajectories. Flexibility in the injection

TABLE 5-5

SPACECRAFT/ENTRY PROBE MASS PROPERTIES

CONFIGURATION	M	X_{CG}	Y_{CG}	Z_{CG}	I_x	I_y	I_z	$\dfrac{2\,I_z}{2\,I_x+I_y}$
43 In. D Probe only	300	0.0	0.0	0.0	5.0	5.0	6.2	1.24
60 In. D Probe only	500	0.0	0.0	0.0	16.9	16.9	21.2	1.25
TOPS	1450	0.0	0.0	+33.0	294.0	1434.0	1506.0	--
Pioneer F/G	550	0.0	0.0	+19.2	383.0	169.0	424.0	1.88
TOPS/43 In. D Probe	1750	-4.2	-1.3	+29.3	329.4	1499.0	1548.0	--
TOPS/60 In. D Probe	1950	-7.9	+1.5	+27.6	352.4	1563.0	1604.0	--
Pioneer F/G/43 In. D Probe	850	0.0	0.0	+3.3	374.7	260.7	430.2	1.36
Pioneer F/G/60 In. D Probe	1050	0.0	0.0	-4.3	436.3	322.3	445.2	1.88

M, mass in lb.

X_{CG}, Y_{CG}, Z_{CG}, entry probe center of gravity in inches, measured from center line at maximum diameter

X_{CG}, Y_{CG}, Z_{CG}, spacecraft center of gravity in inches, measured from center line at spacecraft/booster separation plane

X_{CG}, Y_{CG}, Z_{CG}, spacecraft/entry probe center of gravity in inches, measured from center line at spacecraft/booster separation plane

Subscript x, longitudinal axis

Subscript y, transverse axes

TABLE 5-6

MISSION INDEPENDENT CONSTRAINTS

INJECTION ENERGY

$$C_3 \leq 140 \quad Km^2/Sec^2$$

DAILY LAUNCH WINDOW DURATION

    30 MINUTES MINIMUM

RANGE SAFETY

    LAUNCH AZIMUTH 45 TO 114 DEGREES

PARKING ORBIT

    2 TO 60 MINUTES COAST TIME

    NO DOGLEG OR DIRECT ASCENT TRAJECTORIES

ORBIT DETERMINATION

    TRANSFER TRAJECTORY INCLINATION $\geq$ 0.1 DEGREES

    MINIMUM DLA $\geq |3|$ DEGREES

LAUNCH PERIOD

    LAUNCH PERIOD: 20 DAYS FOR 5 SEG BOOSTER
                        30 DAYS FOR 7 SEG BOOSTER

    TWO LAUNCHES PER OPPORTUNITY

velocity can only be accomplished by varying the payload, and optimum launch periods can normally be established if the upper limit of the injection energy is maintained within 40 to 50 percent of the absolute minimum injection energy. For Jupiter missions during the 1978 and 1980 launch opportunities the minimum injection energies for both Type I and Type II transfers are about 90 Km^2/sec^2, and for this reason a maximum C_3 of 140 Km^2/sec^2 was selected.

Within the matrix of launch date/arrival date combinations that satisfies the payload/injection energy requirements, further restrictions may be imposed by launch, injection and transfer trajectory constraints. Current interplanetary missions are restricted to using a launch azimuth corridor varying from 45 to 114 deg. For interplanetary missions employing a parking orbit with optimum injection onto the departure hyperbola, this launch azimuth corridor constrains the parking orbit inclination to values between 28.3 and 51.6 deg. This, in turn, constrains the declination of the launch asymptote to be less than 51.6 deg.

The parking orbit coast-time constraint imposes restrictions on the inter-planetary trajectory selection by virtue of its relation to launch time for a given azimuth and DLA. With a given launch azimuth and DLA, the matching of the powered booster phase to the post injection phase is accomplished by varing the launch time and parking orbit coast-time. Therefore, within a given launch corridor, where the launch azimuth is continually changing, the daily launch window and parking orbit coast-times can be determined and employed to place constraints on potential transfer trajectories if either the daily launch window is too short or the parking orbit coast-time is excessive. In this study it was assumed that the daily launch window should be in excess of 30 minutes to ensure a high probability of launch or any given day and that parking orbit coast-time should be constrained to values less than 60 minutes because of propellant boil-off rates characteristic of the Centaur stage.

In addition to the maximum DLA constraint associated with range safety there is also a minimum DLA constraint and a minimum transfer trajectory inclination constraint imposed by tracking and orbit determination require-ments. These constraints, at present, appear to be soft. DSN orbit determination accuracy and necessary tracking time that is needed for the first mid-course correction maneuver is based on 1) a minimum value of DLA of less than 3 deg, or 2) a transfer trajectory inclination with respect to ecliptic of less than 0.1 deg. If these constraints are relaxed, then longer tracking times will be required.

5.2.2 Mission Dependent Constraints

The constraints that have been discussed to this point can be considered as mission independent constraints. Mission dependent constraints which pertain to the scientific requirements can now be employed to further restrict the launch date/arrival data matrix. These additional constraints could result from unique interplanetary or planetary encounter trajectory requirements to satisfy specific scientific objectives and could be oriented toward the entry probe or flyby spacecraft. Typical constraints which were considered in the design of the interplanetary transfer trajectory include: 1) arrival date constrained so that probe entry does not occur within 20 days of conjunction because the sun would be directly between Jupiter and the earth and interfere with the telemetry link; 2) location of the approach asymptote such that reasonably shallow probe entry angles can be achieved at any entry longitude 60 degrees in front of the evening terminator; and 3) entry latitude location between 5 and 25 degrees in either the northern or southern hemisphere to satisfy entry site requirements.

In addition to these mission dependent and independent constraints, it is also desirable, if not manditory, to consider launch period selection wherein the payload is maximized and/or the encounter trajectory designed to satisfy post encounter requirements such as 1) an occultation experiment, 2) rendezvous with second planet, or 3) close solar approach or solar system escape.

Analysis of all pertinent constraints applicable to a specific mission will permit an evaluation of the significance of each constraint on the launch period selection and will identify the tradeoffs that must be considered, if the inclusion of all constraints is too restrictive to permit the selection of a reasonable duration launch period.

5.2.3 Transfer Trajectory Parameters for 1978, 1979, and 1980 Launch Opportunities

The pertinent departure and approach trajectory parameters associated with both Type I and Type II transfer trajectories to Jupiter have been analyzed for the 1978, 1979, and 1980 launch opportunities. The variation in the 1) injection energy, C_3, 2) declination of the launch asymptote, DLA, and 3) flight time are presented in Figures 5-11 to 5-13 as a function of the launch and arrival dates. In 1978, the launch dates associated with

FIGURE 5-11

PERTINENT DEPARTURE PARAMETERS - EARTH/JUPITER 1968 TRAJECTORIES

5-34
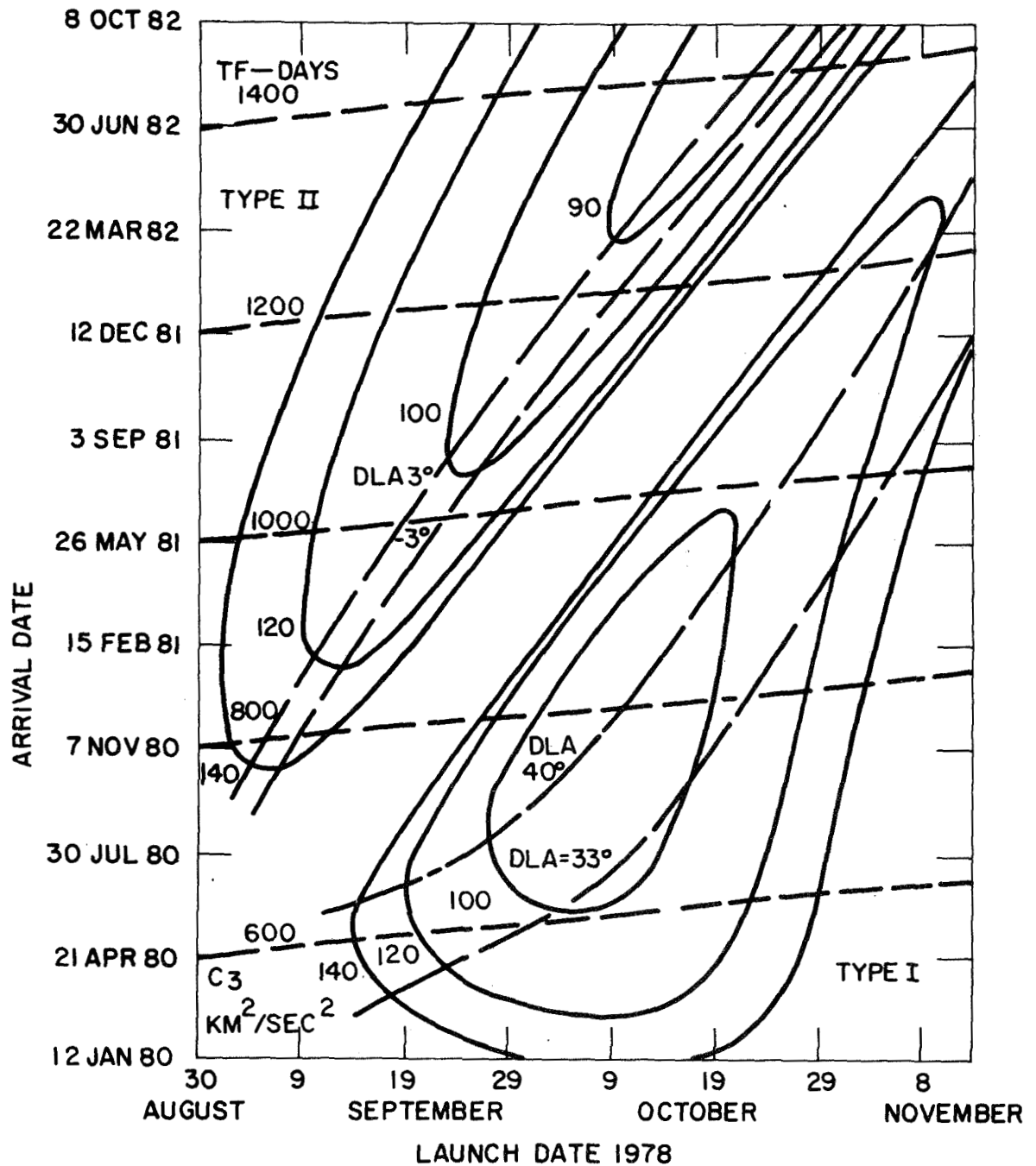
FIGURE 5-12

PERTINENT DEPARTURE PARAMETERS - EARTH/JUPITER 1979 TRAJECTORIES
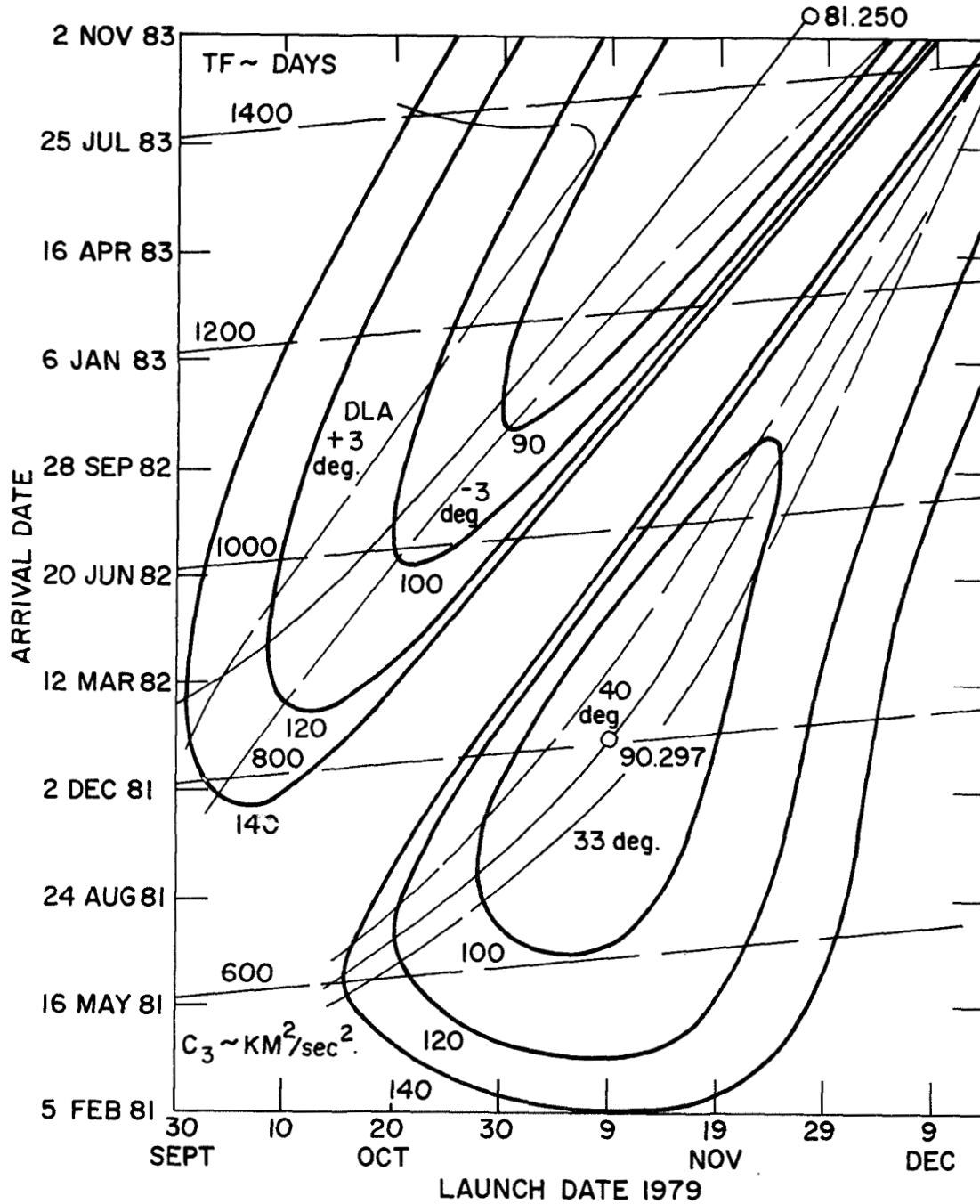
FIGURE 5-13

PERTINENT DEPARTURE PARAMETERS – EARTH/JUPITER 1980 TRAJECTORIES

5-36
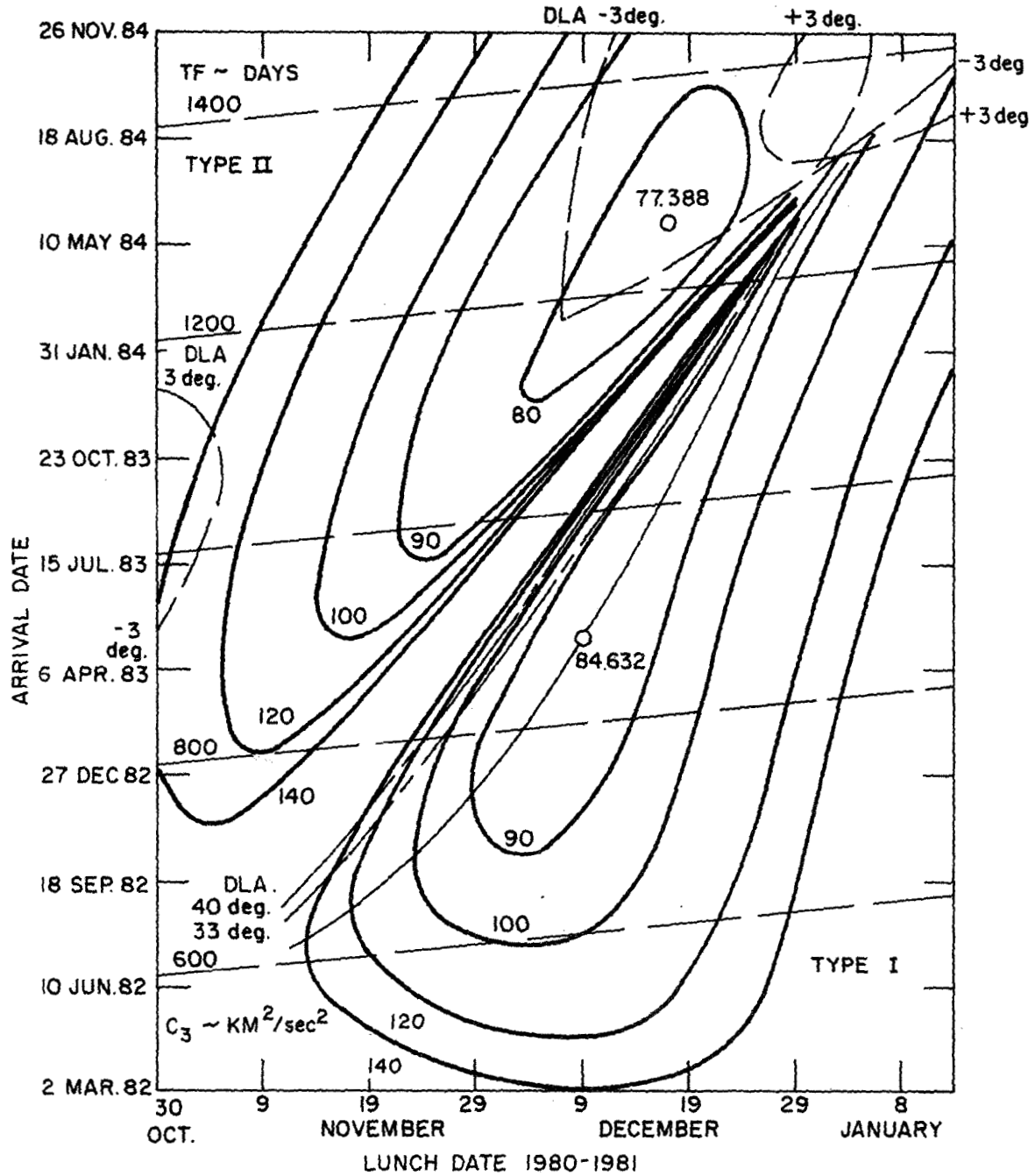
injection energies less than 140 Km^2/sec^2 occur in September and October with arrival dates from early 1980 to late 1982. The flight times vary from about 450 days for a high energy, fast Type I transfer to about 1450 days for a minimum energy Type II transfer. The range safety maximum DLA constraint, eliminates a significant portion of low energy Type I transfers from further consideration. Whereas, the minimum DLA associated with orbit determination considerations, eliminates a narrow swath of Type II transfers in the vicinity of minimum energy.

Similar trends are evident in 1979 and 1980 with the exception that: 1) the launch and arrival dates are approximately one month later in each succeeding launch opportunity; and 2) the maximum DLA constraint associated with Type I transfers becomes less restrictive while the minimum DLA constraint associated with Type II transfers becomes more restrictive. Also, the absolute minimum injection energy for Type I transfers decreases from 91.5 Km^2/sec^2 in 1978 to 90.3 Km^2/sec^2 in 1979 to 84.6 Km^2/sec^2 in 1980.

The variation in the direction of the hyperbolic approach asymptote with respect to the Jupiter-sun line, ZAP angle, the magnitude of the hyperbolic approach velocity (V_{HP}), and the encounter communication range (R_c) is presented in Figures 5-14 to 5-16 for the 1978, 1979, and 1980 launch opportunities, respectively, as a function of launch and arrival dates. (Earth-Jupiter angle and range variations are indicated in Reference 1). These results indicate that basically the magnitude and direction of the hyperbolic approach velocity and the encounter communication range are independent of the launch date and only depend upon the arrival date. The ZAP angle decreases by about 20 degrees for each 200 day increase in flight time, whereas, the hyperbolic approach velocity decreases linearly for flight times, between 450 and 900 days and then remains relatively constant for flight times between 900 and 1450 days.

Because the Earth-Jupiter encounter geometry repeats approximately every 13 months, the encounter communication range cycles through several minimum and maximum values over the matrix of potential arrival dates with a minimum range about 650 million kilometers and a maximum range about 950 million kilometers. The variations in encounter communication range is not a significant parameter in the design of a relay link telecommunication system, but becomes of prime concern in the launch period selection for a direct link telecommunication system in that it tends to restrict the arrival date selection to those in the vicinity of minimum communication range.

FIGURE 5-14

PERTINENT ARRIVAL PARAMETERS - EARTH/JUPITER 1978 TRAJECTORIES

5-38
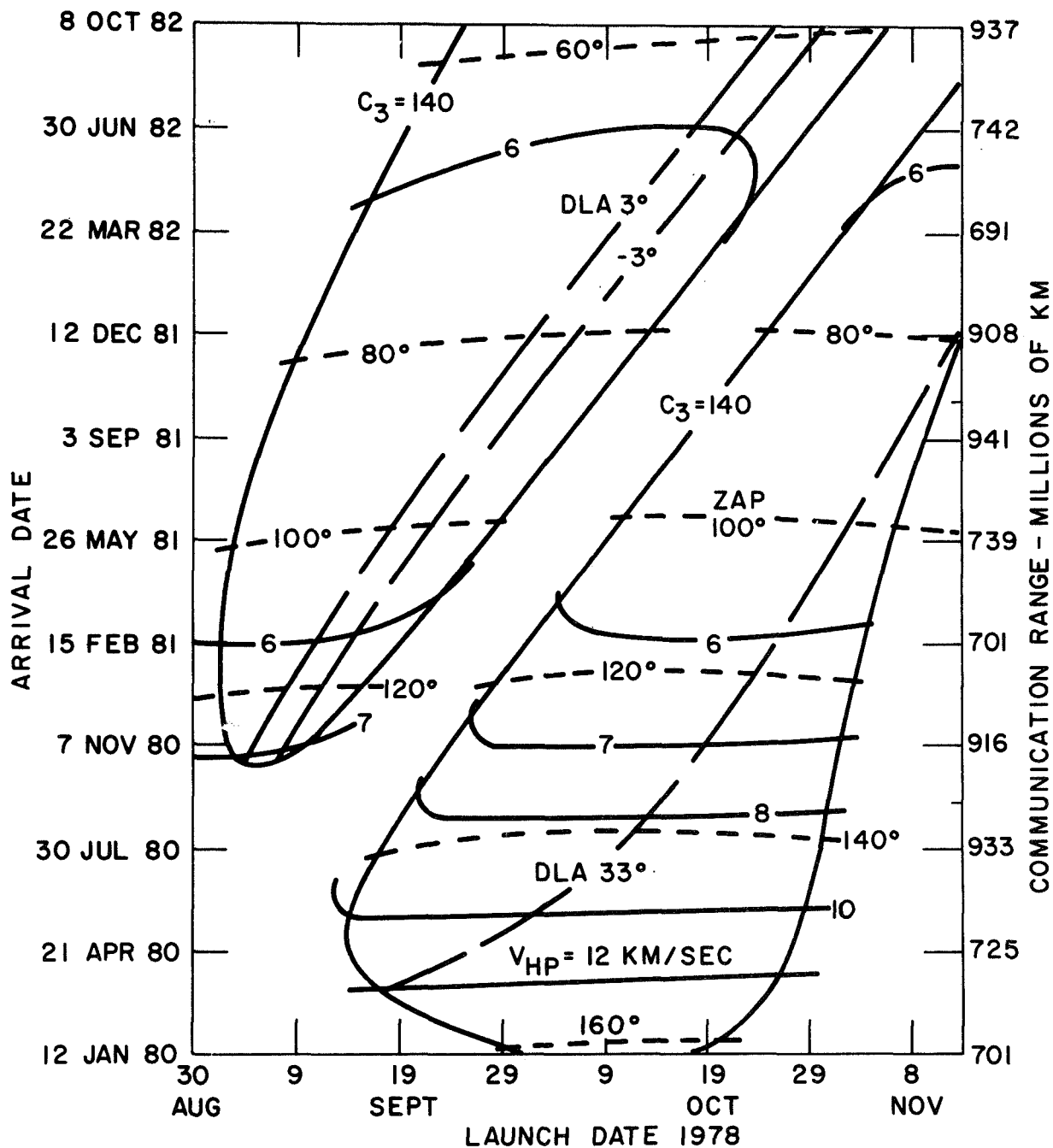
FIGURE 5-15

PERTINENT ARRIVAL PARAMETERS - EARTH/JUPITER 1979 TRAJECTORIES
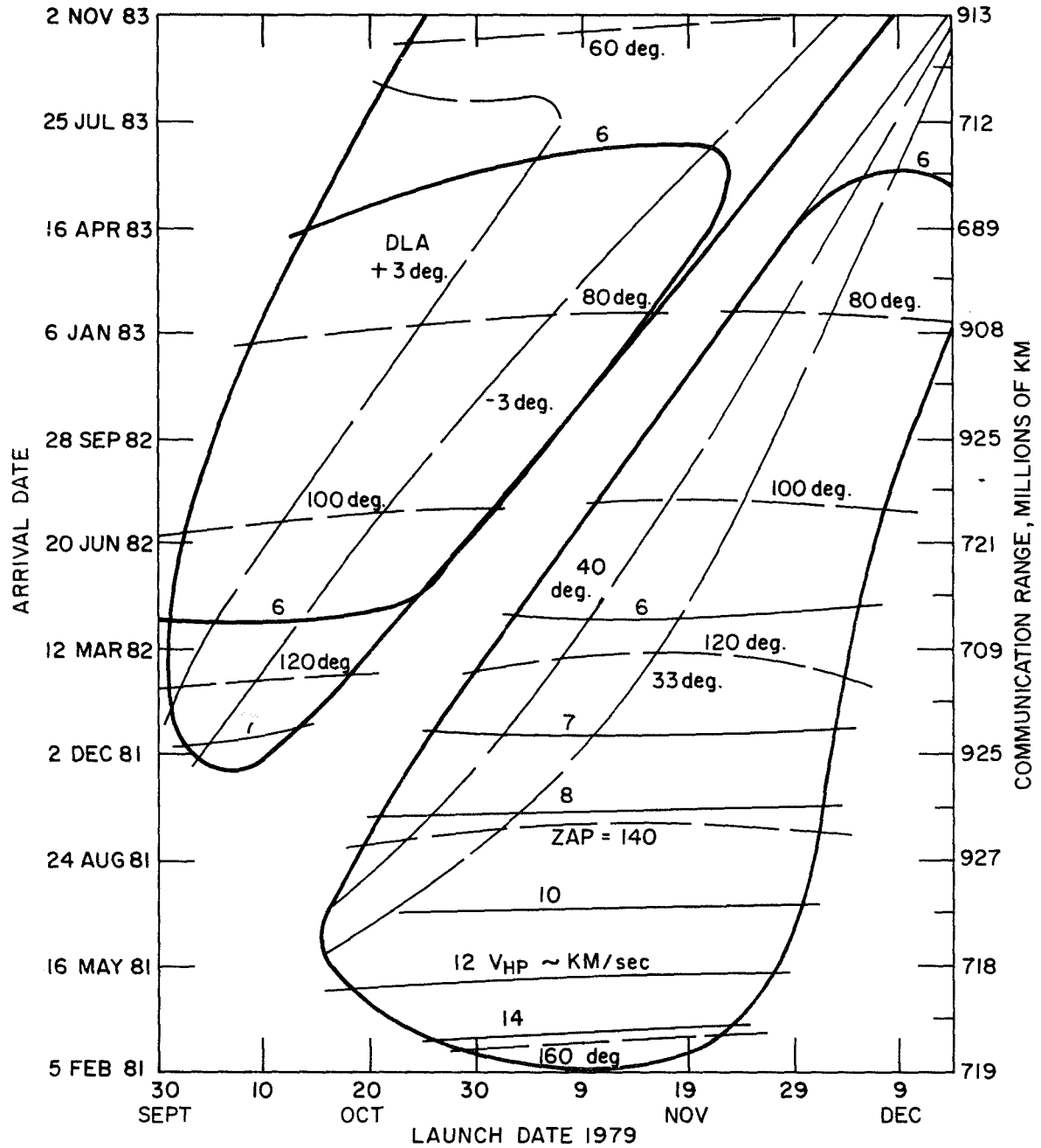
FIGURE 5-16

PERTINENT ARRIVAL PARAMETERS – EARTH/JUPITER 1980 TRAJECTORIES

5-40
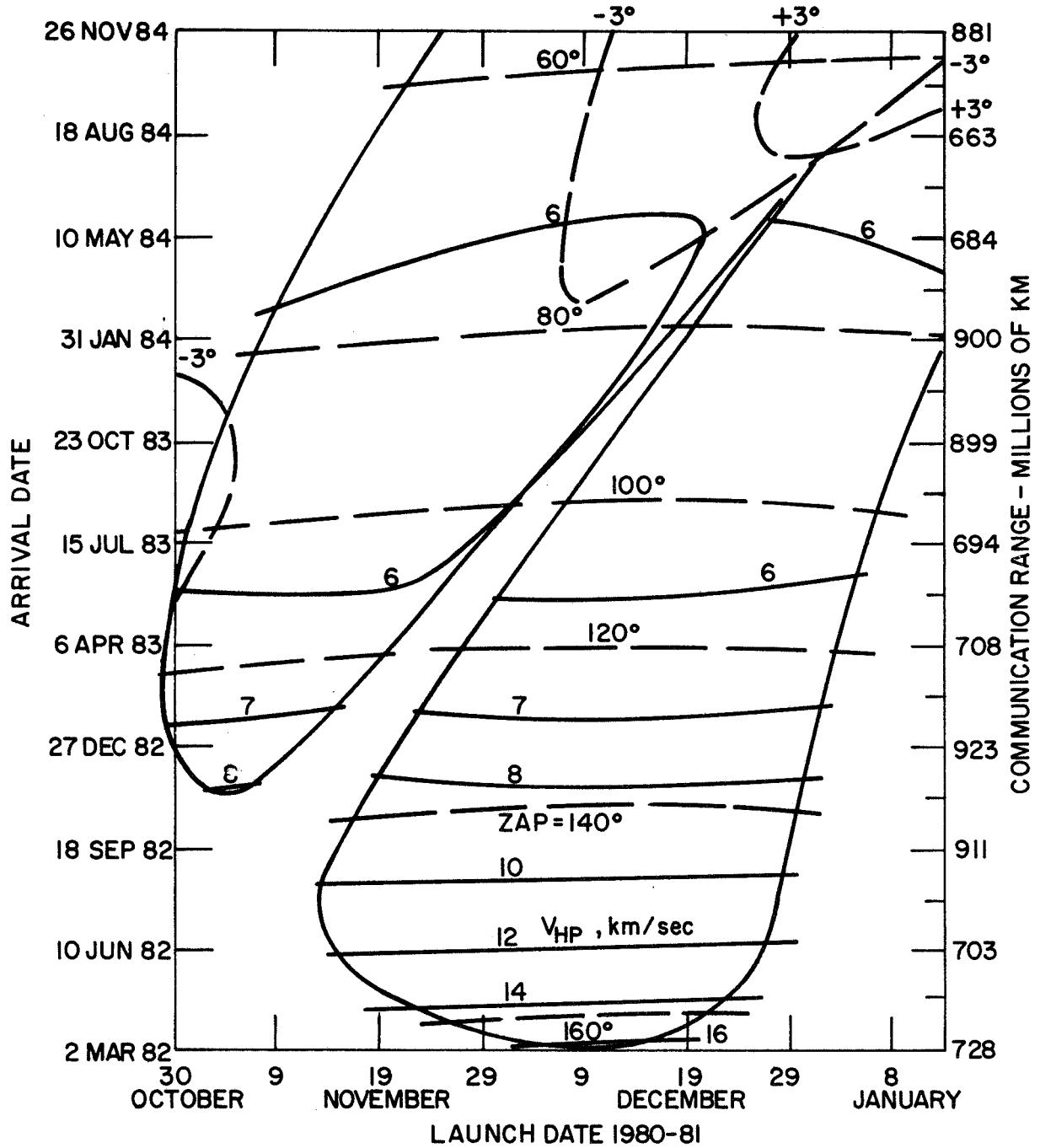
The variation in the encounter trajectory parameters for both Type I and Type II transfer trajectories in the 1978, 1979, and 1980 launch opportunities were analyzed and the results indicated that these parameters are basically not opportunity dependent and only depend upon the flight time. These results are presented in Figure 5-17. The arrows represent the dispersion encountered for the various launch opportunities and transfer trajectory type.

5.2.4 Launch Period Selection

In the process leading to the selection of a specific launch period the implication of the various mission dependent and independent constraints must be evaluated along with the overall mission objectives. For the 1978 launch opportunity a detailed analysis was performed (see Reference 2) to indicate the range of launch and arrival dates that satisfied the specific constraints. The results of this analysis are presented in Figure 5-18. Figure 5-19 illustrates the arrival date regions that must be avoided when the earth is within 20 days of superior conjunction.

Jovian encounter ± 20 days about superior conjunction must be avoided if the sun is not to occult or add unacceptable noise to the communication link. Certainly the probe and spacecraft can arrive 20 days prior to superior conjunction and complete their mission. Likewise, the probe and spacecraft can arrive 20 days after superior conjunction. For this latter case, probe separation time from the spacecraft of less than 40 days is not allowed since the separation must take place in view of DSN. Typical separation times considered range from 30 to 60 days. The targeting analysis is not sensitive to separation time, and the time can be increased.

When these results are combined and further restricted by the desire to maximize the payload within the matrix of launch and arrival dates satisfying all identified constraints the results presented in Figures 5-20 and 5-21 are obtained for 20 and 30 day launch periods, respectively. Within the area defined by the solid lines the payload is truly maximized in that the injection energy on the first and last date in the fixed arrival date launch period is the same. In the dotted region the payload is governed by the injection energy on the latest launch date since the earliest launch date is governed by the parking orbit coast time constraint of 1 hour. Within the payload maximized region for a 20 day launch period several fixed arrival date launch periods were established as a function of injection energy for both Type I and Type II transfer trajectories to identify the pertinent departure and approach trajectory parameters. These results are presented in Table 5-7. Fixed

FIGURE 5-17

EARTH-JUPITER FLIGHT PARAMETERS

1978-1979-1980 LAUNCHES
TYPES I AND II

FIGURE 5-18

MISSION INDEPENDENT CONSTRAINTS

CONSTRAINTS MET IN AREA ABOVE LINE

PARKING ORBIT COAST TIME ≤ 30 MIN.

DAILY LAUNCH WINDOW ≥ 30 MIN.

LAUNCH AZIMUTH BETWEEN 45° AND 115°

$C_3 \leq 140 (KM/SEC)^2$

$i > 0.1$ DEG.

IN THIS AREA

P.O.C.T. BETWEEN 50 & 60 MIN.

LAU. WIND. ≥ 30 MIN.

LAU. AZI. BET. 45° & 72°

$33° \leq DLA \leq 40°$

$C_3 \leq 140 (KM/SEC)^2$

IN THIS AREA

P.O.C.T. BETWEEN 35 & 40 MIN.

LAUNCH WINDOW ≥ 30 MIN.

LAUNCH AZI BET. 100° AND 114°

DLA ≤ 33°

$C_3 \leq 140 (KM/SEC)^2$

$i > 0.1$ DEG.

ARRIVAL DATE

SEPTEMBER   OCTOBER

LAUNCH DATE 1978

FIGURE 5-19

1978 LAUNCH OPPORTUNITY

ARRIVAL DATE CONSTRAINTS IMPOSED BY SUN POSITION

LAUNCH DATE 1978

FIGURE 5-20

AVAILABLE 20 DAY PAYLOAD MAXIMIZED LAUNCH PERIODS – 1978 LAUNCH OPPORTUNITY

AVAILABLE 20 DAY PAYLOAD MAXIMIZED LAUNCH PERIODS

FIGURE 5-21

1978 LAUNCH OPPORTUNITY
AVAILABLE 30 DAY PAYLOAD MAXIMIZED LAUNCH PERIODS

AVAILABLE 30 DAY LAUNCH PERIODS
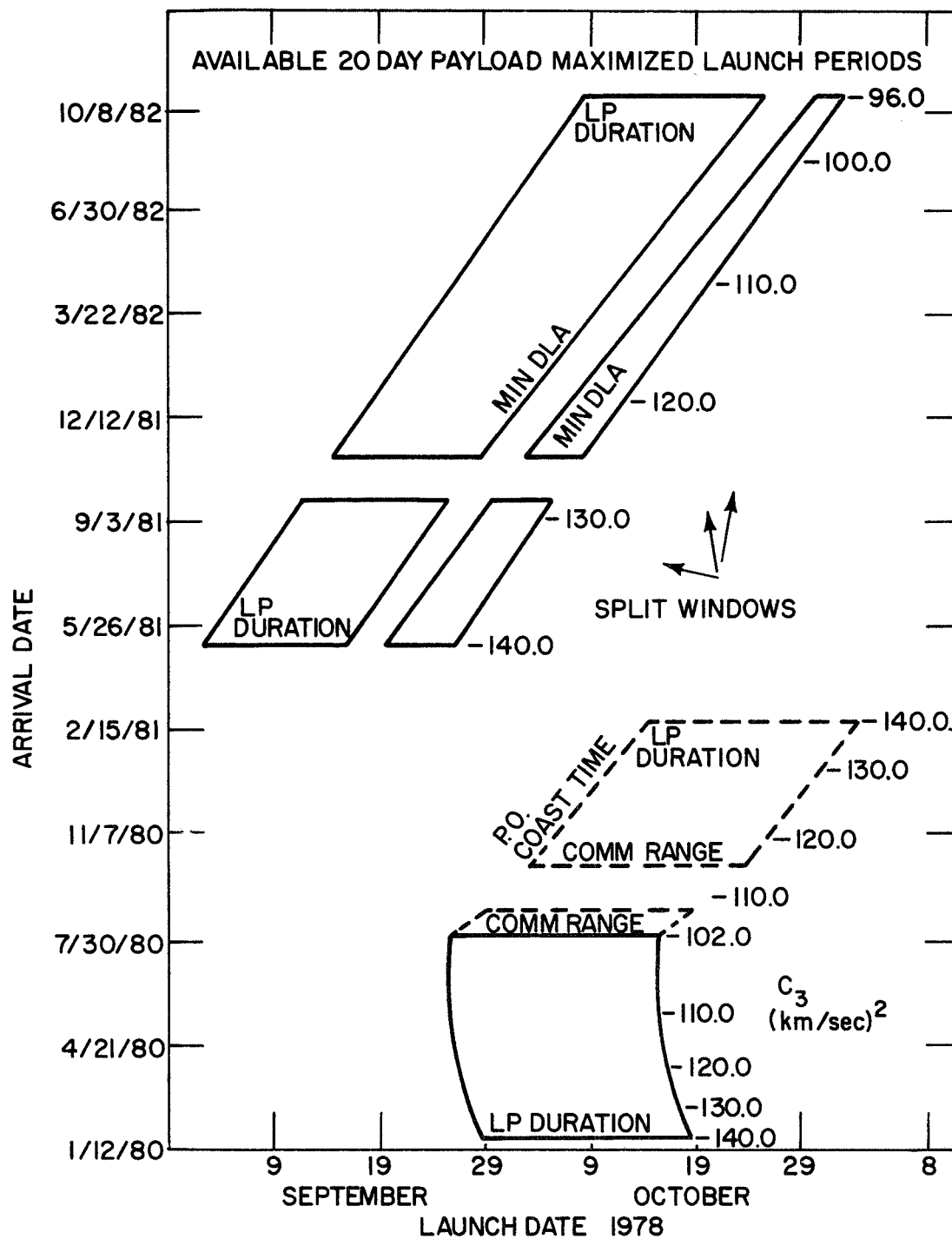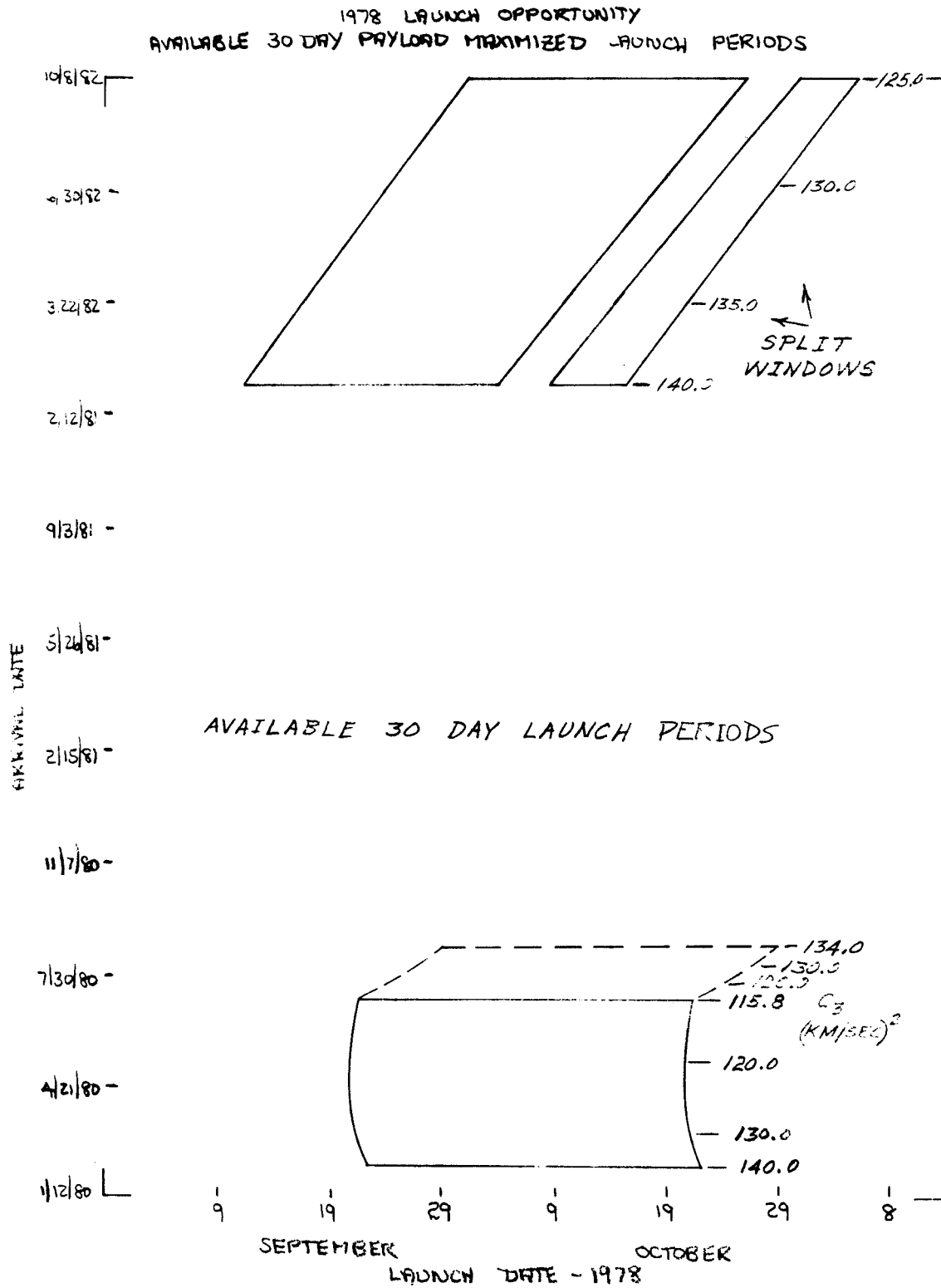
TABLE 5-7

SUMMARY 20 DAY LAUNCH PERIOD TRAJECTORY PARAMETERS - 1978
JUPITER LAUNCH OPPORTUNITY

SUMMARY 20 DAY LAUNCH PERIOD TRAJECTORY PARAMETERS 1978 JUPITER LAUNCH OPPORTUNITY

TYPE	LAUNCH DATE	ARRIVAL DATE	FLIGHT TIME (DAYS)	C_3 (KM²/SEC²)	DLA (DEG)	INCL (DEG)	APPROACH VELOCITY (KM/SEC)	ZAP (DEG)	GP (DEG)	R_C (10⁶ KM)
I	9/29-10/19	1/18/80	~466	140	~28	1.5	14.6	160	-1	690
	9/27-10/17	3/24/80	~534	120	~30	2.0	12.0	155	-1	677
	9/27-10/17	8/3/80	~666	102	~34	2.5	8.5	141	-2	937
	10/5-10/25	10/18/80	~734	120	~34	3.0	7.2	132	-3	943
	10/15-11/4	2/17/81	~846	140	~34	3.0	6.0	116	-3	698
II	9/3-9/27	5/18/81	~976	140	≤|23|	6.0	5.6	101	7	722
	9/15-10/19	11/2/81	~1132	120	≤|19|	6.0	5.5	83	7	958
	10/9-11/2	10/8/82	~1448	100	≤|9|	5.0	6.3	59	6	937

5-47

arrival date launch periods were selected because the magnitude and direction of the approach velocity vector tends to remain constant, which implies that the mission targeting is essentially unaltered by delays in the launch date. For the launch periods selected, the arrival dates vary from early 1980 to late 1982 with injection energies from 100 to 140 Km^2/sec^2 for both Type I and Type II transfer trajectories. For both Type I and Type II minimum energy trajectories ($C_3 \approx 100$ Km^2/sec^2) the communication range is near maximum at 937×10^6 Km. The major differences between the Type I and Type II minimum energy launch periods are: 1) the variation in the direction of the approach asymptote from 50 degrees in front of the morning terminator for Type I to 30 degrees behind for Type II, and 2) the approximate 800 day increase in the flight time for Type II transfers.

If the injection energy is constrained to a value of 140 Km^2/sec^2 or less ZAP angles between 160 and 116 degrees can be achieved with Type I transfers whereas, with Type II transfers, ZAP angles below 101 degrees can be realized. This allowable variation in ZAP angle with trajectory Type is extremely critical as will be shown in Section 6.1 in that it governs the location of probe entry for a fixed entry angle.

In conclusion, the same injection energies and encounter communication ranges can be realized with either Type I or Type II transfers, however, shorter transit times make Type I trajectory attractive from a reliability point while the low ZAP angles associated with Type II trajectories make them more attractive for shallow entry angle missions with entry in the vicinity of the sub solar point.

5.2.5 Launch Vehicle Performance

Launch vehicle data supplied by JPL for use in this study is presented in Figure 5-22. A tabulation of the launch vehicle performance for the injection energies employed in the reference launch period summary in the preceding section is presented in Table 5-8.

This information permits a qualitative assessment of the launch vehicle required when a 400 lb probe is mounted on the 550 lb Pioneer F/G or 1450 lb TOPS spacecraft. For operation in the vicinity of minimum injection energy (Type I or Type II) is is possible to employ either the 5 segment Titan IIID in combination with either the Agena E or Centaur D-IT upper stages for a probe mounted on the Pioneer F/G spacecraft. However, if the same mission were to be flown in the vicinity of maximum C_3

FIGURE 5-22

LAUNCH VEHICLE PERFORMANCE COMPARISON

T5 - TITAN IIID - 5 SEGMENT
T7 - TITAN IIID - 7 SEGMENT
C - CENTAUR D- 1T
A - AGENA - E
B - BURNER (2300)
V - VERSATILE UPPER STAGE
SC - STRETCHED CENTAUR
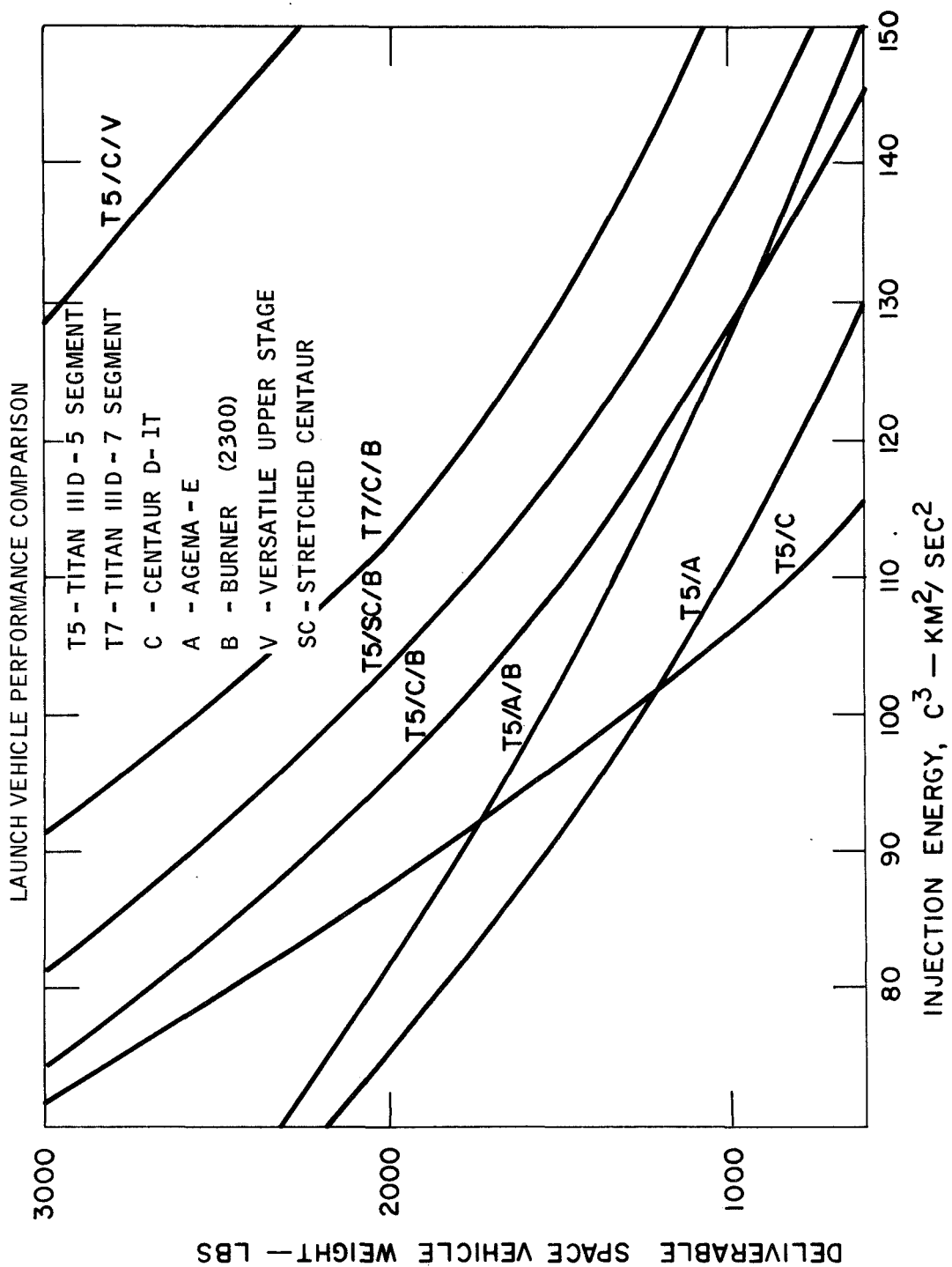
TABLE 5-8

FLIGHT ARTICLE WEIGHT

LAUNCH VEHICLE	INJECTION ENERGY, C_3 Km^2/sec^2		
	100	120	140
5 SEG TITAN IIID/AGENA E	1275 lb	810 lb	375 lb
5 SEG TITAN IIID/CENTAUR D-IT	1300	430	-
5 SEG TITAN IIID/AGENA E/BURNER II (2300)	1560	1150	790
5 SEG TITAN IIID/CENTAUR D-IT/B II (2300)	1810	1225	725
5 SEG TITAN IIID/STRETCH CENTAUR/B II (2300)	2125	1440	950
7 SEG TITAN IIID/CENTAUR D-IT/BII (2300)	2560	1770	1285
5 SEG TITAN IIID/CENTAUR D-IT/VERSATILE UPPER STAGE	-	3300 lbs.	2600

($140 \text{ Km}^2/\text{sec}^2$) because of encounter geometry requirements a 7 segment Titan IIID would be required with both a Centaur D-IT and Burner II (2300) upper stage. With a TOPS spacecraft either the 5 segment Titan IIID/ stretched Centaur/Burner II (2300) or the 7 segment Titan IIID/Centaur D-IT/ Burner II (2300) is required for operation in the vicinity of minimum energy and the 5 segment Titan IIID/Centaur D-IT /Versatile Upper Stage is needed if injection energies greater than $120 \text{ Km}^2/\text{sec}^2$ are employed.

5.3 COMMUNICATION LINK BOUNDARIES

5.3.1 Introduction

The performance of the communication system or any system for that matter is a function of the requirements imposed on the system and the constraints under which the system must operate. Typically for the communication link studies that were conducted, the requirements are imposed by the amount of data that is collected for transmission during the probe descent through the Jovian atmosphere; the constraints are imposed by both internal and external factors which tend to limit or confine the available range of the parameters for which the system may be designed.

During this study, two basic communication approaches were considered: 1) direct link to earth; and 2) relay link via spacecraft to earth. For each of these links, the transmission requirements are identical, however, since the constraining factors are significantly different, the resulting communication system performance can also be different. The objectives of this study were, therefore, to: 1) establish the communication system requirements; 2) define the constraints on the system parameters; and 3) show the communication system performance over the allowable range of the system parameters.

5.3.2 Data Transfer Requirements

The communication system data transfer requirements have been assessed for two science payloads, a nominal and a minimum payload. Profiles of the accumulated data as a function of time $x\sqrt{M/C_D A}$ is shown in Figure 5-23. For the nominal science payload, the data transfer requirement is shown to be about 27000 bits. The accumulated data prior to Mach 0.7 represents the accelerometer, magnetometer, ion mass spectrometer, and assorted engineering measurements. The data accumulation profile for the minimum science payload is shown to be about 6000 bits. The science return for this mission differs in that only ion mass spectrometer data is gathered

FIGURE 5-23

COMMUNICATION SYSTEM DATA TRANSFER REQUIREMENTS

$$(\text{TIME}) \cdot \left(\sqrt{\frac{m}{C_D A}}\right) \sim \text{SEC}\sqrt{\frac{\text{SLUG}}{\text{FT}^2}}$$

MACH 0.7
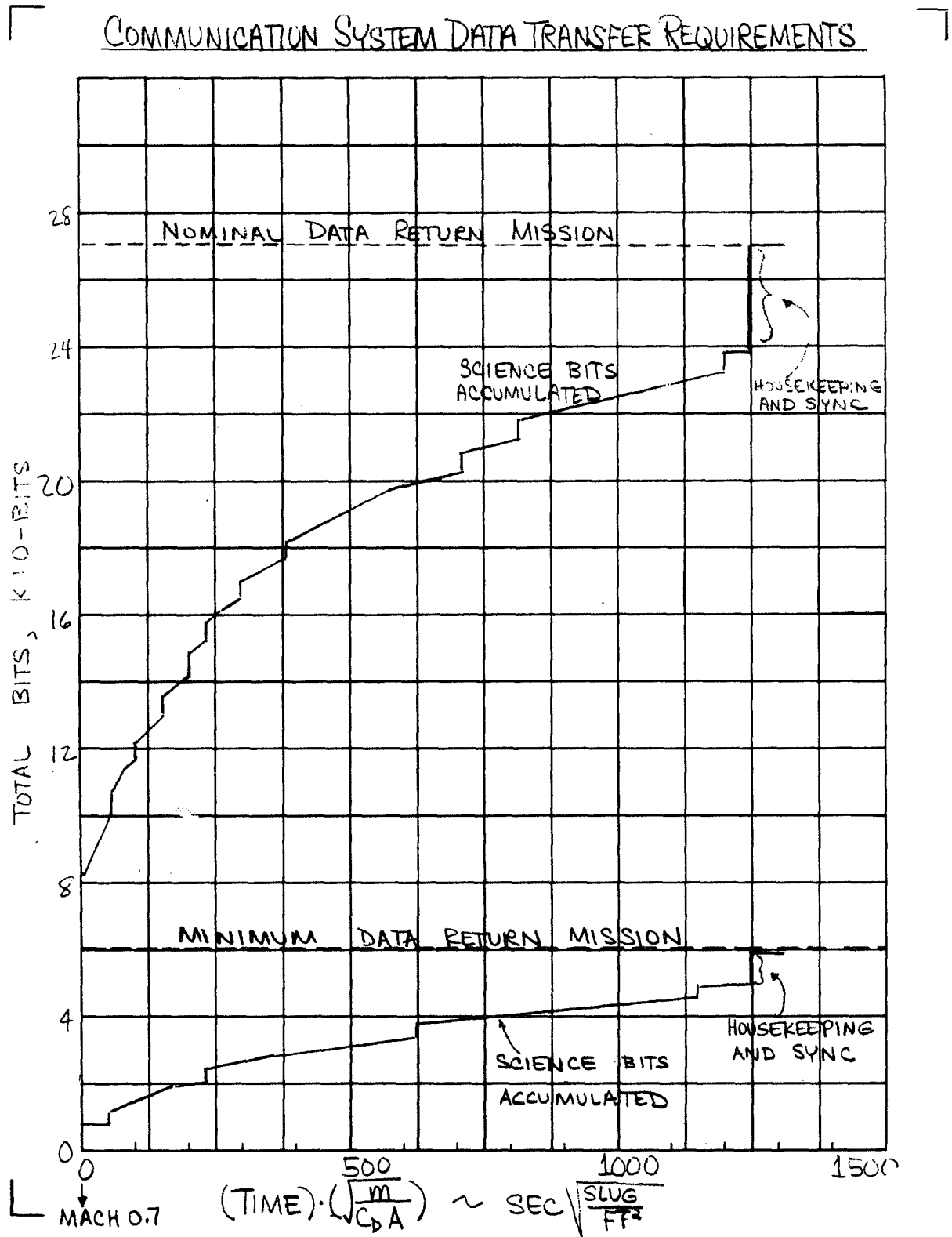
exo-atmospherically and also only limited samples of gas chromatograph and neutral mass spectrometer data along with pressure and temperature are gathered endo-atmospherically. The step increments (12 for the nominal payload, 4 for the minimum) shown in the data profile can be identified with the gas chromatograph measurements. Also included in these profiles are the housekeeping and synchronization data requirements which essentially amount to about 20% of the science data total. A more detailed description of the data samples, sampling rates and the overall data handling format is given in Section 8.1.

The requirement to transmit the bit totals of 27000 and 6000 for each payload translate into a second requirement; namely, data rate, when the probe descent time is considered. Figure 5-24 shows the data rate requirements to achieve a total playout of the accumulated data as a function of descent time for various fractions of the descent period. From a failure analysis point of view, it would be of definite advantage to playout all of the accumulated data as quickly as possible; and from Figure 5-24 the impact of a higher than required data rates to meet this objective can be assessed. For purposes of mission analysis, however, the 100% or minimum required data rate profile will be used as the reference for performing parametric tradeoff studies leading to mission and system configuration conclusions.

5.3.3 Communication System Study Objectives

The basic study objectives of a communication link study are to maximize the total data return and/or data rate within a given time period. However, since these communication related objectives may interact unfavorably with other system parameters, they must be compromised to the extent that all of the interrelated parameters are within acceptable operating boundaries. A summary of these communication system dependent mission parameters is shown in Table 5-9. Viable communication system performance, therefore, must be consistent with these parameter boundaries which, in turn, limit the degree to which the system may be optimized.

The various communication link alternatives that are considered include: 1) direct link to Earth; and 2) relay links via either a TOPS or Pioneer F/G spacecraft to Earth. Figure 5-25 shows these two communication link concepts and the degree of targeting flexibility that exists for each case. For direct links the primary concern is targeting the probe within the narrow band of longitudes which are characterized by having the Earth directly overhead. This targeting requirement to maintain near zenithal probe-to-earth look angles limits to a great extent the flexibility of the overall mission

FIGURE 5-24

Data Rate Requirements
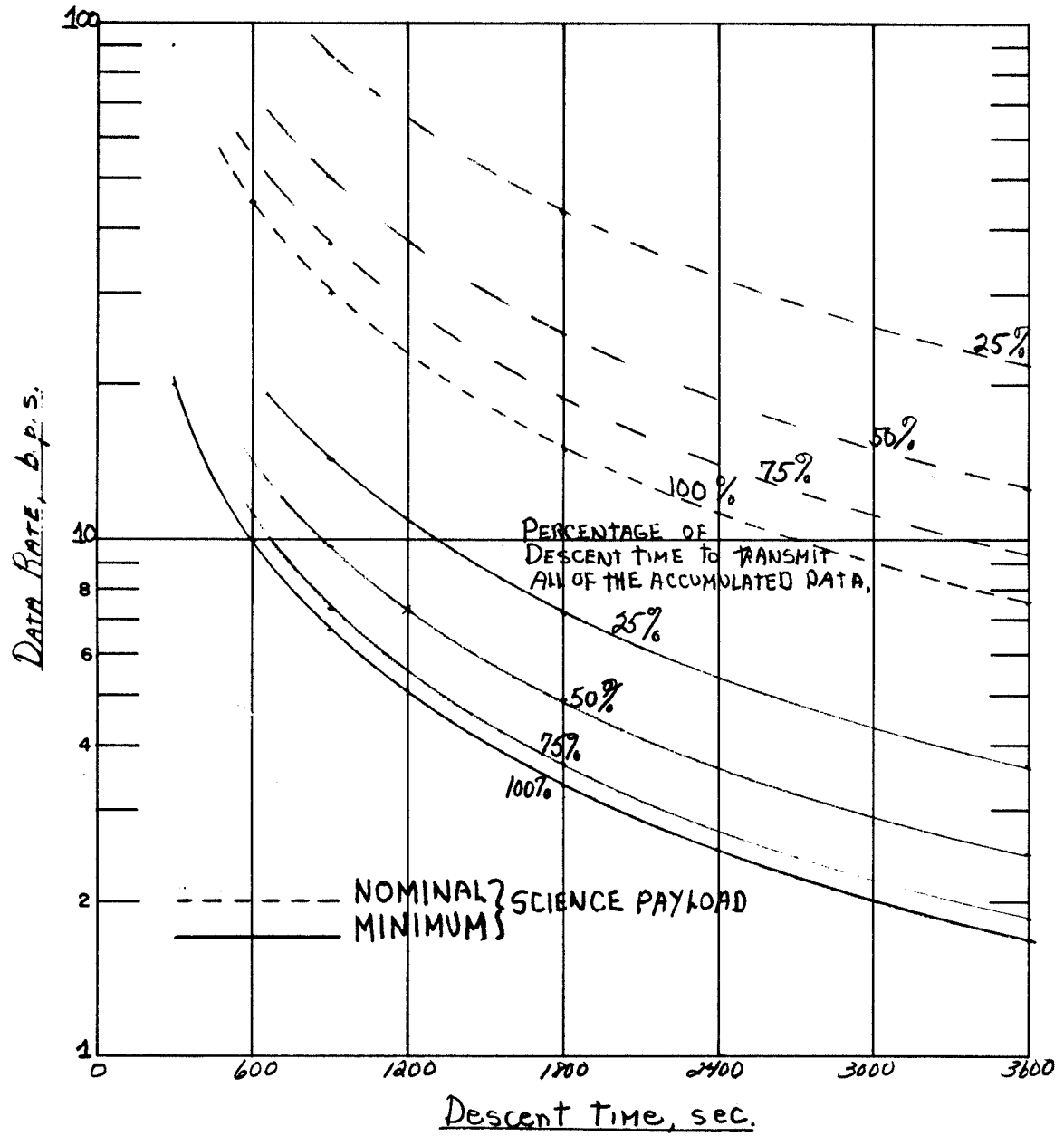
TABLE 5-9

SUMMARY OF COMMUNICATION DEPENDENT MISSION PARAMETERS

Parameter	Operating Boundaries	Criterion For Limits
Approach Velocity Vector Angle (ZAP)	— greater than 60°	Interplanetary transit time < 1300 days
Entry Angle	— less than 45°	Vehicle weight excessive
	— greater than 15°	Preclude skip out.
Probe Longitude For Dayside Missions		
Relay	— greater than 56° from the evening terminator	1 hour daylight mission
Direct	— Within +20° of sub solar point	location of sub earth vector
Descent time	— less than 1 hour	Instrument sampling requirements
	— greater than 15 min.	

5-55

FIGURE 5-25

Communication Link Alternatives

Direct Links

RANGE OF SUB-EARTH
VECTOR ON JUPITER

SUN

Relay Links

Case 1

S/C TRAJECTORY

PROBE TRAJECTORY

APPROACH VELOCITY VECTOR φ

APPROACH VELOCITY VECTOR ANGLE

RANGE OF APPROACH ANGLES

APPROACH VELOCITY VECTOR

SUN

RANGE OF ALLOWABLE TARGETING

Case 2

APPROACH VELOCITY VECTOR φ

PROBE TRAJECTORY

S/C TRAJECTORY
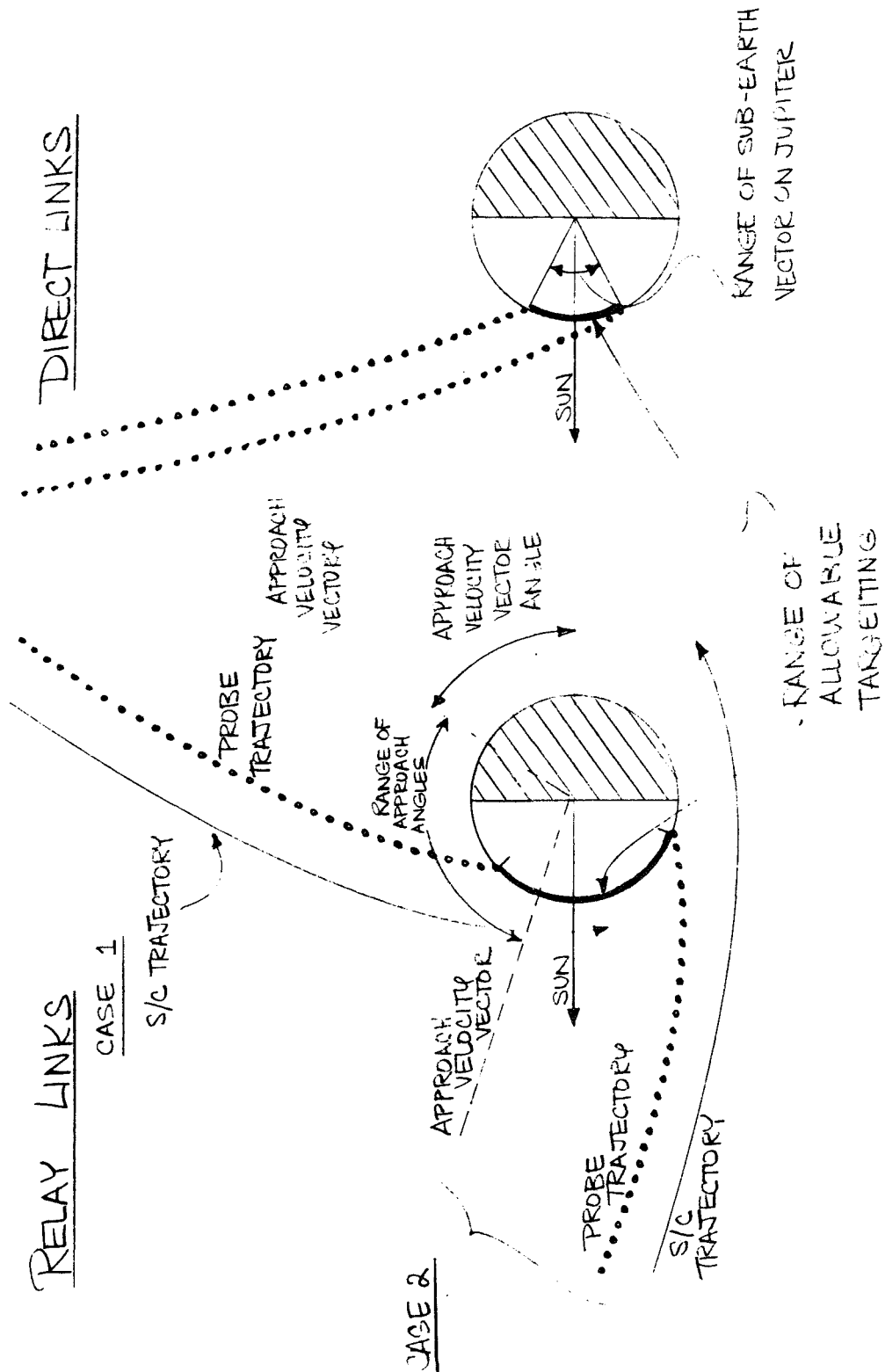
design. In contract, the relay links are not so severely constrained since near zenithal probe-to-spacecraft look angles can almost always be maintained by a proper selection of approach velocity vector angle/lead time combinations for a given probe entry longitude. Figure 5-25 shows the increased targeting flexibility (due mainly to the location of the approach velocity vector) of the relay link concept; also the probe look angles are essentially independent of the probe entry longitudes since with proper spacecraft placement, near zenithal look angles can be maintained throughout the mission. As a result of this targeting flexibility, relay link missions can be of the dayside or nightside variety where as only dayside mission are possible (if near zenithal look angles are required) for direct link missions. The communication study results to be presented in the following sections will describe the communication system performance for the different link alternatives; also shown will be the dependence of link performance on the parameters shown in Table 5-9 such that subsequent tradeoff analyses can be performed to synthesize candidate missions.

5. 3. 4 Direct Link Results

Many direct link mission alternative configurations have been evaluated during this study. A summary of these missions for differing opportunity, trajectory type, antenna configuration and DSN operating mode is shown in Table 5-10.

TABLE 5-10

Direct Link Mission Study Configuration

OPPORTUNITY	ANTENNA TYPE	DSN OPERATING MODE*			
		TRANSMIT S RECEIVE S/X	TRANSMIT S RECEIVE S	RECEIVE S ONLY	
'18	1	———	———	——	TURNSTYLE
'18	2	CONICAL REFLECTOR	CONICAL REFLECTOR	CONICAL REFLECTOR	TURNSTYLE
80	1	———	———	——	TURNSTYLE
80	2	CONICAL REFLECTOR	CONICAL REFLECTOR	CONICAL REFLECTOR	TURNSTYLE

* Selection of a particular DSN operating mode is based on the spacecraft link requirements (either T/M or tracking) during the probe descent phase.

5-57

From Table 5-10, it is shown that a total of 10 different link configurations were studied. The link objectives as they relate to these 10 configurations are: 1) conical reflector antenna cases were used for those links where communications capability of 27000 total bits was the design objective; and 2) turnstyle antenna cases were used for those links where reduced communications capability (6000 bit minimum) in lieu of shallower entry angles (Type II trajectories) or shorter interplanetary transit time was the design objective. For each of these 10 cases, however, the analysis was conducted such that definition of the shallowest entry angle missions could be made based on the two design data return requirements specified in Section 5. 3. 2.

Link Performance

The direct link mission performance based on the study assumptions and constraints and the results of the various link tradeoff studies (see Section 10. 1) is shown in Figure 5-26. This figure shows the sensitivity of data rate to entry angle for 1978 and 1980, Type I and Type II trajectories for a receive S-band only DSN mode. From Figure 5-26, the sensitivity of data rate to changes in the probe entry angles can be attributed to the fact that the probe entry longitudes are further displaced from the sub-earth longitude for shallower entry angles. This effect tends to reduce the link signal strength and available descent time to conduct the mission. The link configurations associated with the conical reflector antenna show significantly better performance than the turnstyle antenna, however, for minimum data return missions (identified by the symbol "o" in Figure 5-26) the turnstyle antenna can provide for a shallower entry angle mission.

Summary and Conclusions

A summary of the 10 direct link configurations with the appropriate mission and performance characteristics is shown in Table 5-11. It should be noted from Table 5-11 that the 10 link configurations can be sectioned off into two groups: 1) the nominal data return mission group associated with the conical reflector antenna; and 2) the minimum data return group associated with the turnstyle antenna. For Group 1 configurations, the range of resulting entry angles are from 29 deg to 39 deg which are considered moderately high. For Group 2 configurations, entry angle missions as high as 47 deg and as low as 15 deg can be achieved.

Based on the results of Table 5-11, the following conclusions can be drawn relative to direct link missions: 1) direct link missions are feasible; 2) the

FIGURE 5-26

DIRECT LINK MISSION PERFORMANCE

- 50 WATT XMTR
- DSN RECEIVE S-BAND ONLY MODE

80 TYPE II

78 TYPE II

NOMINAL DATA RETURN MISSION

TYPE II

80

78

78 80

TYPE I

——— CONICAL REFLECTOR ANTENNA

- - - - - TURNSTYLE ANTENNA

○ 6 K bits Cutoff.

DATA RATE, Kbps

ENTRY ANGLE (δe), DEG
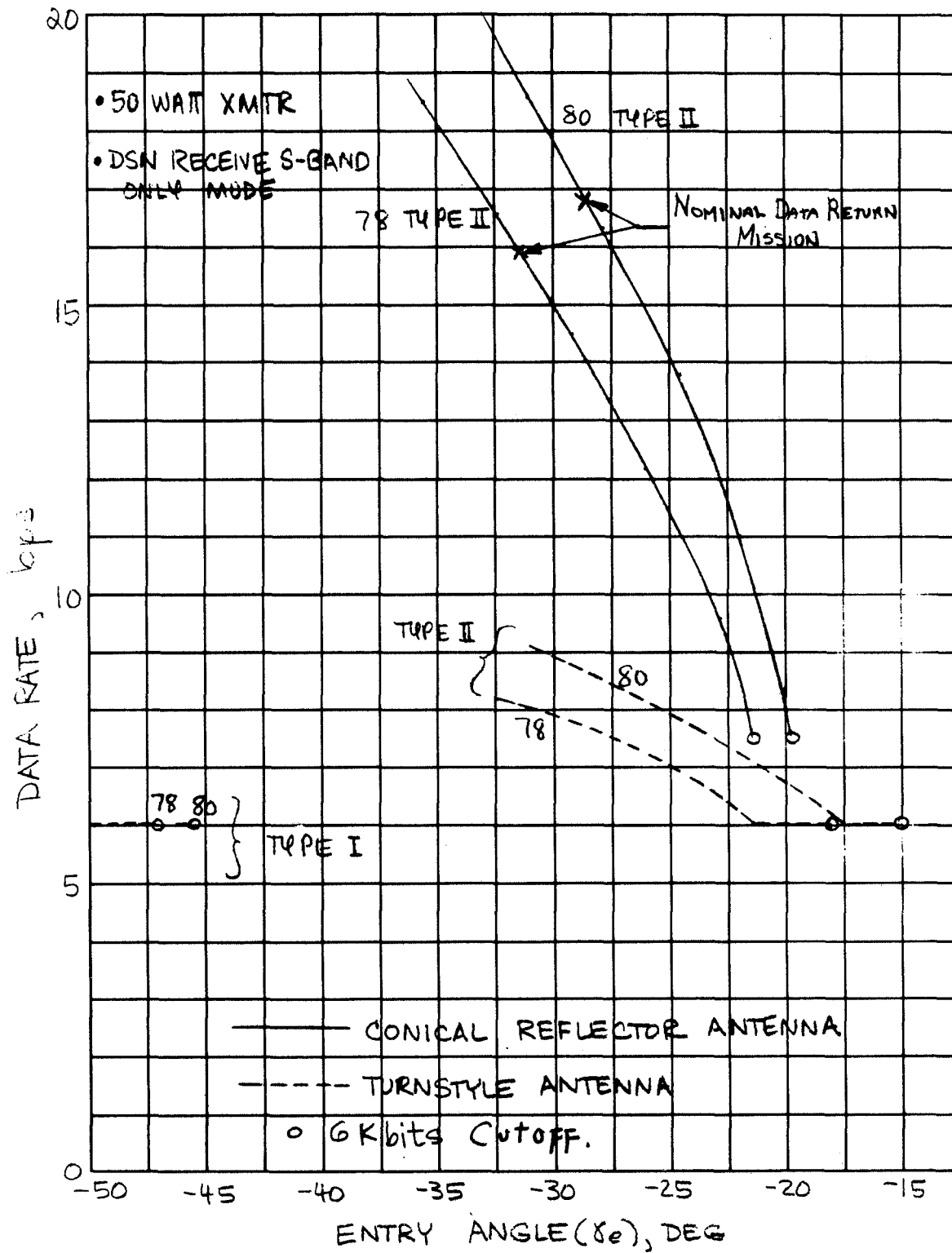
TABLE 5-11

DIRECT LINK COMMUNICATION SUMMARY

PROBE ANTENNA	DSN OPERATING MODE X/RECEIVE	DSN OPERATING MODE S/RECEIVE	DSN OPERATING MODE S/TRANSMIT	TRAJ. YEAR	TRAJ. TYPE	ARRIVAL DATE	FLIGHT TIME (DAYS)	PROBE ENTRY LONG. (DEG.)	PROBE ENTRY ANGLE (DEG.)	DATA RATE (bps)	DESCENT TIME (sec)	TOTAL BITS (bits)	COMMENTS
REFLECTOR	X	X	X	78	2	23 MAR 1982	1265	−6.0	−39.2	11.7	2300	27,000	NOMINAL DATA RETURN MISSION
	−	X	X					−2.1	−36.7	13.5	2000		
	−	X	−					6.2	−32.6	15.9	1700		
	X	X	X	80	2	30 MAY 1984	1384	−3.5	−36.2	12.8	2100		
	−	X	X					4.5	−31.5	15.0	1800		
	−	X	/					8.0	−29.0	16.8	1600		
TRANSMIT	−	X	−	78	1	15 FEB 1981	844	26.9	−47.2	6.0	1000	6000	MINIMUM DATA RETURN MISSION
	−	X	−	78	2	23 MAR 1982	1265	27.8	−18.0				
	−	X	−	80	1	2 MAY 1983	864	28.5	−46.6				
	−	X	−	80	4	30 MAY 1984	1384	29.5	−15.2				

1980 launch opportunity is more favorable than the 1978; 3) Type II trajectories with moderate entry angles are required to achieve the nominal data transfer objectives; 4) shallow entry angle missions (~-15 deg) can be achieved, however, reductions in data return must be accepted; 5) missions with interplanetary flight times of 800 days or less require probe entry angles to be in excess of 45 deg; and 6) the DSN operating mode as necessitated by spacecraft requirements plays a significant role in the overall mission performance.

System Description

The probe communication system characteristics upon which the above performance summary and conclusions are based are listed in Table 5-12.

A. Probe Transmitter

A probe transmitter power level of 50 watts was the basis for this study. This power rating and efficiency is considered consistent with the state of the art technology for 1975 solid state transmitters.

B. Antenna Systems

Two candidate antenna systems were evaluated for the direct link studies. Both of these concepts are considered to be of the simple variety since no beam switching or adaptive steering techniques are employed. A summary of the antenna characteristics is shown in Table 5-12, however, further detail on the antenna design and performance is included in Section 8.6.1.

C. Link Frequency

The S-band downlink frequency is selected for this mission as opposed to X-band based on a frequency trade-off study shown in Section 10.

D. Modulation Scheme

The selected modulation scheme for this link is a coherent coded type. Based on the modulation scheme tradeoff studies (Section 10), it was determined that this approach led to the most efficient communication subsystem.

E. Data Rate

Data rates for the probe transmission system will range from 6 to 17 bits depending on the selected link configuration.

TABLE 5-12

Probe Communication Subsystem Characteristics

Probe transmitter

Type	Solid State	
Power Level	50 watts minimum	
Efficiency	25%	

Antenna System

Type	Conical Reflector	Turnstyle
Peak Gain	7.7 db	4.4 db
Beam Peak	on axis	40° off axis
Aperture (max)	11"	12"
Circuit Losses	.5 db	.5 db
Gain Tolerance**	.5 db	.5 db

Link Frequency	S-Band
Modulation Scheme	Coherent Convolutionally Encoded $(r=\frac{1}{2})$
Data Rate*	6 > 17 b.p.s
Total Data Transfer	6000 or 27000 bits

*Function of the link configuration.
** In addition to a 20° angular tolerance for dynamics and dispersions

5.3.5 Relay Link Results

Summary of Mission Alternatives

The various baseline missions that were considered for relay link studies include: 1) a TOPS spacecraft flyby mission; 2) a Pioneer spacecraft flyby mission; and 3) a TOPS J-U-N mission. For each of these cases, the studies were conducted such that a range of probe entry longitudes/entry angles were evaluated consistent with the range of probable dayside and nightside missions. A matrix of the various link configurations that constituted the relay link studies is shown in Table 5-13.

TABLE 5-13

Relay Link Mission Configurations (78, 79, 80)

MISSION		ANTENNAS	TRAJECTORY			
			TYPE 1		TYPE 2	
			DAY	NIGHT	DAY	NIGHT
TOPS	FLYBY	PROBE	←———— CONICAL REFLECTOR ————→			
		S/C	←———— ELLIPTICAL DISH ————→			
	J-U-N	PROBE	/////	CONICAL REFLECTOR	///////	///////
		S/C	/////	CIRCULAR DISH	///////	///////
PIONEER F/G		PROBE	←——— OPEN ENDED WAVEGUIDE ———→			
		S/C	←——— CIRCUMFERENTIAL ARRAY ———→		AXIAL DISH	CIRCUM. ARRAY

The above link cases can generally be considered independent with launch opportunity (1978 and 1980) since for these two years the resulting approach velocity does not significantly differ. From Figure 5-27 it can be noted that a system configured for a TOPS flyby mission is independent of the trajectory and the science (day/night) features of that mission; however, for the Pioneer F/G cases, it is shown that the S/C receiving system antenna differs for a Type II day mission as compared to the other combinations. This occurs due to the fact that for the spinning Pioneer F/G spacecraft, consideration must be given as to whether the line of sight between probe and spacecraft

FIGURE 5-27

RELAY LINK MISSION PERFORMANCE

	FREQ.	TRANSMIT POWER	DESCENT TIME
TOPS	S	25W	1 HR
PIONEER	L	50W	1 HR
J-U-N	S	50W	½ HR

TOPS FLYBY

PIONEER FLYBY

J-U-N

MINIMUM DATA RATE REQUIRED

DATA RATE, bps

ENTRY ANGLE, DEGREES
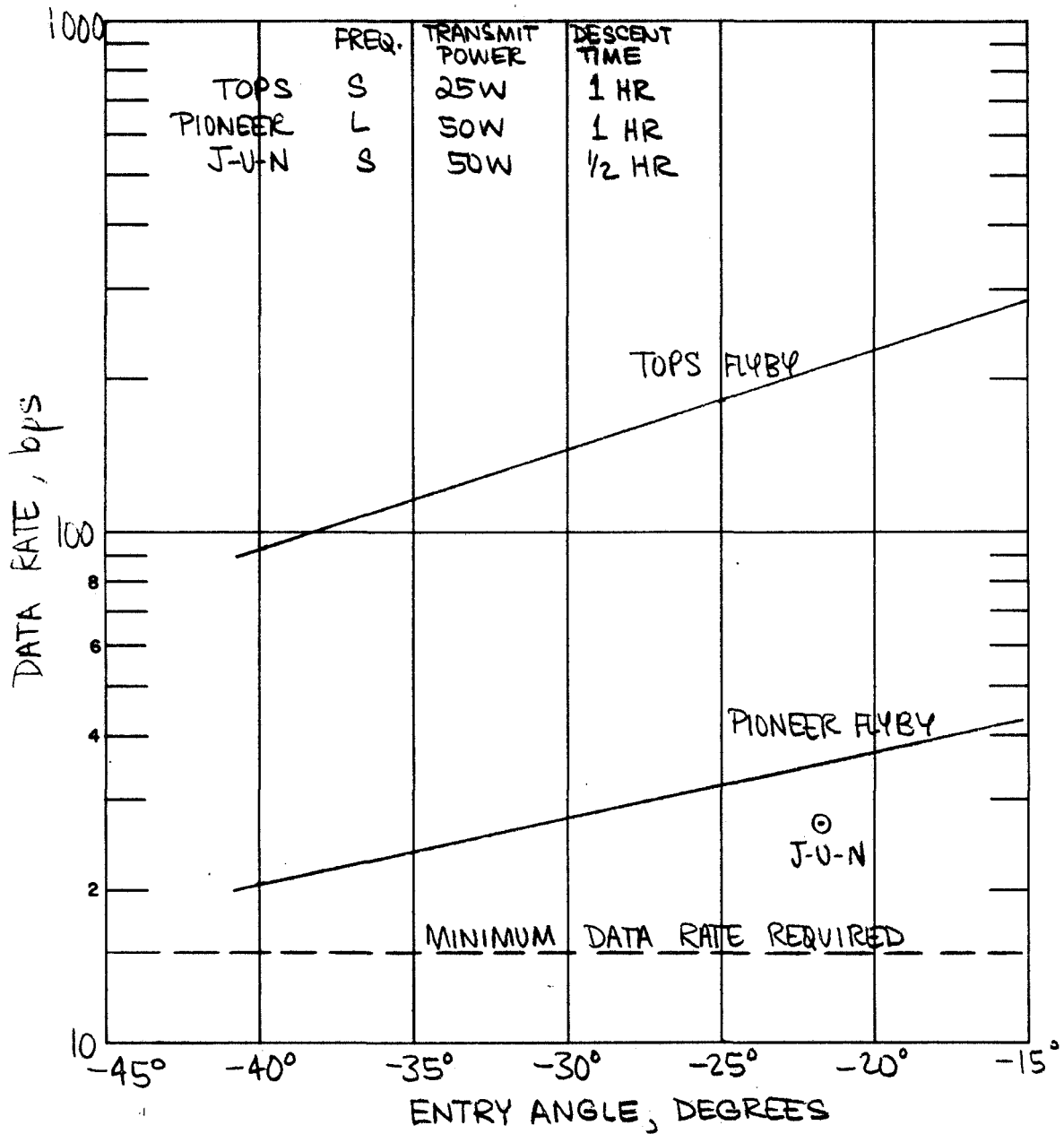
is either parallel or normal to the spin axis of the spacecraft. For the J-U-N mission, only a Type I trajectory was considered due to external restriction; also it was immediately determined that dayside missions would result in excessive entry angle requirements and, therefore, this type mission was discounted from further consideration. In conducting the relay link analysis for these various alternative missions, tradeoff studies were conducted such that the achievable data rates for a given entry angle mission were maximized. The key parameters involved in this tradeoff were: 1) the periapsis radius of the flyby spacecraft; and 2) the spacecraft lead time. Details of the relay link analysis are related tradeoff studies are included in Section 10.2.

Link Performance

Relay link mission performance is shown in Figure 5-27 for the TOPS and Pioneer F/G flyby missions as a function of probe entry angle, and as a single data point for the J-U-N mission. The Pioneer F/G performance shown is based on the circumferential array antenna configuration. No link could be established within the assumed ground rules for the axial antenna and, therefore, Pioneer F/G spacecraft Type II dayside missions were re-evaluated for the circumferential array configuration; this re-evaluation led to realizable Type II dayside missions, however, probe targeting was by necessity limited to $\sim 20^\circ$ of longitude. The results of Figure 5-27 show that the TOPS flyby mission provides the highest performance; this is simply due to the fact that the TOPS spacecraft relay link receiving antenna requirements can be satisfied by a high gain narrow beam elliptical dish. The spinning Pioneer F/G spacecraft on the other hand requires both a despun antenna concept (for missions where the line of sight vector is normal to the spin axis) and considerably larger beamwidth requirements than the TOPS spacecraft. The lower data rate performance of the J-U-N mission can be associated with the fact that this mission is constrained to flyby the planet at 6.8 planetary radii periapsis radius.

The results shown in Figure 5-27 indicate a trend of decreasing data rate capability with increasing entry angle. The two effects which give rise to this trend are: 1) the location of the periapsis point on the planet; and 2) spacecraft lead time dispersions. For steep entry angle missions, the probe descent longitudes are generally further displaced from the longitude at which the spacecraft makes its closest approach to the planet, thereby creating increased communication ranges. Also, lead time dispersions increase with steeper entry angles (mainly due to increased in plane angular errors in probe attitude) thus causing further link degradations due to increased beamwidth requirements.

Summary and Conclusions

Applying the results of Figure 5-27 to specific spacecraft missions is shown in Table 5-14. Summarized in this table are a number of TOPS and Pioneer F/G spacecraft missions identified for different opportunities, trajectory types, and scientific objectives.

In all of the cases shown in the table, the link capability is more than adequate to meet the data requirements of 27000 bits. The range of entry angles covered by these missions extend from -15 deg (the shallowest allowed) to a maximum of -33.2 deg. For all of these missions, the constraint imposed on targeting was not forced by a communication requirement but rather was imposed by a dayside descent requirement. Total data transfer for these missions range from a minimum of 48,600 bits for the J-U-N mission to a maximum of over 1 million bits for selected TOPS spacecraft flyby missions.

Major study conclusions drawn from these results indicate that: 1) TOPS flyby spacecraft performance is generally superior to that of the Pioneer F/G spacecraft; 2) the 1980 opportunity is generally equal to or better than the 1978 opportunity; 3) Type II trajectories can provide for 1 hour of dayside descent in combination with a low entry angle mission; 4) Type I trajectories and dayside descent missions require moderate entry angle missions; 5) a J-U-N mission can be realized for low entry angles, however, only 1/2 hour of nightside descent can be provided; and 6) for all of the missions studied, communications capability is more than adequately satisfied by any of the link configurations studied.

System Description

The probe transmitting and spacecraft receiving system characteristics for which the relay link performance is based are listed in Table 5-15.

A. Probe Transmitter

Probe transmitter power levels of 25 and 50 watts were utilized in synthesizing relay link missions. It was found that TOPS flyby missions could provide adequate performance for a 25 watt power level, however, in order to provide for a sufficient margin of safety, a 50 watt level was utilized for Pioneer F/G flyby and J-U-N missions.

TABLE 5-14

RELAY LINK COMMUNICATIONS SUMMARY

SPACECRAFT MISSION	TRAJECTORY	DAY OR NIGHT	PROBE ENTRY: LONG.	PROBE ENTRY: ANGLE	DATA RATE (bps)	DESCENT TIME (secs)	TOTAL BITS	COMMENTS
TOPS	78 I	DAY	+50°	-33.2°	125.	1800	225,000	1/2 HR OF DAYLIGHT DESCENT
		NIGHT	+102°	-14.9°	282.	3600	1,015,200	MINIMUM ENTRY ANGLE MISSION
	78 II	DAY	+23°	-14.9°	282.	3600	1,015,200	*
		NIGHT						NOT OF INTEREST
FLYBY	80 I	DAY	+50°	-25.7°	175.	1800	315,000	BETTER THAN 1978 TYPE I
		NIGHT	+101°	-14.9°	282.	3600	1,015,200	SAME AS 1978 TYPE I
	80 II	DAY	+25°	-15.0°	218.	3600	1,015,200	*
		NIGHT						NOT OF INTEREST
TOPS JUM	79 I	NIGHT	+100°	-21.7°	27.	1800	48,600	1/2 HR OF NIGHTSIDE DESCENT
PIONEER	78 I	DAY	+50°	-33.2°	75.	1800	135,000	1/2 HR OF DAYLIGHT DESCENT
		NIGHT	+103°	-14.9°	43.	3600	154,800	MINIMUM ENTRY ANGLE MISSION
	78 II	DAY	+25°	-14.9°	43.	3600	154,800	*
		NIGHT						NOT OF INTEREST
FLYBY	80 I	DAY	+34°	-30°	27.5	3600	99,000	BETTER THAN A78 TYPE I
		NIGHT	+103°	-15°	43.	3600	154,800	SAME AS A78 TYPE I
	80 II	DAY	+25°	-15°	43.	3600	154,800	*
		NIGHT						NOT OF INTEREST

* LOW ENTRY ANGLE MISSION WITH 1 HOUR OF DAYLIGHT DESCENT

TABLE 5-15

Probe and Spacecraft System Characteristics

	TOPS	J-U-N	Pioneer F/G
Probe Transmitter			
Type	←	Solid State —	➤
Power Level, watts (min)	25	50	50
Efficiency	←	25%	>
Link Frequency	S-Band	S-Band	L-Band
Probe Antenna System			
Type		Conical Reflector	Open Ended Waveguide
Peak Gain		7.7 db	
Beam Peak		On axis	
Max Aperture		11"	
Circuit Losses		1/2 db	
Gain Tolerance		1/2 db	
Angular Tolerance *		15°	
Modulation Scheme			
Type		Coherent Biorthogonal Coded (n = 6)	
Word Error Rate		$\simeq 10^{-2}$	
Receiving Antenna System			
Type	Elliptical Dish	Circular Dish	Despun Circumferential Array
Peak Gain	24.5 db	27.0 db	15.0db
Beamwidth (3 db)	7° x 10°	7° x 7°	12° x 30°
Max Aperture Dimension	41"	41"	48.6"
Receiver Noise Figure	←	5 db	➤
Data Rates (max) b.p.s.	282	27.5	75.0
Total Data Transfer (max)	1,015,200	48,600	154,800

* Allowance for dynamics only; position dispersions included separately.

B. Link Frequency

Based on the frequency selection tradeoff study reported upon in Section
10.2, it was determined that TOPS flyby and J-U-N missions favored an
S-band frequency whereas the Pioneer F/G flyby missions were optimized
for L-band frequencies. The basic reason for this difference is the fixed
beamwidth requirement; since TOPS spacecraft receiving antenna beam-
width requirements are less than Pioneer F/G, the frequency at which
this beamwidth and the maximum aperture constraint is reached is higher
than that for the Pioneer F/G spacecraft.

C. Probe Antenna Systems

Two relay link antenna concepts applicable to the S and L-band frequency
mission have been evaluated. Again as was the case with the direct link,
only simple antenna concepts were explored; however, for the relay link
cases, both antennas were designed to provide a beam peak on the probe
axis since the flexibilities in spacecraft position provides the necessary
freedom to maintain nearly overhead line of sight conditions. Further
details on the antenna design and performance is included in Section 8.6.2.

D. Modulation Scheme

The favored modulation scheme for the relay link studies was taken as
coherent biorthogonal coded (6 bit word). The performance identified for
these links is based on maintaining a word error rate lower than 1 in 100.
Section 10.2 of this report presents further details relative to this tradeoff
selection.

E. Receiving Antenna System

The receiving antenna type and performance characteristics selected for the
three missions is shown in Table 5-15. The 3 db antenna beamwidths
shown are consistent with maintaining look angle coverage throughout the
descent phase of the mission and also to include angular uncertainties
resulting from probe targeting and lead time dispersions. None of these
antennas are designed to track the probe, however, it is a design require-
ment that the S/C to probe look angles are never outside the antenna 3 db
beamwidth. All of these antennas to some extent, however, track the planet;
the TOPS and J-U-N missions are based on an antenna pointing direction
which is consistent with tracking the center of the planet. The Pioneer F/G
missions assume tracking in the roll plane (hence despun), however, no

continuous tracking axially is assumed. To maintain realistic gain levels for Pioneer missions, it was found necessary to provide for a re-pointing of the antenna beam in the axial plane. This redirected beam approach is designed to occur only once, about halfway in the descent phase. More details relative to these antenna characteristics can be found in Section 8. 6. 2.

5. 3. 6 Communication Link Study Conclusions

In comparing the results of relay and direct link communication capability and related misssion requirements to following overall conclusions are made: 1) relay link missions generally offer a wider range of targeting and also provide for more than adequate communications capability even for shallow entry angle missions; 2) direct link missions are limited in targeting to the vicinity of the sub-earth vector, however, feasible missions (moderate entry angles) can be realized to meet the nominal data transfer requirements; 3) for direct link, it was found that the communications requirement constrained the mission characteristics, while for the relay links, other factors such as science requirements constrained the mission characteristics; and 4) relay link performance can also be considered consistent with other engineering factors that favor shallow entry angle missions; direct link performance, however, differs in this respect since improved communication performance increases with steeper entry angle missions.

5. 4 REFERENCES

1. Earth-Jupiter Geometry, Memo 5-I, Jupiter Atmospheric Probe Study, Section F930, January 1971, Avco Systems Division.

2. Launch Period Selection - 1978 Opportunity, Memo 5-II, Jupiter Atmospheric Probe Study, Section F930, January 1971, Avco Systems Division.

6.0 MISSION SELECTION PROCESS

6.1 MISSION TRAJECTORY TRADEOFFS

This section provides the parametric data to perform tradeoffs with respect to C_3, ZAP angle, entry angle, entry location, probe/spacecraft weight, and launch vehicle requirements. The data is developed and presented in such a fashion that any parameter can be utilized as a starting point with acceptable ranges or specific values of the remaining parameters defined.

6.1.1 Entry Angle-Entry Location-ZAP Angle Tradeoffs

If a probe is separated from the spacecraft at a sufficiently large distance from the planet (infinity with respect to the hyperbolic approach trajectory), there is a unique relationship between the range angle traversed by the probe from separation to entry and the probe inertial entry angle. This relationship is defined in Figure 6-1 for hyperbolic approach velocities of 4 Km/sec and 15 Km/sec which bracket the range of approach velocities to Jupiter on Type I or Type II transfer trajectories during the 1978, 1979, and 1980 launch opportunities. These results indicate that when range angle traversed is 0 degrees, the resulting inertial entry angle is 90 degrees. To realize an inertial entry angle of -20 degrees the probe must traverse a range angle between 120 and 130 degrees depending upon the specific approach velocity. Thus qualitatively it can be seen that with fast Type I transfer trajectories with a ZAP angle of 160 degrees (approach 20 degrees in front of the subsolar point from the leading edge) that shallow entry angles can only be realized with probe entry location in the vicinity of the evening terminator, whereas, with a slow Type II transfer trajectory with a ZAP angle of 60 degrees (approach 30 degrees behind the morning terminator) shallow entry angle result for entry in the vicinity of the sub-solar point.

Since Jupiter rotates once every 9.84 hrs. there is a significant difference between the inertial and relative entry angles as illustrated in Figure 6-2 for entry in the equatorial plane. For example, an inertial entry angle of -16 degrees results in a relative entry angle of -20 degrees.

Considering the relationship between the range angle traversed from separation to entry and the inertial entry angle, in addition to the relationship between the inertial and relative entry angles for equatorial entry, it is possible to relate ZAP angle, entry location relative to sub-solar point

FIGURE 6-1

RANGE ANGLE FROM SEPARATION TO ENTRY

6-2
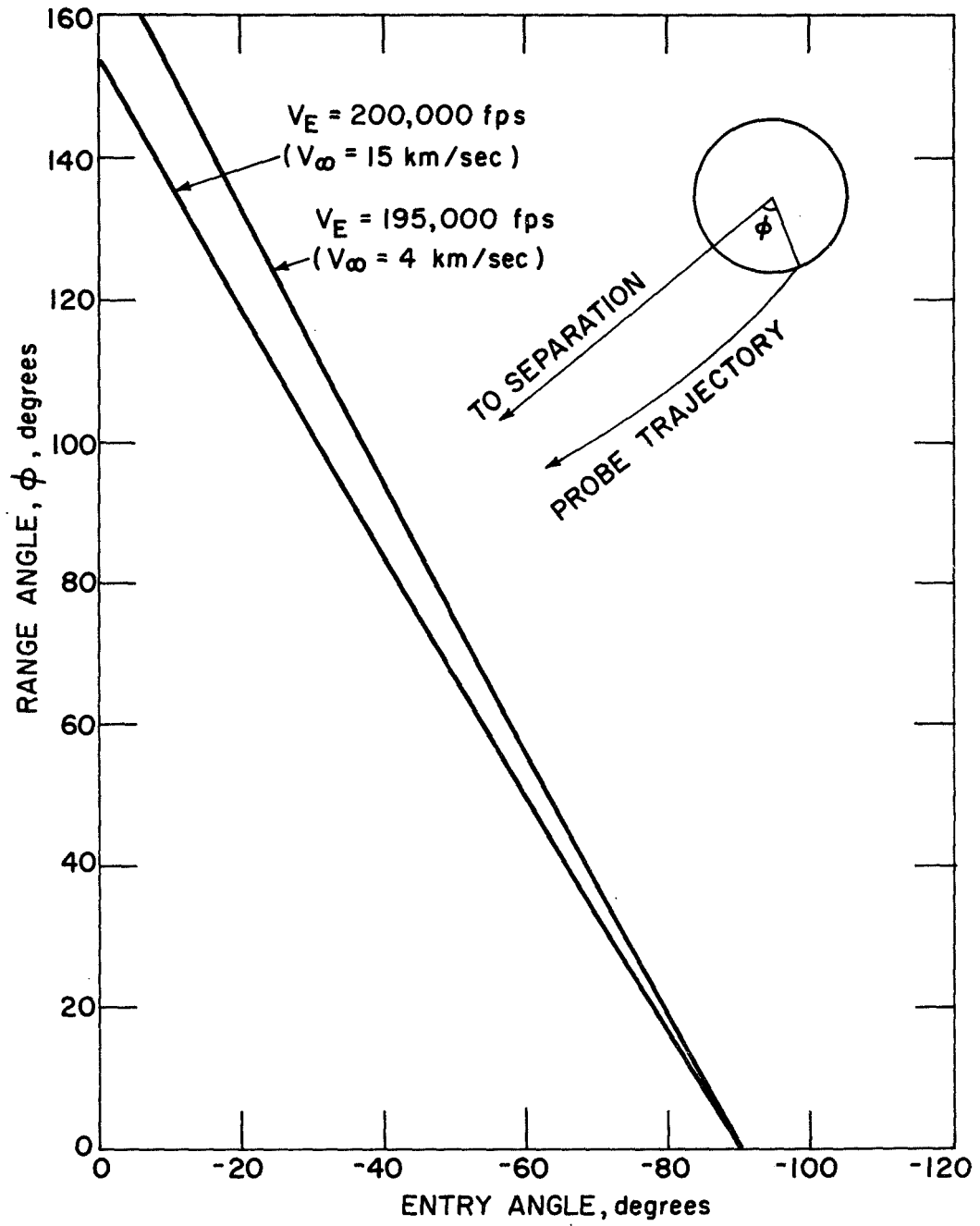
FIGURE 6-2

VARIATION OF RELATIVE ENTRY ANGLE WITH INERTIAL ENTRY ANGLE
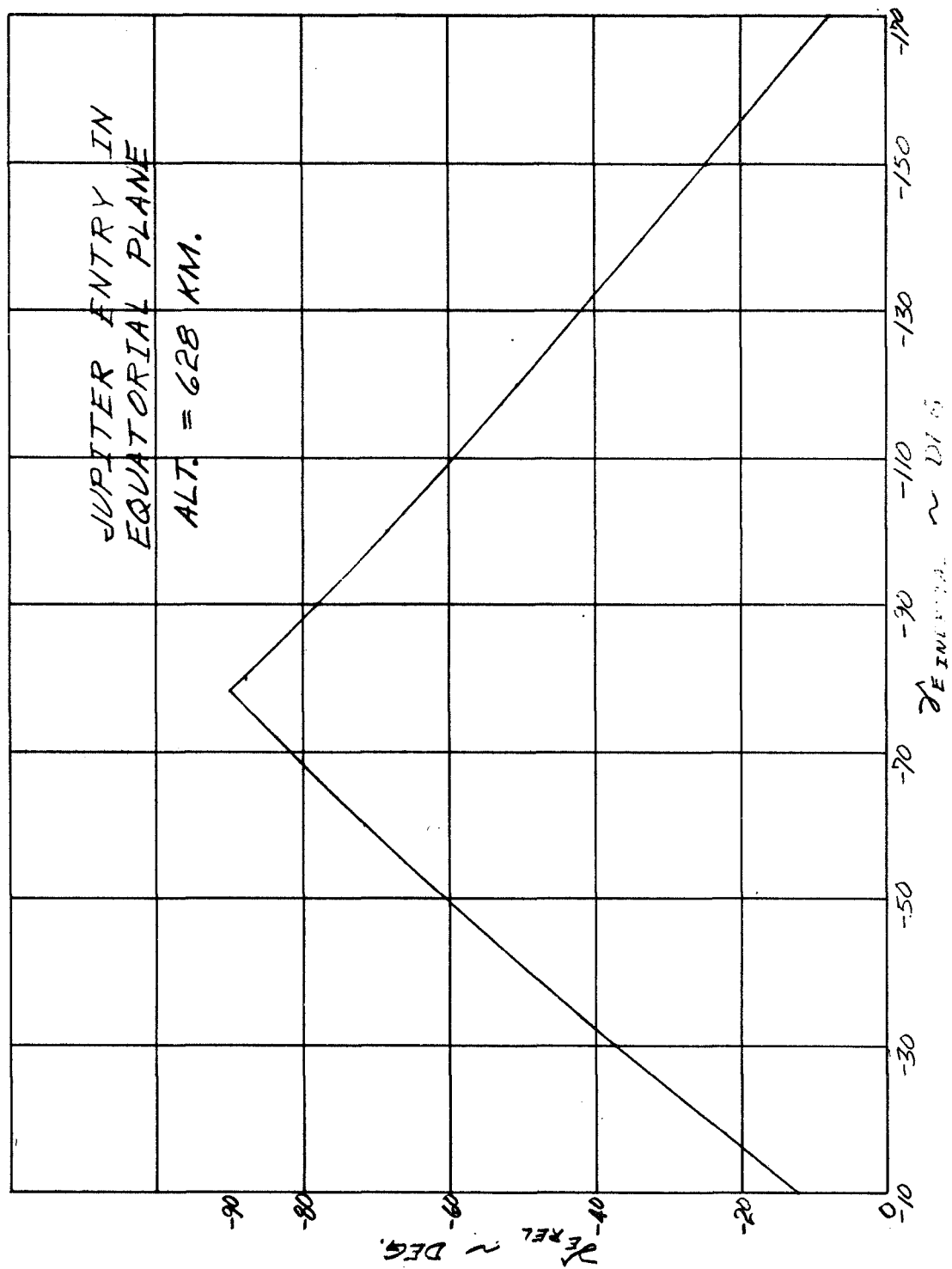
longitude, and the relative entry angle. This relationship is presented in Figure 6-3 and permits tradeoffs to be evaluated between the range of ZAP angles that can be realized from the transfer trajectories, entry locations of scientific interest, and entry angles that can be achieved with reasonable engineering considerations. For example in 1978, the range of ZAP angles that can be obtained with 20 day launch period Type I trajectories varies between 116 to 160 degrees whereas with the significantly slower Type II transfers ZAP angles between 60 and 101 degrees result. If it is desirous to maintain the entry angle to values shallower than -20 degrees from engineering considerations such as loads, heating, etc., the probe is, therefore, constrained to enter at locations from 40 degrees in front of the evening terminator to 30 degrees behind the evening terminator for Type I transfers, and from the vicinity of the sub-solar point to 30 degrees in front of the evening terminator for Type II transfers. These relationships confirm the fact that the scientific objectives and engineering constraints can play a major role in the launch period selection by virtue of their role in the specification of a range of acceptable ZAP angles which, in turn, essentially define both the launch and arrival dates.

6.1.2 ZAP Angle-Injection Energy-Launch Period Duration Tradeoffs

For fixed arrival date launch periods, a relation between the ZAP angle and injection energy can be established where the magnitude of the injection energy is dependent upon the duration of the launch period. Table 5-7 defined this relationship for a 20 day duration launch period for both Type I and Type II transfer trajectories during the 1978 launch opportunity. Similar data is provided in Figures 6-4 to 6-6 for 1, 10, and 20 day duration launch periods for the 1978, 1979, and 1980 launch periods, respectively. In these figures both Type I and Type II transfers are considered, however, the data is presented which minimizes the injection energy if the ZAP angle can be realized with either a Type I or a Type II transfer and the inflection in the curves in the vicinity of a ZAP angle of 100 degrees is the separation between Type I and Type II transfers. These results indicate that for ZAP angles less than 140 degrees (minimum energy Type I transfer trajectories) there is a significant reduction in the injection energy requirements as the launch period duration is reduced. This, in turn, provides additional flexibility in the launch vehicle selection to be discussed later.

For 20 day duration launch periods this data has been assembled for the 1978, 1979, and 1980 launch periods in Figure 6-7 to illustrate the sensitivity of launch opportunity. These results show that the injection energy requirements

FIGURE 6-3

ENTRY ANGLE – ENTRY LOCATION – ZAP ANGLE TRADEOFFS
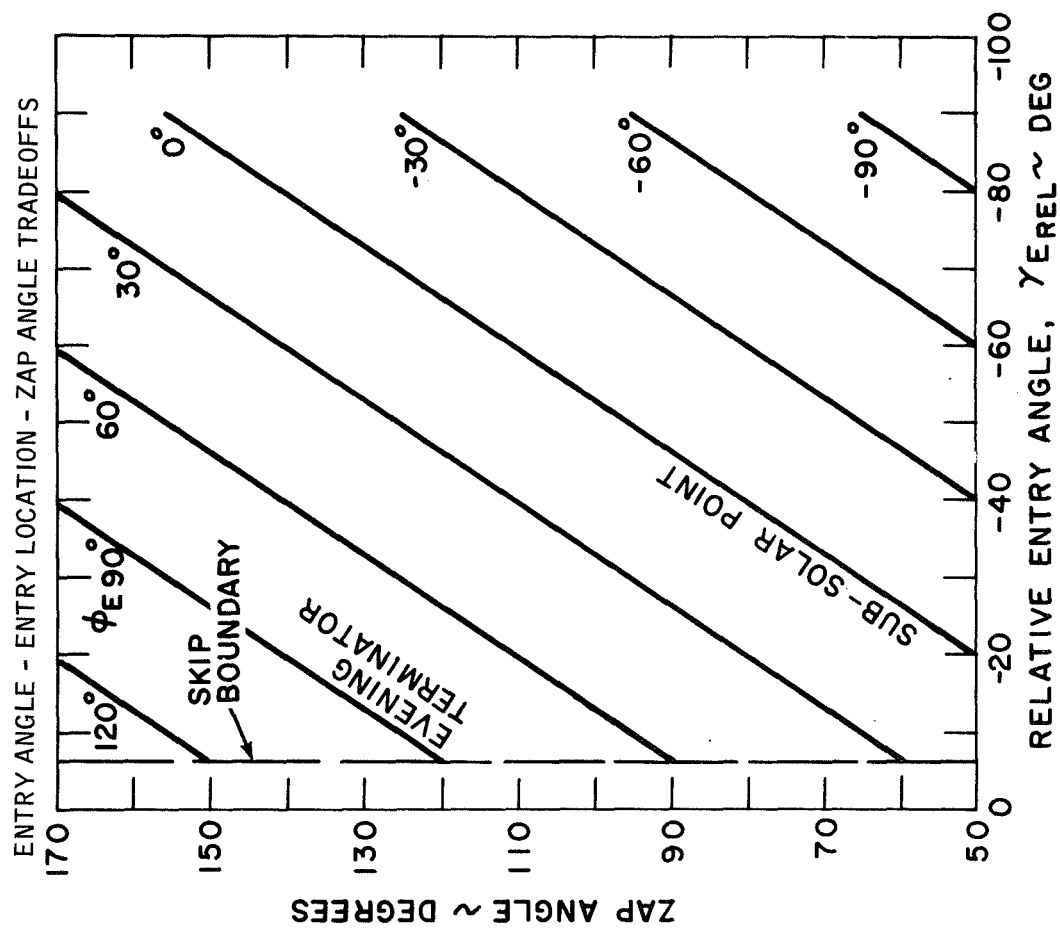
FIGURE 6-4

EARTH –JUPITER 1978 LAUNCH OPPORTUNITY WITH DLA CONSTRAINTS
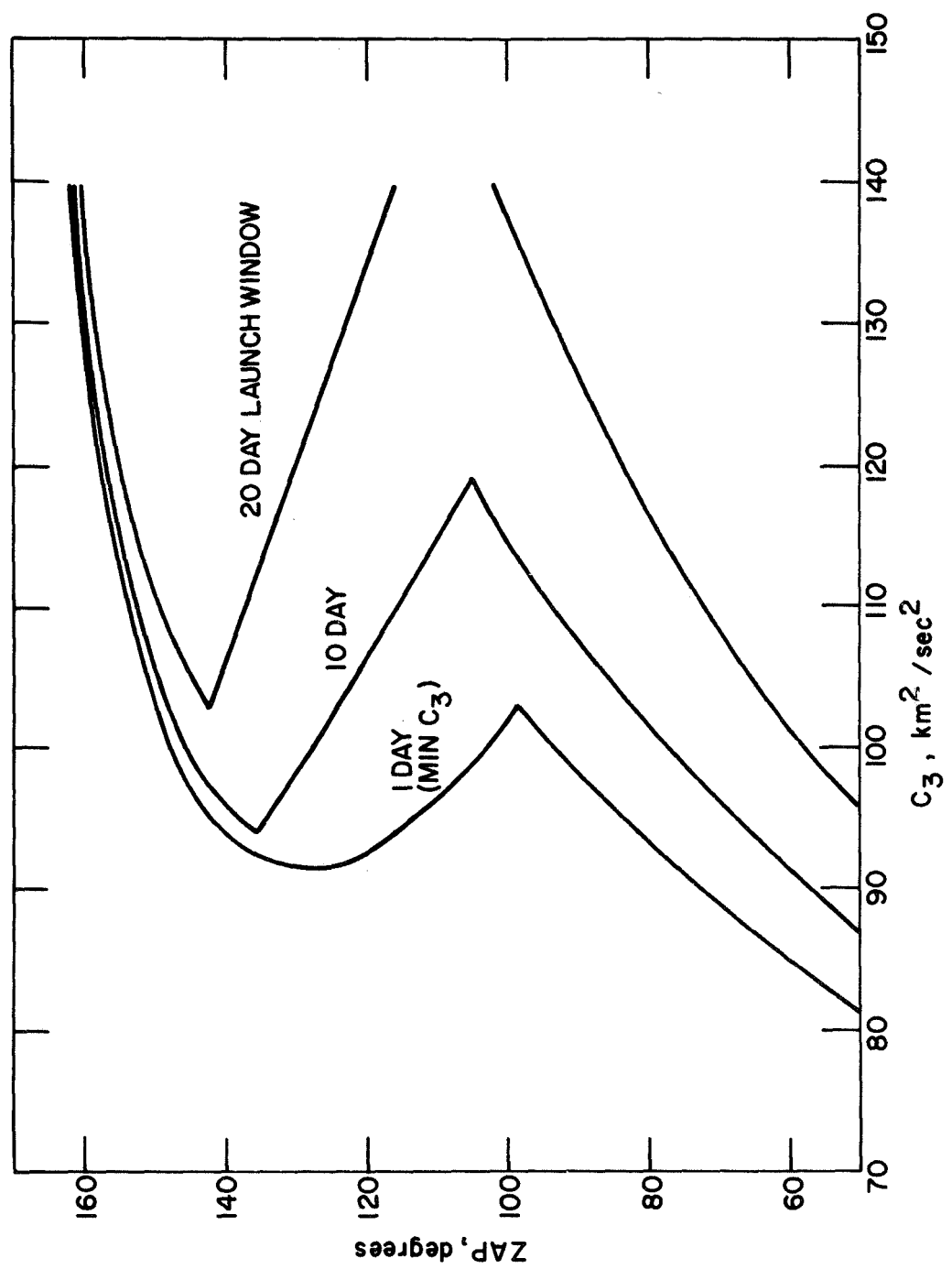
FIGURE 6-5

EARTH-JUPITER LAUNCH
1979 — WITH DLA CONSTRAINTS
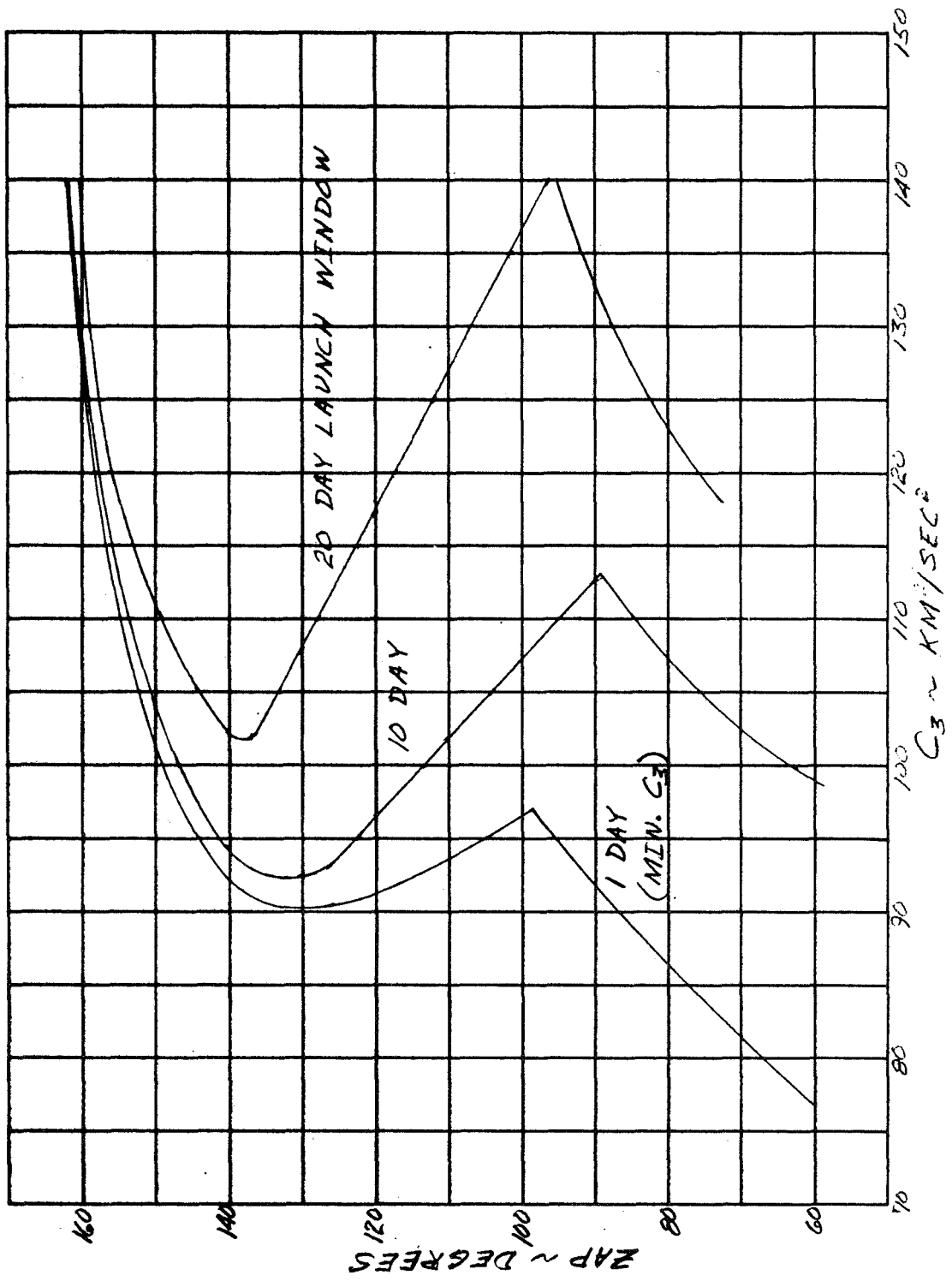
FIGURE 6-6

EARTH—JUPITER LAUNCH
1980 — WITH DLA CONSTRAINT

FIGURE 6-7

VARIATION IN INJECTION ENERGY AND ZAP ANGLE WITH LAUNCH
OPPORTUNITY – WITH DLA CONSTRAINTS

6-9
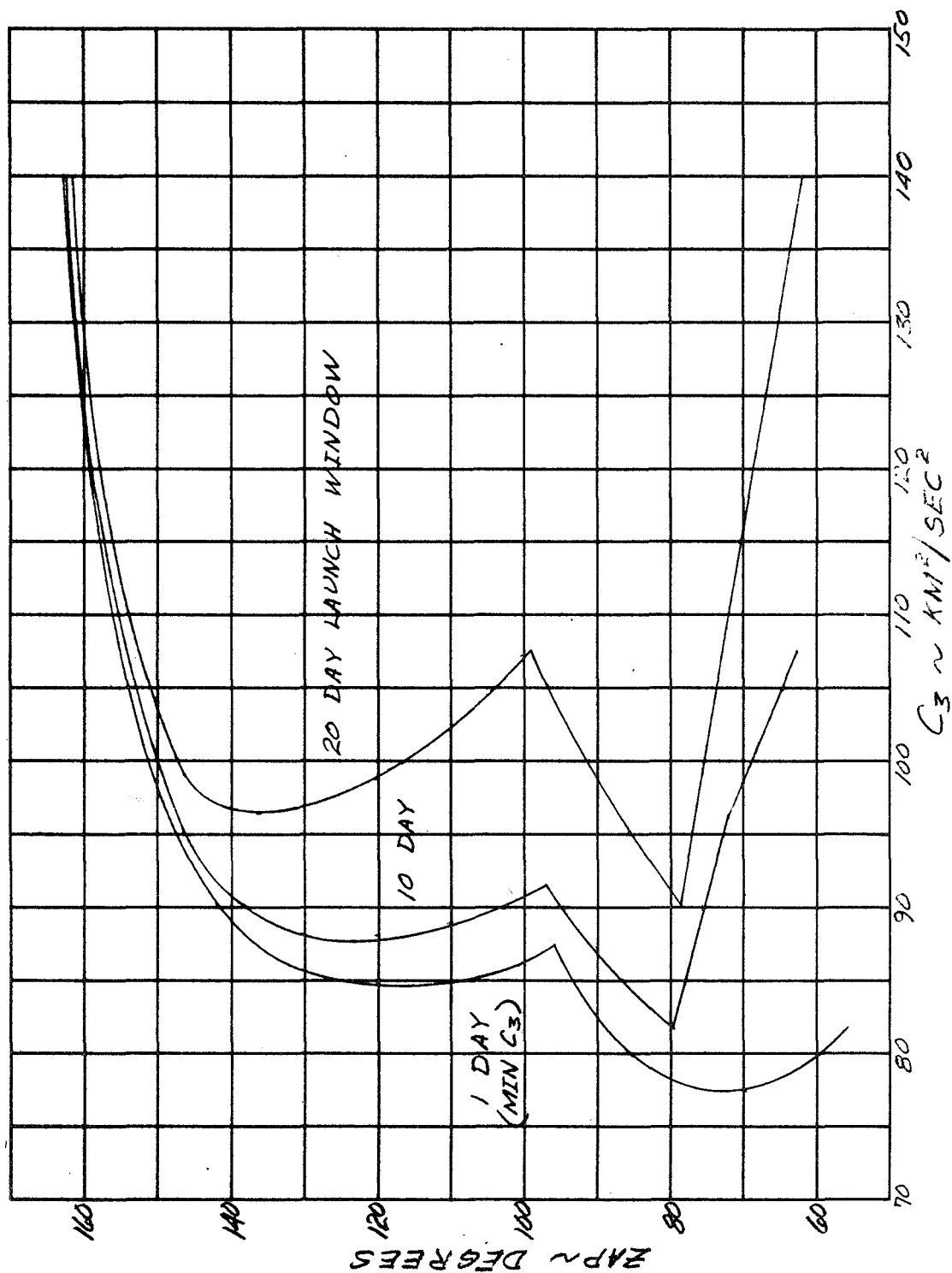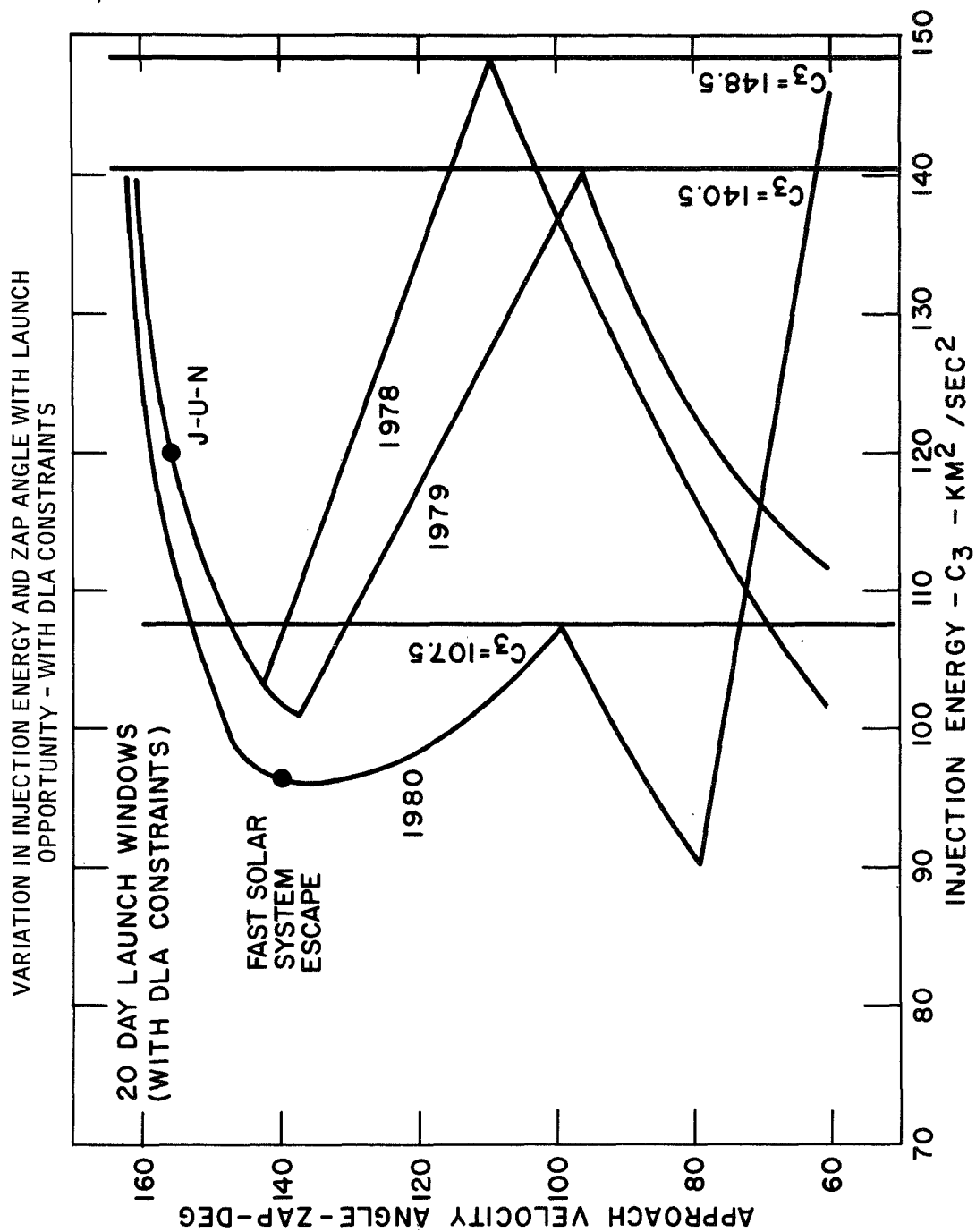
are highest in 1978 and become progressively lower for the later launch opportunities, with the lone exception being long Type II transit times in 1980. This is due to the fact that Jupiter is 1) in the ecliptic plane at encounter for flight time in the vicinity of 1400 days and 2) a large portion of the low energy transfers are negated from further consideration by the minimum DLA constraint. If this minimum DLA constraint (soft constraint associated with orbit determination) is eliminated then its impact on the injection energy can be seen by comparison of Figure 6-7 with Figure 6-8 in which this constraint was removed. Note that the C_3 requirements for 1980 Type II transfers are substantially reduced.

6.1.3 Probe/Spacecraft Launch Weight Sensitivity to Probe Entry Angle

The combined probe/spacecraft launch weight is sensitive to probe entry angle. As the entry angle increases the aerodynamic loads and heating rates increase and this is reflected in higher heat shield, structural, and pressure vessel weights, and hence higher probe weight for a fixed science complement. The variation in probe/spacecraft weight as a function of entry angle is illustrated in Figure 6-9 for the TOPS/probe and Pioneer F/G probe configurations. These results indicate that the combined probe/spacecraft weight increases from 1130 lb for a -15 deg entry angle to 1825 lb for a 50 deg entry angle when the probe is mounted to the Pioneer F/G spacecraft and from 1930 lb to 2525 lb when the probe is attached to the TOPS spacecraft.

6.1.4 Launch Vehicle-Injection Energy Tradeoffs

The last tradeoff area to be considered is the sensitivity of launch vehicle to injection energy. This relationship was discussed in detail in Section 5.2.5 with the tradeoff illustrated in Figure 5-22.

6.2 MISSION SELECTION PROCESS

The pertinent tradeoff information discussed in Section 6.1 has been integrated into Figure 6-10 in a fashion which permits a rapid evaluation of the significance of variations in targeting, engineering, launch opportunity, and launch vehicle requirements. For example, one can specify an entry angle corridor in combination with a desired entry location and define an acceptable range of ZAP angles, injection energies, probe/spacecraft injected weight, and finally the launch vehicle requirements. Alternatively, if specific approach geometry requirements are defined by post encounter

6-10

FIGURE 6-8

VARIATION IN INJECTION ENERGY AND ZAP ANGLE
WITH LAUNCH OPPORTUNITY - WITH 40 DEG. DLA CONSTRAINT ONLY

FIGURE 6-9

FLIGHT ARTICLE LAUNCH WEIGHT

NOMINAL PAYLOAD
NOMINAL ATMOSPHERE DESCENT TO
CLOUD BASE
RELAY LINK

TOPS / PROBE

PIONEER
F/G / PROBE

$\gamma_{E_{REL}} \sim$ DEG

LAUNCH WEIGHT $\sim$ LBS

3000

2000

1000

600

0

-20

-40

-60

-80

-100
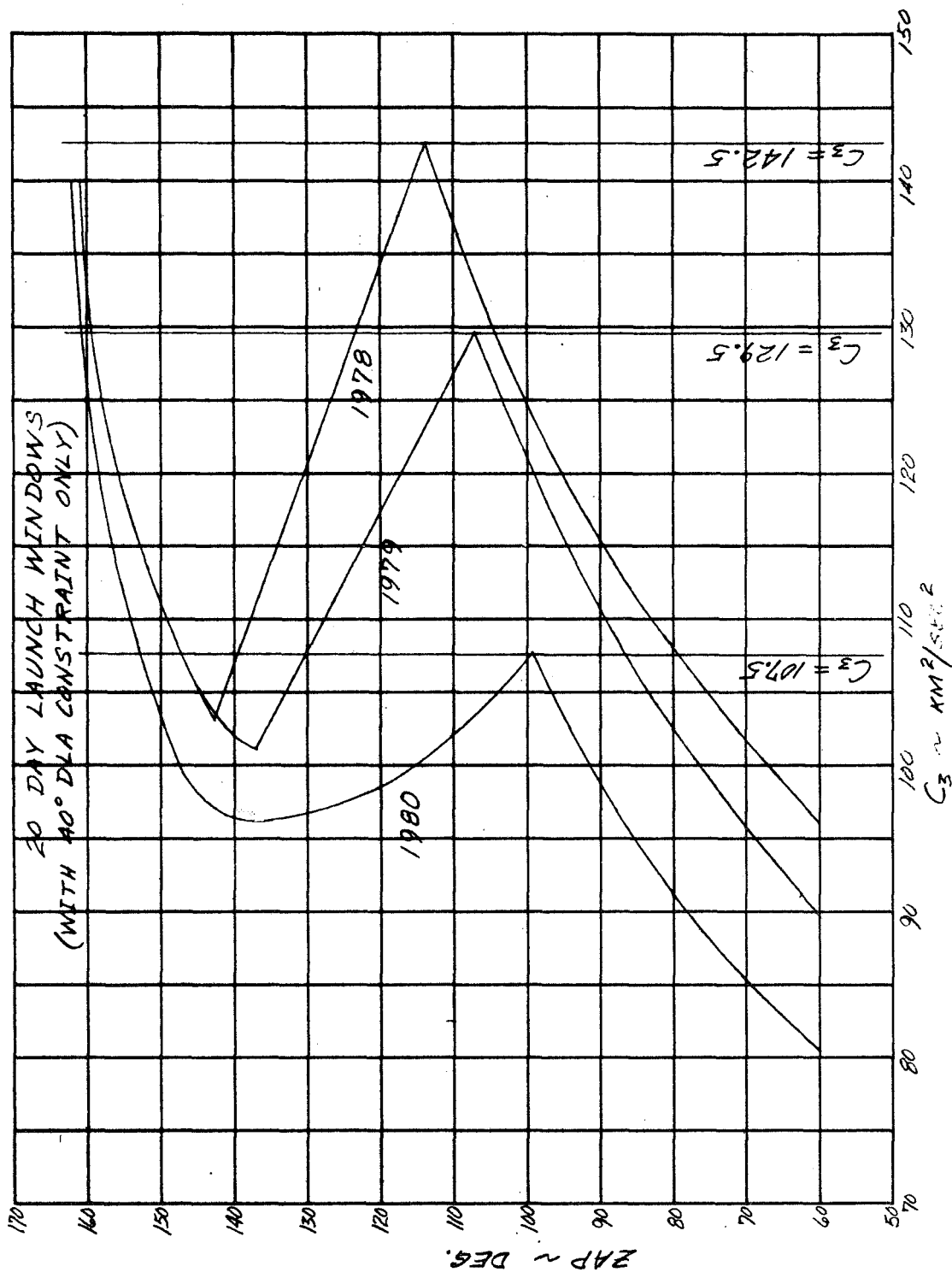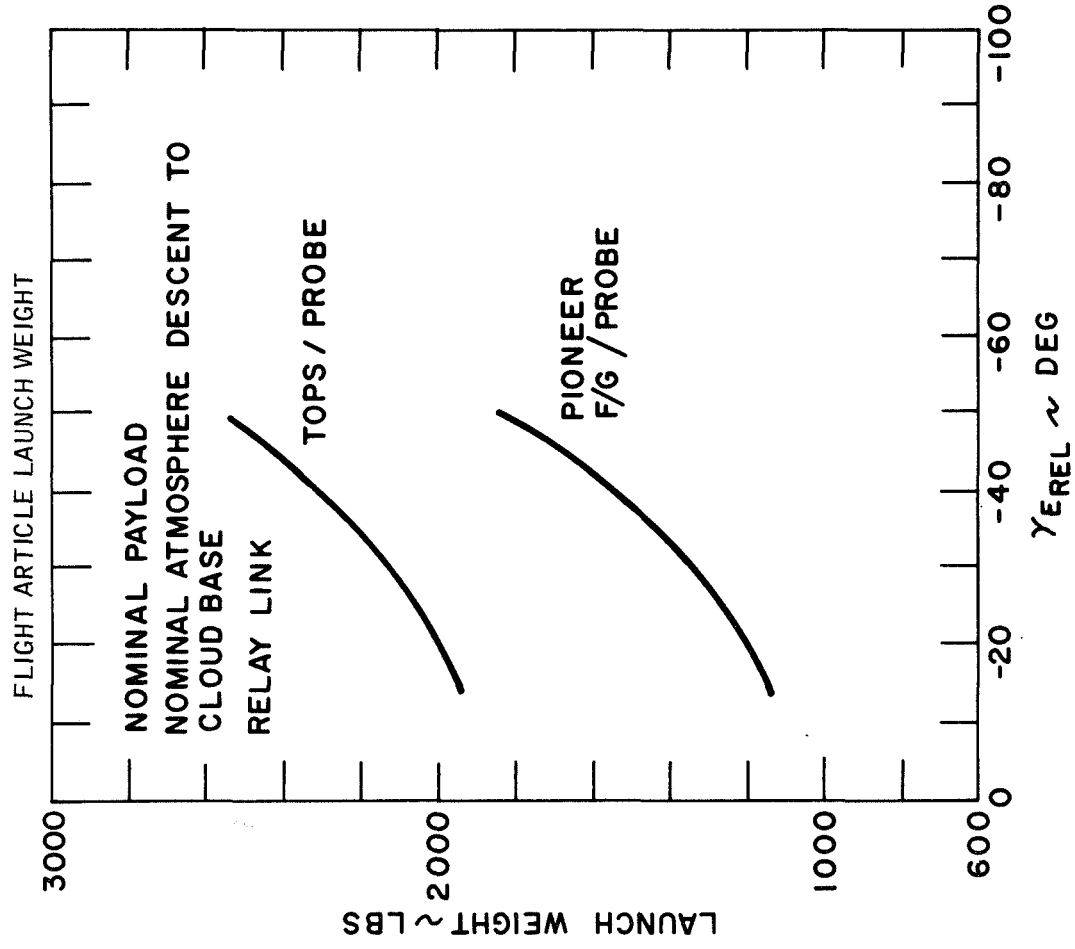
FIGURE 6-10

MISSION ANALYSIS SUMMARY
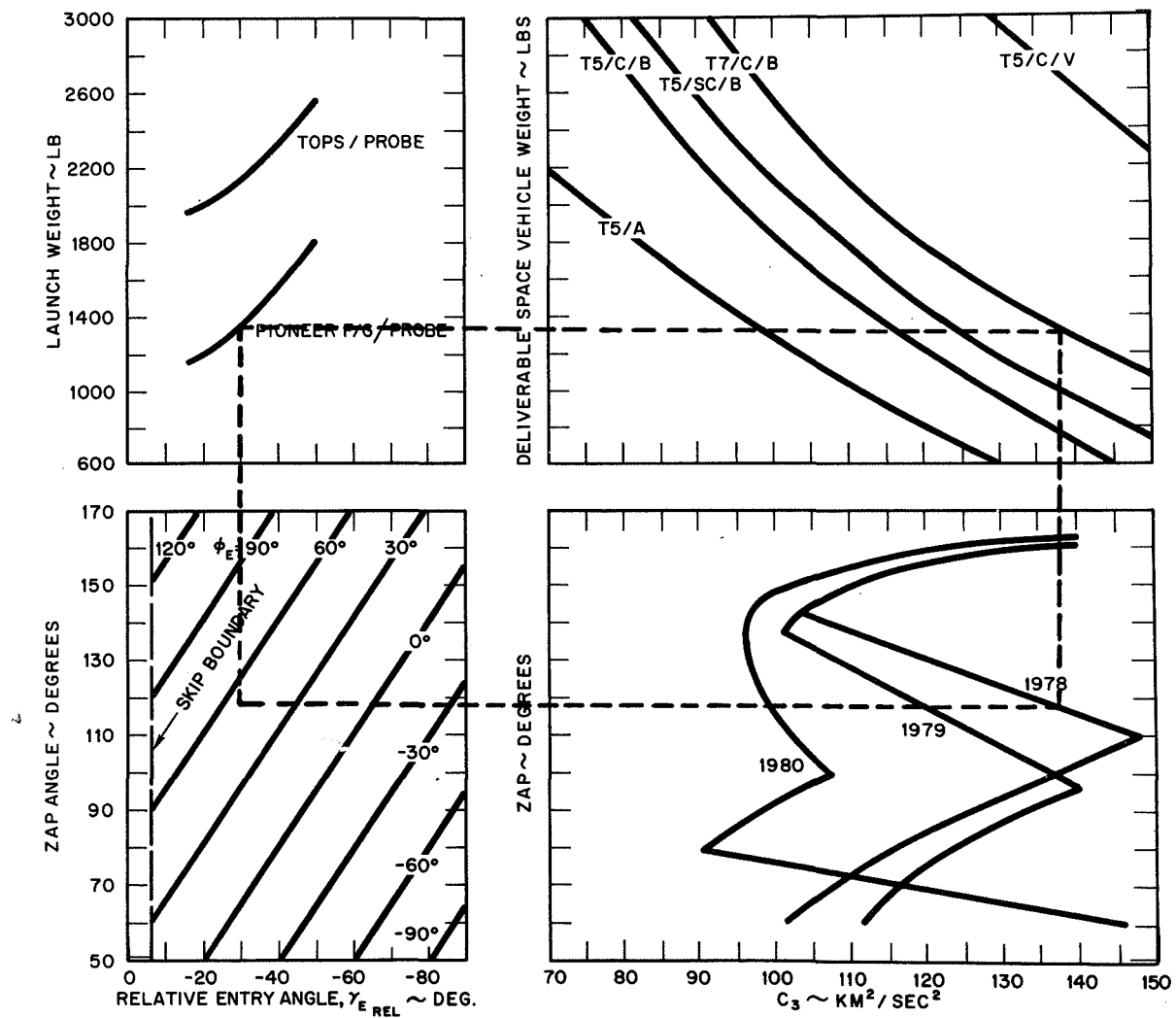
mission requirements one can start with the specified ZAP angle-injection energy conditions and 1) define the allowable variations in the entry angle and entry location, 2) determine the corresponding variations in the probe/ spacecraft injected weight, and 3) identify the launch vehicle that satisfies the injection energy-injection weight requirement. A third option exists wherein a specific launch vehicle can be identified and the various missions that can be accomplished with Type I or Type II transfers over the identified launch opportunities detailed.

Although these mission performance tradeoff maps only identify ZAP angle the information presented in Figure 5-17 illustrates that the flight time, encounter communication range, and hyperbolic approach velocity are basically only dependent upon the ZAP angle and hence are defined by the selection of ZAP angle regardless of the launch opportunity or transfer trajectory type.

With the information provided in Figure 6-10 the targeting parameters, probe/spacecraft injected weight, and launch vehicle data, was obtained for a series of candidate mission considering both Type I and Type II transfer trajectories in the 1978, 1979, and 1980 launch opportunities for a probe mounted on either a TOPS or Pioneer F/G spacecraft, dayside or nightside science complement, and a relay or direct link telecommunication system. In the establishment of the mission parameters the following constraints were observed: 1) entry angle as shallow as possible and in no case steeper than -50 degrees; 2) entry locations and descent time combination for dayside missions such that descent to the base of the clouds was realized 20 degrees in front of the evening terminator; and 3) probe lead time/spacecraft periapsis was optimized to maximize total bits in the presence of separation errors. The results of the analysis are presented in Tables 6-1 to 6-3 with respect to targeting requirements, trajectory parameters and system performance, respectively. Several blocks in the mission/spacecraft tables are obviously not applicable since only the TOPS spacecraft is under consideration for the 1979 J-U-N mission and also, where a good dayside mission could be identified by the targeting parameters for the corresponding nightside mission were not of interest. The results indicate that very shallow entry angles are associated with 1) Type II trajectories and dayside entry, and 2) Type I trajectories and nightside entry. It is also shown for a 1978 Type I trajectory that dayside entry is possible, if the descent time is reduced. The entry angle is no longer shallow, but is increased to an acceptable value.

TABLE 6-1

SUMMARY OF MISSION TARGETING REQUIREMENTS

Mission Classification		Spacecraft					
		PIONEER F/G			TOPS		
		Relay		Direct	Relay		Direct
		Dayside	Nightside	Dayside	Dayside	Nightside	Dayside
Flyby	1978 Type I	116 50 -33.2	141 103 -14.3	116 30 -48	116 50 -33.2	141 102 -14.9	116 30 -48
	1978 Type II	66 25 -15	NA	71 8 -33.5	60 23 -15	NA	71 8 -33.5
J-U-N Grand Tour	1979 Type I	NA	NA	NA	156 72 -44	156 100 -21.7	NA
Flyby	1980 Type I	100 34 -30	140 103 -15	116 30 -48	100 50 -27.7	140 101 -15	116 30 -48
	1980 Type II	64 25 -15	NA	69 9 -31	76 25 -15	NA	69 9 -31
KEY: ZAP Angle, Deg Entry Longitude, Deg Entry Angle, Deg							

TABLE 6-2

SUMMARY OF MISSION LAUNCH CHARACTERISTICS

Mission Classification	Spacecraft					
	PIONEER F/G			TOPS		
	Relay		Direct	Relay		Direct
	Dayside	Nightside	Dayside	Dayside	Nightside	Dayside
Flyby — 1978 Type I	T7/C/B 870 140	T5/A 670 106	TS/C/V 870 140	T5/C/V 870 140	T5/SC/B 670 106	T5/C/V 870 140
Flyby — 1978 Type II	T5/A 1350 100	N/A	T5/A/B 1265 103	T5/C/B 1420 96	N/A	T7/C/B 1265 103
J-U-N 1979 Grand Tour Type I	N/A	N/A	N/A	T5/C/V 528 121	T5/C/V 528 121	N/A
Flyby — 1980 Type I	T5/A/B 970 108	T5/A 670 97	T5/C/B 870 100	T5/C/B 970 108	T5/C/B 670 97	T7/C/B 870 100
Flyby — 1980 Type II	T5/A 1350 82	N/A	T5/A 1285 85	T5/A/B 1350 82	N/A	T5/C 1285 85

KEY: Launch Vehicle
Flight Time, Days
Injection Energy, km^2/sec^2

TABLE 6-3

SUMMARY OF MISSION PERFORMANCE

Mission Classification	Spacecraft					
	PIONEER F/G			TOPS		
	Relay		Direct	Relay		Direct
	Dayside	Nightside	Dayside	Dayside	Nightside	Dayside
Flyby 1978 Type I	850 1800 135,000	590 3600 158,400	1210 1000 6000	720 1800 225,000	500 3600 1,015,200	1050 1000 6000
Flyby 1978 Type II	590 3600 154,800	N/A	850 1600 27,200	490 3600 1,015,200	N/A	720 1600 27,200
J-U-N 1979 Grand Tour Type I	N/A	N/A	N/A	950 1800 ≈48,600	550 1800 48,600	N/A
Flyby 1980 Type I	790 3600 99,000	590 3600 154,800	1210 1000 6000	610 1800 315,000	490 3600 1,015,200	1050 1000 6000
Flyby 1980 Type II	590 3600 154,800	N/A	810 1600 27,200	510 3600 1,015,200	N/A	680 1600 27,200

KEY: Installed Probe Weight, lb
Probe Descent Time, sec
Total Bits

Furthermore, in analyzing the influence of launch opportunity on the mission selection it appears that the 1980 Type II transfers enhance the mission by virtue of lower injection energy requirements which will permit either a higher payload to be employed with the same launch vehicle or a small launch vehicle to be utilized for a fixed payload over the corresponding 1978 missions. Good nightside science missions can be realized with fast Type I transfers in either 1978 or 1980 with the lower injection energy requirement again slightly favoring the 1980 launch opportunity.

For direct link telecommunication system missions lower injection energy requirements, shallower entry angles and significantly higher total bits transmitted again favor Type II transfers with the only apparent detrement being an additional year added to the transfer time. Again as in the relay link missions, the 1980 launch opportunity yield slightly lower injection energy requirements with the result that smaller, less costly launch vehicles can be utilized.

From the mission matrix, five candidate missions were selected. They include: 1) Direct Link Mission - a Pioneer F/G direct link mission with a Type II transfer in 1978, 2) JUN Grand Tour Mission - a 1979 JUN Grand Tour Mission, 3) Early Mission - a short transit time Type I transfer with Pioneer F/G in 1978 with a dayside entry and an 1800 second probe descent mission, 4) Shallow Entry Angle/Pioneer F/G Mission - a shallow entry angle, high data return 1980 Type II transfer with a Pioneer F/G spacecraft utilizing a relay link, and 5) Shallow Entry Angle/TOPS Mission - a shallow entry angle, high data return 1980 Type II transfer with a TOPS spacecraft utilizing a relay link. The parameters associated with these missions are summarized in Table 6-4.

7.0 CANDIDATE MISSION CONFIGURATIONS

The major entry probe tradeoffs that have been investigated in this study include: 1) launch opportunity - 1978 and 1980 opportunities were studied from the viewpoint of tailoring the trajectory to satisfy entry probe requirements, and a 1979 opportunity based on a Jupiter - Uranus - Neptune, Grand Tour trajectory which is not favorable to an entry probe mission, 2) interplanetary bus - either a three-axis stabilized TOPS or spin stabilized Pioneer F/G spacecraft modified to support an entry probe, 3) communication link - a direct link from the entry probe to DSN or a relay link from the entry probe via the spacecraft to DSN, and 4) probe targeting - both dayside and nightside entry. In Section 6.2, the matrix of missions was presented based on the above enumerated tradeoffs. From this matrix of twenty-two mission possibilities, five candidate missions were selected for more detailed investigation.

7.1 GROSS CHARACTERISTICS OF CANDIDATE MISSIONS

The characteristics of the missions that are reported in Table 6-4, tend to emphasize the targeting characteristics whereas the characteristics reported in Table 7-1 for these same missions tend to emphasize the design features. The five missions were selected for the following reasons.

Of the five, only one is a direct link and this mission has been termed the Direct Link Mission. A total of six direct link missions were identified, and of these, the combination of 1978 Type II, and Pioneer F/G interplanetary bus resulted in the most favorable mission. Note that there does not exist a dayside/nightside distinction for a direct communication link. All direct link missions are also dayside missions because of the close angular proximity of the sun to Earth.

The Jupiter - Uranus - Neptune (JUN) Grand Tour Mission was selected as a candidate mission because of its uniqueness and because of the high probability of funding for this mission. It is of value to compare an entry probe that has been designed as the primary mission objective with one that has been designed as a secondary mission objective. Since the JUN Mission is based on the use of the TOPS spacecraft, a Pioneer F/G was not investigated. To satisfy Grand Tour navigation requirements the spacecraft arrives at Jupiter at a large ZAP angle, compatible with shallow angle entry on the nightside. A search was made for a dayside mission. It will be recalled that one of the Avco imposed targeting constraints is entry probe

TABLE 7-1

ENTRY PROBE CHARACTERISTICS

NO.	CHARACTERISTICS \ MISSION	DIRECT	JUN	EARLY	SHALLOW	
					PIONEER F/G	TOPS
1	Launch Opportunity	1978 II	1979 I	1978 I	1980 II	1980 II
2	Spacecraft	Pioneer F/G	TOPS	Pioneer F/G	Pioneer F/G	TOPS
3	Installed Probe Weight	770	572	803	596	508
4	Launch Vehicle	T 5/A/B	T 5/C/V	T 7/C/B	T 5/A	T 5/A/B
5	Communication Link	Direct	Relay	Relay	Relay	Relay
6	Total Data Bits	27,200	48,600	135,000	154,800	1,015,000
7	Flight Time, Days	1265	528	870	1350	1350
8	Solar Longitude, Deg.	8	100	50	25	25
9	Probe Separation Velocity, MPS	84	266	86	76	76
10	Entry Angle, Deg.	-33	-22	-33	-15	-15
11	Maximum G Load	1340	830	1340	525	525
12	Probe Descent Time, Sec	1600	1800	1800	3600	3600
13	Hypersonic Cone $\frac{M}{C_D A}$, Slug/Ft^2	.72	.52	.71	.48	.48
14	Chute $\frac{M}{C_D A}$, Slug/Ft^2	.07	.05	.05	.01	.01
15	Subsonic Sphere $\frac{M}{C_D A}$, Slug/Ft^2	5.5	5.1	5.5	5.0	4.9

BASED ON:

NOMINAL MODEL ATMOSPHERE

NOMINAL DAYSIDE SCIENCE PAYLOAD

DESCENT TO BASE OF AMMONIUM CHLORIDE CLOUDS

mission termination twenty degrees on the dayside of the evening terminator. If this constraint is relaxed and mission termination can occur at the terminator, then for a one-half hour descent time, the probe must enter at a solar longitude of +72 deg. For the JUN Grand Tour targeting, this will result in a -42 deg entry angle. The resulting flight article weight comprising the TOPS and entry probe, and the injection energy to achieve the large ZAP angle will require a launch vehicle of the T5/C/V class. The difficulty of obtaining a dayside mission resulted in the selection of a shallow entry angle, nightside entry mission.

A 1978 Type I mission was selected as one of the five candidate missions because it would allow for the early return of entry probe data. This mission has been termed an Early Mission. An October 1978 launch date is possible. The time of flight is 870 days, and results in returned data as early as March 1982. This mission uses a Pioneer F/G spacecraft as bus, and is based on dayside entry and a relay telecommunication link. It was determined that 1980 Type II targeting resulted in the most favorable entry probe mission configuration. A very shallow entry angle, and dayside targeting is permitted in this launch opportunity. The only unfavorable factor is the long flight time. A candidate mission for both Pioneer F/G and TOPS was selected. The former is termed a Shallow Entry Angle/Pioneer F/G Mission, and the latter a Shallow Entry Angle/TOPS Mission.

The candidate missions that are described in this section have been based on an entry probe: designed to carry the nominal dayside science payload, enter the nominal model atmosphere, and descend to the base of the ammonium chloride clouds which are believed to be the base of all the clouds. Entry probe characteristics for the five candidate missions are presented in Table 7-1. The items in this table are described as:

No. 1 Launch Opportunity – Three launch opportunities have been considered, and both Type I and Type II trajectories. A spacecraft launched along a Type I trajectory encounters Jupiter prior to apoapsis passage along the transfer ellipse. This trajectory can be characterized by short flight times, and approach on the dayside of the morning terminator, thus resulting in nightside entry for a shallow angle entry. A spacecraft targeted to Jupiter along a Type II trajectory, encounters Jupiter after apoapsis passage. Flight times are long, but the spacecraft encounters Jupiter on the nightside of the morning terminator. This type of encounter is compatible with shallow entry angle, dayside entry.

No. 2 Spacecraft - The Pioneer F/G is a spin stabilized spacecraft that weighs 550 lb., and the TOPS is a three axis stabilized spacecraft that weighs 1450 lb.

No. 3 Installed Probe Weight - This weight is comprised of the entry probe weight and the weight of all modifications to existing spacecraft subsystems, and additional spacecraft subsystems that are used to support the entry probe mission. The installed probe weight plus the spacecraft weight result in the flight article weight.

No. 4 Launch Vehicle - A Titan III D family of launch vehicles have been used in this study. The Titan III D is a two-stage booster. The 5 and 7 refer to use of a two, five segment or two, seven segment zero stage solid propellant motors. The letter A refers to an Agena upper stage; B, Burner II; C, Centaur, and V, a Versatile Upper Stage (a paper configuration).

No. 5 Communication Link - A direct link is communication from the entry probe to DSN, whereas a relay link is based on telemetry from the entry probe to the spacecraft bus, and subsequent retransmission from the bus to DSN. Note all direct link missions are also dayside missions. The Early and Shallow Entry Angle Missions are based on a 25w transmitter output power, whereas the Direct Link and JUN missions are based on 50w transmitted power.

No. 6 Total Data Bits - The total bits transmitted during probe descent from 0.7 Mach No. to the cloud base plus the ion mass spectrometer and accelero-meter stored data. Use of the nominal dayside science payload results in 27,000 bits that must be transmitted.

No. 7 Flight Time - The time along the trajectory from Earth launch to Jupiter periapsis passage.

No. 8 Solar Longitude - Jovian longitude is measured from the sub-solar point. Positive longitude is measured from the sub-solar point in the direction of the Jovian rotation towards the evening terminator. Thus, a +90 deg. solar longitude implies entry at the evening terminator, and a -90 deg. solar longitude implies entry at the morning terminator.

No. 9 Probe Separation Velocity - This is the velocity increment necessary to deflect an entry probe which is on a flyby of Jupiter to an impact trajectory. Large periapsis passing distances and steep entry angles result in large impulse

requirements. The periapsis passing distance of the JUN mission is almost 7 planetary radii, and the periapsis passing distance of the other missions is about 3 planetary radii.

No. 10 Entry Angle - All entry is in the direction of Jovian rotation, and the angle is measured relative to the rotating planet. For example, the relative entry angle of -15 deg. and relative entry velocity of 49 Km/sec, corresponds to an inertial entry angle (for a non-rotating planet) of -12 deg. and inertial entry velocity of 60 Km/sec.

No. 11 Maximum G Load - Maximum G load has been calculated based on entry into the nominal model atmosphere and accounts for variable entry probe mass, that is consistent with the anticipated massive ablation. Loss of mass during entry results in an increase in the maximum G load and a shift upward in altitude at which events occur. For example, a constant mass entry probe that enters the nominal model atmosphere at -15 deg. entry angle will experience a maximum load at 486 G and achieve 0.7 Mach No. at an altitude of 47 Km above the cloud tops. Consideration of variable mass results in a maximum load of 525 G, and occurrence of 0.7 Mach No. at 51 Km.

No. 12 Probe Descent Time - This is the time from 0.7 Mach No. to the base of the cloud layers. A Mach No. of 0.7 has been arbitrarily selected as a representative high subsonic Mach No. at which the parachute can be deployed and the payload container extracted from the 60 deg. half-angle cone aeroshell, so that the instrumentation is enabled to gather data.

No. 13 Hypersonic Cone $\dfrac{M}{C_DA}$ - This is the value of the ballistic parameter of the entry probe at entry before the commencement of ablation and reduction in ballistic parameter. All probe configurations use a 4 ft. diameter aeroshell.

No. 14 Chute $\dfrac{M}{C_DA}$ - This is the value of the ballistic parameter of the payload container suspended from the parachute. The chute has been sized so that for a one-hour descent time, the time from 0.7 Mach No. to the base of the water clouds is at least 2100 seconds. This will permit the securing of seven samples from the gas chromatograph (each sample requires five minutes to process). For the one-half hour descent time, the time to the base of the water clouds must be greater than 1200 sec to allow for four gas chromatograph samples.

No. 15 Subsonic Sphere $\dfrac{M}{C_D A}$ - This is the value of the ballistic parameter of the spherical payload container configuration that descends to the base of the clouds after the parachute is released. A torus is added to the sphere just to the rear of the maximum diameter station to provide stability.

7.2 GENERAL CHARACTERISTICS OF ENTRY PROBE CONFIGURATIONS

An inboard profile of the entry probe configuration is indicated in Figure 7-1. The primary features of the configuration are: 1) the 60 deg half angle cone aeroshell with a 1/4" nose radius, and 2) the spherical payload container. This aeroshell configuration was provided as a groundrule for this study. It has been determined that the inside diameter of the spherical payload container necessary to contain the nominal dayside science payload will vary from about 20 to 21 inches. The variation is caused by the influence of descent time and transmitter power, and resulting power and thermal control perturbations. The container dimension is based on summing the volume of all of the packages that must be contained, and multiplying this volume by a factor of 2.5. Studies have indicated that a packaging efficiency of 40% is obtainable. The pressure vessel thickness and insulation thickness will add about 0.9 inches to the container diameter. For a 60 deg. cone, the center of pressure will lie to the rear of the maximum diameter. Therefore, static stability can be obtained by having the center of gravity lie on the maximum diameter or forward. It was determined that the center of gravity of the probe would lie near the base of a four foot diameter aeroshell. Note that a meteoroid container surrounds the forebody of the entry probe. During the interplanetary flight the forebody will be exposed to the meteoroid environment, whereas the afterbody will be shielded by the spacecraft. The mounting of the entry probe to the TOPS is shown in Figures 5-7 and 5-8, and the mounting of the entry probe to Pioneer F/G is indicated in Figure 5-9 and 5-10. This meteoroid container is separated about one hour prior to entry. A typical sequence of events is provided in Table 7-2.

7.3 SPECIFIC CHARACTERISTICS OF ENTRY PROBE CONFIGURATIONS

In Section 7.1, the general broad characteristics of the entry probe configuration were described. In this section the specific characteristics of the many subsystems will be described, and differences between the five candidate missions will be indicated.

FIGURE 7-1

INBOARD PROFILE OF ENTRY PROBE POST SEPARATION CRUISE
CONFIGURATION – 48 IN. DIAMETER AEROSHELL
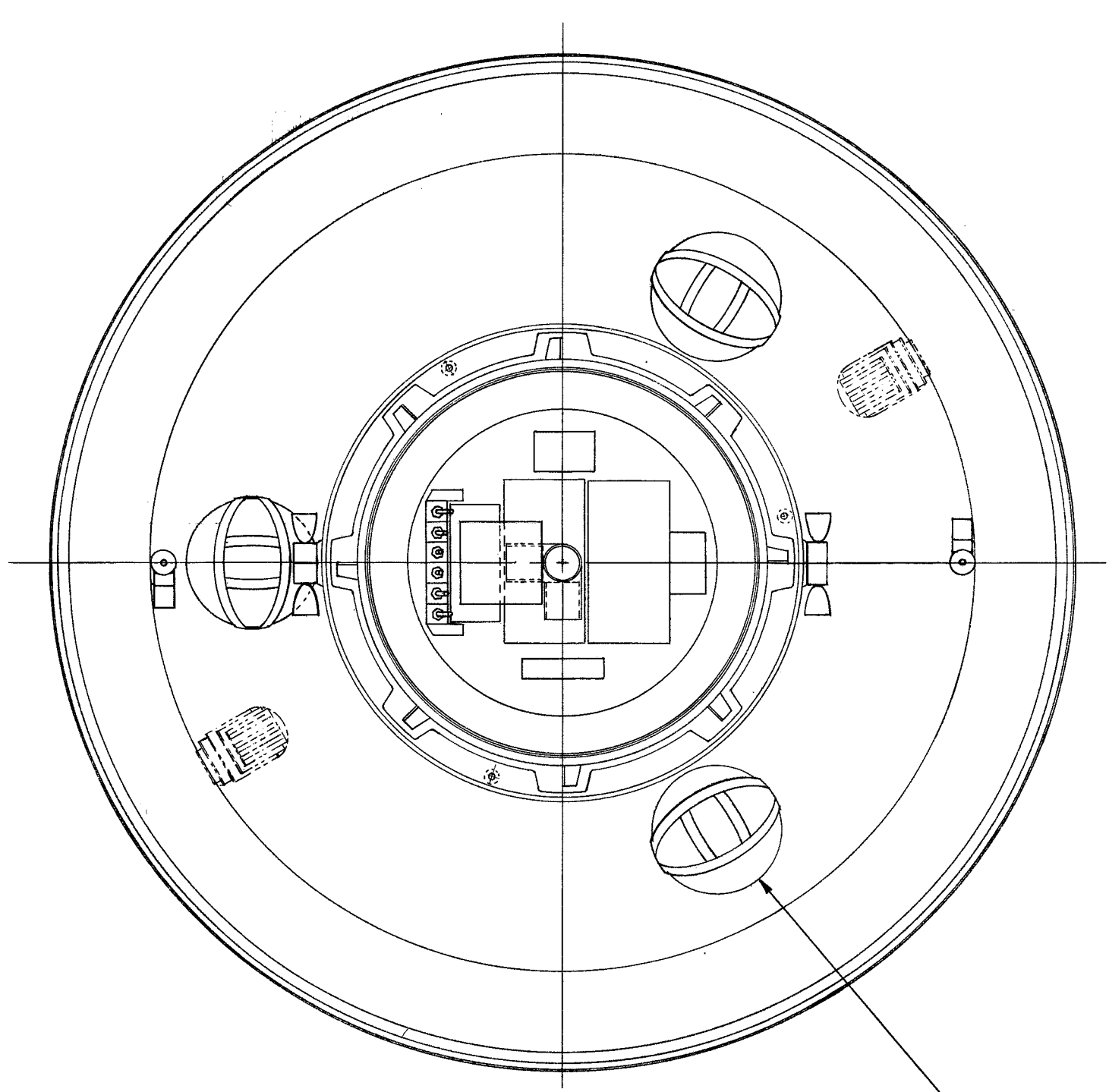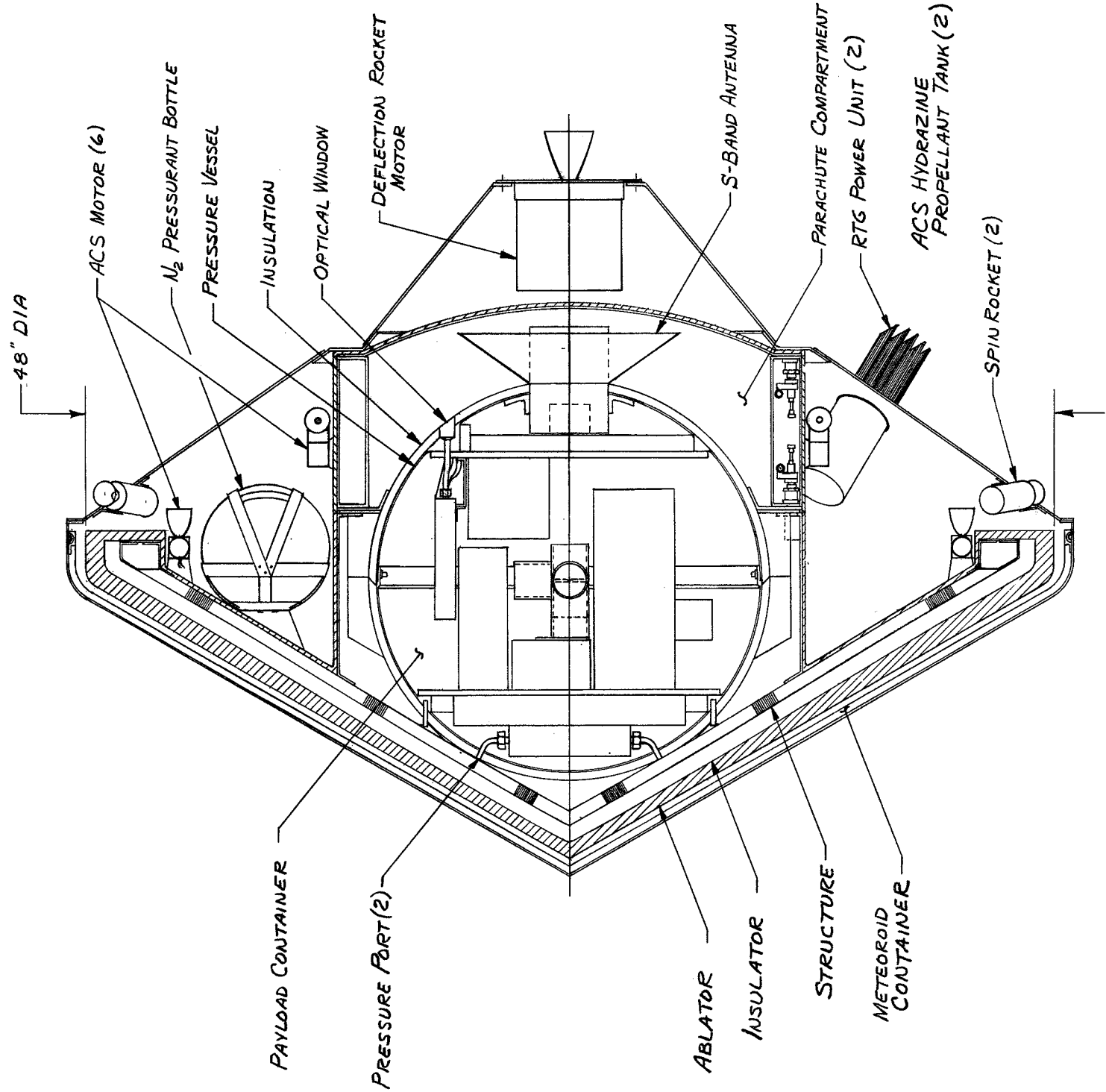
VIEW SHOWN WITH AFT METEOROID SHIELD, AFT CYLINDER
AND AFT SPHERE WITH ANTENNA REMOVED

ACS MOTOR (6)
N₂ PRESSURANT BOTTLE
PRESSURE VESSEL
INSULATION
OPTICAL WINDOW
DEFLECTION ROCKET MOTOR
S-BAND ANTENNA
PARACHUTE COMPARTMENT
RTG POWER UNIT (2)
ACS HYDRAZINE PROPELLANT TANK (2)
SPIN ROCKET (2)

48" DIA

PAYLOAD CONTAINER
PRESSURE PORT (2)
ABLATOR
INSULATOR
STRUCTURE
METEOROID CONTAINER

TABLE 7-2

JUPITER ATMOSPHERIC ENTRY PROBE MISSION PROFILE

NO.	EVENT	TIME DIRECT	JUN	EARLY	SHALLOW	REMARKS
1	Earth Launch	L = 0	L = 0	L = 0	L = 0	Event
2	Separate from Spacecraft	L + 1194 day S = 0 E - 71 day	L + 486 S = 0 E - 42	L + 800 S = 0 E - 70	L + 1102 S = 0 E - 73	45 x 10^6 KM from Jupiter
3	Initiate Deflection Maneuver	S + 60 sec	S + 60	S + 60	S + 60	Reduce transfer of energy and momentum to spacecraft
4	Rocket Motor Burnout	S + 75 sec	S + 75	S + 75	S + 75	Spin-stabilized, ~30 RPM
5	Checkout	EVERY FIVE DAYS				Telemeter engineering diagnostic data and ion mass spec & magnetometer data
6	Separate from Meteoroid Container	E - 1 hr	E - 1	E - 1	E - 1	Endoatmospheric magnetic field measurements terminated
7	Null Angle of Attack	E - 1 min	E - 1	E - 1	E - 1	Achieve zero angle of attack
8	Enter Atmosphere	E = 0	E = 0	E = 0	E = 0	Event = 0.1G (Rising); end ion mass spec storage - begin accelerometer storage
9	Peak G	E + 8 sec	E + 13	E + 8	E + 18	Unique time reference for backup time sequencing
10	Emerge from Blackout	E + 9 sec	E + 19	E + 9	E + 32	V = 10,000 Ft./sec
11	Deploy Chute	E + 32 sec	E + 60	E + 32	E + 73	M = 0.7, P ≈ 0.1 atm
12	Extract Payload Container	E + 37 sec	E + 65	E + 37	E + 78	Enable descent science
13	Enter Cloud Tops	E + 244 sec	E + 303	E + 278	E + 622	P = 0.38 atm
14	Separate Chute	E + 1279 sec	E + 1467	E + 1479	E + 3260	P = 3.1 atm base of H_2O clouds
15	Achieve Base of Clouds	E + 1600 sec	E + 1800	E + 1800	E + 3600	P = 17 atm, base of NH_4Cl clouds

7. 3. 1 Separated Probe Configuration

A weight summary of the separated probe configuration for the five candidate missions is presented in Table 7-3. From the viewpoint of entry probe design, there exists four different separated probe configurations. This is due to use of similar probes for both the Shallow Entry Angle/TOPS Mission and Shallow Entry Angle/Pioneer F/G Mission.

The various subsystems presented in Table 7-3 are described in the following paragraphs.

No. 1 Internal Science - The internal science is comprised of all of the instruments that appear in the nominal dayside science payload of Figure 3-1, except for the ion mass spectrometer and one magnetometer. A second magnetometer is part of the external science payload.

No. 2 Communication - This subsystem is comprised of an antenna and transmitter. For the Direct Link Mission and the JUN Mission, a 50w output power S-band transmitter is required. The Early Mission and the Shallow Entry Angle/Pioneer F/G Mission requires a 25w output power L-band transmitter, and the Shallow Entry Angle/TOPS Mission, a 25w output power S-band transmitter. A 25% efficiency has been used for the S-band transmitter, and 28% efficiency for the L-band transmitter.

No. 3 Programmer and Data Handling - This subsystem provides all programming, data storage, multiplexing, encoding, timing, analog to digital conversion, and processing for all probe science and engineering subsystems.

No. 4 Cabling - Accounts for all wires and connectors that carry power, input timing, and output data signals between the subsystems.

No. 5 Power (Descent) - The primary power source is a silver-zinc battery that is rated at 50 whr/lb. The total time of operation is the descent time plus one-half hour that accounts for warm-up and uncertainty in entry time. Energy requirements are increased to account for an 80% converter efficiency. The resulting total watt hours are increased by a factor of two to provide for good regulation. Total energy requirements can range from 350 whr to 550 whr. Also included in the power subsystem is the weight of the converter and regulator.

TABLE 7-3

JUPITER ATMOSPHERIC ENTRY PROBE WEIGHT SUMMARY

NO.	SUBSYSTEM ⟍ MISSION	DIRECT	JUN	EARLY	SHALLOW *
1	Internal Science	36 Lb.	36 Lb.	36 Lb.	36 Lb.
2	Communication	6	6	5	5
3	Programmer & Data Handling	4	4	4	4
4	Cabling	12	12	12	12
5	Power (Descent)	13	13	9	12
6	Thermal Control (Internal)	6	4	4	6
7	Internal Structure	38	23	38	15
8	Pressure Vessel	16	15	15	15
9	Thermal Control (External)	6	6	6	9
10	Sphere Probe Configuration	127	119	129	114
11	Parachute	5	5	5	12
12	External Structure	26	15	26	10
13	Parachute Probe Configuration	168	139	160	136
14	External Science	6	6	6	6
15	Communication (Endo Ant.)	2	2	2	2
16	Attitude Control	16	13	16	13
17	Aeroshell	113	49	112	34
18	Heatshield	157	123	157	120
19	Entry Probe Configuration	462	332	453	311
20	Thermal Control (RTG)	6	6	6	6
21	Canister	22	22	22	22
22	Rocket Motor	20	43	20	13
23	Separated Probe Configuration	510 Lb.	403 Lb.	501 Lb.	352 Lb.

*Same Separated Probe Configuration used for both TOPS and Pioneer F/G

No. 6 Thermal Control (Internal) - Local temperature modification is effected by use of phase change salts in the vicinity of the subsystems that dissipate large quantities of energy such as the transmitter. A phase change salt that melts at 97 deg. F and absorbs 114 Btu/lb. was utilized. Total internal power dissipation can range from 135 to 215 whr. Local temperature extremes are moderated also by use of an internal atmosphere. Use of sulfur hexafluoride provides good convective coupling and also inhibits voltage breakdown.

No. 7 Internal Structure - An internal structure to support the payload was estimated for the Shallow Entry Angle Mission, and the weights were scaled for the other higher G load missions. This aluminum structure is used to provide complete support for the various subsystem packages. It should be pointed out that high G loads are not the fundamental design problem but rather the stresses that are induced by the loads. These stresses can be reduced by providing complete contoured support for the packages.

No. 8 Pressure Vessel - A 20 to 21 inch diameter titanium pressure vessel is used to contain the payload and so provide protection against the high external pressure of 17 atm at the base of the clouds. This vessel is of monocoque construction and the wall thickness is about 0.06 inch.

No. 9 Thermal Control (External) - The principal component of the external thermal control subsystem is the insulation system that envolops the payload container. This insulation retards the flow of heat from the atmosphere into the payload container. At the cloud base, the ambient temperature is 305 deg. F whereas the payload temperature is not allowed to exceed 165 deg. F. A MIN-K insulator is used; the thermal conductivity, accounting for the low molecular weight atmosphere, the high pressure, and elevated temperature is about 0.1 Btu/hr-deg F-ft. The thickness of insulator varies from 0.2 to 0.4 inches. The other components of the thermal control subsystem include coatings, and multilayer insulation for localized protection.

No. 10 Sphere Probe Configuration - This is the configuration that descends to the cloud base after the parachute and external structure are released.

No. 11 Parachute - A parachute is used to retard the descent velocity in the upper cloud layers to provide sufficient sampling time for the gas chromatograph instrument and to also reduce the bit rate requirements on the telemetry subsystem. Dynamic pressure at chute deployment (0.7 M) for the Direct and Early Mission is about 90 lb/ft^2 whereas for the JUN and Shallow Entry Angle

Missions, about 60 lb/ft^2. For the short descent time, like 1800 sec, Direct Link, JUN, and Early Missions, a 13 ft. diameter (based on total surface area) ring-sail chute is indicated, and for long descent times, like 3600 for the Shallow Entry Angle Missions, a 25 ft. diameter chute is indicated.

No. 12 External Structure - The external structural requirements were estimated for the Shallow Entry Angle Mission and scaled up for the other higher G load missions. This structure includes the parachute compartment, aeroshell attachments, parachute harness ring, and part of the aft cover.

No. 13 Parachute Probe Configuration - This is the configuration of the probe as it descends from 0.7 Mach No. to below the base of the water clouds.

No. 14 External Science - Two instruments comprise the external science, i.e., external to the payload container. The entry probe carries two magnetometers, one is deployed during atmospheric descent and the other during post separation cruise. This latter magnetometer is part of the external payload. The magnetometer is enabled after entry probe separation and operates up to meteoroid container separation. The ion mass spectrometer is attached to the aeroshell and is carried through entry. This allows for ion mass spectrometer measurements for one minute prior to probe achievement of the entry point 0.1 G rising).

No. 15 Communication - During post separation cruise there will be a require-ment to determine the status of the probe systems and also to record the out-puts of the external science instrumentation. The antenna that is used during atmospheric descent is covered by a titanium structure that supports a heat shield so as to protect the entry probe afterbody from the wake heating. The presence of this metallic structure will require the addition of a second antenna mounted to the outside of the cover to provide post separation communications.

Other design alternatives such as 1) no cover, and use of a non-charring material as the antenna window, or 2) a dielectric cover structure that is transparent to R.F. radiation, could possibly result in a design that avoids the necessity of two antennas.

No. 16 Attitude Control - An attitude control system is provided to 1) null the angle of attack prior to entry, and 2) despin the probe prior to entry. The entry probe attitude during the deflection maneuver is maintained by spin stabilization. It has been determined that the angle of application of the

impulse will not generally result in a zero angle of attack at entry. Due to the extreme heating environment is is desirable to ease the heat shield design requirements whenever possible. Greater confidence could be placed in heat shield performance and probe survival if the angle of attack is small at entry. Therefore, it is desirable to null the angle of attack prior to entry. Magnetic field perturbations can also cause an increase in the angle of attack at entry. It is also desirable to have a near zero spin rate, but to ensure maintenance of a preferred attitude up to the presence of aerodynamic forces some low rate is required. Also during cruise, magnetic field distrubances could cause probe despin to an unacceptable level for maintenance of stability. A monopropellant hydrazine system provides impulse for a set of six thrusters that control spin, despin, pitch, and yaw. About one pound of hydrazine is required, and nitrogen gas is used to pressurize the system. Spin rate can be sensed by a rate gyro. Attitude can be sensed by using the outputs of the lateral accelerometers and this would probably require that the attitude control sybsystem be carried through entry. A set of ion sensors can be used to provide the necessary inputs to align the entry probe longitudinal axis with the velocity vector prior to entry. If ion sensors are used it is possible to eject the system prior to entry. The weight of the plumbing, motors, valves, and electronics is about 7 lb. , and the weight of the hydrazine and nitrogen and respective tankage about 8 lb.

No. 17 Aeroshell - A titanium aeroshell is used to resist the high stagnation pressures. For the Shallow Entry Angle Mission, a maximum stagnation pressure of about 8 atm is experienced, and for the Direct Link and Early Missions, about 30 atm. The JUN Mission experiences about 13 atm. Honeycomb sandwich construction is used. The titanium core thickness is about one inch, and the titanium face sheet thickness varies from .020 in. for the low stagnation pressure to .080 for the high stagnation pressure.

No. 18 Heatshield - The heatshield performance was provided by JPL for this study. A high-density graphite material is used for the ablator, and a low-density carbonaceous material is used as an insulator. The average ablator thickness is about 2.25 cm, and can vary by about 60% from the nose cap to the maximum diameter. To this 2.25 cm thickness is added one-half centimeter of high-density graphite to provide a nominal safety margin. The low-density insulator is 2 cm thick.

No. 19 Entry Probe Configuration - This is the hypersonic configuration that enters the atmosphere of Jupiter, and used to dissipate the kinetic energy that is associated with entry at 49 Km/sec.

No. 20 Thermal Control - An RTG is used to provide power for thermal control and for electrical checkout and timer operation during post separation cruise. A SNAP 19 type of unit was considered. Each plutonium heat source unit is encapsulated in a POCO graphite container to satisfy abort safety requirements. The unit can provide 10w of electrical power. The battery power supply that is used during entry is also used during the checkout of entry probe systems. RTG electrical power is used to recharge the battery. Also, the electrical energy is used for thermal dissipation in remote probe locations. Heat radiation and heat conduction paths are used to distribute thermal energy that is rejected by the RTG cycle. For 10w electrical output, 140w of thermal energy must be rejected: this energy is available for thermal control. An RTG performance figure of 2w electrical power per pound was used. The RTG is jettisoned prior to entry.

No. 21 Canister - A meteoroid container was used to protect the ablator from pitting and cracking that could result from meteoroid impact. The container weight based on a 95% probability of zero penetrations and a Type I mission is 22 lb., and for a Type II mission 32 lb. A sandwich construction is employed. A .02 inch aluminum bumper is used to shatter the meteoroid; a 2 inch polyurethane foam is used to disperse the shattered meteoroid particles, and a .04 inch backup plate is provided to stop the particles.

No. 22 Rocket Motor - A single end-burner solid rocket motor is used to provide the impulse to deflect the entry probe from a flyby to an impact trajectory. The propellant mass fraction varies from 0.74 for the low impulse Shallow Entry Angle Mission to 0.81 for the higher impulse JUN Mission.

No. 23 Separated Probe Configuration - This is the post separation cruise mode configuration of the Jupiter atmospheric entry probe.

7.3.2 Flight Article Configuration

A weight summary of the flight article for the five candidate missions is presented in Table 7-4. The subsystem additions or subsystem modifications that must be made to the spacecraft to support the entry probe mission are described below.

No. 1 Separated Probe Configuration - This is the post separation configuration of the entry probe.

No. 2 Separation - This subsystem must be added to the spacecraft. It includes: separation pyrotechnics, clamps and springs.

TABLE 7-4

JUPITER FLIGHT ARTICLE WEIGHT SUMMARY

NO.	SUBSYSTEM OR MODIFICATION	DIRECT	JUN	EARLY	SHALLOW	
					PIONEER F/G	TOPS
1	Separated Probe Configuration	510 Lb.	403 Lb.	501 Lb.	352 Lb.	352 Lb.
2	Separation	7	7	7	7	7
3	Probe to Spacecraft Adapter	6	8	6	5	7
4	Spacecraft Structure	2	7	2	2	7
5	Relay Receiver	0	8	8	8	8
6	Data Storage	0	0	3	3	0
7	Relay Antenna	0	15	24	24	15
8	Cabling	3	3	3	3	3
9	ACS & Midcourse Correction	62	14	62	44	14
10	Flight Vehicle Adapter	52	12	53	49	11
11	Entry Probe & Spacecraft Sub-System & Modification Weight	642	477	669	497	424
12	Contingency (20%)	128	95	134	99	84
13	Installed Weight	770	572	803	596	508
14	Spacecraft	547	1450	547	547	1450
15	Flight Article	1317 Lb.	2022 Lb.	1350 Lb.	1143 Lb.	1958 Lb.

No. 3 Probe to Spacecraft Adapter - This is the subsystem that is used to structurally mount the entry probe to the spacecraft.

No. 4 Spacecraft Structure - Some structural modification must be made to the spacecraft to provide a load path for the entry probe inertial loads induced during launch.

No. 5 Relay Receiver - All relay link missions require the addition of an up-link terminal to the spacecraft for receipt of the entry probe telemetry.

No. 6 Data Storage - The received relay data must be stored. Due to the very large storage capacity aboard the TOPS spacecraft, no additional data storage is required. For a Pioneer F/G, some additional capacity must be provided.

No. 7 Relay Antenna - A two-axis elliptical antenna is substituted for the single-axis medium gain antenna on the TOPS. The elliptical antenna can serve as an up-link S-band antenna for receipt of probe telemetry and as an X-band down-link medium gain antenna for the spacecraft. An electronically despun antenna is used for receipt of entry probe data by the spinning Pioneer F/G spacecraft.

No. 8 Cabling - This is the cabling for the entry probe to spacecraft electrical interface.

No. 9 ACS & Midcourse Correction - This is the modification that must be made in the TOPS and Pioneer F/G attitude control and midcourse correction sub-systems to accommodate the increased mass and greater moments of inertia that have resulted from the addition of an entry probe. For the Pioneer F/G, a greater propellant weight loading must be provided. For the TOPS, more propellant must be added, a set of ACS nozzle blocks moved, and a set of nozzle blocks added.

No. 10 Flight Vehicle Adapter - This is the modification that must be made in the existing adapter to support the entry probe. For the TOPS, the adapter must be strengthened. For a Pioneer F/G, a new adapter must be provided.

No. 11 Entry Probe and Spacecraft Subsystem and Modification Weight - This is the total weight penalty for carrying an entry probe.

No. 12 Contingency - The entry probe and spacecraft subsystem and modifica-tion weight has been increased by 20% to account for the many uncertainties in these conceptual design estimates.

8.0 SUBSYSTEM TRADEOFFS AND DESCRIPTION

The following eleven sections contain a description of the subsystems that were selected in the design of the entry probe system. These sections also include: 1) a discussion of the tradeoffs that were considered in making the selection, 2) the alternative approaches that were considered, and 3) the technology limitations that constrain the subsystem performance.

8.1 DATA HANDLING SUBSYSTEM

The total number of data bits generated while the entry probe descends to below the cloud layers in the Jupiter atmosphere will depend on the scientific instruments selected for the mission and the manner in which these instruments are sampled. To a first approximation the total number of data bits will be independent of the descent time, although it may turn out to be desirable to transmit some real time data along with stored scientific and engineering data with the result that there will be a small increase in total amount of transmitted data as the descent time increases.

8.1.1 Science Options

The types of instruments to be included on the entry probe will depend on the type of mission to be flown, i.e. whether the descent will be on the dayside or on the nightside. A total of five payloads have been selected as follows: 1) nominal dayside descent, 2) expanded dayside descent, 3) nominal nightside descent, 4) expanded nightside descent, and 5) small science payload.

The instruments to be included in each of the five payloads are indicated in Figure 3-1.

The nominal dayside descent payload will be selected for the reference design, and a data handling unit capable of processing the data from this set of instruments will be outlined. The optional science payloads will be discussed only to the extent of their gross effect on the data handling unit.

8.1.2 Dayside Science Sampling Requirements

The instruments that make up the nominal dayside payload have been listed in Table 8-1 which also summarizes the sampling requirements. Methods by which this sampling can be accomplished in a practical manner will be briefly discussed in this section. The methods discussed here should not be considered the only practical solutions to the sampling problems. Rather, they should be considered as specific examples of a design approach intended to show the feasibility of the mission.

TABLE 8-1

NOMINAL DAYSIDE SCIENCE PAYLOAD

No	Instrument	Bits/ Sample	Note No.	Total Samples	Total Bits	Remarks
1	Accelerometers (4)	40	1	90	3600	Peak axial acceleration must be determined
2	Temperature (2)	9	2	128	1152	Redundant sensors - range switched
3	Pressure (2)	9	2	128	1152	Redundant sensors - range switched
4	Gas Chromatograph/ Neutral Mass Spec.	500	3	10	5000	Gas Chromatograph requires 5 min. per analysis
5	U. V. Photometer	40	5	32	1600	5 channels
6	Aerosol Photometer	20	4	32	640	2 channels
7	H:D Photometer	10	4	32	320	1 channel
8	R. F. Click Detector	9	2	128	1152	Coincidence with optical flash detector indicated
9	Optical Flash Detector	9	2	128	1152	Coincidence with R. F. Click Detector indicated
10	I. R. Radiometer	50	3	10	500	5 detectors
11	Microwave Radiometer	20	3	10	200	2 detectors
12	Magnetometer	18	2	128	2304	2-axis instrument - also exo-atmospheric
13	Turbulence Indicator	9	2	128	1152	
14	Ion Mass Spectrometer	90	5	30	2700	Some pre-processing required

Note: 1. Acceleration will be measured in 3 axes with a 4th redundant axial instrument. Resolution: 10 bits/axis

2. 1 sample per kilometer

3. One sample above clouds, one within each cloud layer and one between each cloud layer.

4. One sample above clouds, then every 10% pressure increase.

5. Exoatmospheric - 1 scan every 2 sec for 1 minute prior to blackout.

Table 8-2 shows the 14 instruments grouped according to their sampling requirements. They can conveniently be broken up into four groups, as shown. One instrument, the magnetometer, has been listed in two different groups, since this instrument will be sampled prior to atmospheric entry as well as during the atmospheric descent.

8.1.2.1 Pre-entry and Blackout Data

The magnetometer as well as the ion mass spectrometer will be sampled periodically during the time from separation to entry into the Jovian atmosphere. However, during the last few minutes before entry, and after the protective canister has been jettisoned, the sampling will be done at a rate too high for direct transmission. For this reason, data from the magnetometer and from the ion mass spectrometer, will be stored in memory, and played back during the atmospheric descent period.

The time of entry, and consequently the beginning of communications blackout cannot be predicted closer than +35 minutes (typical 3 σ value) at the time of separation from the bus. For this reason the instruments will be turned on approximately 40 minutes prior to the predicted time of entry. The additional 5 minutes is for warm-up. Sampling of the magnetometer and the ion mass spectrometer will begin immediately on turn-on. However, to keep the number of stored bits to a minimum, the concept of continuous store-and-dump (Ref. 1) is recommended for use. A fixed number of memory locations, sufficient for about 1 minute of magnetometer and ion mass spectrometer data will be assigned to these instruments. When the memory locations have been filled, the oldest sample in the memory will be erased and replaced with the next sample. A special tag will be assigned to mark the boundary between "new" and "old" data. In this manner, the memory will always contain a one-minute time history from the two instruments. The sampling will be discontinued when 0.1g is sensed, signaling the onset of communications blackout. At that time, the new/old boundary may be anywhere within the memory block assigned to the two instruments.

The number of magnetometer samples stored during the last minute before blackout will be quite small, typically 10 or less, while the ion mass spectrometer will generate a substantial amount of data. Most of this data will be zero, since data for m/e greater than 4 is not expected, except possibly at the very base of the exosphere. For this reason it is considered essential that the data be preprocessed to reduce the number of bits that have to be stored and transmitted.

The accelerometer triad, with a redundant axial instrument, will be sampled during communications blackout, and immediately following emergence from blackout. Depending on entry angle, the sampling period may last 70 seconds or longer. For a 15 deg entry angle, peak acceleration of 523g will occur 18

TABLE 8-2

INSTRUMENT SAMPLING REQUIREMENTS

Group I   Instruments whose sampling will be completed before transmission of data begins:

1. Magnetometer (exoatmospheric)
2. Ion Mass Spectrometer (exoatmospheric)
3. Accelerometers (during and immediately after communication blackout)

Group II   Instruments which are sampled according to the expected temperature of the postulated cloud layers. Backup sampling may be done as a function of pressure or time.

1. Neutral Mass Spectrometer/Gas Chromatograph
2. I. R. Radiometer
3. Microwave Radiometer

Group III   Instruments whose sampling is done as a function of atmospheric depth.

1. Temperature Gauges
2. Pressure Gauge
3. R. F. Click Detector
4. Optical Flash Detector
5. Magnetometer
6. Turbulence Indicator

Group IV   Instruments which are sampled every 10% increase in pressure

1. U. V. Photometer
2. Aerosol Photometer
3. H:D Photometer

seconds after 0.1g has been detected. Communications blackout will last about 31 seconds, and chute deployment at 0.7M will occur about 73 seconds from the beginning of entry (0.1g). If a fixed sampling rate were used, it would be necessary to take one sample (40 bits) every 0.1 seconds to ensure that the peak acceleration is determined. This would result in storage requirements of about 12,000 bits (through emergence from blackout), or about 30,000 bits (through chute deployment). In both cases the total number of bits that must be transmitted is high.

The main objectives of the accelerometer measurements are to determine peak acceleration, and the shape of the acceleration curve in all three axes. If the peak acceleration is determined separately, the shape of the curve can be determined from relatively few measurements. The time and amplitude of the peak acceleration from the two axial accelerometers with the simultaneous readings from the two transverse accelerometers could be stored in specially assigned memory locations, while the samples taken at fixed time intervals could be stored in sequence in a specially assigned memory block.

The four accelerometers should be sampled "simultaneously". For all practical purposes, it would appear that the four samples may be taken over a time period of about 1 millisecond. This is well within the current state of the art for 10 bit analog to digital converters.

8.1.2.2 Instruments Sampled In or Between Cloud Layers

The Group II instruments (Table 8-2) should be sampled once above the clouds, within each cloud layer, between cloud layers, and below the clouds. The sampling may be done as a function of: 1) temperature, 2) pressure, and 3) time.

Temperature is by far the most sensitive indicator, although it does not appear possible to select one set of temperatures that simultaneously satisfy all model atmospheres. One set of samples suitable for the nominal atmosphere has been shown in Table 8-3. This table also shows that, even for a 1 hour descent, it may be difficult to obtain 10 complete measurements from the gas chromatograph. If the gas chromatograph requires 5 minutes for each analysis, it may only be possible to obtain 4 samples during a half hour descent.

TABLE 8-3

GROUP II EXPERIMENT SAMPLING

NOMINAL ATMOSPHERE

Sample No.	Temp. °K	Pressure ATM	Time Sec 1/2 Hr. Descent	Time Sec 1 Hr. Descent	Location
1	115	.25	120	470	Above clouds
2	140	.45	175	690	Within NH_3 clouds
3	165	.81	255	1000	Between NH_3 and NH_4 clouds
4	190	1.14	315	1250	Within NH_4SH clouds
5	205	1.35	355	1380	Between NH_4SH and H_2O (solid) clouds
6	240	1.95	450	1759	Within H_2O (solid) clouds
7	270	2.95	580	2300	Within H_2O (solution) clouds
8	285	3.60	660	2600	Between H_2O and NH_4CL clouds
9	400	13.5	1550	3550	Within NH_4CL clouds
10	430	17.5	1850	3650	Below clouds

8. 1. 2. 3 Sampling as a Function of Atmospheric Depth

The Group III instruments listed in Table 8-2 should ideally be sampled once every kilometer of vertical descent. If it were essential to sample at equal vertical intervals, this could best be accomplished by storing (in a read-only memory) the various pressures corresponding to every kilometer of descent. This would require a substantial amount of storage, in particular if all three atmospheric models have to be considered.

An alternate sampling scheme would involve the use of a non-linear time base according to which samples would be taken close together at the top of the atmosphere, and less frequently (by a factor of 4 or 5) near the bottom of the clouds. This latter sampling method has the advantage that it is clock synchronous, can be made fairly close to the desired sampling rate, and yields a fixed number of samples. It is expected that 128 such samples will be adequate.

8. 1. 2. 4 Instruments Sampled as a Function of Pressure

The three instruments listed in Group IV (Table 8-2) must be sampled once above the clouds, then every 10% increase in pressure down to the bottom of the clouds would require about 45 samples. A possible way to sample would again be to store the pressure values where samples are to be taken in a read-only memory. A fairly substantial amount of storage would be required. Fortunately, it turns out that a 10% pressure increase in the nominal atmosphere comes close to 4 km descent. The simplest way to sample the Group IV instruments would be to take one sample for every four samples from the Group III instruments. This would result in 32 samples being taken from the top to the bottom of the clouds.

8. 1. 2. 5 Composite Sampling

Figure 8-1 shows the total number of science data bits generated as a function of time while the probe descends through the Jovian atmosphere. A fixed $\frac{m}{C_D A}$ has been assumed. The curve does not start at zero because of the exoatmospheric and blackout data which has been stored in memory prior to the beginning of data transmission and also atmospheric sampling.

A typical mission might require about 24, 000 bits of scientific data. In addition to that, engineering and housekeeping data must be added.

FIGURE 8-1
DATA ACCUMULATION PROFILE

SCIENCE BITS
GENERATED

SCIENCE BITS
READ OUT

TIME = 0 AT
P = 10⁻² ATM.

No. Bits/10³

$TIME \times \sqrt{\frac{m}{C_D A}} \sim SEC \sqrt{\frac{SLUG}{FT^2}}$
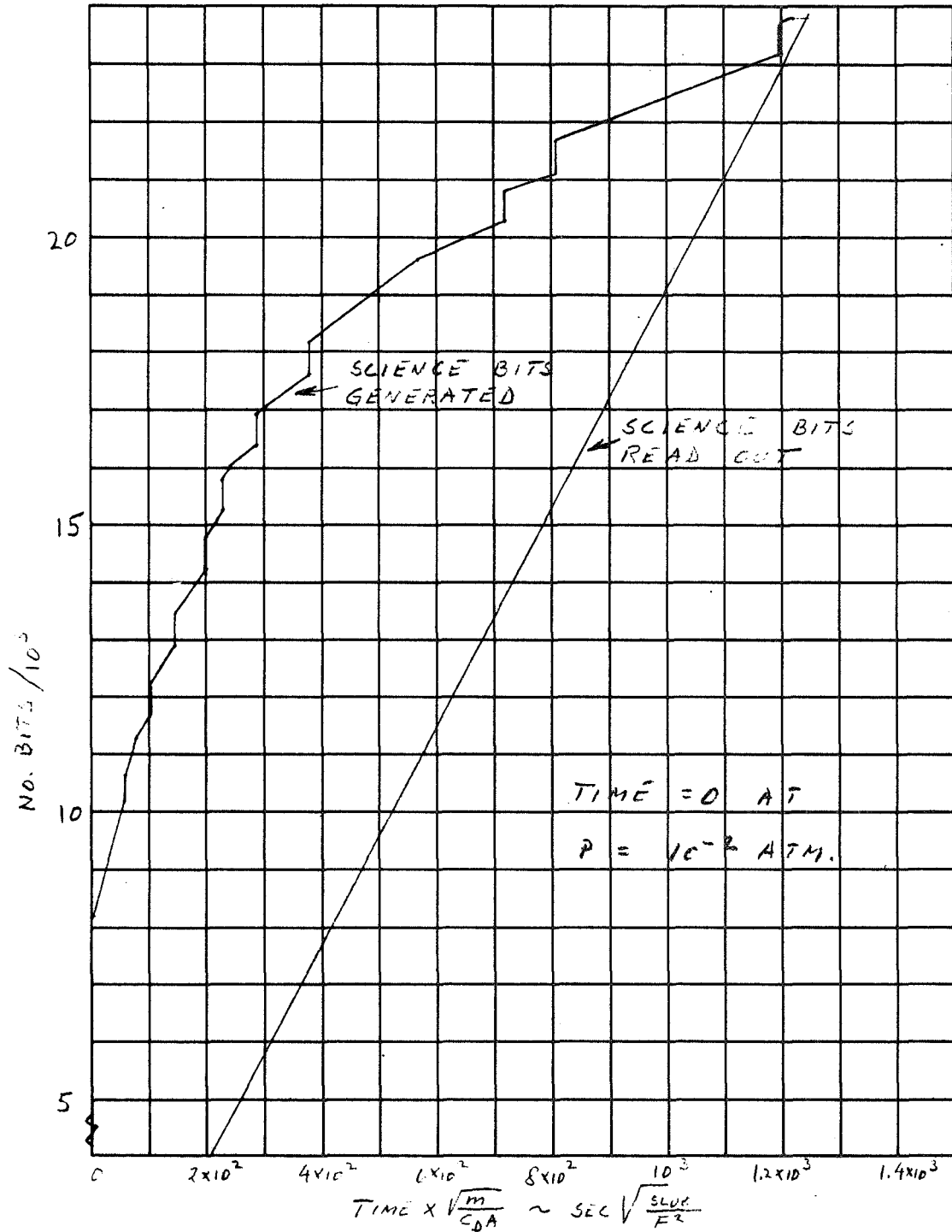
The sloping, straight line portions of the curve represent data from the Group III and Group IV experiments, and the changes in slope represent rate changes in the non-linear time base. The vertical "jumps" in the curve correspond to the Group II data.

The long, straight line represents the readout of the scientific data at a constant rate. For a 1/2 hour descent more than 13 bits per second is required for the science, while engineering and housekeeping data will bring the rate above 15 bps.

The difference in Figure 8-1 (vertically) between the upper curve and the straight line readout corresponds to the amount of data in storage at any time. The maximum is in the neighborhood of 16,000 bits.

8.1.3 Other Science Payloads

In the event one of the other science payloads is selected, the principal effect on the data handling unit will be a change in sampling and programming requirements, as well as the total number of bits generated during the atmospheric descent.

8.1.3.1 Expanded Dayside Payload

The expanded dayside payload replaces the U.V. photometer with a U.V. spectrometer, and adds a condensimeter-evaporimeter. The net result of this will be to nearly double the total number of bits to be transmitted. As a consequence, only a relay transmission scheme appears feasible. For a 1 hour descent time the bit rate requirements will be about 20 bps, which is well within the capabilities of the typical relay link. At the same time, the data storage requirements will increase by about a factor of three over that required for the reference mission. Some additional hardware will be required for the purpose of controlling requirement sampling and programming.

The more favorable relay links will permit bit rates more than an order of magnitude higher than the 20 bps assumed above. Higher bit rates will allow a reduction in on-board data storage requirements, but at the same time it will increase the storage requirements on the bus, while the total amount of useful data will remain roughly the same.

8. 1. 3. 2 Nominal Nightside Payload

The nominal nightside payload is similar to the reference payload. Three
photometers will be replaced by a nephelometer whose total bit require-
ment during the descent will be somewhat less than the bit requirements
for the photometers. The difference will be about 1000 bits or less, and
the effect on the data handling unit will be negligible when compared to the
reference mission.

8. 1. 3. 3 Expanded Nightside Payload

On the expanded nightside payload the small gas chromatograph will be
replaced with a more extensive gas chromatograph package. In addition, a
condensimeter-evaporimeter will be added. The total number of science
bits generated during the mission will be somewhat less than for the expanded
dayside mission, but definitely too large for a direct telemetry link. Con-
sequently, a relay link will be required.

8. 1. 3. 4 Minimum Science Payload

The minimum science payload will make it possible to drastically simplify
the data handling unit on the probe, particularly if a relay link is used. A
relay link capable of a 200 bps data rate would eliminate the requirement for
on-board storage, and all data could be transmitted in real time. If a direct
link is used, even a half hour descent time would result in bit rates below
10 bps ($\sim$5. 5 bps for a total of 10, 000 bits). A memory with a capacity of
about 8000 bits would be required.

8. 1. 4 Engineering and Housekeeping Data Requirements

In addition to the scientific data which has already been discussed, allowance
must be made for the engineering and housekeeping data requirements.
Typical requirements would include ablation measurements and bond line
temperatures which would be stored along with the accelerometer data during
the atmospheric entry. In addition, it will be desirable to measure tem-
peratures at key internal points, as well as various voltages and currents.
It will also be necessary to include synchronization codes and sufficient time
tags to permit non-ambiguous identification of all data.

8. 1. 5 Data Handling Implementation

At the present time, it appears that adaptive data handling will result in
maximum useful data obtained from the probe. This is particularly true in
the event a direct link is desirable. A block diagram of a candidate data
handling unit has been shown in Figure 8-2, and a brief discussion follows.

8.1.5.1 General Characteristics

The data handling unit should be capable of operating in a number of different modes, and must be able to modify its sampling of the instrument outputs as a function of the readings obtained from some of these instruments. Thus, the number of science bits generated each second will not remain constant, while the transmitted bit rate stays constant. The difference between the total number of bits generated at any point in time during the descent, and the total number of bits transmitted at the same point in time, must be stored in memory. The amount of stored data will reach a maximum in the upper portion of the atmosphere. The scientific data will not necessarily be read out in the same order that it was sampled.

Post Separation Cruise

After the probe has been separated from the bus, certain instruments will occasionally be turned on, and data from these instruments transmitted. In addition, there will be checkout of the other instruments. During the cruise, the data handling and programming will be controlled by a clock, and switch-over to the next operating mode will occur at a pre-selected time loaded by means of ground commands into a timer register prior to separation from the bus.

Exoatmospheric Mode

The exoatmospheric mode will be initiated by the timer and terminated when the onset of communications blackout is sensed by the accelerometers. During this operating mode the magnetometer and the ion mass spectrometer will be sampled in a continuous store-and-dump process, while the transmitter and the remaining instruments will be turned on in preparation for the atmospheric descent.

Communications Blackout Mode

During and immediately following communications blackout, data from the accelerometers along with some engineering data will be stored in memory. The duration of the blackout mode will depend on the entry angle of the probe.

Atmospheric Descent

During the atmospheric descent, all data stored in memory, as well as data obtained during the descent, will be transmitted. At the same time, an adaptive program will control the sampling of the various instruments, perform the required data processing, and store the data in memory until it can be read out to telemetry.

FIGURE 8-2

DATA HANDLING SUBSYSTEM

SIZE: 200 In.^{3}

WEIGHT: 6 Lb.

POWER: 3 W
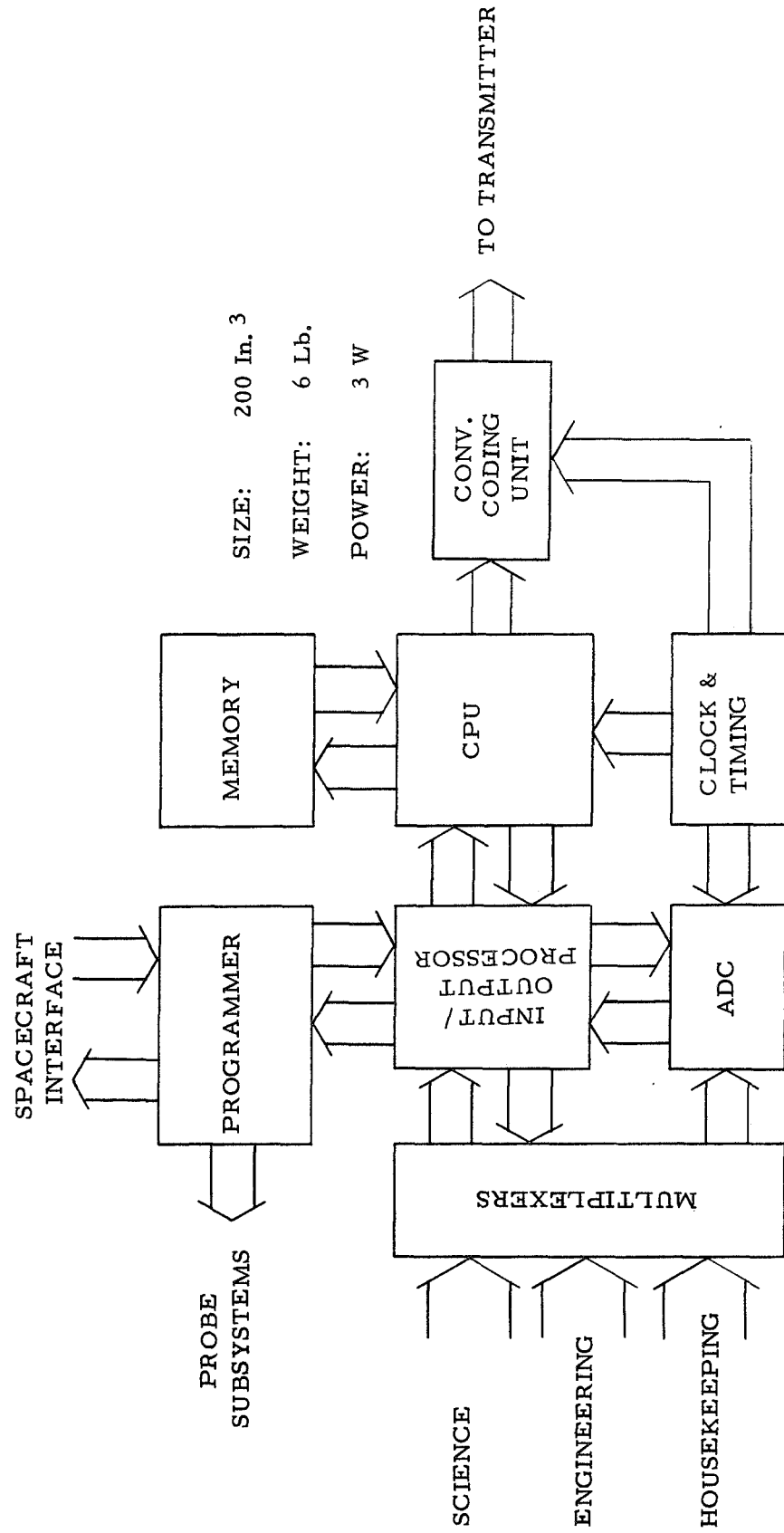
Test Mode

Facilities for testing the probe subsystems must be designed such that
testing can be accomplished: a) while the probe is attached to the bus;
b) after separation from the bus, but before the meteoroid canister is
ejected; and c) after ejection of the meteoroid canister, but before the
exoatmospheric mode begins.

8. 1. 5. 2 Data Handling Components

The various components to be used in the data handling unit on the entry
probe, do not appear to put excessive demands on technology. In fact, all
major components can be built with 1971 technology. In addition to the
procedures normally used in the design of reliable, high-performance
space equipment, the electronics for the Jupiter entry probe must be
designed to survive the intense radiation belts surrounding Jupiter, as well
as operate in a satisfactory manner in the strong Jovian magnetic fields.

The most critical component appears to be the memory. The intense radia-
tion belts appear to rule out MOS memories, and bipolar memories have
excessive power requirements. Magnetic memories are susceptible to the
strong magnetic fields, but it is considerably easier to shield against the
magnetic field than it is to shield against the high energy electrons in the
radiation belt.. Candidate magnetic memories are the ferrite core and the
plated wire types. With proper shielding both types of memories should per-
form in a satisfactory manner, and the choice must be based on other
qualities, such as primarily reliability, power, and special properties such
as the NDRO characteristics of the plated wire memories.

The other major components, such as the analog to digital converter,
multiplexer, clock, central processing unit, etc. , can be designed to survive
the radiation belts and to function properly in the magnetic fields, using
present-day technology.

8. 1. 6 Data Compression

Data compression can be performed as desired by the central processing unit
(CPU) in combination with the memory. In most cases, simple compression
algorithms can be implemented using hard-wired subroutines. If complex
algorithms are required, they can be stored in memory, while arithmetic
capability can be added to the CPU if needed. The accelerometer data, for
instance, can have the bit requirements cut by an order of magnitude or more
if data compression techniques are used.

8.1.7 Programming

It is convenient to include most programming features within the data handling unit. In some cases, such as for the pyrotechnic subsystem, additional control and sequencing circuits external to the data processor, may be desirable. Typical areas where programming may be required are: 1) attitude control electronics; 2) mode selection for the data handling unit; 3) instrument control; 4) test programming; 5) R.F. subsystem control; and 6) initiation of pyrotechnic events. The programmer may also contain the circuits required for the interface between the probe and the bus.

8.1.8 Redundancy and Reliability

The long mission duration coupled with the severe environmental requirements will lead to unusually strict reliability requirements. Reliability can best be achieved with a careful design based on proven components and technology. In addition, consideration must be given to redundancy as a means of enhanced overall subsystem reliability. The use of redundancy may also imply that self testing and repair functions have to be built into the equipment. Such technology has been investigated extensively at JPL.

8.1.9 Data Handling Tradeoffs

The design of the data handling unit is a strong function of the science payload as well as the selected descent time and the available bit rate. When these parameters have been established, various other choices affecting the data handling design can be evaluated. Some possible choices will be briefly described in the following section.

8.1.9.1 Minimum Mission

The minimum mission concept assumes that the minimum science payload (Figure 3-1) is combined with a 10 minute descent time and a direct link to Earth that provides a 10 bit/second rate. Figure 8-3 illustrates the number of science bits generated as a function of time, as well as the number of bits read out to telemetry. The difference between bits generated and bits read out is never greater than about 2,000 bits, and this, then, becomes the minimum memory size. The minimum mission allows two to four ion mass spectrometer samples, four neutral mass spectrometer samples (at about $100^\circ K$ intervals), two gas chromatograph samples (coincident with the first and third neutral mass spectrometer samples), as well as pressure and temperature readings at one to two km intervals.

FIGURE 8-3

MINIMUM SCIENCE MISSION

10 MIN. DESCENT

SCIENCE DATA READ OUT.

SCIENCE DATA GENERATED

RATE = 8.45 BITS/SEC
SYNC, HSKP, 1.55 "

TOTAL RATE 10.0 BITS/SEC

TIME ~ SEC

No. BITS
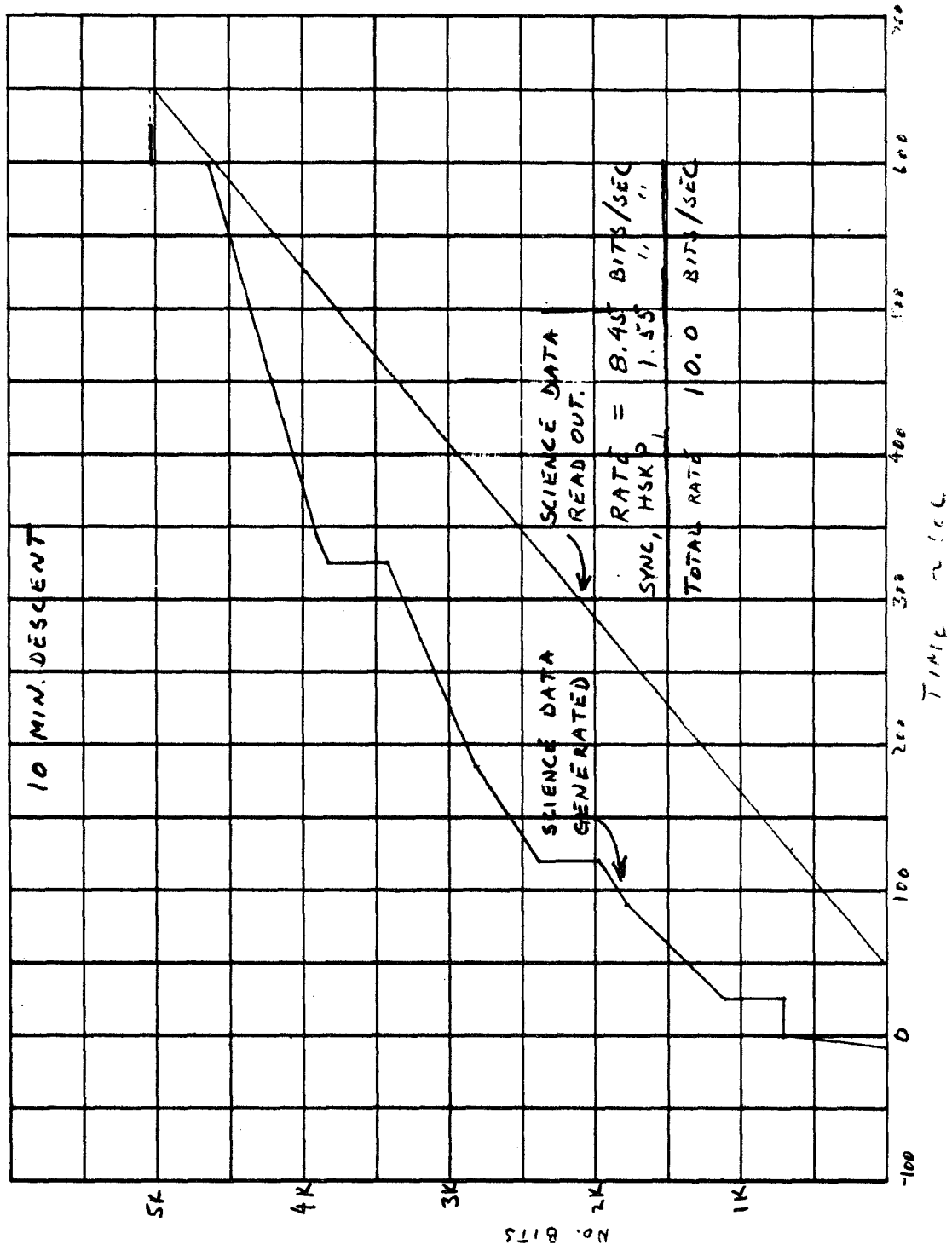
8.1.9.2 Nominal Mission

A nominal mission may be based on the nominal dayside science payload, 1 hour descent time, and relay transmission to DSN via the bus at a data rate of 100 bits per second or less. If a total of 27,000 bits is generated during the descent to the bottom of the clouds, the required bit rate is only 7.5 bits per second. This option is similar to the one illustrated in Figure 8-1, where about 3,000 bits could be added for engineering, housekeeping and some limited real time data.

8.1.9.3 Multiple Transmissions

The two mission alternatives which have been described so far, suffer from one potentially serious drawback, i.e., the data is transmitted only once, and not in real time. Should data be lost during the mission, either temporarily due to such factors as wind gusts, or permanently due to an early mission failure, scientific data which was already obtained and stored in memory would be lost. The use of multiple transmissions of data would minimize such losses, in particular those of a temporary nature.

One multiple transmission alternative has been illustrated in Figure 8-4 where it is assumed all data will be stored in memory. Each memory location will be read out at least three times, making possible the recovery of data lost during a temporary transmission dropout. Additionally, the higher bit rate will mean less data is lost in case of an early mission failure.

8.2 STRUCTURAL SUBSYSTEM

The Jupiter entry probe structural subsystem consists of two major elements, the aeroshell and the scientific payload pressure vessel. Other structural elements of the probe, including the launch vehicle adapters, external equipment support, Δ V rocket support, etc. are strongly dependent on design configuration and hence are presented in the design section of the report. Similarly, the environmental container was sized primarily for micrometeoroid protection as discussed in Section 2.1. In the following subsection, only the aeroshell and pressure vessel parametric analysis will be discussed.

8.2.1 Aeroshell

The aeroshell structure provides the probe aerodynamic configuration during Jupiter entry. In this role, it must react the high aerodynamic pressure load,

FIGURE 8-4
MULTIPLE DATA TRANSMISSION

TOTAL DATA BITS
GENERATED

BITS READ OUT TO
TELEMETRY

TOTAL BIT RATE ~ 67 BPS

1, 2, 3 DENOTES DATA MODE

THOUSANDS OF BITS

TIME — SEC
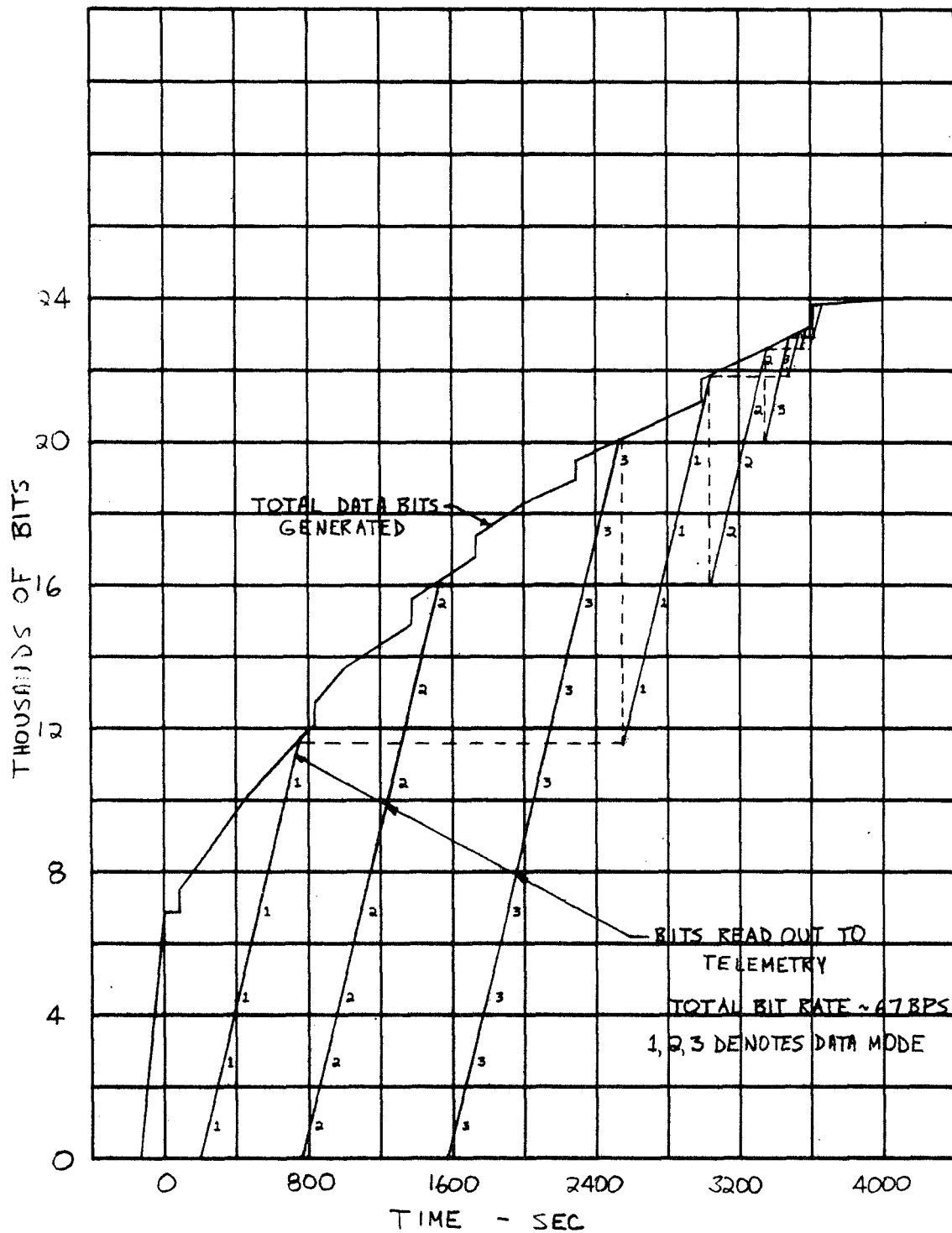
support the internal payload, and support the heat shield protection sub-
system. For this study, a 60 deg blunted cone, aerodynamic configuration
was selected. Previous aeroshell studies have indicated that the most
optimum structural configuration will be a sandwich shell consisting of face
sheets and honeycomb core. Using this type of construction, parametric
weight curves where generated as a function of external aerodynamic
pressure (in equivalent Earth atmospheres) for several candidate materials;
titanium, beryllium, aluminum, and glass reinforced plastic (fiberglass).
These curves are shown in Figure 8-5 along with the material properties
utilized. The structure was assumed to be at 200 deg F when the probe is
experiencing peak aerodynamic loads. In addition, a multiplication factor of
1.7 is included in the weight parameter to account for the face sheet to core
bonding, the payload attachment ring, the base ring required to stabilize
the conical shell against buckling, and local fittings necessary for mounting
miscellaneous equipment on the aeroshell

The weight parameter curves presented in Figure 8-5 clearly illustrates the
advantage of titanium as a light weight aeroshell for pressures above 7 atm.
Below this pressure level, beryllium is slightly lighter. The reason
titanium is attractive at the higher pressures is that the face sheet weight
is predominant and governed by the yield strength of the material. This is
more clearly illustrated by the total weight equation* for a 60 deg blunt
conical, honeycomb shell,

$$W_{TOTAL} = 12.3 R^3 \left[\left(\frac{\rho_f}{\sigma_{cy}} \right) P + 159 \left(\frac{\sigma_{cy}}{R E_c} \right)^{0.704} \frac{\rho_c}{R} \right]$$

where

P	=	applied external pressure, psi
R	=	base radius of shell, in.
ρ_f	=	face sheet density, #/in^3
ρ_c	=	core density, #/in^3
σ_{cy}	=	face sheet yield strength, psi
E_c	=	face sheet elastic compression modulus, psi

The first terms in the bracket represents the face sheet weight and the
second term is the honeycomb core weight. It is apparent that the weight is
a strong function of face sheet, ρ_f / σ_{cy} parameter. For titanium this para-

---

*This equation is only applicable when the face sheets are governed by yield
stress. When the face sheet is limited by minimum gage (for the case in
point this is at $P < 1.0$ atm applied pressure) this equation no longer is
applicable.

8-18

FIGURE 8-5

AEROSHELL PARAMETRIC WEIGHT

MATERIAL	DENSITY ρ, lb/in^3	COMPRESSION YIELD STRENGTH σ_{cy}, psi	COMPRESSION ELASTIC MODULUS E_c, psi
TITANIUM	0.16	135,000	16.4×10^6
BERYLLIUM	0.067	40,000	44.0×10^6
ALUMINUM	0.101	60,000	10.0×10^6
FIBERGLASS	0.069	80,000	5.0×10^6

PROPERTIES AT 200°F

NOTE: WEIGHT PARAMETER INCLUDES A FACTOR OF 1.7 FOR BONDING RINGS, FITTINGS, ETC.
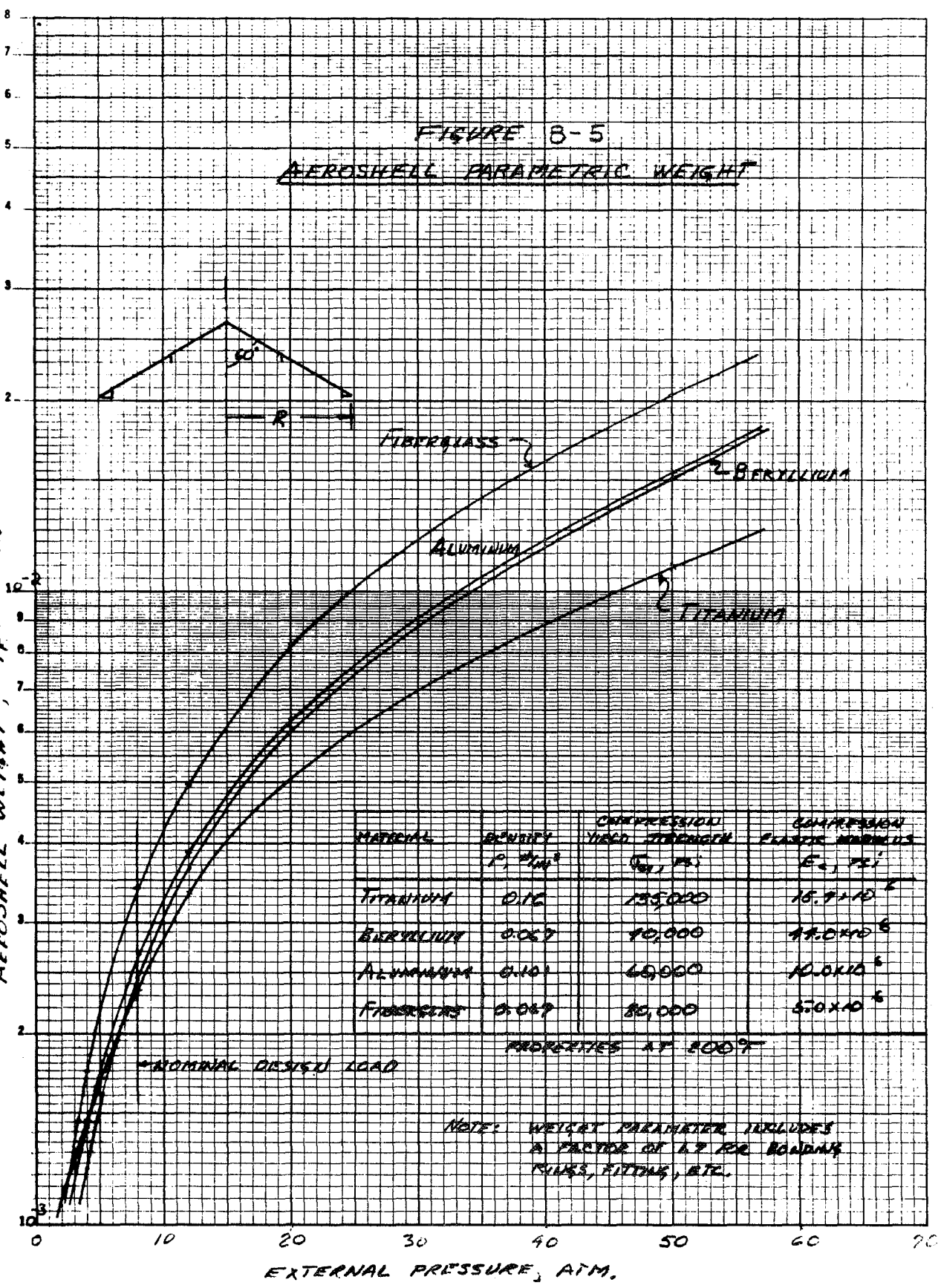
meter is 36% smaller than beryllium. As the external pressure becomes smaller, the core weight becomes a larger percentage of the total weight, since it is independent of external pressure and thus, is a constant for given material properties. This is the reason for the titanium curve crossing the other materials at low pressure levels. If an aluminum or beryllium core were used with titanium face sheets, additional weight saving could be realized over the all titanium construction.

For the nominal probe design presented in this document, a titanium aeroshell was employed. The aeroshell diameter is 48 inches which results in a 32.5 pound aeroshell at an external pressure of 8 atm. A beryllium aeroshell structure could also have been employed at this pressure level with a slight weight increase (1.3 pounds) over titanium; however, the fabrication cost would be significantly higher.

8.2.2 Pressure Vessel

The descent payload for the Jupiter probe is a spherical pressure vessel which must support and contain the scientific instruments during descent into the Jupiter atmosphere. Since the pressure vessel is maintained at approximately one atmosphere internal pressure, and the Jupiter atmospheric pressure is high (17 atmospheres to 525 atmospheres, depending on the atmosphere model used) the pressure vessel is subjected to severe external pressure loads. As a result of the large operating pressure range, there exists significant pressure vessel weight tradeoffs that are sensitive to material selection.

Under external pressure, the spherical vessel may be governed by buckling stability criteria or by the material yield strength depending on the magnitude of external pressure and material properties.

In reality, the perfect spherical pressure vessel is unobtainable and critical buckling pressure is strongly dependent on the degree of departure from sphericity. Experimental buckling pressures are frequently as low as one fourth or less of the classical predicted pressures. Recent testing on near-perfect spherical shells, however, indicate that a critical buckling pressure of 70 percent of the classical prediction is a reasonable design point, hence the elastic buckling critical pressure of near-perfect spherical shells can be expressed as:

$$P_{CR} = 0.84 \; E_c \left(\frac{t}{R}\right)^2$$

where P_{CR} = elastic buckling critical pressure, psi
E_c = compression modulus of elasticity, psi
t = pressure vessel thickness, in.
R = pressure vessel radius, in.

Utilizing this buckling criteria, the weight parameter for the spherical pressure vessel can be expressed as:

$$\frac{W}{D^3} = \frac{\pi}{2} \sqrt{\frac{P}{0.84}\left(\frac{\rho^2}{E_c}\right)}$$

where P = applied external pressure, psi
D = pressure vessel diameter, in.
ρ = material density, lb/in^3

It is evident that the pressure vessel weight, governed by buckling, is strongly dependent on the ρ^2/E_c ratio, i.e., the vessel weight is reduced as the ratio is diminished.

Similarly, if yield strength is the governing design criteria, where the average stress in the spherical pressure vessel is:

$$\sigma_{AVG} = \frac{PR}{2t} \quad , \quad \text{for} \quad R/t > 10$$

then the vessel weight can be expressed as:

$$\frac{W}{D^3} = \frac{\pi}{4}\left(\frac{\rho}{\sigma_{CY}}\right)P$$

where σ_{CY} = material yield strength, psi

Hence, the weight of the spherical pressure vessel that is governed by yield strength, is then strongly dependent on the ρ/σ_{CY} ratio.

Based on these criterion several candidate materials were selected for evaluation which included: two conventional metals, (aluminum and titanium); beryllium, glass reinforced plastic, two advanced composites (boron/epoxy and boron/aluminum, which represent 1975 technology), and two high compressive yield strength materials, alumina and bulk glass. A comparative summary of these materials is presented in Table 8-4 along with their respective room temperature properties. In the study it was assumed that the pressure vessel will be operating at a temperature of less than 160 deg F (providing it is protected by a layer of MIN-K or similar type of insulation).

TABLE 8-4

PRESSURE VESSEL - CANDIDATE MATERIAL PROPERTIES
(At Room Temperature)

Material	Density ρ, $\#/IN^3$	Compression Yield Strength σ_{cy}, PSI	Compression Modulus E_c, PSI	$\frac{\rho}{\sigma_{cy}} \times 10^{-4}$ $\frac{1}{IN}$	$\frac{\rho^3}{E_c^2}$ $\#/IN^4 \times 10^{-9}$
Beryllium	.067	40,000	45 x 10⁶	.168	.100
Alumina	.130	300,000	45 x 10⁶	.043	.372
Boron-Epoxy	.071	70,000	15 x 10⁶	.100	.334
Titanium (6AL-4V)	.160	150,000	16 x 10⁶	.107	1.600
Aluminum (7075-T6)	.101	70,000	10 x 10⁶	.145	1.010
Boron-Aluminum	.090	150,000	19 x 10⁶	.060	.426
Bulk Glass	.080	150,000	9 x 10⁶	.053	.710
Glass Reinforced Plastic	.067	30,000	6 x 10⁶	.223	.750

Of the materials presented in Table 8-4, beryllium, alumina and boron epoxy appear to be the most attractive for the spherical pressure vessel from the weight standpoint. Boron/aluminum and bulk glass could also be considered except both are difficult to fabricate in spherical shapes and are not that much better than boron/epoxy or alumina which are presently being used for spherical shells. Neither conventional aluminum nor glass reinforced plastic materials are attractive because of their low compressive strength and modulus.

A comparison of pressure vessel weight parameter as a function of external pressure for these materials is presented in Figure 8-6. A titanium weight curve was also included in this figure since it can be easily fabricated in spherical shapes and allows for a weight comparison of a conventional material to the minimum weight candidates. To provide realistic design data curves, the weight parameter was generated using safety factors applied to the external pressure of 1.5 for buckling and 1.0 for yield as well as a factor of 1.25 on both criteria for rings, fittings, bosses, etc.

The discontinuity in the weight curves presented in Figure 8-6 represents a change in criteria from buckling stability at low pressure levels to yield stress at higher pressure levels. This discontinuity point occurs when the weight for buckling criteria equals the weight for yielding criteria. This point is higher than the actual transition point because the safety factor is higher on buckling than on yielding. It is important to note that for beryllium the discontinuity point occurs at a low pressure ($\sim$17 atm) because of its low compressive yield strength. The opposite is true for alumina, where buckling governs up to 1000 atm since it has both a high compression modulus and yield strength.

In general, the results of the study has indicated that beryllium is the lightest material in the low external pressure region ($<$ 60 atm) and alumina is lightest in the high pressure region ($>$ 150 atm). In between these pressure regions the advanced composite, boron/epoxy, results in a slightly lower weight than alumina. With the rapid advancement that is presently underway in advanced composites, particularly boron/epoxy and boron/aluminum, this picture may improve greatly by 1975.

One of the major difficulties in using alumina as a pressure vessel is its brittle nature and its low tensile strength. These problems can be somewhat minimized by careful design techniques at joints and penetrations along with tempering and chemical strengthening. A possible alternative solution is

FIGURE 8-6

PRESSURE VESSEL WEIGHT AS A FUNCTION OF
EXTERNAL PRESSURE

EXTERNAL PRESSURE, ATM.

8-24
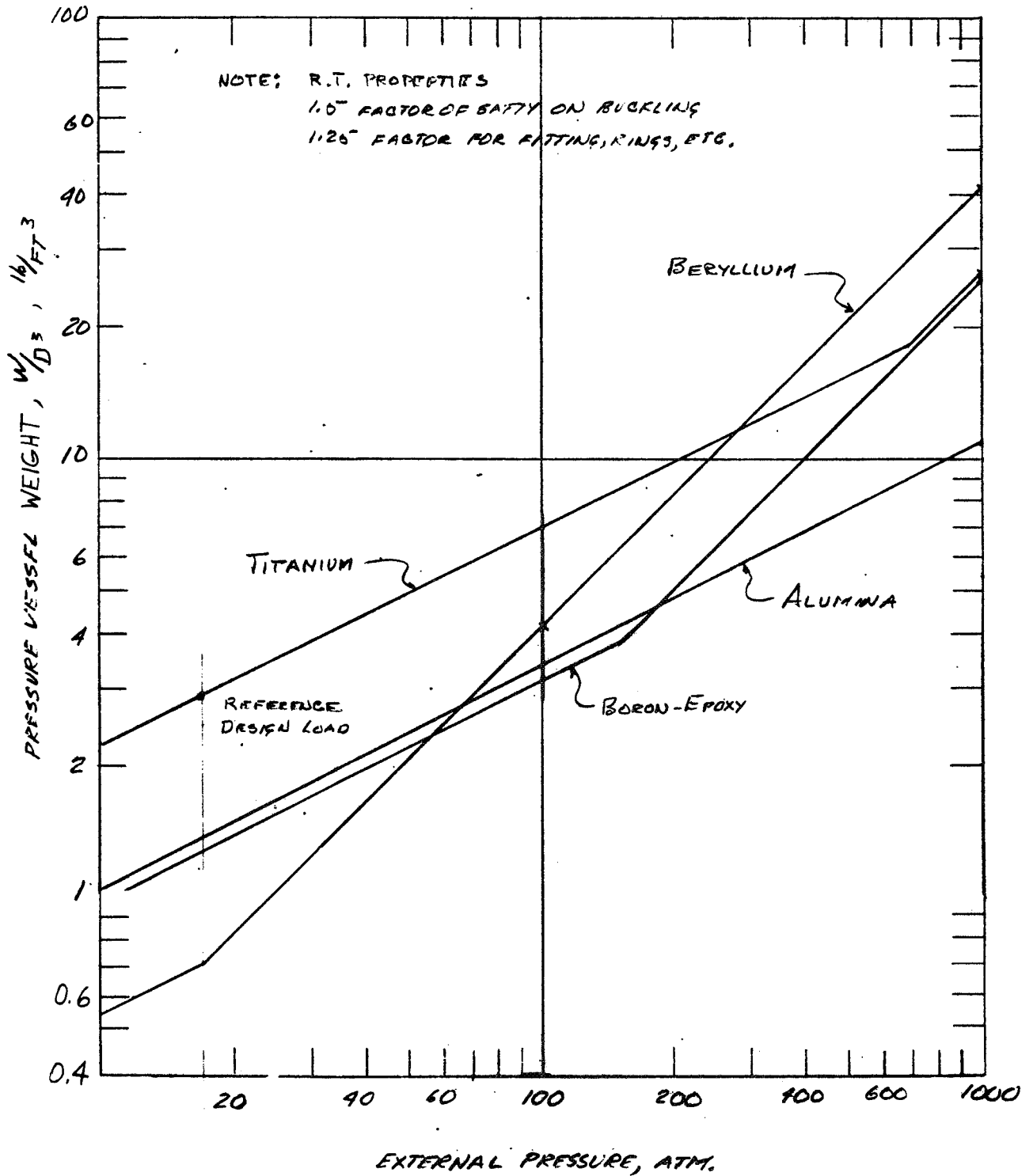
to use a composite of alumina and fiberglass. In this construction the
alumina is made into a series of sphere segments and wrapped with fiberglass.
By this technique, the fiberglass reacts all tension, vibration and fitting
loads and the alumina reacts the high Jupiter descent pressure loads.
Similar techniques are being employed today for deep submerging ocean
vessels that are made of bulk glass or ceramics.

For the nominal reference design presented for this study the external pressure
during Jupiter descent is 17 atmospheres. To allow some conservatism in
the structures weight estimate, titanium was used for the pressure vessel
which is 21.3 inches in diameter. The weight of the titanium pressure vessel
as presented in Figure 8-6 will be 16.6 pounds. It is obvious that significant
weight savings can be made by using beryllium or alumina in place of titanium
at this pressure; however, fabrication cost is significantly higher. In future
studies of the Jupiter probe where more detail conceptual designs will be
considered, with atmospheric pressure more clearly defined, these lighter
weight materials must be further evaluated to arrive at an optimum probe
design.

8.3 THERMAL CONTROL SUBSYSTEM

The basic function of the thermal control subsystem is to maintain the tem-
perature level of the entry probe within defined operating limits during
exposure to the changing environment from Earth launch to descent to base
of the Jovian clouds. The probe will be exposed to the following environments:

Launch Phase - The probe will be attached to the spacecraft under an environ-
mentally controlled shroud. This phase of the mission should not impose any
unusual design requirements.

Interplanetary Cruise Phase - After injection onto an interplanetary transfer
trajectory the high gain antenna of the TOPS and Pioneer F/G will be oriented
towards the sun for the 450 to 1450 day cruise. This provides an invarient
solar aspect during cruise. At Jovian encounter, the high gain spacecraft
antenna will also be oriented towards Earth due to the relative proximity of
the sun to Earth in comparison to the distance of the Jovian orbit from the
sun. Based on use of an open mesh construction for the antenna and mounting
of the probe axis normal to the spacecraft longitudinal axis, the entry probe on
TOPS will be partially exposed to sunlight. On Pioneer F/G, the entry probe
will be mounted to the structure opposite the high gain antenna and so it will
be in the shade. For both TOPS and Pioneer F/G, the entry probe could be
exposed to direct sunlight for a period of a few hours during the midcourse
correction maneuvers.

A thermal design problem exists due to the conflicting requirement of: 1) low solar absorptivity and high infrared emissivity near Earth so that the probe temperature does not rise above the design limits, and 2) high solar absorptivity and low infrared emissivity near Jupiter so that the probe temperature does not drop below the design limits. Use of electrical heaters near Jupiter that derive their energy from a spacecraft power source can be used to reduce the dynamic range of the temperature excursion. Temperature regulation during this phase of the flight should not tax present technology.

Post Separation Cruise Phase - Some thirty to sixty days prior to spacecraft periapsis passage, the probe will be separated from the spacecraft. During this phase, the major problem will be to prevent the probe temperature from dropping below the design limit of 60 deg F. Approaches to thermal control during this phase are discussed in Section 8.3.1.

Atmospheric Descent Phase - The probe descends into the atmosphere of Jupiter and must survive for a period of up to one hour. During the descent, the ambient temperature and pressure is rising. The ambient temperature at the base of the clouds of 305 deg F is greater than the maximum operating temperature, 160 deg F, of the probe payload. Therefore, the atmosphere cannot be used as a thermal sink for the payload. An approach to thermal control during this phase of operation is discussed in Section 8.3.2.

8.3.1 Post Separation Cruise Thermal Control

During the interplanetary cruise and post separation cruise, the entry probe is contained within a meteoroid container which is aluminum sandwich with a polyurethane foam filler. An aluminum coating was assumed for this container and the equilibrium temperature in the sun-space environment was assumed for a range of internal dissipation rates. The results of these calculations are shown in Figure 8-7. Depending on the orientation of the probe spin axis relative to the sun line, the internal heating required to maintain an uninsulated probe at a temperature of 60 deg F can vary from 43 to 52 watts. For a 60 day coast time, some 75,000 whr or 250,000 Btu of energy are required. Primary batteries can contain about 50 to 100 whr/lb. The resultant weight of the energy source is not acceptable. A hydrazine chemical reaction liberates about 700 Btu/lb. If this energy can be released at a low rate, and distributed, then this approach could be feasible. If the probe is enveloped in 102 layers of super-insulation (with a resultant weight penalty of about 21 lb) then the thermal control power requirements drop to 1 to 2 watts. There exists an important subsystem tradeoff.

FIGURE 8-7

JUPITER PROBE POST SEPARATION THERMAL CONTROL POWER REQUIREMENT

NO INSULATION
ALUMINUM COATING

$\alpha/\epsilon = 5.0$
$\epsilon = 0.05$

TOTAL AREA = 33 FT^2

LOWER LIMIT BEFORE ENTRY

SUN PARALLEL

SUN NORMAL

INTERNALLY DISSIPATED HEAT - W

ENTRY PROBE TEMPERATURE - DEG F
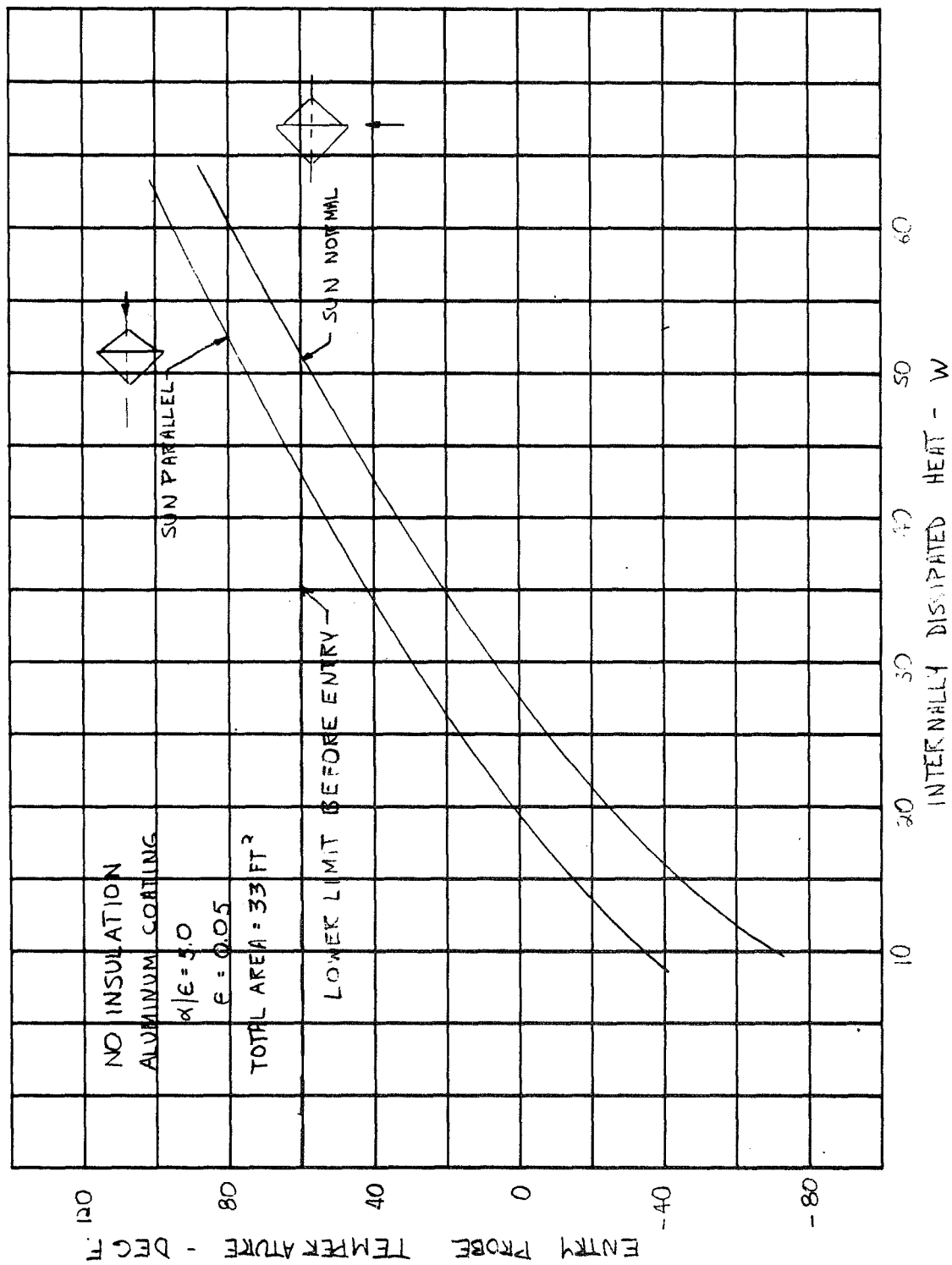
The power can also be supplied by a number of radioisotope heaters. Five watt output and larger plutonium heaters have been developed. A five watt heater weighs 0.35 lb., and this includes the weight of a thermal protection system to prevent burnup of the source in the event of a launch failure. Assuming 50 watts of power are required for post separation cruise, then ten heaters can be distributed to provide a uniform temperature distribution within the probe. Another approach is to use an RTG. The added advantage of the RTG is that it can provide a trickle charge for a battery power supply subsystem. For example, after a checkout of the probe and transmission of cruise science and probe diagnostic data, if a 3w recharge rate is required, then based on a 7% thermal to electrical conversion efficiency, about 40w of thermal energy are available for dissipation. Unlike the isotope heaters, the RTG would be a single unit. Its thermal energy must be distributed by radiation and conduction heat paths, and could result in local hot and cold spots. If for example, 10w of thermal energy must be provided in a certain location, then an RTG with a 10w electrical output could provide the energy to a set of resistors. Ten watts of electrical power will result in about 140w of thermal power that must be rejected. Based on a specific performance of 2w/lb., an RTG that supplied 10w electrical would weigh 5 lb., not counting regulation weight. It is possible to consider a thermal switch to shunt the dissipated energy to internal conduction heat paths if the temperature drops too low or to an external radiator if the temperature rises too high.

A passive approach can also be considered. This approach would be based on: 1) elevating the probe temperature by dissipating spacecraft power within the probe prior to separation, and 2) providing a good insulator about the entry probe to retard the leakage of the stored thermal energy during post separation cruise to Jupiter. The feasibility of this approach was established, and the temperature-time profile for a cool down is indicated in Figure 8-8. The entry probe temperature was raised to 160 deg F, and the probe was wrapped with 102 layers of superinsulation. This insulation weighs 0.6 lb/ft^2 and for a 48 in. diameter probe, the total insulation weight is 21 lb.

8.3.2 Atmospheric Descent Thermal Control

The descent phase environment is characterized by an external ambient temperature rise of 3 deg F/min (see Figure 8-9), during a 60 minute descent, and an internal heat dissipation of 340 watts. Descent thermal control is based on use of an internal phase change material within the payload container to soak up the electrical energy dissipated internally and an external insulator around the payload container to provide a high thermal resistance to the high temperature atmosphere in which the entry probe is immersed. Shown in

FIGURE 8-8

COOLDOWN OF INSULATED PROBE DURING POST SEPARATION NEAR JUPITER
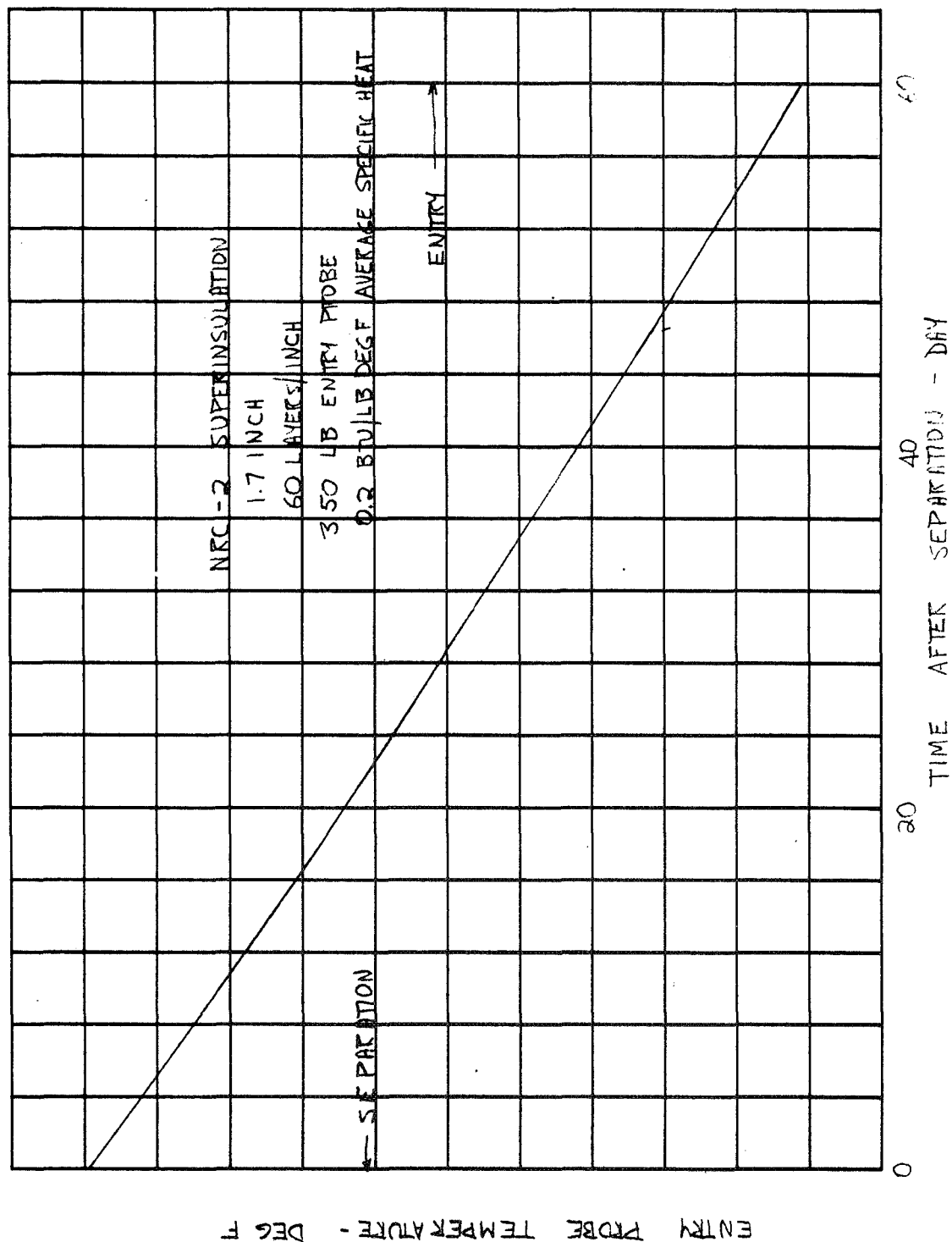
FIGURE 8-9
JUPITER PROBE DESCENT TEMPERATURE PROFILE
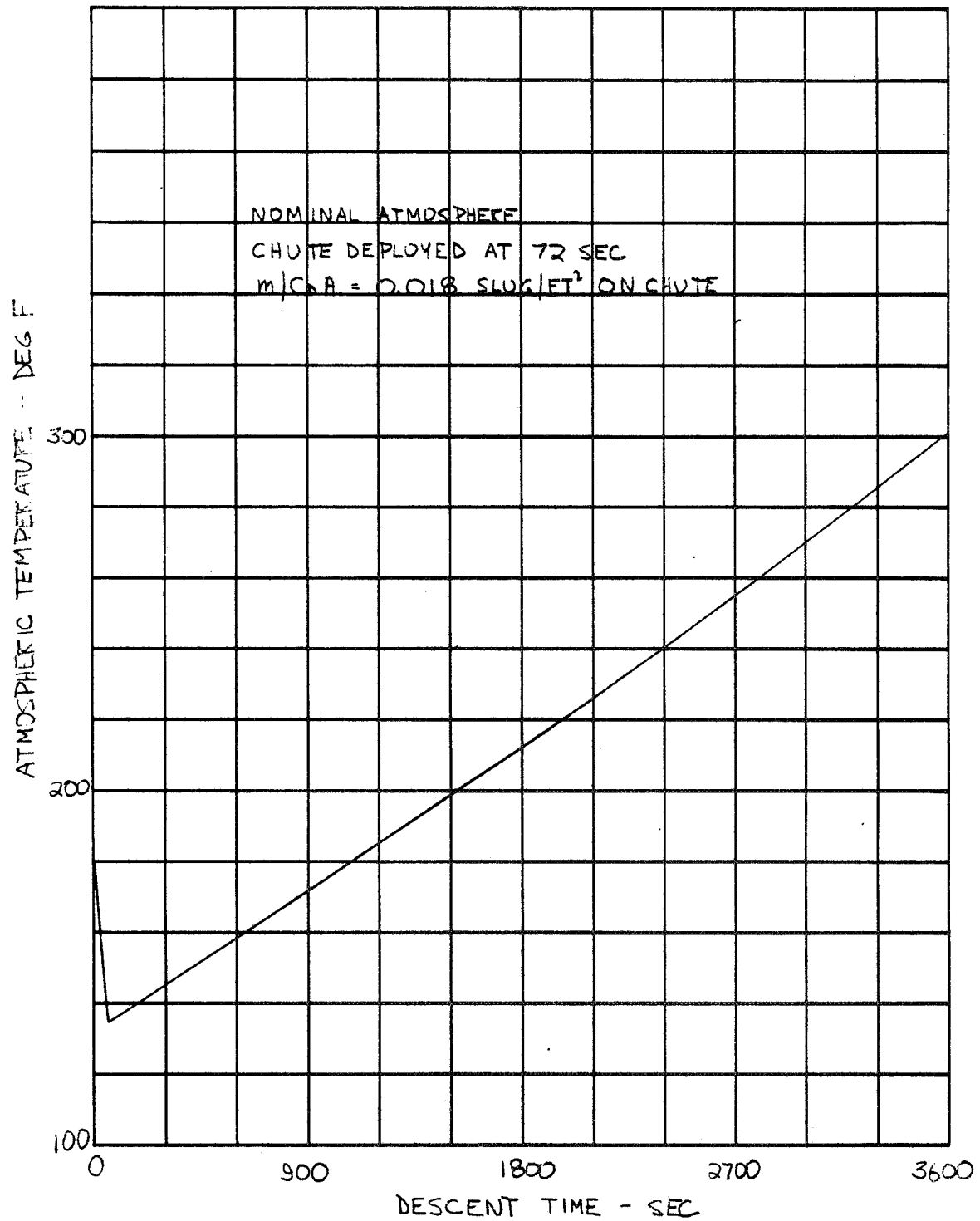
Figure 8-10 is a tradeoff between insulation thickness and phase change material. It can be seen that as the insulation thickness increases, the phase change material decreases. The phase change material used in this analyais absorbs 114 Btu/lb at the melting temperature of 97 deg F, and the insulator is MIN-K TE1200 with a thermal conductivity of 0.14 Btu/ft-hr-deg F when exposed to a hydrogen/helium atmosphere at a temperature of 305 deg F and a pressure of 13,000 torr. It is indicated in Figure 8-10 that if the insulation thickness is 0.76 in., then the need for phase change material can be removed. It is also shown that this will not result in a weight penalty for the case considered. As the insulation thickness is increased beyond 0.76 in., the payload temperature at the base of the clouds is reduced.

8.3.3 Thermal Control Subsystem Description

The probe thermal control design is indicated in Table 8-5, and consists of passive devices such as coatings, insulation, and phase change materials, and active devices such as heaters, and an isotope heat source. Coatings with selected electromagnetic properties are applied to all surfaces involved in radiant heat interchange. Good payload container design requires that an unbroken insulation barrier be provided. However, several penetrations of this barrier are required to enable the passage of: structural supports, optical windows, pressure ports, electrical power, antenna coaxial cable, and cabling that carries data. These penetrations are designed to minimize the leakage of heat.

8.4 HEAT SHIELD SUBSYSTEM

Heat shield subsystem performance was provided as a guideline in the ground-rules for the conduct of this study. The information contained in Reference 2, was based on the work of Tauber and Wakefield (Reference 3) and Wilson (Reference 4). It could be said that these preliminary analyses are speculative since there has not been any laboratory or flight simulation of the heating, or laboratory or flight test evaluation of the interaction between the ablator and the heating environment.

The purpose of this study has been to advance the state-of-the-art of Jupiter entry probe development. At first thought, it might seem inappropriate to conduct a study for the entry probe system when there exists a significant feasibility question i.e., the survivability of a probe that enters at 160,000 ft/sec (49 Km/sec), or a significant subsystem penalty such as the possibility of a very large subsystem weight requirement. To await the results of an in-depth heat shield investigation would result in a serial development of the entry probe system which would tend to increase the development time. If

FIGURE 8-10

JUPITER PROBE THERMAL CONTROL SYSTEM WEIGHT
EXTERNAL MIN-K INSULATION
TITANIUM PRESSURE VESSEL

60 DEG F INITIAL TEMPERATURE
340 W DISSIPATED POWER

0.14 BTU/FT-HR-DEG F INSULATION CONDUCTIVITY
160 DEG F FINAL TEMPERATURE AT CLOUD BASE

T = 160 DEG F $\longrightarrow$ T < 160 DEG F

COMPOSITE

INSULATION

PHASE CHANGE MATERIAL

WEIGHT - LB

20   15   10   5   0

0.3   0.4   0.5   0.6   0.7   0.8
EXTERNAL INSULATION THICKNESS - IN.
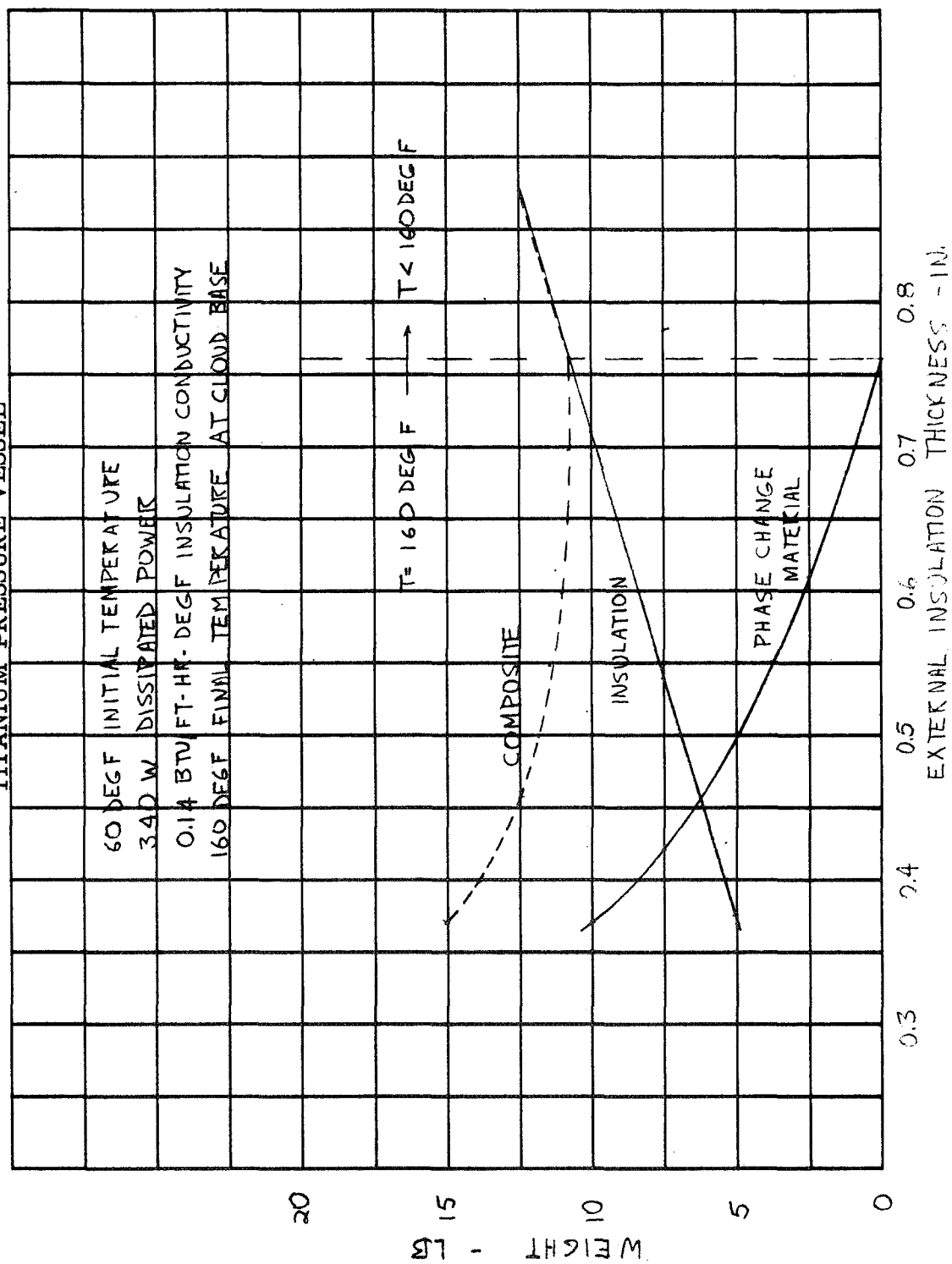
TABLE 8-5

JUPITER ENTRY PROBE THERMAL CONTROL DESIGN

	Component	Aluminum/Polyurethane	Thermal Control Approach
1.	Meteoroid Container	Aluminum/Polyurethane	Radiation: High α/ϵ coating
2.	Heatshield	High density carbon	Thermal environment controlled by container and heaters
3.	Aeroshell	Titanium H. C.	Thermal environment controlled by container and heaters
4.	Support Structure	Titanium	Conduction: Low-k material and cross-section minimization
5.	Insulation	MIN-K TE1200	Low-k material specification
6.	Pressure vessel Penetration, structural	Titanium Titanium	Conduction: Low-k material and cross-section minimization
	Penetration, electrical	Al/Ceramics	Conduction: Low-k materials and wire cross-section minimization
	Penetration, optical window	Quartz/Ti	Conduction: Low-k materials, cross-section minimization. Radiation: Filters
	Penetration, antenna	St. Stl. /MgO	Conduction: Low-k materials and coax-cable cross-section minimization.
	Penetration, pressure port	St. Stl.	Conduction: Low-k materials and tube cross-section minimization
7.	Phase change material	TH-97	High heat of fusion, high density, high specific heat material
8.	Science, communications, Data Handling	Various	MIN-K insulation
	Power-Battery	Various	TH-89 phase change material
9.	Insulation support shell	Titanium	
10.	Afterbody	Titanium/high density carbon	Thermal environment controlled by container and heaters
11.	Antenna	Titanium	No specific
12.	Rocket Motor		Thermal environment controlled by container and heaters
13.	Parachute	Nylon	Thermal environment controlled by container and heaters
14.	RTG	Plutonium source	Thermal source

heat shield subsystem performance is estimated and an entry probe study conducted, then it is possible to identify other entry probe long lead time items, and engage in a parallel development program which would tend to reduce the development time.

The generation of the heat shield weights have been based on identification of and use of physical phenomena that would tend to reduce the heating or block the transport of energy from the bow shock layer to the ablator. Based on previous heat shield development programs there should exist new self-limiting mechanisms that will result in performance that should be significantly better than that estimated, based on simple extrapolation from current technology.

8.4.1 Heat Shield Performance

Heat shield performance is presented in Figure 8-11 as a function of ballistic parameter and flight path angle at probe entry. These weights are based on: 1) shallow angle entry in the direction of the Jovian rotation, entry velocity of 49 Km/sec., 2) a 1.6M (or 58.5 in) diameter entry probe, and 3) a 60 deg half angle cone with a one-quarter inch nose radius. The heat shield weight includes the weights of the ablator and insulator.

Note that the influence of the model atmosphere on the heat shield weights was not considered. Based on a preliminary assessment by Avco, it can be expected that the total heating and the maximum heat transfer rates (no heat shield interaction considered) increase as the scale height of the atmosphere decreases. Therefore, it would be expected that the cool/dense model atmosphere would result in the greatest thermal protection penalty.

Although the heat shield mass fraction, i.e, the heat shield weight to total entry probe weight, decreases as the ballistic parameter increases for a constant entry angle and entry probe diameter, the absolute heat shield weight increases as the ballistic parameter increases. For example, the heat shield weight can be written as:

$$M_H = \left(\frac{M_H}{M_E}\right)\left(\frac{M_E}{C_D A}\right)\left(C_D A\right) F_D$$

FIGURE 8-11

HEAT SHIELD MASS FRACTION

$V_F = 4.9$ KM/SEC.

$D = 1.6$ M

DIAMETER WEIGHT FACTOR - F_D

DIAMETER - IN

-15 DEG FLIGHT PATH ANGLE AT ENTRY

-30

-45

-60

-90

HEAT SHIELD MASS FRACTION - M_H/M_E

BALLISTIC PARAMETER - $M_E/C_D A$ - SLUG/FT^2
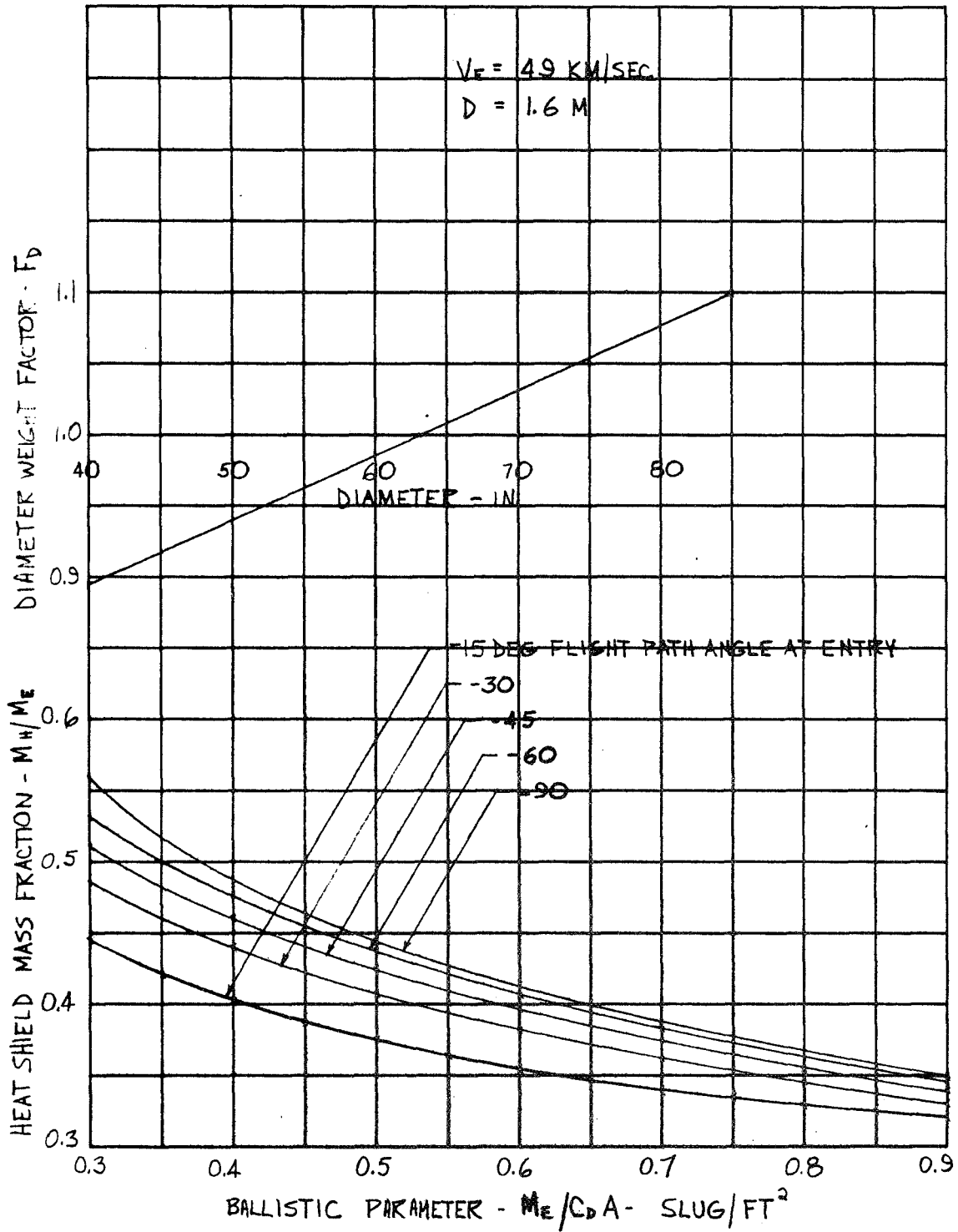
where M_H is the   weight of the heat shield

M_E weight of probe at entry

A   cross section area of probe

C_D drag coefficient based on A

F_D scaling factor for diameter

From Figure 8-11, it can be shown that the quantity $\left(\dfrac{M_H}{M_E}\right) \left(\dfrac{M_E}{C_D A}\right)$ which is a function of total heat shield weight increases as $\dfrac{M_E}{C_D A}$ increases. Also shown in Figure 8-11 is a correction factor from Reference 1 to be applied to the weight to account for an entry probe diameter that is different than 1.6M.

In Reference 1 it has been assumed that the total heat shield thickness is comprised of a high-density graphite ablator (density 1.75 gm/cm^3), and a low-density carbonaceous insulator (density 0.1 gm/cm^3). A schematic of the structure and heat shield is shown in Figure 8-12. Note that one-half cm of ablator is added to all stations other than the stagnation point region. At the vicinity of the stagnation point one cm of ablator has been added.

8.4.2 Heat Shield Mass and Dimensions

The distribution of heat shield on the aeroshell structural cone has been based on the following case given in Reference 1.

V_E = 170,000 Ft/Sec (52 Km/Sec)

γ_E = -30 deg

D   = 40.3 In (or R = 0.55M)

$\dfrac{M_E}{C_D A}$ = 0.45 $\dfrac{Slug}{Ft^2}$ (70.3 Kg/M^2)

Normalized distribution at several stations is shown in Figure 8-13. The required ablator thickness can be calculated in the following manner. Heat

FIGURE 8-12

CROSS SECTION OF AEROSHELL STRUCTURE AND HEAT SHIELD
SHALLOW ANGLE ENTRY
MID-POINT ON CONE
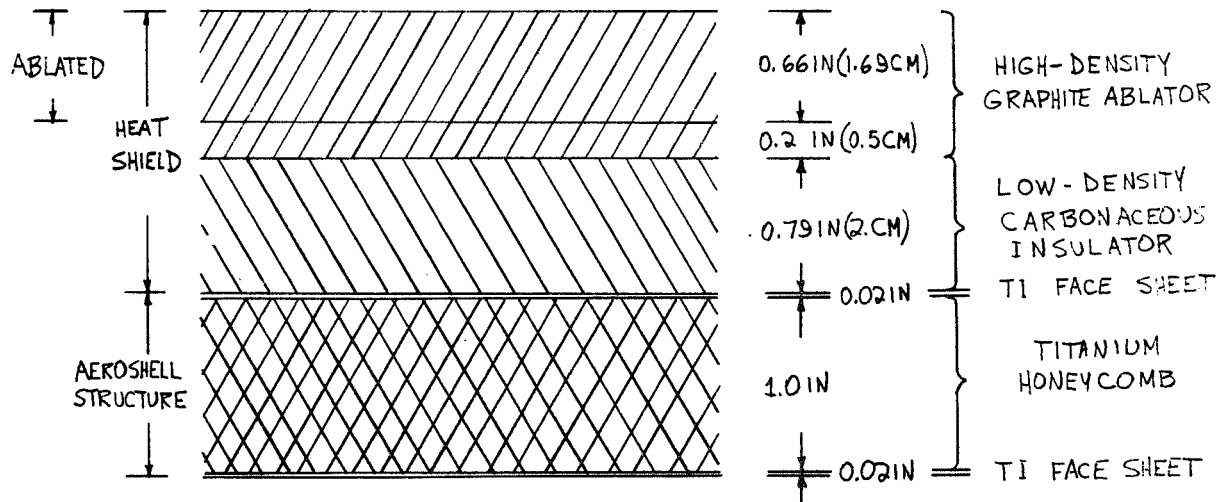
FIGURE 8-13

DISTRIBUTION OF HEAT SHIELD SHALLOW ANGLE ENTRY
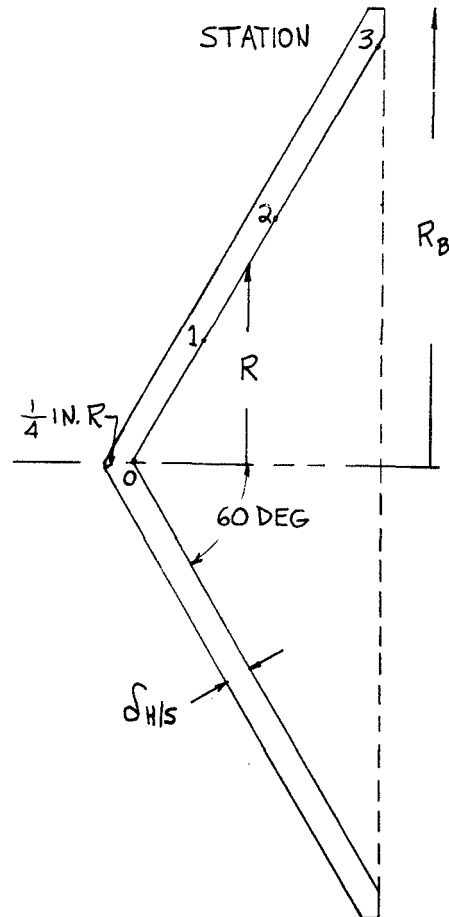
Station	$\frac{R}{R_B}$	δ_{Fixed}	$\left(\frac{\delta}{\delta_o}\right)_{ABL}$	$\delta_{H/S}$*
0	0.0	3.0cm	1.0	4.16 cm
1	.283	2.5	0.92	3.6
2	.574	2.5	1.35	4.2
3	.987	2.5	1.55	4.4

$$\delta_{H/S} = \delta_{Fixed} + \left(\frac{\delta}{\delta_o}\right)_{ABL} \delta_o$$

* δ_o = 1.16 cm for shallow angle entry

shield weight can be calculated based on Figure 8-11. The weight of the insulator is calculated from

$$\frac{M_I}{M_E} = \frac{8.3}{\frac{M_E}{C_D A}}$$

where $\frac{M_E}{C_D A}$ is the ballistic parameter in Kg/M^2; note 1 $Slug/Ft^2 = 157$ Kg/M^2, and the mass of ablated material is then

$$\frac{\Delta M_H}{M_E} = \frac{M_H}{M_E} - \frac{M_I}{M_E}$$

An equation was written that incorporated the distributions shown in Figure 8-13, and allowed for calculation of the absolute ablated thickness require-ments at the stagnation point. This equation is

$$\delta_o = 0.056 \left(\frac{\Delta M_H}{M_E}\right)\left(\frac{M_E}{C_D A}\right)$$

Once the ablated thickness at the stagnation point is known, the ablated thickness at the other stations can be calculated from the ratio data pre-sented in Figure 8-13. The average ablated thickness can be estimated from

$$\delta_{AVE} = 1.33 \, \delta_o$$

8.5 ATTITUDE CONTROL SUBSYSTEM

The entry probe attitude control subsystem is used for orientation of the probe during the maneuver that deflects the probe from a Jovian flyby tra-jectory onto a planetary impact trajectory. It has been determined that the precision with which this maneuver is conducted has a significant impact on the dispersion in the lead time, the dispersion in the entry longitude, and the dispersion in the entry angle. Lead time and longitude dispersions degrade the performance of the relay communications link during subsonic descent, and entry angle dispersions aggrevate the heating and loads experienced by the probe during the initial deceleration. There are three error sources that contribute to these dispersions, and they include: 1) the uncertainty in the position of Jupiter relative to the spacecraft, 2) the uncertainty in the magnitude of the velocity increment to deflect the probe, and 3) the uncertainty in the direction in which the velocity increment is applied relative to the spacecraft velocity vector. These uncertainties and

their influences are presented in Section 9.0. It is shown that the Jupiter ephemeris error of 2000 km (one sigma) dominates the other two error sources. However, the uncertainty in angle of application of impulse is of comparable importance although smaller. There is the possibility that following the Pioneer F/G flight that the position error could be reduced to the point where the angular error becomes most significant.

The most important requirement of the attitude control system is to provide orientation during this deflection maneuver. A second requirement for the attitude control system is to null the probe angle of attack immediately prior to entry and to reduce the spin rate. These two alterations are important to enhance the survival of the heat shield subsystem and allow for deployment of the parachute after descent to subsonic velocity. Nulling the angle of attack tends to reduce the size of the stagnation point region to a point about the forward tip of the entry probe, and so reduces the heat shielding requirements. A finite spin rate helps to maintain gyroscopic stability up to the point where the dynamic pressure on the probe will maintain aerodynamic stability and assure forward entry at near zero angle of attack. In the event of nonsymmetrical ablation, the possible torques which will tend to spin the probe up, (less significant for a blunt cone like 60 deg than a slender cone) will be lower if the initial spin rate is low. This assumes that spin buildup is not dependent on the initial spin rate. High probe spin rates at 0.7M can hinder the deployment of the parachute.

The attitude control system selected for the baseline design utilizes: 1) a spacecraft maneuver to provide the probe orientation and a probe spin-up to maintain attitude during the entry probe deflection onto an impact trajectory, and 2) two transverse accelerometers to sense angle of attack at the top of the atmosphere and a hydrazine reaction control system for torquing the probe to near zero angle of attack.

There are many ways to implement the requirements for orientation of the probe during application of the deflection impulse maneuver, and for nulling the angle of attack and reducing the spin rate. Three approaches are discussed.

8.5.1 Passive ACS Approach

This first approach to entry probe attitude control depends on utilization of the spacecraft sensors and attitude control subsystem. About thirty to sixty days prior to spacecraft periapsis passage, the entry probe deflection maneuver in initiated. This maneuver occurs near the Jovian sphere of

influence at a range of about 45×10^6 km. At this range the deflection velocity requirements are very small, and so result in only a small propulsion subsystem weight penalty. It has been determined that the entry angle and entry position dispersions are nearly independent of the separation range. For separation at a great distance from Jupiter, the deflection velocity is small, and so is the error. However, this error has a longer time to propagate. For separation near Jupiter the deflection velocity is greater, and also the error in deflection velocity. This error has a shorter time to propagate. The net result of these opposing trends is to make the dispersion independent of separation range, i.e., no apparent optimum.

At command from DSN, the spacecraft begins a maneuver to orient the entry probe and the thrust axis of the entry probe deflection rocket motor. After the proper orientation is achieved, the restraining clamp that holds the entry probe to the spacecraft is released and a preloaded set of springs are freed to react against the probe and spacecraft. After the entry probe has translated a few feet to clear the spacecraft, the entry probe spin rockets are initiated to spin the probe to maintain the attitude of separation. After the probe has moved about one km from the spacecraft, the deflection motor is initiated. This separation distance is required to reduce the impingement of the rocket motor exhaust plume. This impingement causes the recovery of momentum which can perturb the spacecraft, and recovery of energy which can cause local heating of the spacecraft surfaces. Following burnout of the rocket motor, the probe attitude remains fixed in inertial space until the vicinity of entry. Since the entry probe is designed so that the spin moment of inertia is greater than the transverse moment of inertia, the probe attitude is stable in the presence of internal dissipation mechanisms. Near entry, after the probe subsystems are turned on, the entry probe is despun from about 30 rpm to about 5 rpm. This despin can be accomplished by spin rockets, yo-yos, or a reaction control subsystem. A high spin rate is maintained during this post separation cruise to ensure that the probe attitude or spin rate is not seriously perturbed by the application of external torques, i.e., from the solar flux and Jovian magnetic field. As the probe enters the threshold of the Jovian atmosphere, the transverse accelerometers of the triad of accelerometers will sense an input if the angle of attack is not zero. This sensor output can be used to drive a reaction control subsystem to null the angle of attack. There is a tradeoff between the available time to null the angle of attack and the thrust level and response time of the reaction control system. It is possible to arrive at a smaller reaction control system by adding ion sensors to provide entry probe attitude information, and so permit the nulling of the angle of attack above the atmosphere where more time is available.

An analytical equation for the dispersion in the thrust application angle can be derived and is valid for 1) small angular errors so that the function is approximately linear, 2) independent error sources so that the variance in the subsystem performance is equal to the sum of the squares of the error sources, and 3) bivariate error sources, with equal variance, to allow for equal probability of an error in both pitch and yaw. The errors that contribute to the dispersion in thrust application angle are: 1) the initial alignment to the reference frame, i.e. the spacecraft, 2) the separation error caused by spring misalignment, 3) the spin up error, and 4) the thrust misalignment error. The standard deviation (one sigma) error in the thrust application angle can be calculated from:

$$\sigma_{\Theta_{OP}}^2 = b_{\alpha_o}^2 \, \sigma_{\alpha_o}^2 + b_{\omega_o}^2 \, \sigma_{\omega_o}^2 + b_{\Delta L_S}^2 \, \sigma_{\Delta L_S}^2 + b_{\Delta L_T}^2 \, \sigma_{\Delta L_T}^2$$

(See Table 8-6) for definition of terms)

where the influence coefficients are

$$b_{\alpha_o} = 1$$

$$b_{\Delta L_S} = \left(2 N R^2 \right)^{-\frac{1}{2}}$$

$$b_{\Delta L_T} = \frac{m \Delta V}{I_S \Omega_S^2 L_b}$$

The contribution to the initial alignment error $b_{\alpha_o} \, \sigma_{\alpha_o}$ is comprised of the spacecraft limit cycle dead band, the spacecraft sensor error and the entry probe to spacecraft mounting accuracy, so that

$$\sigma_{\alpha_o}^2 = \sigma_{DB}^2 + \sigma_{SEN}^2 + \sigma_A^2$$

The separation error can be written as

$$b_{\omega_o} \, \sigma_{\omega_o} = \frac{m S}{I_T} \, \sigma_\epsilon$$

Spin-up alignment error can be calculated from

$$\sigma_{\Delta L_S}^2 = \sigma_{\Delta X_S}^2 + X^2 \, \sigma_{\Delta K_S}^2 + \left(R^2 + X^2 \right) \sigma_{\xi_S}^2$$

TABLE 8-6

PARAMETER VALUES FOR PASSIVE ACS-THRUST ACCURACY ANALYSIS

PARAMETER	DEFINITION	VALUE
$\sigma_{\theta_{op}}$	Thrust Application Angle Error	DEG.
σ_{α_o}	Initial Alignment Error	DEG.
$\sigma_{\Delta L_s}$	Spin Rocket Moment Arm Error	IN.
$\sigma_{\Delta L_T}$	Deflection Rocket Moment Arm Error	IN.
σ_{DB}	Spacecraft Limit Cycle Bandwidth	.066 deg.
σ_{SEN}	Spacecraft Sensor Error	.144 deg.
σ_A	Probe to Spacecraft Mounting Accuracy	.17 deg.
m	Probe Mass	16.7 Slug
S	Separation Distance for Clearance	3 Ft.
ΔV	Deflection Velocity	164 Ft/sec.
I_T	Transverse Moment of Inertia	12.2 Slug-ft^2
a_ϵ	Error in Distance from Probe C. G. to Line of Action of Spring Forces	.03 in.
N	No. of Spin Rockets	2
R	Radius of Spin Rocket Circle	22.5 in.
$a_{\Delta\lambda_s}$	Spin Rocket Location Error	.040 in.
$\sigma_{\Delta K_s}$	Standard Deviation in Variance of Spin	1%
a_{ξ_s}	Spin Rocket Angular Misalignment	.17 deg.

TABLE 8-6 (concl'd)

PARAMETER VALUES FOR PASSIVE ACS-THRUST ACCURACY ANALYSIS

PARAMETER	DEFINITION	VALUE
X	Distance of Plane of Spin Rockets from Probe C. G.	4. 5 in.
Ω_s	Probe Spin Rate	30 R. P. M.
I_s	Spin Moment of Inertia	15. 1 Slug-ft^2
t_b	Thrust Duration	15 sec.
$a_{\Delta X_T}$	Error in Location of Thrust Rocket from Probe Center Line	. 04 in.
$a_{\Delta CG}$	Error in Location of Prlbe C. G. from Probe Center Line	. 03 in.
$a_{\Delta \delta_T}$	Deflection Motor Misalignment	. 17 deg.
L	Distance from Point of Application of Thrust to Probe C. G.	21 in.

σ Standard Deviation

a Tolerance

$\sigma = \dfrac{a}{\sqrt{2}}$ for transforming a uniform distribution to a bivariate Gaussian distribution.

and finally, the contribution due to thrust misalignment can be calculated from

$$\sigma_{\Delta L_T}^2 = \sigma_{\Delta x_T}^2 + \sigma_{\Delta cc}^2 + L^2 \sigma_{\Delta \xi_T}^2$$

Based on the values shown in Table 8-6, it was determined that the comparative values of the error sources are

$$b_{\alpha_o} \sigma_{\alpha_o} = 0.232 \text{ Deg}$$
$$b_{\omega_o} \sigma_{\omega_o} = 0.414$$
$$b_{\Delta L_s} \sigma_{\Delta L_s} = 0.091$$
$$b_{\Delta L_T} \sigma_{\Delta L_T} = 0.106$$

The square root of the sum of the squares of these errors is 0.49 deg. Therefore, based on error sources and nominal values used, the error in thrust application angle is about 0.5 deg (one sigma). Note that the separation error is the principal contributor. If the other error sources were reduced to zero, then the thrust application angle error would be 0.41 deg. The spacecraft system error sources are considered typical of the performance that can be achieved during a maneuver for three-axis stabilized spacecraft like TOPS, and is also considered typical of the performance that can be achieved for a spinning spacecraft like Pioneer F/G. It should be pointed out that the pointing accuracy of the two spacecraft were not provided for this study.

The weight of the pyrotechnic release elements, clamps, springs, and spin rockets is estimated to be about 7 lb.

The major limitation of this scheme to use the spacecraft for probe orientation is the requirement to conduct a maneuver at Jovian range, and the possible conflict in flight sequence with the spacecraft encounter science requirements. Also this maneuver will alter the thermal balance, and require switching of antennas.

A listing of the elements that comprise the attitude control subsystem used to null the angle of attack at entry is given in Table 8-7. A six nozzle arrangement is used which will provide spin, despin, pitch, and yaw control. The arrangement of nozzles is shown in Figure 7-1.

8.5.2 Active ACS Approach

The second approach is based on the use of gyro sensors for entry probe orientation prior to impulse addition. Spacecraft attitude information is

TABLE 8-7

WEIGHT OF REACTION CONTROL SUBSYSTEM

ELEMENT	WEIGHT
Hydrazine Propellant	0.9 lb
Three Axis Fluidic Rate Sensors and Logic Module	1.0
Gaseous N_2	1.0
Tankage	4.3
Plumbing and Valves	1.8
Motors (6)	4.0
	13.0 lb.

provided to the entry probe gyro package, and also the required attitude information is supplied to the entry probe subsystem memory. The spacecraft remains fixed in the cruise mode attitude, and the entry probe is separated. Following separation the entry probe reaction control subsystem is actuated, and the probe is maneuvered to the attitude for the deflection maneuver. At the termination of the impulse maneuver, the probe can be spun up for spin stabilization. If the influence of external torques are small, then it is possible to maneuver the entry probe after the impulse addition so that the angle of attack will be zero at entry. Typical error sources and parameter values are shown in Table 8-8. The square root of the sum of the squares of the values given in Table 8-8 result in a 0. 25 deg (one sigma) error in thrust application angle. It has been assumed that comparable performance can be achieved for both a three-axis stabilized spacecraft like TOPS as well as a spin-stabilized spacecraft like Pioneer F/G.

The weight of the gyro sensors and electronics subsystem is given in Table 8-9, and the weight of the reaction control subsystem will be the same as that shown in Table 8-7.

This approach tends to decouple the spacecraft requirements from the entry probe requirements, and so eliminate a possible spacecraft failure mode. However, this reduction in spacecraft failure mode, imposes the requirement of an additional complex probe subsystem with its own failure mode characteristics.

8. 5. 3 Spacecraft Maneuver Approach

It is also possible to consider initial targeting of the spacecraft onto an impact trajectory that will result in the required probe flight path angle at entry. Prior to separation, the spacecraft is maneuvered to provide the probe with an orientation that will result in a near zero angle of attack at entry. Following probe separation the spacecraft is maneuvered to align its midcourse propulsion subsystem so that the spacecraft is slowed down and deflected from the planet. This will result in the correct lead time and periapsis passage that are necessary for a good relay communication link geometry.

Referring back to Section 8. 5. 1, it is to be noted that if this approach is used then the error in the thrust application angle can be reduced to about 0. 48 deg (one sigma) since the thrust misalignment error contribution is eliminated. The system total impulse requirement is increased. Although the velocity

TABLE 8-8

PARAMETER VALUES FOR ACTIVE ACS - THRUST ACCURACY
ANALYSIS

PARAMETER	DEFINITION	VALUE
$\sigma_{\Theta op}$	Thrust Application Angle Error	DEG.
σ_{DB}	Spacecraft Limit Cycle Dead Band Width	.066 deg.
σ_{SEN}	Spacecraft Sensor Error	.053
σ_{GYRO}	Probe Sensor Error	.144
σ_{LC}	Probe Limit Cycle Dead Bandwidth	.066
σ_A	Probe to Spacecraft Mounting Accuracy	.17
σ_{PACK}	Probe Gyro Package Alignment	.09

TABLE 8-9

WEIGHT OF GYROSENSORS AND ELECTRONICS SUBSYSTEM

ELEMENT	WEIGHT
Inverter	1.0 lb.
Gyro Package	3.0
Control Electronics	2.0
Analog Integrator	1.0
Cables	1.0
	8.0 lbs.

increment remains unchanged, the total mass that must be accelerated is increased, since the spacecraft, not the probe, is deflected. This approach tends to reduce the entry probe requirements and places greater burden on the spacecraft subsystems.

8.6 ANTENNA SUBSYSTEM

In this section there is presented a discussion of entry probe antennas for both direct and relay links, and a discussion of antennas for use on both TOPS and Pioneer F/G to support a relay link.

8.6.1 Direct Link Antennas

The probe direct link communications antenna must provide adequate gain at 2295 MHz over look angles that vary from a minimum of 60 deg ($\pm$ 30 deg off-axis) to a maximum of 120 deg ($\pm$ 60 deg off-axis). The particular look angles at any instant of time are determined by the probe dynamics, trajectory dispersions, and azimuthal shift in probe position. Under these conditions, two missions are defined from the communications view point. These are: 1) an optimum mission with $\pm$ 30 deg look angle, and 2) an off-optimum mission with a $\pm$ 60 deg look angle. An antenna concept is proposed for each of these missions in the following paragraphs.

8.6.1.1 Optimum Communication Capability Mission

The antenna for the optimum mission must provide adequate gain over $\pm$ 30 deg centered about the probe spin axis. The minimum gain required by the probe is shown in Figure 8-14. This gain coverage requirement is satisfied by the low gain omni-antenna concept of Mariner '64 shown in Figure 8-15. The antenna aperture is seen to be the generic form of the Mariner '64 low gain omni which is an open ended circular waveguide with a conical reflector designed to provide wider angle coverage at higher gain levels than conventional open ended waveguides. The antenna is circularly polarized by exciting two spatially orthogonal TE_{11} modes in phase quadrature. The antenna gain is plotted against the requirements in Figure 8-14. To meet the severe environmental conditions, the antenna is fabricated of titanium. The estimated weight of the antenna is .8 lb.

8.1.6.2 Off-Optimum Communication Capability Mission

The look angle requirement ($\pm$ 20 deg) in this option is centered anywhere from 0 deg to 40 deg off the spin axis. A single antenna capable of meeting

8-49

FIGURE 3-4

OPTIMUM MISSION; ANTENNA CHARACTERISTICS

Probe Direct Link
Optimum Communication
Capability Mission

$f = 2300\ mhz$

Flared Guide
Antenna

Minimum Probe
Antenna Gain

Look Angle (Deg)
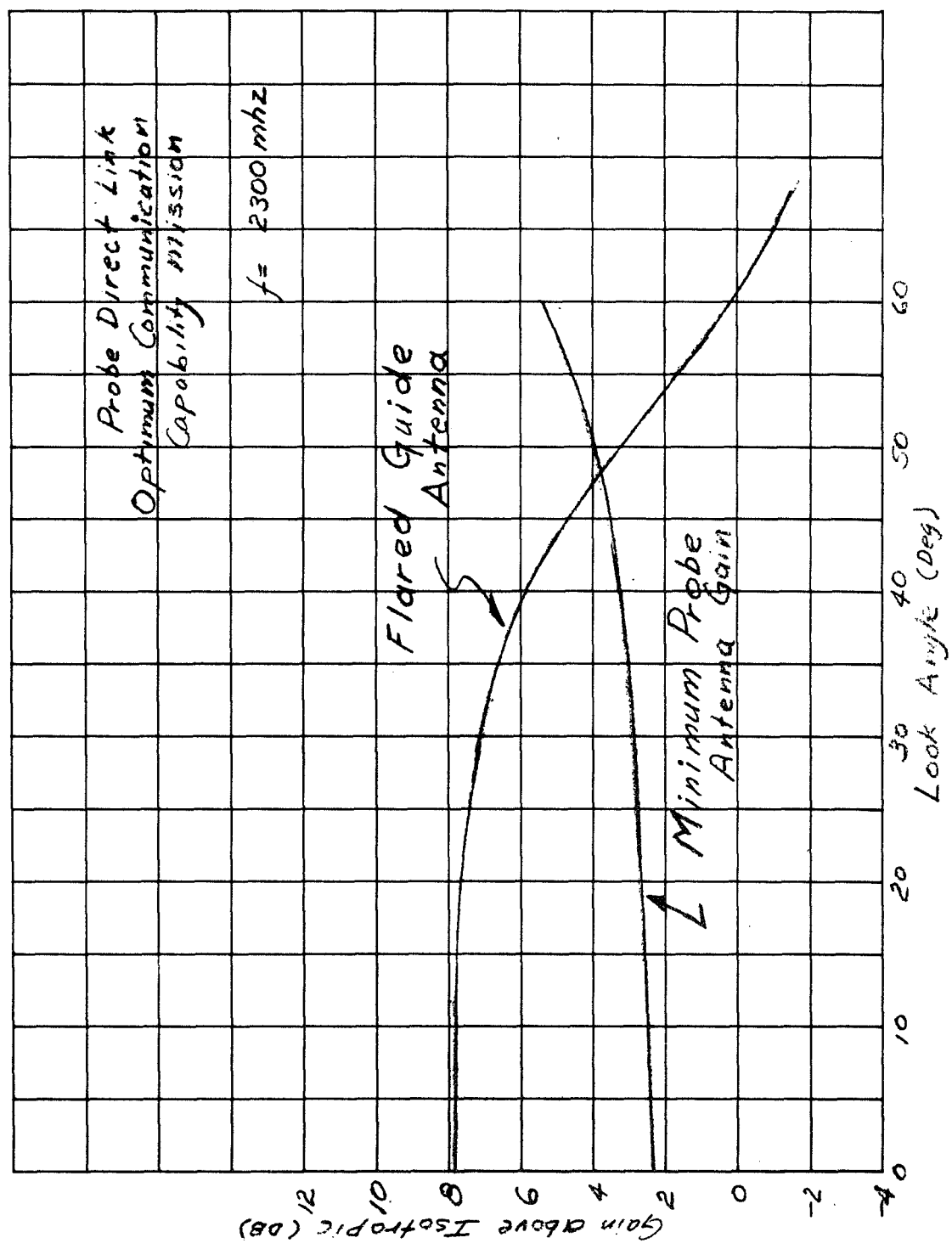
Gain above Isotropic (DB)

FIGURE 8-15

ENTRY PROBE ANTENNA
OPTIMUM DIRECT LINK MISSION
CONICAL REFLECTOR CONFIGURATION
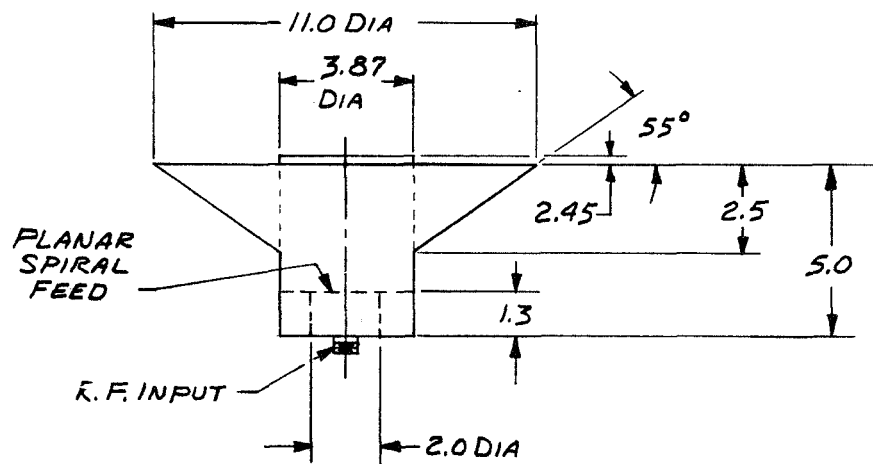
this requirement with adequate gain is the turnstyle over a two wavelength diameter ground plane. In practice, the surface of the probe can serve as the ground plane thereby decreasing weight and utilizing probe substructure in a dual capacity. The turnstyle, two half wavelength dipoles fed by a split cylindrical balun, protrudes two inches above the probe. A plot of the gain characteristics against the system requirement is shown in Figure 8-16. For the expected temperature environment, the turnstyle is fabricated of titanium with an expected weight of .8 pounds. A sketch of the antenna is shown in **Figure 8-17.**

8.6.2 Relay Link Antennas

8.6.2.1 Entry Probe Antenna

The probe relay link transmit antenna is required to provide coverage over look angles $\pm$ 40 deg centered about the vehicle spin axis. The frequency of operation is 1350 MHz. A cupped turnstyle radiating a circularly polarized wave, is an adequate solution. The required gain vs look angle is shown plotted against the system requirement in Figure 8-18. The system specification is seen to be achieved beyond the required $\pm$ 40 deg. To meet the high thermal environment titanium is selected as the material from which the antenna is made. The estimated weight is .8 lbs. A sketch of the antenna is given in Figure 8-19.

8.6.2.2 Spacecraft Antenna

TOPS Spacecraft Antenna - To receive the telemetry signals from the probe, a relay receiving antenna with 25 db gain is required on the TOPS spacecraft. To provide packaging compatibility with the spacecraft, the antenna aperture must be less than 41 inches on the side. Because of the look angle variations between probe and spacecraft, an antenna beam configuration of 10 deg x 7 deg is required at a frequency of 2295 MHz.

An antenna capable of meeting the above-mentioned requirements and constraints is an elliptically shaped parabolic dish of the generic form of Mariner '64. A sketch of the proposed elliptical dish is shown in Figure 8-20. The actual beam requirements are met with an aperture of 31" x 41" with a beam width and gain of 10 deg x 7.5 deg and 24.5 db respectively at 2295 MHz.

The dish is excited by a circularly polarized feed having an E-H plane illumination taper of approximately 13 db. The physical configuration of the

FIGURE 8-16
OFF-OPTIMUM MISSION ANTENNA CHARACTERISTICS

Probe Direct Link
Non-Optimum Communication
Capability Mission

f = 2300 mhz

Turnstyle Above
Ground sheet

Minimum Probe
Antenna Gain Required

Look Angle (Deg)

Gain Above Isotropic (DB)
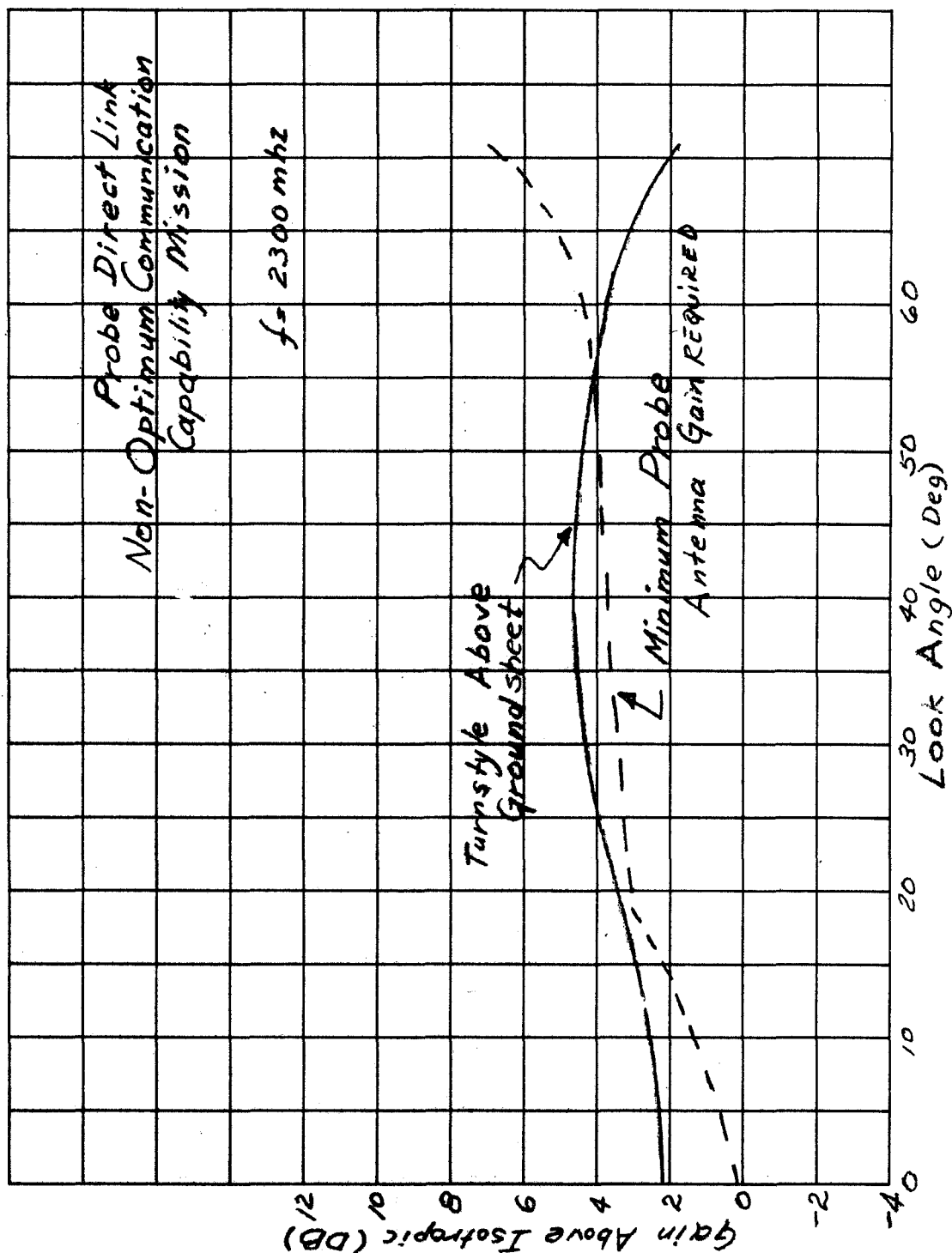
FIGURE 8-17

ENTRY PROBE ANTENNA

OFF-OPTIMUM DIRECT LINK MISSION

TURNSTYLE OVER GROUND PLANE CONFIGURATION
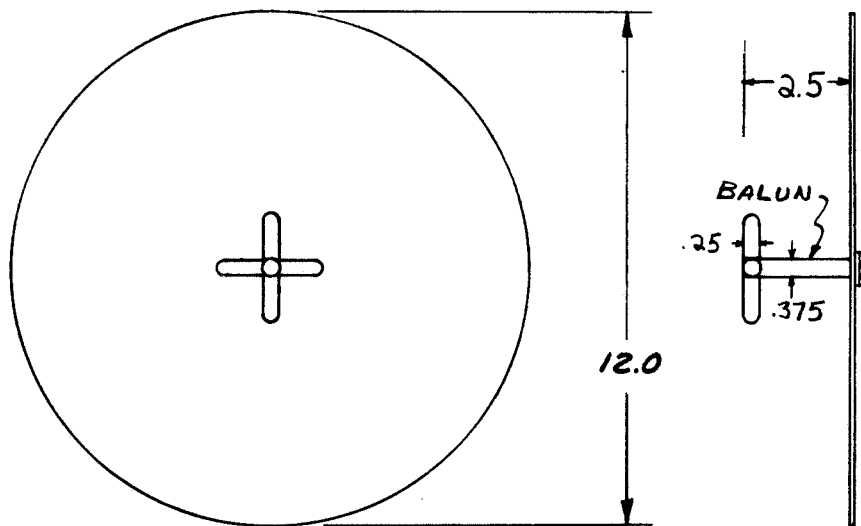
FIGURE 8-18
Antenna Radiation Pattern

Probe Relay Link

$f = 1350$ mhz

CRESSLINE CAPPED TURNSTYLE
($Dia = \frac{1}{2}\lambda$)

Minimum Probe
Antenna Gain

Gain Above Isotropic (DB)

Look Angle (Deg)
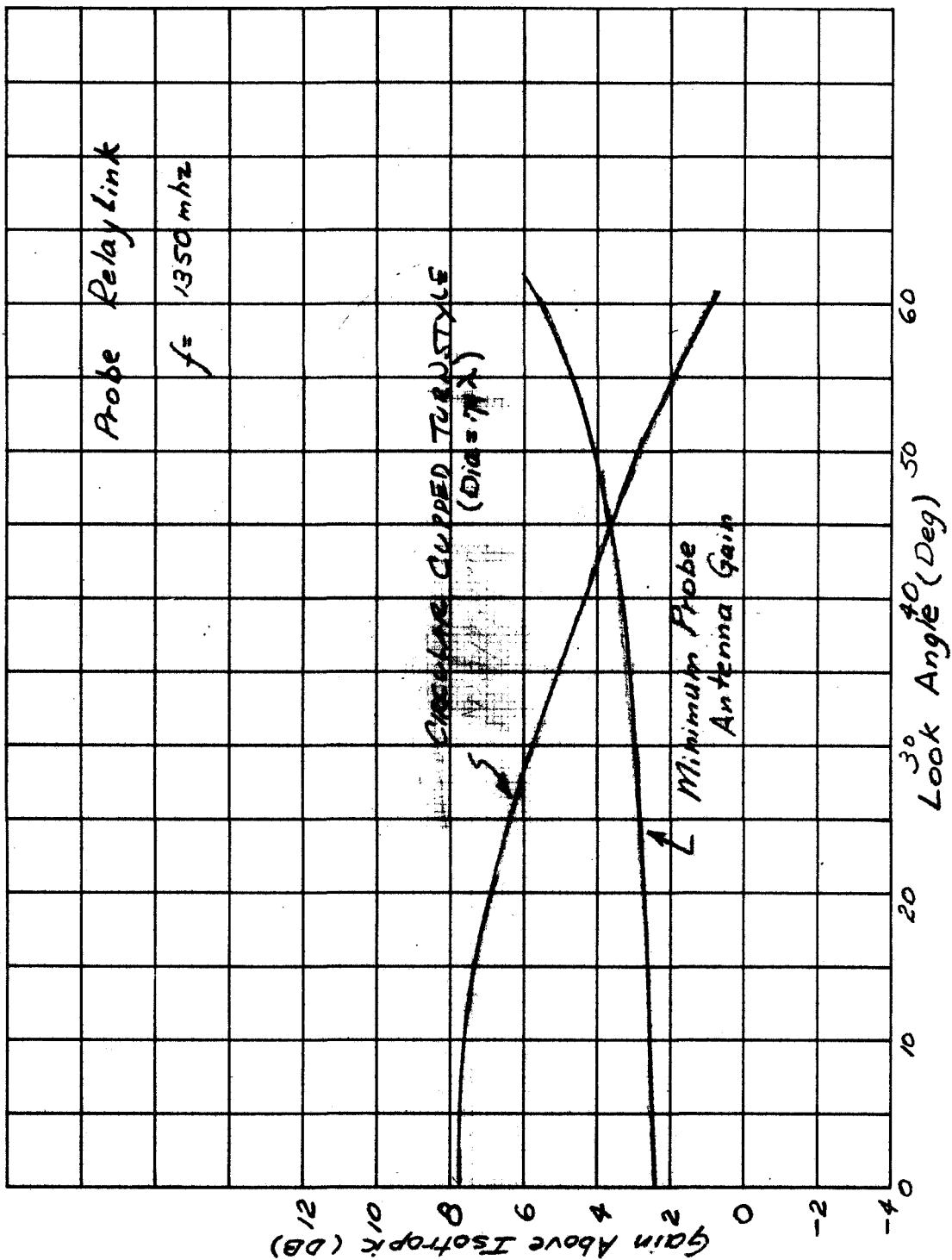
FIGURE 8-19

ENTRY PROBE ANTENNA

RELAY LINK MISSION

CIRCULAR CUPPED TURNSTYLE CONFIGURATION

TURNSTYLE ELEMENT

CIRCULAR CUP

6.4

2.5
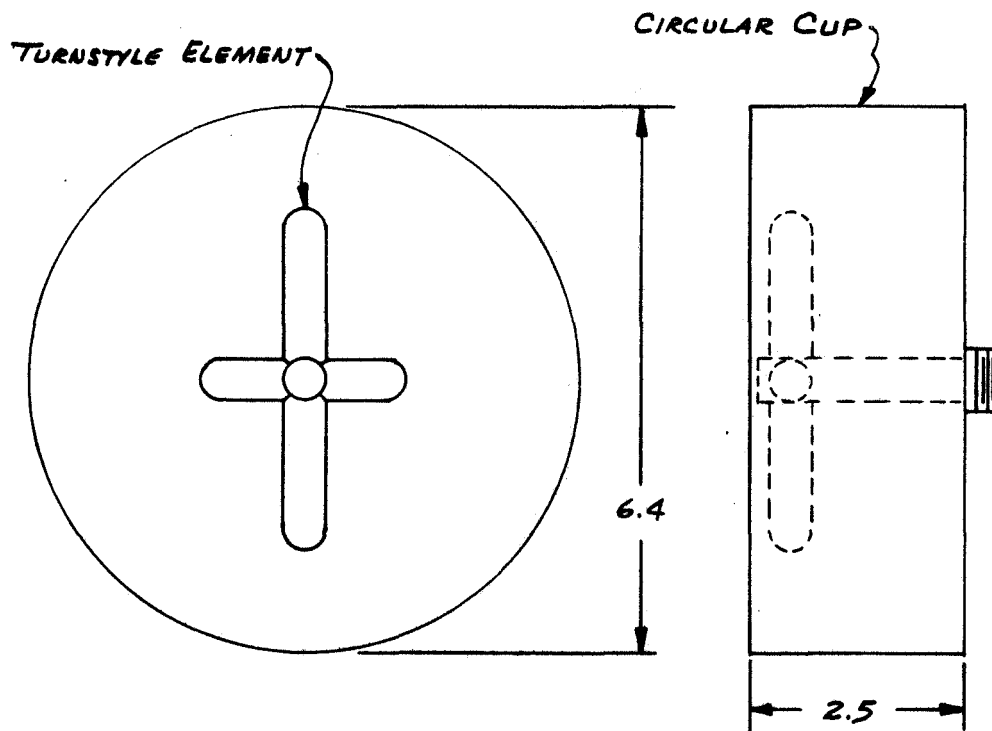
FIGURE 8-20

TOPS SPACECRAFT RELAY LINK ANTENNA
ELLIPTICAL PARABOLIC REFLECTOR CONFIGURATION
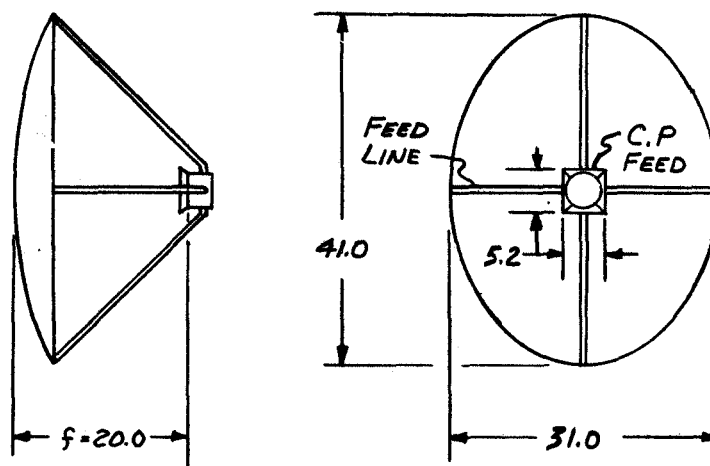
feed is conceived as a modified Mariner '64 array of two cupped turnstyles arrayed along the minor axis of the elliptical dish. The radiation pattern in the principal planes to be expected is approximated by the well known $J_1(u)/u$ function. The estimated weight of the antenna is 12.7 pounds.

The proposed antenna system can be made to withstand the thermal environment by utilizing state of the art materials and fabrication technology.

Pioneer F/G Spacecraft Antenna - The Pioneer spacecraft relay communications system is required to operate under two possible mission configurations. In the first mission option, the line of sight from the spacecraft to the probe is near parallel to the Jupiter sub-earth vector and parallel with the spacecraft spin axis. In the second mission option, the line of sight from the spacecraft to the probe is normal to the Jupiter sub-earth vector and requires a beam normal to the spacecraft spin axis for relay communications.

Mission Option 1 - In this option, a 20 deg x 20 deg beam is required to point along the direction of the spin axis. This requirement is adequately met with a parabolic dish mounted coaxially with the spin axis of the Pioneer F/G spacecraft. The parabolic dish is sized at 34" in diameter and is excited with a circularly polarized cupped turnstyle feed of circular configuration. At 1350 MHz, the 3 db beamwidth is 20 deg x 20 deg with a gain of 19.7 db. Again, the radiation pattern is the classical parabolic dish pattern with side lobe levels approximately 22 db down from the beam peak. The parabolic dish can be fabricated utilizing state of the art material and construction technology.

Mission Option 2 - In the second mission option, the spacecraft probe trajectory geometry requires that the beam be propagated in a direction that is approximately normal to the spacecraft spin axis. Since the spacecraft is spin stabilized, a despun antenna is required.

It is required that gain coverage be provided from broadside (Θ = 90) to an angle 45 deg from broadside. The gain required in this region is 12 db minimum.

The Planetary Explorer spacecraft has an electronically despun antenna (EDA) prototype system currently operating with a 10 deg x 18 deg beam with a maximum possible gain of 19 db. (See Reference 5). A modification of the feed excitation scheme and aperture geometry could be utilized to simplify the RF complexity for application on Pioneer F/G. The Planetary Explorer EDA antenna is currently linearly polarized and the proposed Jupiter

requirement could not be met with the associated 3 db polarization loss. Replacement of the linear radiating elements of the EDA with circularly polarized elements could make this antenna a viable candidate for use on a Pioneer F/G.

An alternate electronically despun concept for the Pioneer F/G Mission Option 2 requirements is discussed below:

An array of circularly polarized radiating elements arranged in the configuration shown in Figure 8-21 is a candidate approach.

The array consists of a sub-array of 3 antenna elements stacked 0.5λ apart along the axial direction. These 3 element sub-arrays are arrayed circumferentially about the spacecraft. The radiation pattern for this arrangement has been computed utilizing Avco's antenna prediction program #2712. The patterns of Figures 8-22 and 8-23 are for broadside pointing (Θ = 90 deg) and represent the patterns in the circumferential and axial planes respectively. The patterns represent an aperture with an aperture efficiency of approximately 60 percent. The physical portion of the aperture utilized to generate the beam consists of three rows of seven antenna elements spaced in an 80 deg circumferential sector. The computed beamwidth in the circumferential plane and axial plane is obtained from Figures 8-22 and 8-23 as 12 deg and 30 deg respectively. The corresponding directivity is 18.0 db. In the following discussion, we assume a 50% circuit loss for conservative gain predictions.

In operation, the radiating sector will be "despun" by stepping the sector circumferentially about the spacecraft in a direction opposite to the spin vector of the spacecraft and at a rate equal to the spin rate of the spacecraft.

To provide the coverage required in the axial plane, the beam must be switched to "off broadside" pointing positions which are assumed to be known apriori. As a reference design, one switching function is required if the initial beam pointing position is set to 15 deg off broadside (i.e. Θ = 75 deg). This will provide 12 db of gain at Θ = 90 deg, 15 db at Θ = 75 deg, and 12 db at Θ = 60 deg. When the look angle to the probe is at Θ = 60 deg (30 deg off broadside), the elements in the axial 3 element sub-arrays are rephased to switch the beam to a boresight position at Θ = 45 deg. The gain coverage will then be similar to broadside with a degradation in gain from 1-2 db due to element pattern tapers. The beamwidth will correspondingly increase to offset the degradation in gain.

The schematics of Figures 8-24 and 8-25 illustrate the antenna element excitation scheme. Figure 8-24 shows that each three element sub-array in

FIGURE 8-21

PIONEER F/G SPACECRAFT RELAY LINK ANTENNA

DESPUN CIRCUMFERENTIAL ARRAY CONFIGURATION
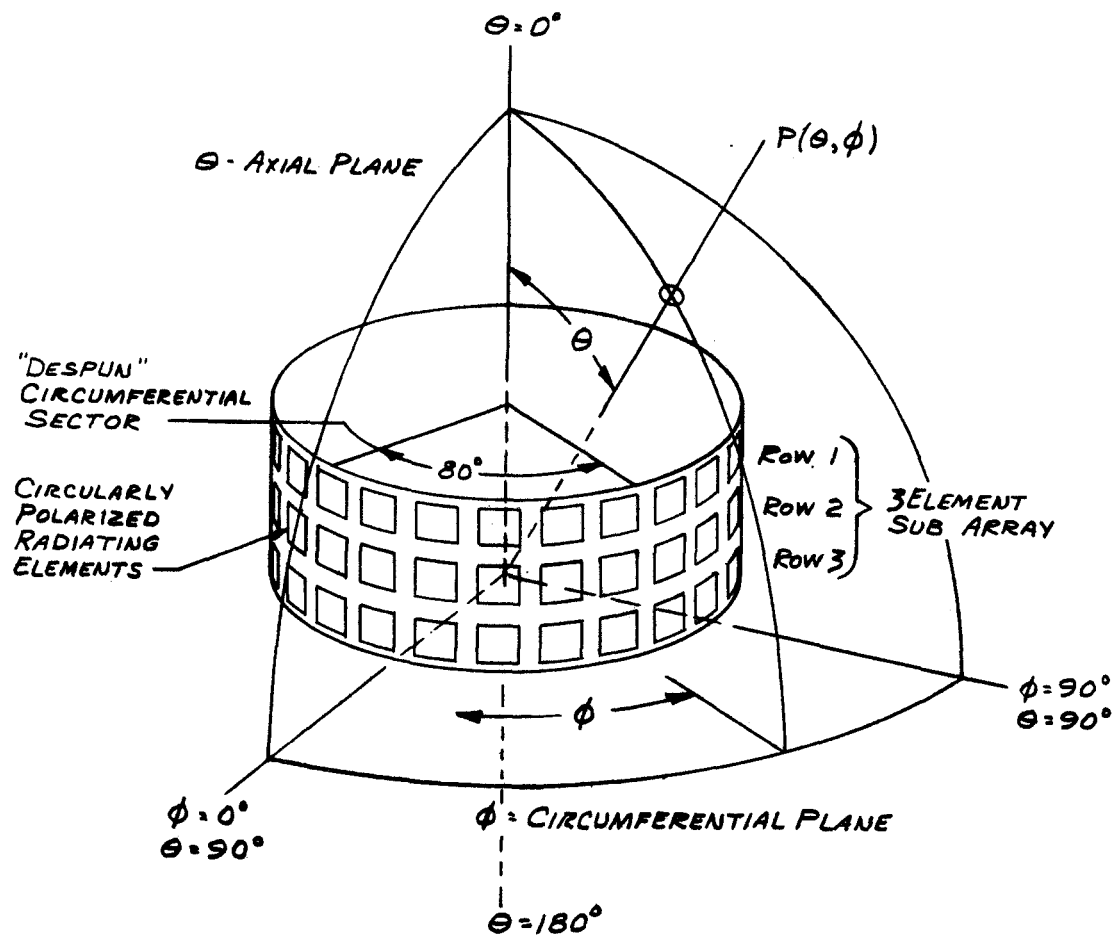
FIGURE 8-22

JUPITER PROBE DESPUN ANTENNA - PATTERN OF CIRCUMFERENTIAL PLANE
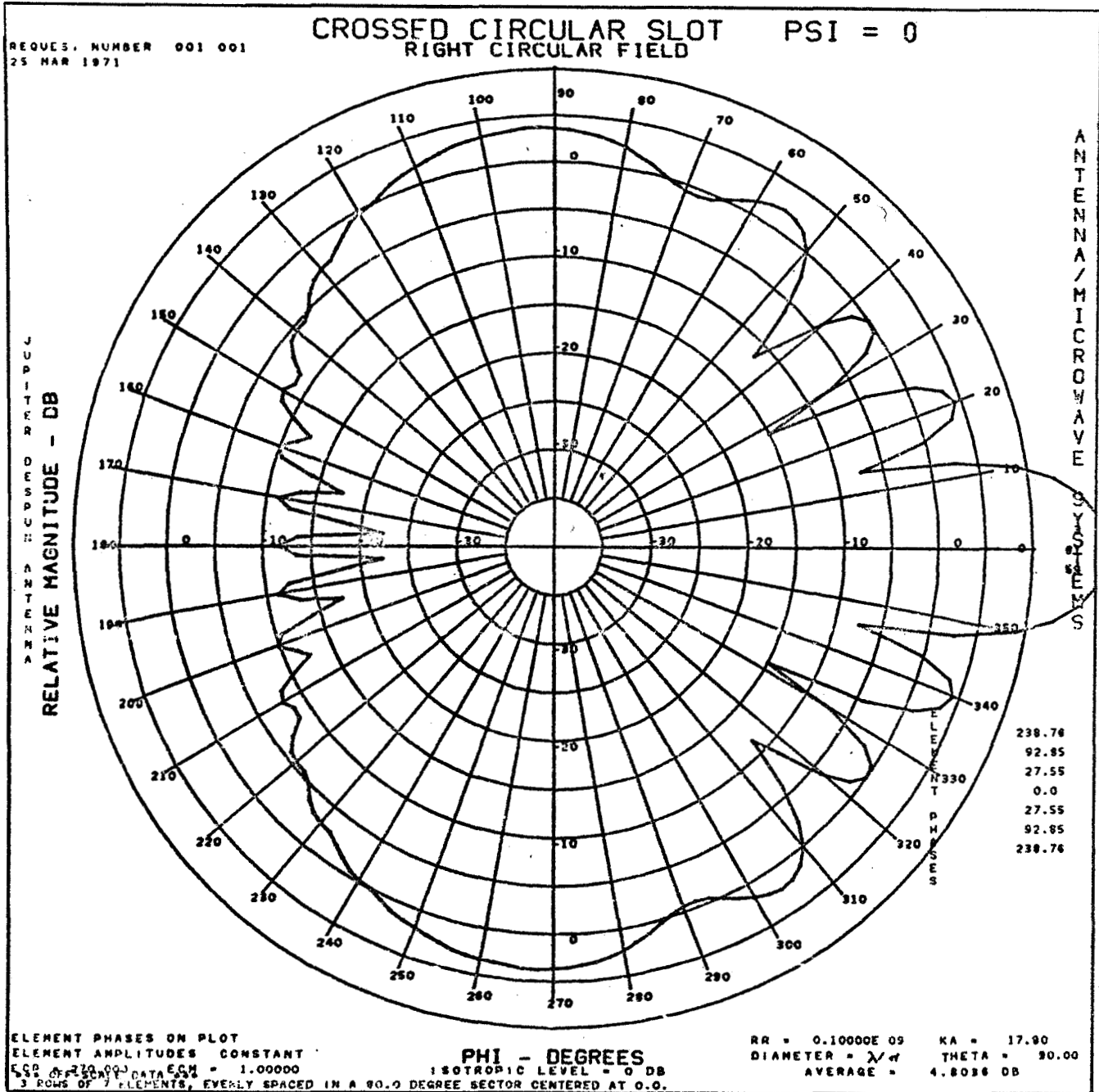
FIGURE 8-23

JUPITER PROBE DESPUN ANTENNA - PATTERN OF AXIAL PLANE
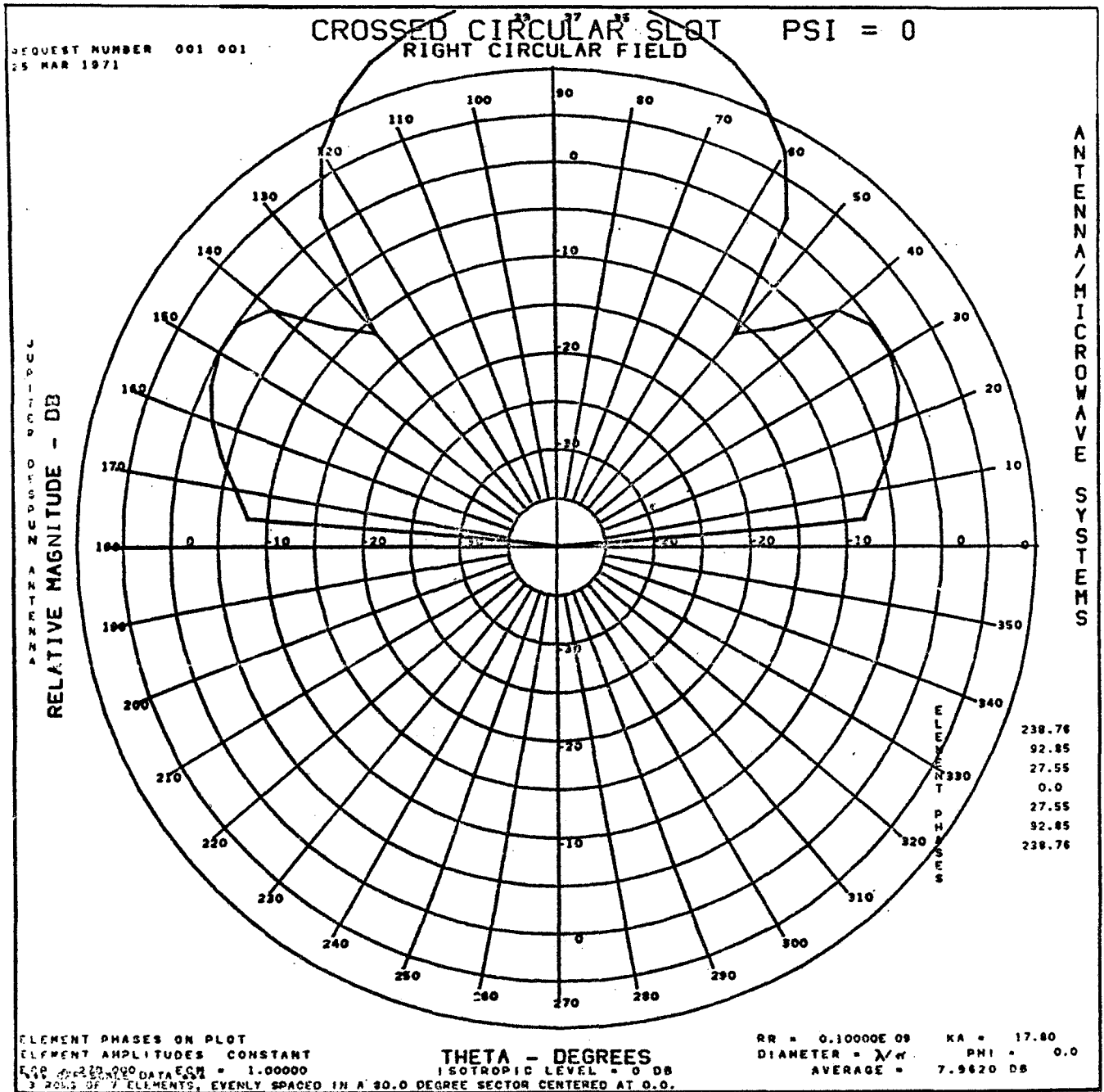
FIGURE 8-24

PIONEER F/G SPACECRAFT - 3 ELEMENT AXIAL SUB-ARRAY
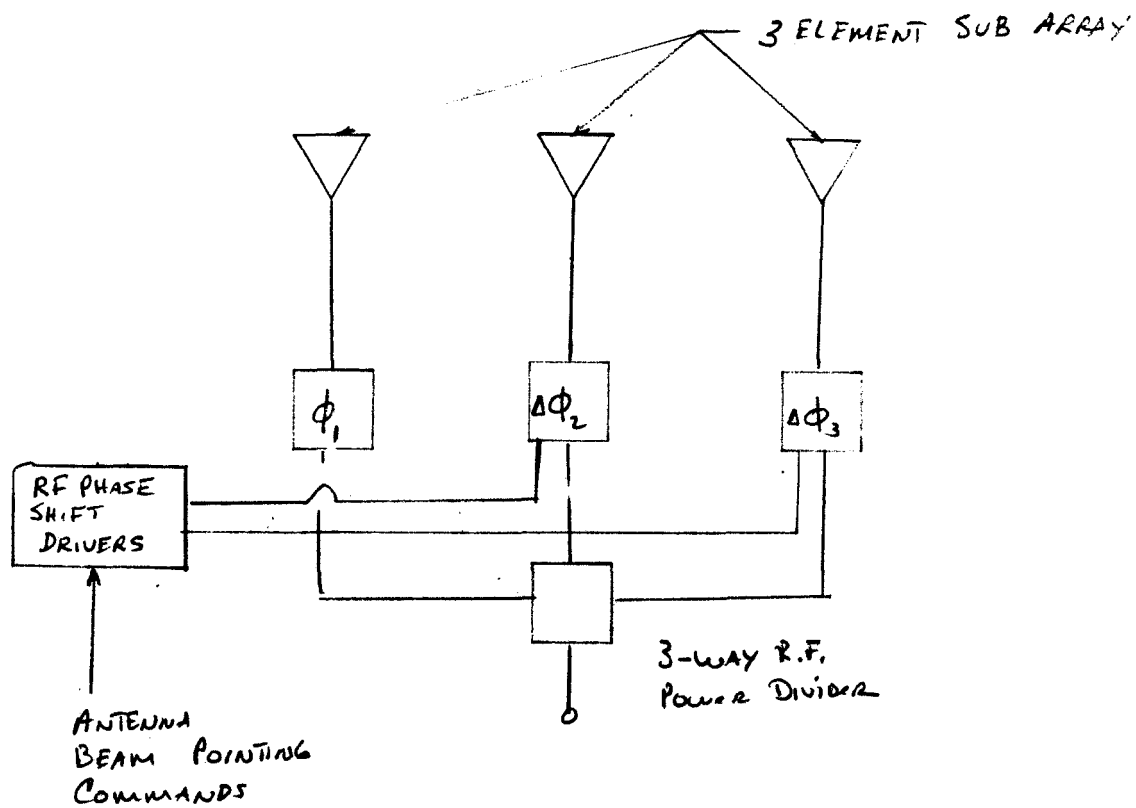
FIGURE 8-25

DESPUN JUPITER ANTENNA SWITCHING SCENARIO
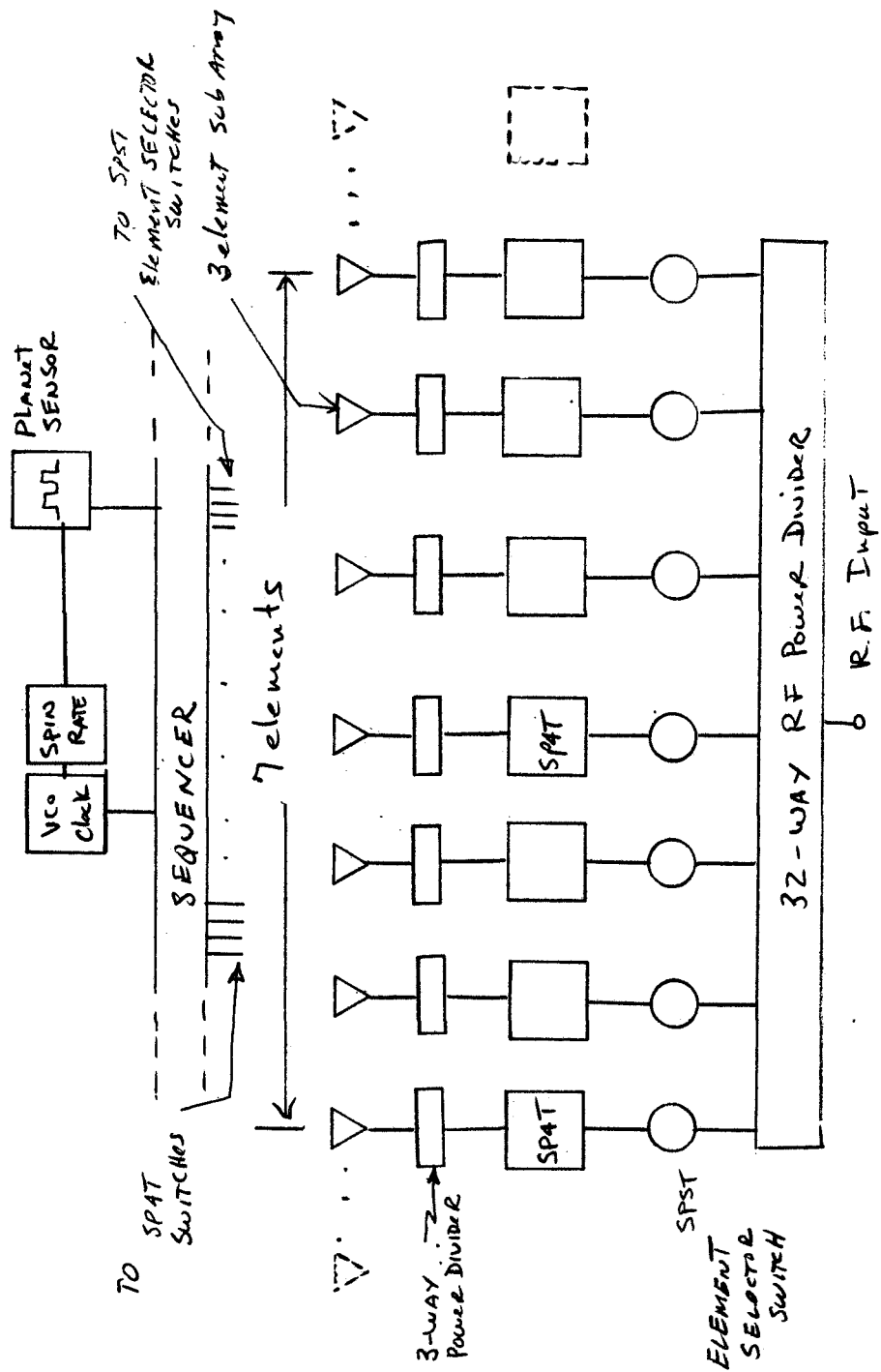
the axial plane is fed from a single three way power divider. The phase shifter of elements two and three are preprogrammed to provide a single step in phase of the three element array to shift the beam in the axial plane at a preprogrammed time in the trajectory. All three element sub-arrays about the cylinder have identical axial plane phase characteristics.

The circumferential array excitation scheme is illustrated in Figure 8-25. The 12 deg beamwidth in the circumferential plane is formed by exciting a sector of 7 elements phased to produce a beam mode of operation (each element considered to be a sub-array of three axial elements). While only seven elements are excited at any one time, there are a total of 32 of the three element sub-arrays equally spaced about the circumference of the spacecraft.

The despin mode is accomplished in Figure 8-25 by sensing the planet on each spacecraft spin cycle. The output of the planet sensor is used to deduce spacecraft spin rate which in turn provides information for driving a sequencer (binary counter).

The sequencer provides the switching signals which drive the RF switches (element selector and SP4T switches) in the 32 element circumferential array, into the appropriate on or off position depending on whether the element is in the illuminated sector or not. The appropriate phase is inserted into the element within the sector by the SP4T RF switch. The 32 element circumferential array is fed by 32 way stripline power divider with a single RF input connector.

8.7 POWER SUBSYSTEM

There are three flight regimes which must be considered in the selection and design of an entry probe power subsystem. These are the interplanetary cruise, post-separation cruise, and atmospheric descent regimes. During interplanetary cruise, spacecraft power will be used to provide all subsystem checkout and engineering diagnostic status, and thermal control (electrical dissipation) needs. It was determined that either the TOPS or Pioneer F/G spacecraft serving as a bus can provide the required power (See Section 5.1.6). During the post-separation cruise, entry probe power is required for subsystem checkout and engineering diagnostic status; and during descent through the clouds, entry probe power is required for operation of all subsystems.

8.7.1 Power Requirements

The power requirements for both the post-separation cruise regime and atmospheric descent regime is discussed in the following section.

8.7.1.1 Post-Separation Cruise Regimes

Immediately prior to entry probe separation from the spacecraft, the timer that is part of the programming and data handling subsystem will be initiated. The timer power requirement is about 100mw, and based on separation 60 days prior to entry, a total energy requirement of 144 whr will result. For the shallow flight path angle entry mission, which is based on 25w of transmitter power for a relay link, the total power consumption is 132w continuous during atmospheric descent. If it is assumed that the probe will be checked out once every five days, for a total of 15 minutes per checkout, then a total energy capacity of 396 whr will be required. The thermal control analysis of Section 8.3 has indicated that from about 45 to 50w of continuous power will be required for an uninsulated probe, with an aluminum coating, that is in equilibrium with space and the sun. If insulation is used, Section 8.3 also indicates that the thermal power requirements during post-separation cruise can be reduced to 1 to 2 watts. Therefore, depending on the approach followed, the power requirements for thermal control during post-separation cruise can range from 0 to 50w. The nominal thermal control design, however, is based on the use of insulating blankets and an RTG to provide electrical and thermal energy. The post separation power requirements are summarized in Table 8-10. It can be seen that the electrical power requirements can be satisfied by a power source that can provide 0.4w for a period of sixty days, or 0.1w for sixty days and 132w for 15 minutes for 12 subsystem checkouts. Some thermal control power may have to be provided in the form of electrical power rather than thermal power to supply energy at locations which have a high thermal resistance.

8.7.1.2 Atmospheric Descent Regimes

The shallow flight path angle entry mission is based on a 3600 sec descent time. An analysis of uncertainty in entry time as presented in Section 9.2 has indicated that there could exist a 1700 sec, three sigma, uncertainty in probe arrival at the entry point. A total entry probe nominal operation time of 5400 sec (1.5 hr) was selected and includes the time necessary for operation in the clouds, the three sigma error in arrival time, and warm-up time.

TABLE 8-10

ENTRY PROBE POWER REQUIREMENTS

REGIME	FUNCTION	REQUIREMENTS	POWER	ENERGY	CONTINUOUS POWER
Post-Separation	Timer Operation	Continuous for 60 days	0.1 w	144 whr	0.1 w
	Subsystem Checkout	12 times for 15 minutes	132 w	396 whr	0.275 w
	Thermal* Control	Continuous	0 to 50 w	0 to 72,000 whr	0 to 50 w
Descent	Subsystem Operation	Continuous for 1.5 hr	132 w	198 whr	132 w

*Most of this power can be thermal

8.7.2 Power Subsystem Candidates

A brief survey was made to screen and select candidate power energy sources for entry probe application. Based on the power and energy levels presented in Table 8-10, both solar and radioisotope power sources can be considered, as well as electrochemical battery and fuel cell energy sources. Some consideration was given to an open-cycle, hydrazine powered turboalternator. It was determined that this type of device has been designed where power levels of the order of 1 to 3 kw are required for short periods of time, like the order of tens of minutes. In addition, there are some integration problems such as angular momentum perturbations caused by the rotating machinery and the necessity of balancing. Also, it is necessary to eject the exhaust gases from the unit without inducing disturbance torques. The turboalternator approach did not appear to offer any advantages.

Solar Photovoltaic Array - Since the probe will be spinning from separation to entry, use of a solar concentrator to drive a thermal boiler or thermoelectric device is not feasible. A simple photovoltaic power converter affords the easiest integration. At Jupiter, the solar flux is about 5 to 6 mw/cm^2, and the temperature of solar cells in equilibrium with space and the sun is about 140 deg K. The solar flux is reduced to about 4% of the value that exists near Earth, and so the performance of the cells is greatly reduced. However, near Earth the solar cells tend to run at a temperature of about 300 deg K, so that the cooler operation near Jupiter tends to slightly increase their performance. Near Jupiter, a silicon cell can provide about 0.9 mw/cm^2 and a cadmium sulfide thin-film cell 0.22 mw/cm^2. The weight of a solar array comprised of silicon cells can be written as

$$W_{PANEL} = \frac{f \, m \, P}{r \cos\theta \, \eta}$$

where W_{PANEL} is the panel weight in lb.

f	f = π when array is along spin axis, and f = 1 when the array is perpendicular to the spin axis.
r	power output of cell per unit area (0.9 mw/cm^2)
P	power output
m	is the specific weight of panel (0.6 lb/ft^2)
θ	angle of incidence between array and sun
η	packaging efficiency of panel (75%)

For a normal angle of incidence, and a 1w output, the solar array can weigh from about 1 to 3 lb, and the total area requirement will vary from 1.6 to 5.0 ft^2 depending on whether the array is mounted parallel to the spin axis or perpendicular to the spin axis.

Radioisotope Thermoelectric Generator - A static power converter was determined to be appropriate for the power levels presented in Table 8-10. A thermoelectric unit was selected over a thermionic unit because there appears to be a greater technology investment in the former. Use of a radioisotope power source permits probe orientation at any angle to the sun. This is certainly not true for the solar array. Use of a radioisotope does impose some special design problems for the entry probe spacecraft interface, However, since the RTG will be located external to the payload container, it can be integrated late in assembly. It should be pointed out that both the TOPS and Pioneer F/G spacecraft use RTG's. However, these units are located on booms and are removed from the spacecraft payload compartment. The entry probe will be integrated in close proximity to the spacecraft payload compartment. Plutonium 238 was the fuel selected because of its long half-life and low gamma radiation. For an RTG that provides 10w of electrical power, the thermal to electrical efficiency is about 6.5% and the specific weight about 1.4 w/lb, whereas at the 2w level, the electrical efficiency is reduced to 5% and the specific weight is about 0.5 w/lb.

Electrical Chemical Batteries - Various types of batteries can be considered for this mission, and these types are listed in Table 8-11. It can be seen from this table that the greatest performance can be gained by use of silver-zinc batteries in their primary mode. From Table 8-10, the total energy requirement (not counting thermal energy) is 738 whr. Based on a performance figure of 50 whr/lb, some 15 lb of battery are required. The major limitation to the use of a battery in its primary mode is the relatively short shelf life. During the 60 day cruise, the cell separation material will deteriorate and the battery will lose charge. From this viewpoint of mission reliability, it is highly desirable to activate the battery prior to entry probe separation. It is the introduction of electrolyte that causes the deterioration. One way to get around this problem is to consider use of a battery operating in a secondary mode, and to suffer the lower performance penalty. If the power requirements were split between the post-separation and descent regime, then it would be possible to use a remotely activated primary battery within the payload container, and a secondary battery, activated at separation, either within the payload container or attached to the meteoroid container.

TABLE 8-11

ELECTROCHEMICAL BATTERY PERFORMANCE

SYSTEM	OPERATING MODE	OPERATING TEMPERATURE	SPECIFIC WEIGHT	ENERGY DENSITY
Silver-Zinc	Primary	-40 to 130 Deg. F	50 to 100 whr/lb	3.5 to 7.5 whr/in^3
Silver-Zinc	Secondary	-20 to 110	30 to 80	2.0 to 4.5
Silver-Cadmium	Secondary	-40 to 110	15 to 30	1.0 to 2.1
Nickel-Cadmium	Secondary	-40 to 160	8 to 16	0.6 to 1.5

Fuel Cells - A 1 kw-hr hydrogen-oxygen fuel cell system has a specific weight of about 330 whr/lb if cryogenic storage can be considered. However, due to the long cruise times, the boil-off losses could be prohibitive. If gaseous storage (in tanks) is used to avoid the boil-off problem, then the specific weight of a 1 kw-hr system is reduced to about 140 whr/lb. This latter pressurized system can provide a greater performance than can be obtained with the electrochemical battery. Deterioration of performance for long storage times is not a problem for the fuel cell as it is for the electrochemical battery that is charged. For each whr of electrical energy provided about 0.9 whr of thermal energy is dissipated. This energy dissipation could be combined with an insulation system to provide the necessary post-separation thermal control. There may be a problem in providing regulation of the fuel cell. During cruise 100 to 400 mw of continuous power is required, and during checkout and at entry the power requirement increases to 132w.

8.7.3 Power Supply Description

There are many combinations of power supply configurations that can be considered. For this study, a secondary silver-zinc battery serving as a primary source was used to provide the energy requirements for the atmospheric descent regime. A total of 198 whr of power were required. Using a 50% depth of discharge and an 80% battery efficiency, it was determined that a 10 lb battery would suffice. During post-separation cruise an RTG was used as the primary power source to provide all electrical needs. The secondary battery provided the energy for the checkout, and the RTG recharged the battery to full capacity and provided a trickle charge during the post-separation cruise. A 10w electrical output RTG was used to supply all electrical energy during post-separation cruise. The excess capacity can be used to provide electrical energy for dissipation in remote or highly insulated locations. The thermal output power can be radiated or conducted into the probe when needed or radiated to space. A specific weight performance figure of 2 w/lb was used for the RTG and a 7% thermal to electrical efficiency was assumed as performance based on 1975 technology. Using an efficiency of 7% some 140w of thermal power are available for thermal control. Two pounds were added for all power conditioning elements.

8.8 COMMUNICATION SUBSYSTEM

The communication subsystem conceptual design for the probe transmitting (direct and relay) and the spacecraft receiving systems is detailed in this section.

During the course of the study, four different probe communication links were evolved. Each one of these communication links, differ in antenna concept, and/or modulation scheme. A summary of the four probe transmitting concepts is listed in Table 8-12.

TABLE 8-12

Probe Transmitting Subsystems

No.	Antenna Type	Link Frequency	Transmitter Power	Modulation Scheme	Application
1	Conical Reflector	S-Band	50 watts	Convolutional Coding	Direct Link
2	Turnstyle over ground plane	S-Band	50 watts	Convolutional Coding	Direct Link
3	Conical Reflector	S-Band	25-40 watts*	Biorthogonal Coding	Relay Links
4	Cupped Turnstyle	L-Band	50 watts	Biorthogonal Coding	Relay Links

*25 watts for TOPS Missions; 40 watts for J-U-N Mission.

The basic block diagram for the probe transmitting system is shown in Figure 8-26. Also shown are the elements of the system that differ for each of the four study concepts.

Modulation Approaches - The data to be transmitted is either block or convolutionally encoded into binary symbols (a stream of ± 1). For either of the coding schemes (bi-orthogonal or convolutional) the code symbols appearing at the modulator in the form of a binary waveform are used to biphase modulate a square wave data subcarrier shown as S(t). S(t) is a square wave unmodulated carrier having ± 1 states. The modulated data subcarrier $Z_k(t)$ also of ± 1 in turn phase modulates the RF carrier C(t) which is then amplified and radiated from the probe antenna as $y_k(t)$.

where
$$Y_k(t) = \sqrt{2P} \, \sin\left[\omega t + (\cos^{-1} m) Z_k(t)\right]$$

$$K = 1, 2, \ldots 2^6$$

FIGURE 8-26 PROBE TRANSMITTING SUBSYSTEM

Figure 8-26 Probe Transmitting Subsystem

Block diagram: FROM DATA HANDLING SYSTEM → ENCODER → $x_k(t)$ → BI-PHASE MODULATION (input $S(t)$) → $z_k(t)$ → PHASE MODULATOR → POWER AMPLIFIER → $y_k(t)$ → ANTENNA

SYSTEM	ENCODER		POWER AMPLIFIER	ANTENNA
1	CONVOLUTIONAL	SAME	50 WATTS	CONICAL REFLECTOR
2	CONVOLUTIONAL		50 WATTS	TURNSTYLE OVER GROUND PLANE
3	BLOCK		25-40 WATTS	CONICAL REFLECTOR
4	BLOCK		50 WATTS	CUPPED TURNSTYLE

where P is the radiated power and m is the percentage of the total power allocated for the carrier component; i. e. $m^2 = Pc/p$, where Pc is the carrier power at frequency f.

Figure 8-27 is presented to show how each of the two different encoding schemes are generated. In the case of the block coded scheme, a 6 bit pseudo random (PR) bi-orthogonal encoder which has the property that each code word $x_k(t)$ (From Figure 8-26) has a near comma free property. The data bits x_1, x_2, x_3 .... x_5 shown in Figure 8-27 provide a PR sequence of length 31 which approaches the orthogonal code. The x_6 data bit determines the sequence polarity thus providing for the good synchronization property of the bi-orthogonal code.

For the generation of the convolutional code a shift register of length k is used to pass the information bit sequence. If some registers are used for parity check, then the convolutional code is called systematic otherwise as shown in the figure it is a nonsystematic code. For a given number of bits (L) in the message stream, the n modulo -2 adders are sampled in sequence by a commutator and the number of bits in the output code is n (L + k). Typically with $L \gg k$, the rate of the binary convolutional code, R_n, can be calculated as $\frac{1}{n}$ (bits/transmitted symbol).

Transmitter Power - Proposed transmitter power levels of from 25 to 50 watts of S and L-band frequencies have been configured for this study. All solid state transmitters have been selected since development technology in diode and power transistor efficiency, increased oscillator stabilities, and smaller packaging volumes and weights will, by 1975, show these trans- mitters to be the more attractive candidate.

The block diagram of such a transmitter is shown in Figure 8-28. The modula- tion input signal is applied to the exciter via an RFI filter to minimize cable conducted electromagnetic interference. The exciter provides an RF output power in the milliwatt range to the power amplifier at a drive frequency Fo/n where Fo is the transmitter carrier frequency and n is varactor diode frequency multiplier factor. After frequency multiplication the signal is passed through an RF load isolation and filter to protect the transmitter final stages from overload resulting from high VSWR conditions. Transmitter efficiencies on the order of 25 to 28 percent are anticipated for 1975 for these transmitter configurations.

FIGURE 8-27 ENCODING SYSTEMS
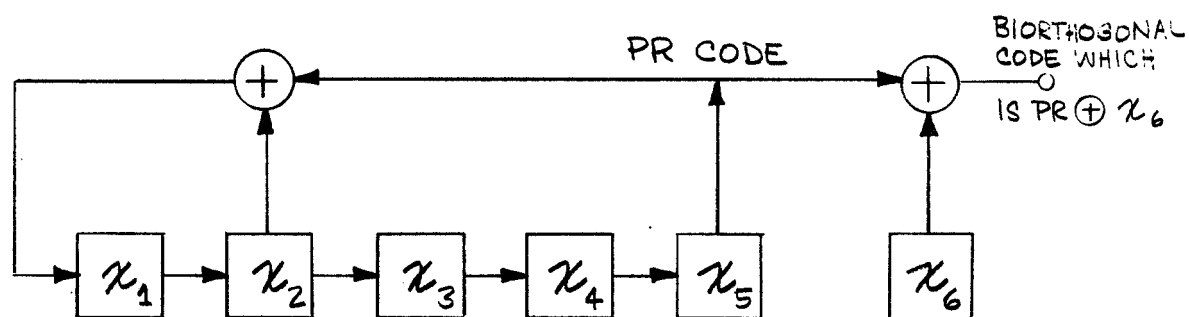
(a.) 6 BIT BIORTHOGONAL ENCODER
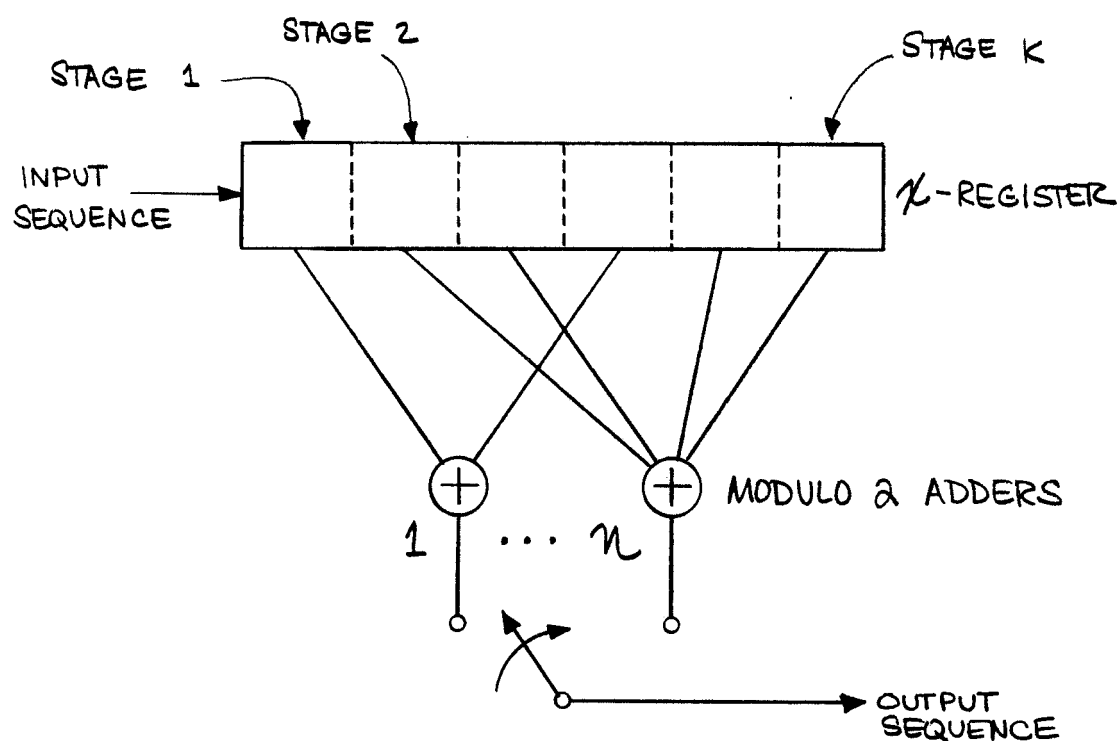
(b.) NONSYSTEMATIC BINARY CONVOLUTIONAL ENCODER

FIGURE 8-28 PROBE TRANSMITTER BLOCK DIAGRAM
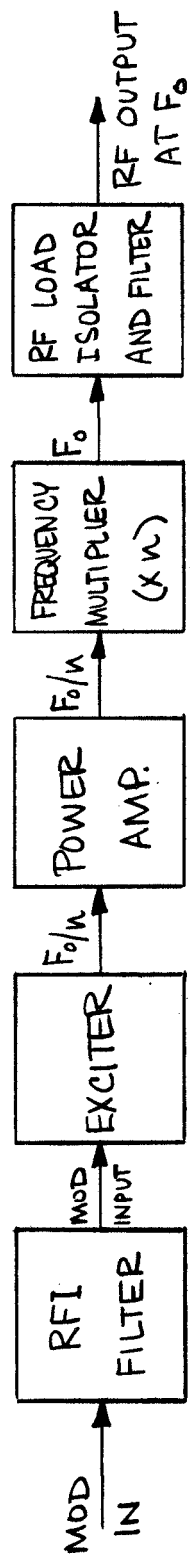
Antenna Systems and RF Transmission Circuits - The probe transmission systems configured for this study will not require any power splitting to feed the antennas; therefore, only a single line from transmitter to antenna feed is required. The various antenna systems associated with the probe transmission system have been discussed in Section 8.6.

Characteristics of Probe Transmission System - A summary of the electrical and mechanical characteristics of the probe transmission system is summarized in Table 8-13.

TABLE 8-13

Summary of Probe Transmission Characteristics

Transmitter		
Operating Frequency	L-Band/S-Band	
Frequency Stability	±0.0001%	
Output Power Required	50 watt max.	
Input Power Required	200 watts max.	
Modulation	Coded PCM	
Antenna Types	Turnstyle/Conical Reflector	
Polarization	Circular	
Maximum Aperture	11"	
Efficiency	Above 50%	
Power Handling	Greater than 50 watts	
	Weight	**Volume**
Telemetry System		
Video	2 lb	50 cu. in.
R.F.	3 lb	8 x 4 1/2 x 1 1/2
Antenna System	.8 lb	- - - - -

Receiver - The receiver employs a phase-locked loop (PLL) to track the observed RF carrier component thus providing a coherent reference for synchronously demodulating the received signal. The received signal is denoted as U(t), where

$$U(t) = \sqrt{2P} \sin\left[\omega t + (\cos^{-1} m)\, z_k(t) + \Theta\right] + n(t)$$

where Θ is the random phase shift and $n(t)$ is the additive Gaussian noise The output of PLL is

$$r(t) = \sqrt{2} \cos\left[\omega t + \hat{\Theta}(t)\right]$$

where $\hat{\Theta}$ is the estimate of the phase of the observed carrier component. Multiplying $U(t)$ by $r(t)$ and neglecting double frequency terms, the result $v(t)$ is the input of the data detector:

$$v(t) = \sqrt{S} \; Z_k(t) \cos\phi + \mathcal{M}'(t)$$

where $S = (1-m^2)P$ and $\phi = \Theta - \hat{\Theta}(t)$ is the receiver phase error. The additive noise $\mathcal{M}'(t)$ is the low pass equivalent of $M(t)$.

A subcarrier tracking loop is assumed to exist for the purpose of providing subcarrier or bit synchronization. The phase jitter may be kept small by designing a very narrow-band subcarrier tracking loop. Note that $Z_k(t)$ may be considered as a modulated waveform. It is obtained by modulating $S(t)$ with $X_k(t)$. Finally, word sync may be derived at the receiver symbol loop by making use of the comma-free properties of the transmitted code. Thus the necessary timing information is provided for triggering the cross-correlation detector in Figure 8-29. The output data is the recovered bit stream and may be recorded for the data user.

Characteristics of Receiving Subsystem - A summary of the electrical and mechanical characteristics of receiving system is shown in Table 8-14.

TABLE 8-14

Summary of S/C Receiving System

Antenna System*		TOPS	Pioneer F/G
	Link Frequency	S-Band	L-Band
	Type	Elliptical Dish	Circumferential Accuracy
	Gain	24.5 dB	15 dB
	BW	10° x 7°	10° x 30°
	Polarization	Circular	Circular
	Power Divider	None	32 x 3
	Weight	12.7 lb	25 lb
Receiver			
	Noise Figure	5 dB	5 dB
	Noise Spectral Density	-197.6 dBW/Hz	-194.8 dBW/Hz
	Modulation Scheme	Biorthogonal Coded	
	Error Rate	$<10^{-2}$	
	Carrier Loop BW	50 Hz	
	Acquisition Times	< 60 seconds	
	Input Power	2.0 watts	
	Weight	4.0 lb	
	Volume	100 cu "	

*See Section 8.6.2 for further details

FIGURE 8-29 RECEIVING SYSTEM BLOCK DIAGRAM
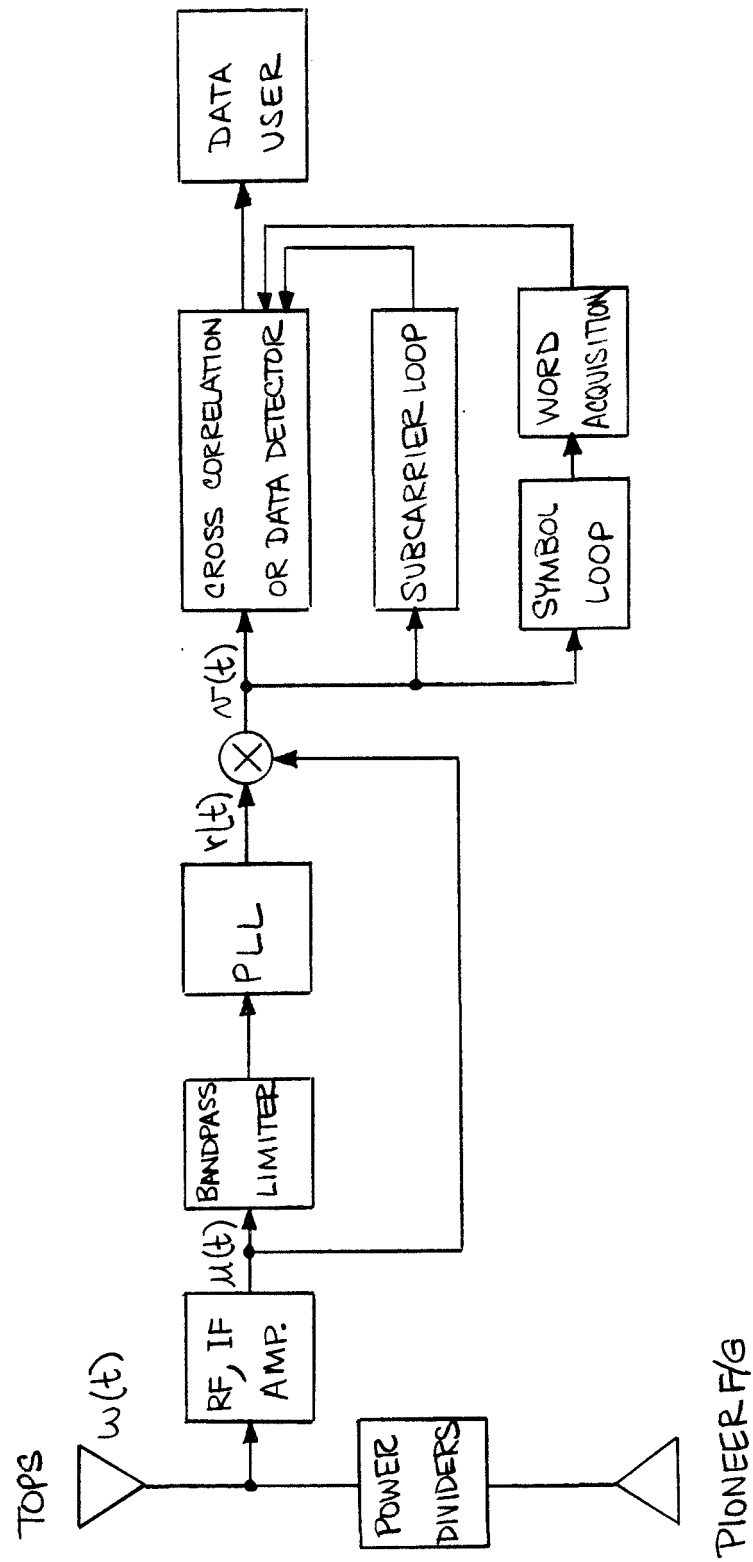
8.9 PARACHUTE SUBSYSTEM

Following deceleration of the entry probe from the high entry velocity that results from the kinetic energy of the approach velocity and the fall through the Jovian gravitational field: 1) the heat shield must be separated, 2) the payload container extracted, and 3) the payload container descent velocity reduced to provide "a long and slow descent through the cloud layers". Extraction and separation is required to jettison a relatively low drag 60 deg cone aerodynamic configuration which will have suffered massive ablation losses and no longer have a predictable shape, and to discard a subsystem which, by continuing to outgas, can contaminate the mass ingestion science experiments. It is further necessary that heat shield separation and payload container extraction which will enable deployment and operation of the scientific instrumentation, be accomplished prior to entrance into the clouds. In the cool/dense model atmosphere, the nominal model atmosphere, and warm/ expanded model atmosphere, the tops of the clouds occur at a pressure of about 65, 38, and 20 mbar. respectively. A parachute was selected as the device to accomplish the tasks of separation, extraction, and long and slow descent. Other types of deceleration devices could be employed, however, a parachute can 1) meet the objectives, 2) provide high reliability, 3) is light in weight, and 4) is well within the 1975 state-of-the-art.

8.9.1 Parachute Environment

In selecting the type of parachute, the environments must be specified so that the material and general subsystem can be characterized and described. There are three distinct environments. These include: 1) dormant and packaged throughout the interplanetary and post separation cruise, 2) the deployment of the parachute and loads attendant during extraction of the container, and 3) the aerodynamic loads and thermal environment of atmospheric descent.

Interplanetary Cruise Phase - During the interplanetary cruise and post separation cruise, the nominal temperature of the entry probe and hence the parachute compartment will be held to about +60 deg F. Thermal control analysis indicated that this favorable temperature can be achieved with minimal impact on spacecraft subsystems, and careful insulation of the entry probe.

During the long cruise of 450 to 1450 days the parachute will be exposed to the solar wind and cosmic rays. However, during the five to seven hours prior to entry, the probe will be subjected to the high flux levels of the Jovian trapped radiation belts. Lightweight parachute subsystems are based on use of organic materials which are, in general, sensitive to this radiation, and

could suffer serious degradation of their physical properties. This is a problem that is noted, but was not investigated in this study.

Extraction and Separation Phase - A typical entry trajectory is presented in Figure 8-30 for the nominal model atmosphere, variable mass probe, and -15 deg flight path angle at entry. The Mach No., dynamic pressure, and deceleration load are shown as a function of local pressure. A constant dynamic pressure and deceleration load indicate that the entry probe is in terminal descent. For this study, it was assumed that parachute deployment would occur at a Mach No. of 0.7. It was determined that over the range of model atmospheres, ballistic parameters, and entry angles studied that if deployment would occur at 0.7 Mach No., then the entry probe would be above the clouds when the payload container was extracted and instrument sampling initiated. For the case under consideration the dynamic pressure at chute opening is 57 lb/ft^2. The dynamic pressure and the local temperature are the important factors in the determination of chute design. In Table 8-15, there is indicated the dynamic pressure and altitude above clouds at 0.7 Mach No. for the range of model atmospheres, entry angles, and ballistic parameters considered. The variable mass (caused by heat shield ablation) cases shown in Table 8-15 tend to decrease the dynamic pressure and increase the altitude at 0.7 Mach No. in comparison with constant mass cases.

Terminal Descent Phase - During descent the aerodynamic loads on the chute are greatly reduced to about one sixtieth the value experienced at deployment. The aerodynamic loads could increase due to wind shears and gusts. The main factor in the chute design is the local ambient temperature. For descent into the nominal model atmosphere the local temperature varies from 113 deg K at 0.7 Mach No. to 425 deg K if the chute remains attached to the probe to the base of the clouds. In the warm/expanded model atmosphere the temperature excursion is 118 to 387 deg K and in the cool/dense model atmosphere, 113 to 490 deg K.

8.9.2 Parachute Configuration

There are many types of parachute canopy configurations that can be utilized, depending on the specific application and performance requirements. A ring sail configuration was selected for the Jupiter probe decelerators, because it has well defined performance characteristics and high drag (C_{DO} = 0.7 to 0.9).

The size of the parachute will depend on the required descent time. A discussion of descent time is given in Section 5.1.5, and resulted in a terminal descent

FIGURE 8-30

TRAJECTORY PARAMETERS AT PARACHUTE DEPLOYMENT

NOMINAL ATM.
VARIABLE MASS
$m/C_DA_{INIT} = 0.5 \ SLUG/FT.^2$
$m/C_DA_{SUBSONIC} = 0.648 \ SLUG/FT.^2$
$\gamma_E = -15°$

PRESSURE ~ ATM

MACH NO. ~ M
LOAD ~ G's × 10^{-1}
DYN. PRES. ~ q ~ (LBS/FT²) × 10^{-2}
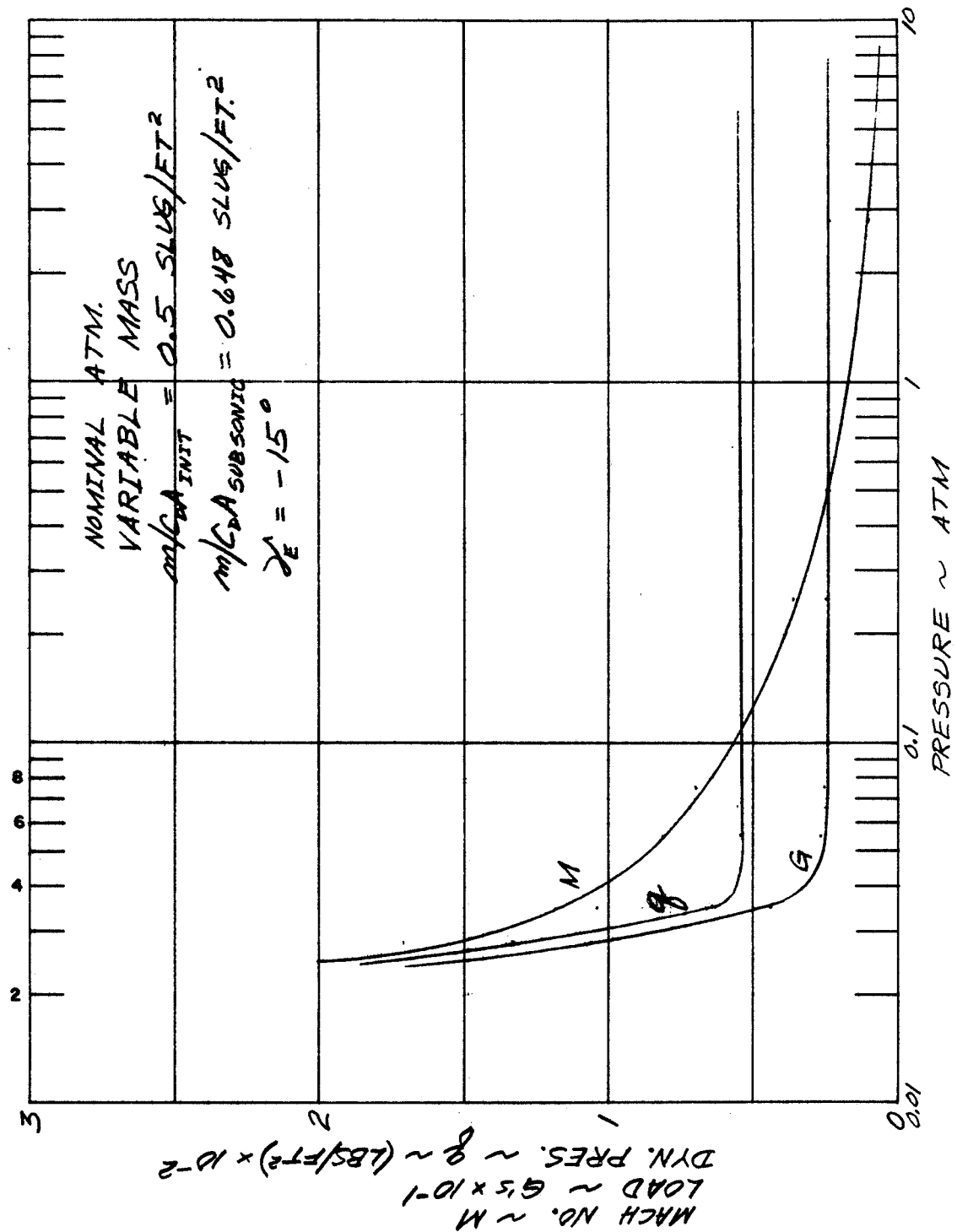
TABLE 8-15

DYNAMIC PRESSURE AND ALTITUDE AT PARACHUTE DEPLOYMENT*

$\dfrac{M}{C_D A}$ $\dfrac{SLUG}{FT^2}$	γ_E DEG	ATMOSPHERE	q LB/FT^2	h** KM
0.3	-15	Nominal	34	59
	-30		41	55
↓	-60		57	47
0.5	-15		57	50
	-30		67	47
↓	-60		97	39
0.7	-15		79	45
	-30		94	41
↓	-60	↓	137	34
0.5	-30	Warm/Expanded	63	66
		Nominal	67	47
↓	↓	Cool/Dense	83	33

* Mach No. = 0.7 at Deployment Variable Probe Mass

** Altitude Above Cloud Tops

ballistic parameter of 0.01 slug/ft^2 (see Table 7-1). Based on a spherical container weight of 114 lb. (Earth) and iterating to account for chute weight, it was determined that a 25 ft. diameter ring sail chute is required.

A number of organic textile materials are available for the construction of parachute systems. These include Nylon, Dacron, and Nomex. In addition, an excellent material like PBI (polybenzimidozole) which has good high temperature performance if needed, could be considered. Use of PBI is consistent with the groundrule of use of 1975 technology.

The selected parachute material must possess the necessary strength, energy absorption ability, and porosity characteristics, and provide a low weight; but at the same time, the selected material must be capable of operating in and surviving the environments. In Table 8-16, there is shown the comparative performance of Nylon, Dacron, and Nomex. The favorable strength to weight ratio of Nylon fabric, in comparison to the other parachute materials, along with its availability in many textile forms, make it a good choice for the parachute. However, Nylon has definite limitations in respect to its maximum operating temperature, and also the radiation damage threshold of Nylon is lower than the other materials. A comparison of Nylon fabric with other possible parachute material fabrics is shown in Figure 8-31. This figure illustrates the strength retention during exposure to elevated temperature. At the base of the clouds in the nominal model atmosphere the temperature is 425 deg K. If a Nylon chute was exposed to this temperature for 30 min., the strength would be reduced to 40% of the initial value. But it is important to note that the reduction in strength occurs after the loads are reduced.

Nylon was selected with the knowledge that the radiation damage problem must be assessed, and that it is not satisfactory for all model atmospheres. Its main advantage is the lighter weight subsystem that can result based on the design data used.

The parachute system is made up of the main chute and a pilot chute to extract the main chute, along with their respective packaging containers. Each of these chutes will have a canopy. suspension lines, and riser lines. In addition, the main chute will have a harness assembly to attach the parachute to the suspended payload container. The diameter of the main chute canopy is governed by the descent time requirement of the suspended weight to satisfy the science requirements. The parachute system weight is primarily governed by the opening shock load which is a function of the dynamic pressure and chute diameter. It is, therefore, possible to express the total parachute weight in

TABLE 8-16

PERFORMANCE OF CANDIDATE PARACHUTE MATERIALS

MATERIAL	STRESS TO DENSITY RATIO OF FABRIC	STRESS TO DENSITY RATIO OF WEBS, TAPES, AND CORDS	RADIATION DAMAGE THRESHOLD	CONTINUOUS MATERIAL TEMPERATURE RANGE
Nylon	69,000 Ft.	180,000 Ft.	5×10^7 Rad	78 to 420 Deg. K
Dacron	69,000	110,000	1×18^8	20 to 420 Deg. K
Nomex	78,000	120,000	5×10^8	20 to 590 Deg. K

FIGURE 8-31

TOTAL SUBSYSTEM WEIGHT OF PARACHUTE
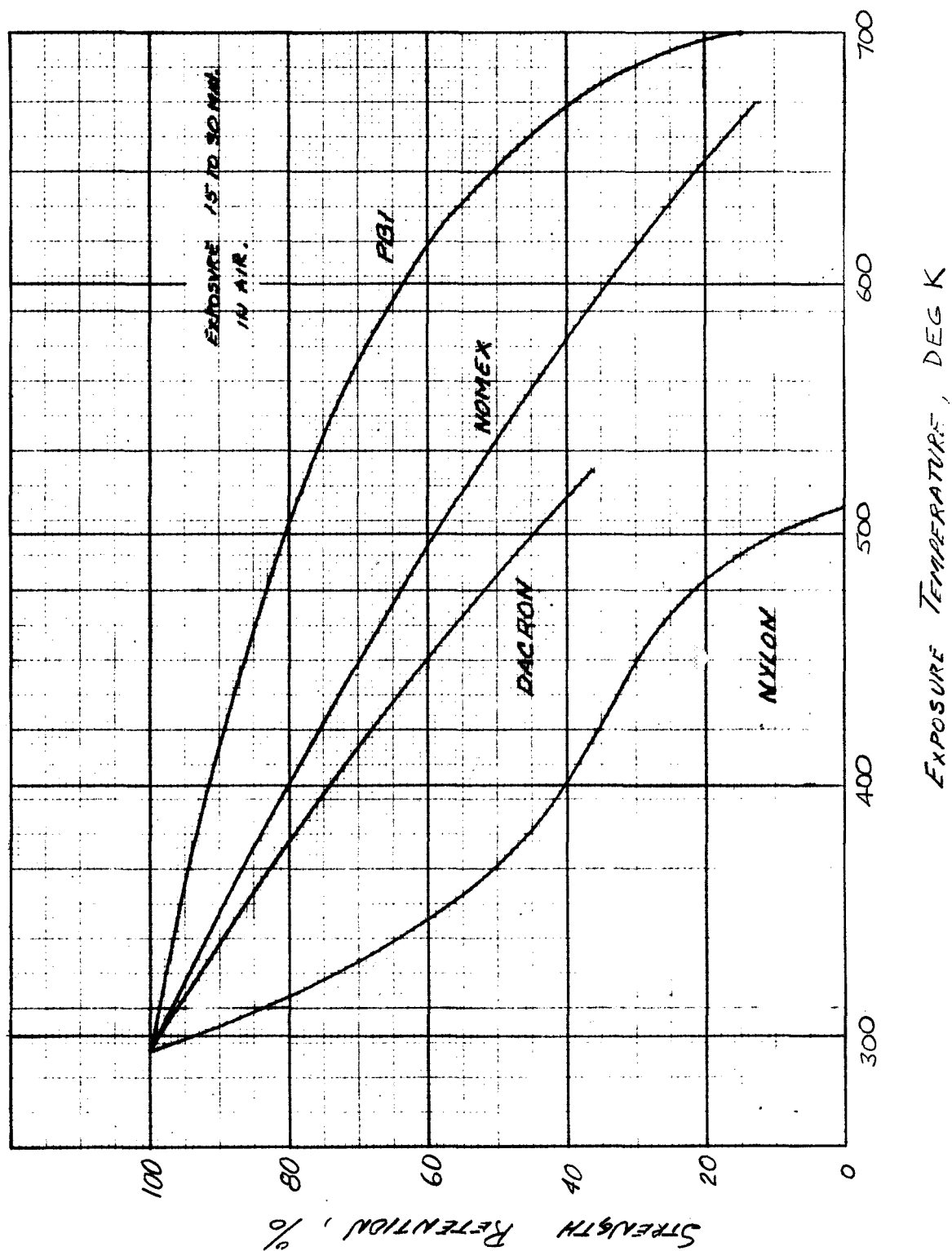
in terms of these parameters, for a given material and parachute configuration. The following total parachute weight equation was developed for a ringsail parachute canopy using Nylon material:

$$W = 14.5 \times 10^{-6}\left(q\, D_o^3\right) + 2.44 \times 10^{-4}\left(q\, D_o^3\right)^{\frac{2}{3}} + 2.6 \text{ lb.}$$

where, q = dynamic pressure at deployment, lb/ft^2

   D_O = nominal diameter, ft.

In this equation the first term represents the weight of the main chute, pilot chute, and harness, including suspension and riser lines. The second term is the weight of the containers for both the main chute and pilot chute. The constant in the equation accounts for fixed hardware, typically, attachments, swivels, collars, etc. This equation is presented graphically in Figure 8-32. Also shown in Figure 8-32 is the nominal atmosphere design condition for a 25 ft. diameter chute deployed at q = 57 lb/ft^2 dynamic pressure (M = 0.7), which gives a total parachute system weight of 18 lbs. The G load on the probe during parachute deployment is 177. Following deployment the dynamic pressure during descent is reduced to a constant value of 0.8 lb/ft^2 (in the absence of shears and gusts).

8.10   DEFLECTION SUBSYSTEM

The entry probe is on a flyby of Jupiter while attached to the spacecraft. Sometime following penetration of the Jovian sphere of incluence, the probe must be separated, oriented, and an impulse applied to deflect the probe onto an impact trajectory. The magnitude of the impulse is dependent upon the probe mass and the deflection velocity.

8.10.1   Deflection Subsystem Requirements

The magnitude of the deflection velocity is dependent on the entry angle, lead time, approach velocity, separation range, and periapsis passing distance. It is shown in Tables 9-1 to 9-5 that the deflection velocity requirements increase as the flight path angle at entry, lead time, approach velocity, and periapsis passing distance increase; the deflection velocity decreases as the separation range increases. It is also important to note from these tables that the dispersion in entry angle is only a function entry angle. It might be expected that as the separation range decreased, the increase of velocity requirements and greater absolute magnitude in velocity error would propagate into a larger entry dispersion. This larger velocity error is offset by the

Load Parameter, $q D_o^3$, lb-ft

Parachute System Weight, lb

NOMINAL DESIGN
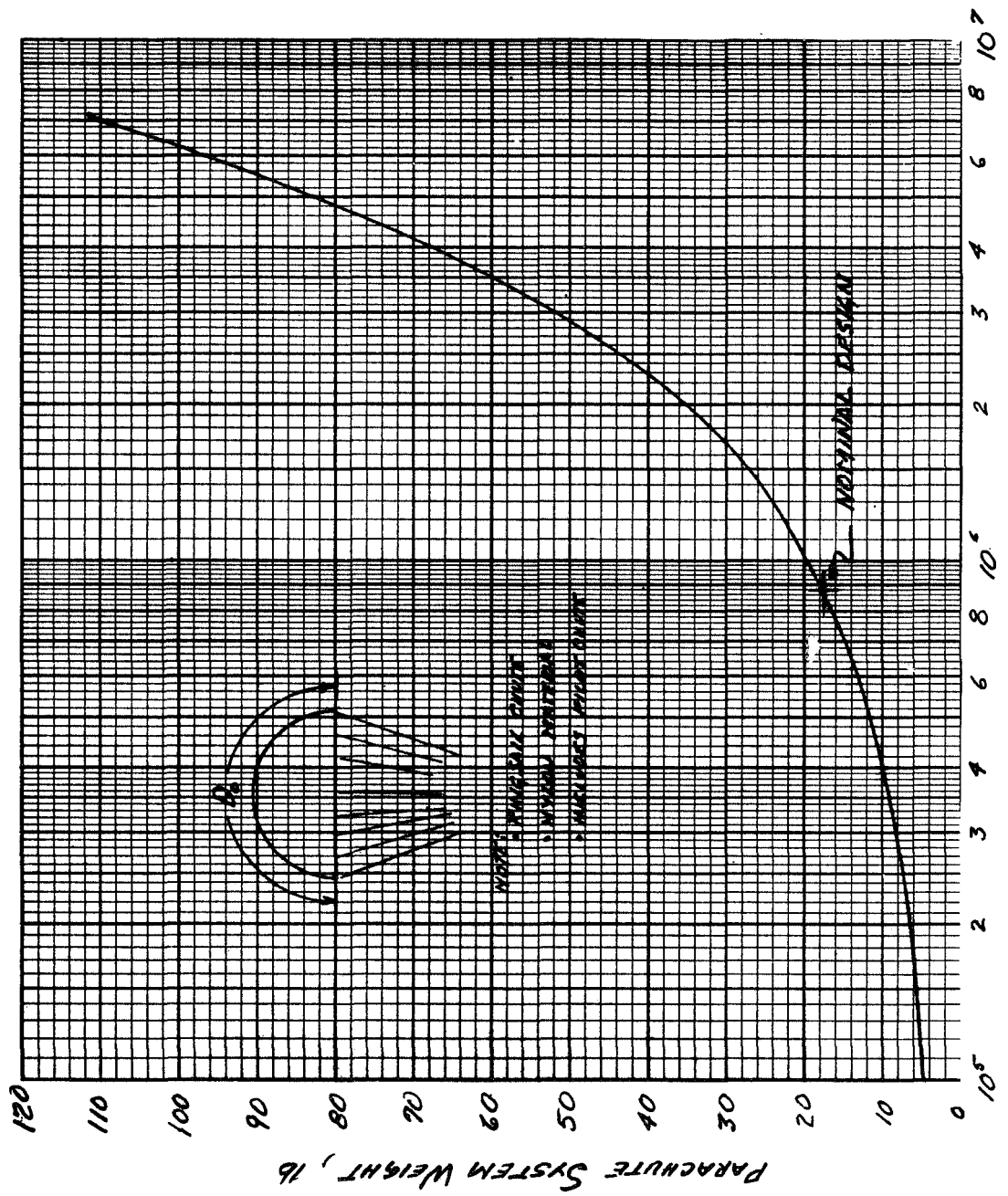
decrease in time from separation to entry due to the larger velocity, and so does not have the time to propagate into a larger entry dispersion.

The advantage of separation of the probe near to Jupiter is that it allows for greater utilization of spacecraft subsystems. If the time of separation from the spacecraft can be made very small, then only the flight regimes of interplanetary cruise while attached to the spacecraft and atmospheric entry must be considered. As the post separation flight time increases, the post separation cruise becomes an important new regime. If a separation range of 45 million km is chosen, the post separation flight time is 47 days and the velocity increment for probe deflection is 54 m/sec. At 15 million km, the flight time is reduced to 14 days and the velocity is increased to 162 m/sec. A 14 day flight time will lead to requirements for post separation thermal control and post separation power for operation of entry timer, and power for checkout, as will certainly a 60 day post separation cruise. Since there **did** not appear to be a clear cut advantage at a 14 day flight time as compared to a 47 day flight time based on qualitative considerations, separation at the sphere of influence or 45 million km was chosen. The velocity increment can range from 50 to 300 m/sec based on the range of approach and targeting parameters considered. Probe mass can range from about 250 lb for a probe designed to contain the small payload and enter at shallow angle to about 800 lb for a probe designed to contain an expanded payload and enter at steep angles. The total impulse, therefore, can range from 400 to 8000 lb-sec. Another requirement is long burn time to facilitate the ability of adding impulse in the proper direction. Note that for a spin stabilized configuration long burn times allow for many probe revolutions and an averaging o) t of misalignment errors. Also for an active attitude control system, the thrust levels needed for control and the response of the system can be reduced, if a long burn time can be provided.

8. 10. 2 Deflection Subsystem Performance

Both solid and liquid propulsion systems could be considered. An end-burner grain configuration solid rocket motor propulsion system was selected because design studies had indicated that a compact assembly resulted. In addition, technology studies are being conducted to develop long burn time/low acceleration end burner grain configuration motors for a Jupiter spacecraft orbit insertion motor. The shelf life reliability and the environmental hardening problems that would be solved for the spacecraft orbital motor could be applied to the entry probe deflection motor.

Two rocket motor configurations are presented in Figure 8-33, and the corresponding performance is indicated in Table 8-17. Both configurations are end burners. A propellant mass fraction equation was developed, that would permit estimates for a mid-range class of motors. The equation for the propellant mass fraction, λ, of an end burner solid rocket motor is a function of propellant mass, M_P,

$$\lambda = \frac{M_P}{0.123 + 0.734 \, M_P^{2/3} + M_P}$$

Propellant mass fraction is defined as the ratio of the propellant mass to the propulsion subsystem mass. It can be seen from Table 8-17, that the specific impulse is a function of the nozzle area ratio. For this study, an area ratio of 20 was used with a corresponding specific impulse of 274 lb-sec/lb. The somewhat lower performance and weight increase was offset by a reduction in the length of the motor. The mass of propellants can be calculated from:

$$M_P = M_{PROBE} \left[\frac{\frac{\lambda \Delta V}{g \, I_{sp}}}{\lambda - (1-\lambda) \frac{\Delta V}{g \, I_{sp}}} \right]$$

and the equation for λ by an iterative process. For example, the velocity requirement for the JUN Mission is 266 m/sec, and the separated mass of the probe before the addition of a propulsion subsystem is 360 lb. The propellant mass is 28 lb., the propellant mass fraction is 0.82, and the propulsion subsystem mass is 46 lb. Of the five candidate missions considered the greatest propulsion requirements were for this mission and resulted from the large periapsis passing distance required at Jupiter for trajectory guidance to Uranus. The length of an end burner motor is to a first approximation a function of the length of the grain plus the length of the nozzle. The length of grain is directly proportional to the propellant burn rate, and the length of the nozzle is dependent on the mass rate of flow of propellants and the area ratio of the nozzle.

8.11 ENVIRONMENTAL CONTAINER SUBSYSTEM

An environmental container serves to provide a set of physical conditions for the entry probe that tend to approach laboratory conditions. Three containers can be defined and include: 1) the meteoroid container to protect the entry

FIGURE 8-33

SOLID PROPELLANT ROCKET MOTOR CONFIGURATIONS

24.20 DIA

20.51 DIA

68.00
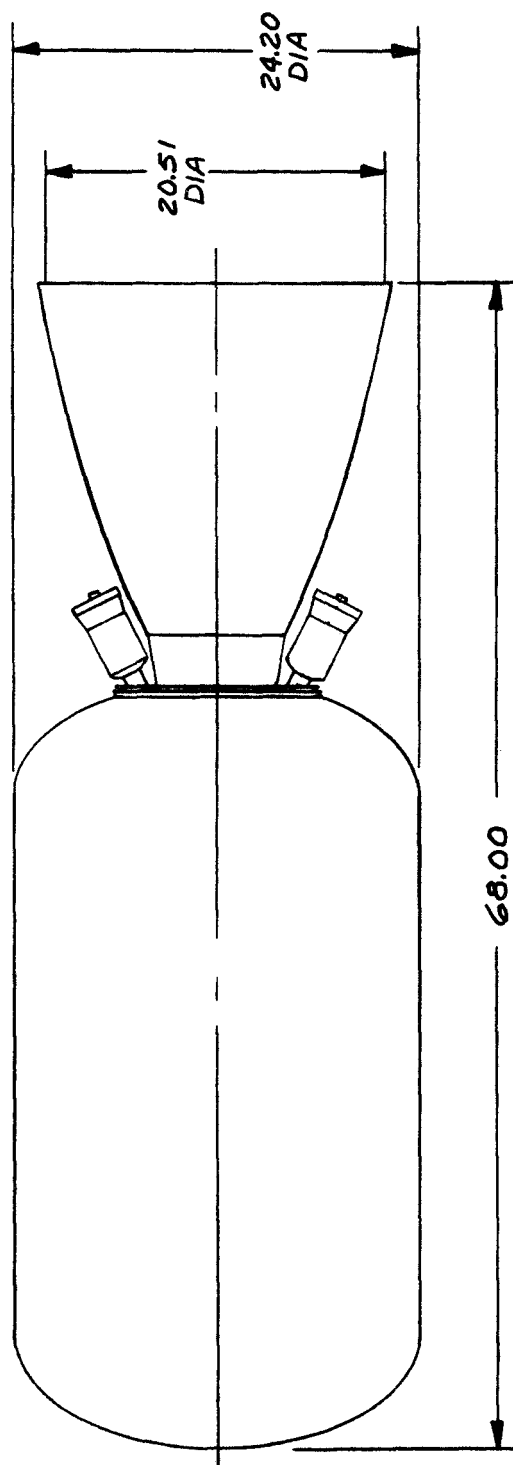
LARGE MOTOR

TOTAL IMPULSE 301,000 LB-SEC

$\frac{1}{10}$ SCALE

7.750

2.50 DIA
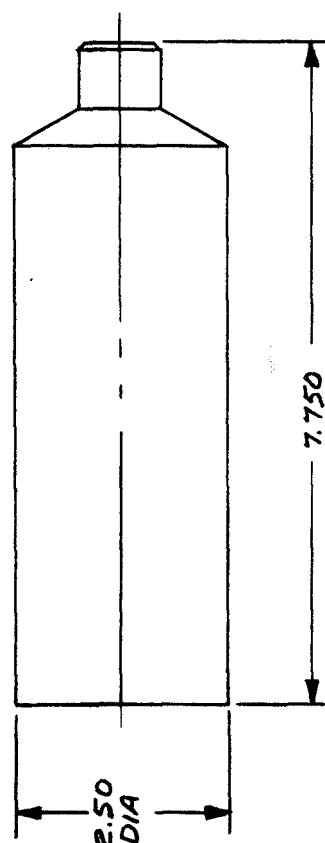
SMALL MOTOR

TOTAL IMPULSE 280 LB-SEC

$\frac{1}{2}$ SCALE

TABLE 8-17

SOLID PROPELLANT ROCKET MOTOR PERFORMANCE
END-BURNER GRAIN CONFIGURATION

CHARACTERISTIC	SMALL MOTOR	LARGE MOTOR
Total Impulse, Lb-Sec	280	301,000
Burn Time, Sec	15	260
Average Thrust, Lb.	19	1,160
Specific Impulse, Lb-Sec/Lb	247	297
Average Chamber Pressure, Lb/In^2	500	158
Burn Rate, In/Sec	0.37	.15
Expansion Ratio	8.5	80
Propellant Weight, Lb.	1.13	1,015
Motor Weight, Lb.	2.47	1,089
Propellant Mass Fraction	.55	.93
Propellant Density, Lb/In^3	.061	.063
Specific Heat Ratio	1.22	1.21
Vendor	Atlantic Research Corporation	Thiokol Corporation

probe from the hazard of impact with meteoroid and cometary debris, 2) the heat shield and aeroshell structure to protect the payload from the aerodynamic dissipation of energy and momentum that results from interaction of the probe with the Jovian atmosphere, and 3) a payload container to protect the payload from the high temperature, and high pressure gases of the Jovian lower atmosphere. A discussion of the meteoroid container is presented in Section 2.1. The heat shield discussion is presented in Section 8.4, and the aeroshell structure discussion can be found in Section 8.2.1. The design concept for the payload container is indicated in Section 7.2, and specific discussion of the pressure vessel subsystem and insulation subsystem can be found in Section 8.2.2 and Section 8.3.2 respectively. In this section there is presented the arguments for the selection of the payload container design concept, and a comparison of the design concept with alternatives that were considered.

8.11.1 Payload Container Concept Evaluation

A study was made to evaluate the comparative performance of alternative payload container concepts. The reference design approach that has been pursued during this study is based on use of an insulated pressure vessel to isolate the payload from the local environment, and maintain an Earth-sea level like environment. The pressure vessel is designed to resist the tensile loads induced by the interplanetary flight, and the buckling loads (or compressive loads) induced during descent into a high pressure atmosphere. An insulating material is wrapped around the exterior of the pressure vessel to provide protection for the payload against the high temperature atmosphere that is associated with descent to high atmospheric pressure levels. This approach removes the requirement for development of a payload that must be designed to operate at the elevated temperature and pressure associated with penetration of the Jupiter atmosphere. This approach also removes the necessity of having to qualify all of the subsystems in an environment that is significantly different than local ambient conditions within a laboratory at the surface of the Earth. On Earth, the local conditions are that of an atmosphere of air at a pressure of 1 atm and a temperature of 289 deg K (60 deg F) whereas the local environmental conditions at the base of the ammonium chloride clouds in the Jovian nominal model atmosphere corresponds to a hydrogen:helium atmosphere, a pressure of 17 atm and a temperature of 425 deg K (305 deg F).

Three alternative payload container concepts were evaluated and compared. All three concepts are based on maintaining the thermal protection system,

but relaxing the pressure requirements. In Table 8-18, the three alternative con-
cepts are summarized, and are compared with the nominal design approach
which maintains the payload environmental pressure at one atmosphere. The
weights shown in Table 8-18 are for the pressure maintenance system alone,
and do not reflect the weight of the insulation system. Weights are given for
titanium pressure vessel construction, and also for lightweight pressure vessel
construction. For the lightweight construction, beryllium is used to a pressure
of 90 atmospheres and yield stress governs; from pressures of 90 to 590
atmospheres, alumina is used and buckling stress governs; from 590 to 1000
atmospheres, alumina is also used, but yield stress governs.

The first concept is based on admitting the atmosphere during descent. With
this approach the need for a pressure vessel is eliminated, and instead a
lighter structure is provided to support the insulation during the application
of launch loads and entry deceleration loads. It has been assumed that the
holes that admit the atmosphere are of sufficient dimension that during
atmospheric descent the internal pressure follows the external pressure, and
that the holes are sufficiently baffled so that the convective heat transfer paths
with the atmosphere are negligible. It has been further assumed that the pay-
load is maintained at a constant temperature of 100 deg F during the descent.
Table 8-18 shows the quantity of heat absorbing salts (106 Btu/lb) that must
be used to absorb the energy of the admitted gases. For descent to low
atmospheric pressure levels there appears to be a weight advantage. However,
account must be taken of protection of sensitive components from the local
pressure, and from the condensed gases which will probably be present.

A second concept was investigated based on the use of a stored gas to equilibrate
the atmospheric pressure. This concept removes the requirement to provide
a pressure vessel for the payload, and substitutes a pressure vessel for the
containment of the regulation gas. Note that the payload will realize the local
pressure of descent. The results of this analysis is also presented in Table 8-18.
From the point of view of minimization of weight of gas and weight of storage
tank, it is desirable to use a very high storage pressure and a very low
molecular weight gas. Accordingly, a storage pressure of 100,000 psia was
used for hydrogen gas. The weights shown in Table 8-18 do not account for
regulation and plumbing, and are based on use of a safety factor of two for
the titanium storage tank design. It was further assumed that the packaging
factor for the two foot diameter payload container was 50%, and the quantity
of stored gas required was reduced accordingly. At low atmospheric descent
levels, the weights shown in Table 8-18 indicate that the regulated system may
have some advantage. However, it is felt that after account is taken of the
regulation and plumbing weights, protection of pressure sensitive components,

TABLE 8-18

COMPARISON OF PAYLOAD CONTAINER CONCEPTS

Atmospheric Descent Level	Pressure Vessel Concept		Admission of Atm. Concept	Pressure Regulation Concept		Pressurized Concept	
	Wt. of Titanium Design	Wt. of Light-weight Design	Wt. of Salts	Wt. of Tank & Gas	Dia. of Tank	Internal Pressure	Wt. of Pressure Vessel & Gas
10 atm	14.8 lb.	2.7 lb.	.06 lb.	4.8 lb.	.23 ft.	9.9 atm	3.5 lb.
30	25.6	8.0	1.2	12.3	.33	28.9	9.7
100	46.4	25.3	13.9	38.8	.49	89.	26.2
300	81.0	43.8	79.5	118.	.72	233.	57.6
1000	181.0	104.	433.	439.	1.1	500.	123.

and the integration of the tank (see tank dimensions also given in Table 8-18) that the pressure vessel concept will yield lighter weights and result in a simpler system concept. It should be added that the presence of the mass of gas would probably remove the requirement for an internal energy absorption system such as salts. Also the design of pressure seals for experiment parts and windows will be eased since the internal and external pressure is equalized.

The third and last concept is termed the pressurized concept. In this approach, the payload container is pressurized such that thickness of titanium required to resist the tensile load induced by the vacuum of space (due to one atm internal pressure) is equal to the thickness required to resist the buckling loads induced by the atmospheric descent. A factor of safety of two is used to account for launch range safety requirements. It can be seen from Table 8-18 that only at the low atmospheric descent pressure levels, is there a weight advantage. As before, account must be taken of pressure sensitive components, since they will be exposed to a pressure which is always lower than the local ambient value.

Based on this preliminary assessment, the pressure vessel concept was pursued in the preparation of probe configurations for this study. It is believed that the advantages that might be realized from an in-depth design of an alternative approach will be very small, and thus will not alter the results of this study.

8.11.2 Payload Container Design

The payload container design for containment of the nominal day side science payload and entry into the nominal model atmosphere and descent to the base of the ammonium chloride clouds is given in Section 7.2, and it is indicated that the 20 in. diameter pressure vessel is of monocoque construction and the wall thickness is about .06 in. A MIN-K insulator of about 0.3 in. envelops the exterior of the vessel. MIN-K is selected because of its low thermal conductivity, and because this material when exposed to high temperature will not outgas with possible contamination of the ingested atmospheric samples.

The payload container is filled with sulfur hexaflouride molecular weight of 146. This gas inhibits the voltage breakdown of components, such as the accelerator for the mass spectrometer which operates at high voltage. Sulfur hexaflouride also has a very high convective heat transfer coefficient that promotes the distribution of energy away from heat sources such as the

transmitter, and so prevents local hot spots. Air or nitrogen gas could be used as a filler but are not as effective in resisting voltage breakdown and transporting energy as sulfur hexaflouride. The small disadvantage of sulfur hexaflouride is the greater weight; the mass of gas to fill a 20 in. diameter container (50% volumetric efficiency) to 1 atm at 60 deg F is 0.46 lb whereas the weight of nitrogen gas is 0.09 lb.

It could be argued that if no internal gas was used and that a vacuum was provided that the heat transfer from the inside wall of the pressure vessel to the payload could be reduced. Maintenance of this vacuum would be difficult since the various components would tend to outgas and form a "thin atmosphere". From the viewpoint of voltage breakdown, Pachen's Law indicates that the likelihood is greatest at a low pressure rather than for near vacuum or very high pressure.

The reference design is based on application of the insulator on the outside of the pressure vessel. This results in the possible use of the heat sink capacity of the pressure vessel to soak up internally dissipated energy. Use of an external insulator also results in a lower operating temperature for the pressure vessel. Also since the pressure vessel temperature tends to be low (like the payload temperature) the mechanical design problems caused by differences in thermal expansion coefficients between the science experiment feed through and the pressure are reduced. It was found that the performance of the MIN-K insulator is sensitive to temperature, pressure, and gas composition. If the insulator was placed inside the pressure vessel, the vessel diameter would have to be made larger (for the same internal volume) but the thickness would be reduced since the thermal conductivity would be higher due to the reduced pressure and increased molecular weight. There probably exists an optimum split in the division of internal and external insulator.

8.12 REFERENCES

1. Ultraviolet and Microwave Horizon Sensor Satellite Experiment, Final Report, Avco Systems Division, AVSD-0103-70-RR, March 1970.

2. JPL Section Document 131-12, "Forebody Heat Shield Weight Estimates for Jupiter Entry, June 5, 1970.

3. Tauber, M. E., and Wakefield, R. M., Heating Environment and Protection During Jupiter Entry, AIAA Preprint 70-1234, 1970 October 21.

4. Wilson, K. H., Massive Blowing Effects on Viscous, Radiating Stagnation Point Flow, AIAA 8th Aerospace Science Meeting, New York, January 1970, AIAA Paper No. 70-203.

5. Planetary Explorer Universal Bus Study, Final Report, Avco Systems Division, AVSD-0503-70-RR, October 1970.

9.0 PROBE DEPLOYMENT AND ENTRY TRAJECTORY TRADEOFFS

This section discusses the influence of the various separation parameters on the entry parameters, defines the probe separation requirements and spacecraft targeting to optimize the relay link geometry, and finally, addresses the influence of atmosphere, probe $m/C_D A$ on probe skip angle and descent time requirements.

9.1 PROBE DEPLOYMENT ANALYSIS

A parametric probe deployment analysis study was performed to define the influence of entry angle, lead time, approach velocity, deployment range, and spacecraft periapsis radius on the separation and entry parameters. In this analysis the sensitivity of each parameter was analyzed by varying one parameter at a time and holding all other parameters fixed at a nominal value. The effect of entry angle on the separation and entry parameters is presented in Table 9-1 where the entry angle was allowed to vary between -10 degrees and -150 degrees where entry angles greater than -90 degrees indicate retrograde motion. These results indicate that the magnitude of the separation velocity and the angle-of-attack at entry (probe spin stabilized in deployment attitude) tend to increase proportionally with entry angle, whereas the thrust application angle is relatively insensitive to variations in entry angle in that it only varies between 89 and 100 degrees for entry angle variations between -10 and -150 degrees. The probe spacecraft communication range at probe entry, the probe spacecraft communication angle (which is the angle from the probe longitudinal axis to the spacecraft) and the entry angle dispersion all have minimums for entry angles in the vicinity of -60 to -90 degrees. In this analysis the one sigma entry angle dispersion arises from one sigma errors of 1% in separation velocity, 1 degree in thrust application angle, and a 2000 km spherically distributed position uncertainty relative to Jupiter at separation.

The major influence of lead time on the separation and entry parameters as illustrated in Table 9-2 is in the reduction in the thrust application angle, angle-of-attack, and the significant increase in the probe/spacecraft communication range at entry for increases in the lead time.

The influence of approach velocity on the separation and entry parameters is presented in Table 9-3 and illustrates that as the approach velocity increases there is a slight increase in the probe/spacecraft communication angle at entry, however, the most significant variation is in the reduction in the time from separation to entry where the reduction in flight time is almost inversely proportional to the increase in the approach velocity.

TABLE 9-1

INFLUENCE OF ENTRY ANGLE ON SEPARATION AND ENTRY PARAMETERS

V_∞ = 10 Km/sec

R_0 = 45 x 10^6 Km

L.T. = 2 Hrs.

R_p = 144000 Km

INERTIAL ENTRY ANGLE (deg)	SEPARATION VELOCITY (m/sec)	THRUST APPLICATION ANGLE (deg)	ANGLE-OF-ATTACK AT ENTRY (deg)	COMMUNICATION PARAMETERS		1σ ENTRY ANGLE DISPERSION (deg)
				RANGE (10^3 Km)	ANGLE (deg)	
-10	43	89	25	240	32	2.3
-30	54	95	43	199	33	0.9
-60	90	100	66	191	19	0.7
-90	138	98	87	244	9	0.9
-120	186	95	106	302	11	1.3
-150	221	92	130	328	18	2.8

TABLE 9-2

EFFECT OF LEAD TIME ON SEPARATION AND ENTRY PARAMETERS

γ_E = -30 Deg

V_{∞} = 10 Km/Deg

R_o = 45 x 10^6 Km

R_p = 144000 Km

LEAD TIME (hrs)	DEPLOYMENT VELOCITY (m/sec)	THRUST APPLICATION ANGLE (deg)	ANGLE-OF-ATTACK AT ENTRY (deg)	COMMUNICATION PARAMETERS	
				RANGE (10^3 km)	ANGLE (deg)
0	59	115	63	110	69
2	54	95	43	199	33
4	56	74	23	383	34
6	65	57	5	548	75
8	78	46	7	699	18

TABLE 9-3

EFFECT OF APPROACH VELOCITY ON SEPARATION AND ENTRY PARAMETERS

γ_E = -30 Deg

L.T. = 2 Hrs.

R_p = 144000 Km

R_o = 45 x 10^6 Km

APPROACH VELOCITY (km/sec)	TIME FROM SEPARATION TO ENTRY (days)	DEPLOYMENT VELOCITY (m/sec)	THRUST APPLICATION ANGLE (deg)	COMMUNICATION ANGLE (deg)
5	81	53	101	25
7	63	53	99	29
10	47	54	95	33
15	33	58	82	32

The influence of separation range on the separation and entry parameters presented in Table 9-4 indicates that the selection of the separation range only affects the magnitude of the separation velocity and the time from separation to entry. The magnitude of the separation velocity is inversely proportional and the time from separation to entry varies proportionally with change in the separation range.

The effect of the periapsis radius on the separation and entry parameters is presented in Table 9-5 and illustrates that all parameters with the exception of probe/spacecraft communication angle show significant increase as the spacecraft periapsis radius is increased with the most significant increases being in the areas of deployment velocity, probe/spacecraft communication range and entry angle dispersion.

In Reference 1 there is reported the encounter targeting study data from which data was extracted to form Tables 9-1 through 9-5. Based upon this preliminary analysis the following conclusions are:

1. For shallow entry angles, short lead times and low spacecraft periapsis radii the separation range only affects the magnitude of the separation velocity. A separation velocity of about 50 mps is required for a separation range of 45 million kilometers from Jupiter. If it proves desirable to improve the knowledge of the planetocentric orbit parameters prior to the probe release, then 25 days of tracking time can be provided by decreasing the separation range to 22.5 million kilometers at the expense of an additional 50 mps in the probe separation velocity.

2. Consistent with angle centering the spacecraft within the probe antenna beam during the terminal descent portion of the mission the shortest possible values of probe lead time coupled with the lowest feasible value of the spacecraft periapsis radius should be employed to minimize the probe spacecraft relay link communication range.

9.2 PROBE DISPERSION ANALYSIS

A parametric probe dispersion analysis was conducted to define the influence of the separation parameters and perturbations in these parameters on dispersion in the probe entry angle, entry location, and entry time. In this preliminary analysis the following one sigma error sources were employed: 1) spherically distributed position error of 2000 km; 2) spacecraft pointing accuracy of 0.5 deg; and 3) propulsion system accuracy of 0.33 percent (of total applied impulse), to define the magnitude of the contribution from each

TABLE 9-4

EFFECT OF DEPLOYMENT RANGE ON SEPARATION AND ENTRY PARAMETERS

γ_E = -30 Deg

V_{oo} = 10 Km/sec

L.T. = 2 hrs.

R_p = 144000 Km

SEPARATION RANGE (10^6 km)	TIME FROM SEPARATION TO ENTRY (days)	DEPLOYMENT VELOCITY (m/sec)
15	14.1	162
30	30.5	81
45	47.3	54
60	64.3	41

TABLE 9-5

EFFECT OF PERIAPSIS RADIUS ON SEPARATION AND ENTRY PARAMETERS

γ_E = -30 Deg

R_o = 45 x 10^6 Km

V_{oo} = 10 Km/sec

L.T. = 2 hrs.

SPACECRAFT PERIAPSIS RADIUS (Jupiter Radii)	DEPLOYMENT VELOCITY (m/sec)	THRUST APPLICATION ANGLE (deg)	ANGLE-OF-ATTACK AT ENTRY (deg)	COMMUNICATION PARAMETERS RANGE (10^3 km)	ANGLE (deg)	1σ ENTRY ANGLE DISPERSIONS (deg)
1	18	45	7	236	14	0.6
1.5	35	84	32	210	37	0.7
2.0	54	95	43	199	33	0.9
3.0	90	104	52	214	17	1.3
5.0	151	111	59	316	1	2.1
10.0	279	116	64	653	3	4.1

error source and hence to define where efforts should be applied to improve the hardware capability. In this analysis a coordinate system was established with the X-axis along the hyperbolic approach velocity vector, the Y-axis normal to the hyperbolic approach velocity vector in the trajectory plane and the Z-axis normal to both the hyperbolic approach velocity vector and the trajectory plane completing the right hand orthogonal triad. The results of this analysis are presented in Tables 9-6 to 9-8 for selected values of entry angle, lead time, and spacecraft periapsis radius in terms of the individual contributions and the root-sum-square uncertainty. (In Reference 2-II there is reported the influence of periapsis radius, lead time, separation range, and approach velocity on the dispersion in entry angle). In this analysis a fixed deployment range of 45×10^6 km was employed along with a hyperbolic approach velocity of 7 km/sec.

The entry angle dispersion analysis presented in Table 9-6 illustrates that for shallow entry angles (γ_{Erel}) between -15 and -30 degrees , short lead times and low values of the spacecraft periapsis radius the in-plane position uncertainty normal to the approach asymptote is the major contributor to the entry angle dispersion. As the spacecraft periapsis is increased from 1.5 to 3.0 planetary radii the deployment velocity dispersion, in-plane thrust application dispersion, and the in-plane position uncertainty normal to the approach velocity vector are all essentially equal contributors to the entry angle dispersion.

Similar results are evident in the entry location dispersion analysis presented in Table 9-7 with the exception that the total undertainty in entry position is approximately twice as large as the entry angle uncertainty.

The entry time dispersion analysis presented in Table 9-8 shows that this dispersion is essentially independent of lead time and entry angle and strongly dependent upon the spacecraft periapsis radius. The primary contributors to this dispersion are the position uncertainty along the approach velocity vector and the uncertainty in the in-plane thrust application angle. For low values of spacecraft periapsis, the position uncertainty is the largest contributor and is basically just a function of the position uncertainty and the hyperbolic approach velocity, whereas, when the spacecraft periapsis radius is raised to 3.0 Jupiter radii, the in-plane thrust application angle uncertainty becomes, by far, the predominant error source and is almost a factor of 2 larger than the position uncertainty. The contribution of in-plane thrust application angle uncertainty to entry time variations is non-linear with respect to periapsis radius in that the contribution increases by a factor of approximately 3 as the spacecraft periapsis radius is doubled.

TABLE 9-6

1σ ENTRY ANGLE DISPERSION ANALYSES

Contributor	Error Source	$\gamma_E = -15°$				$\gamma_E = -30°$			
		LT = 0		LT = 1		LT = 0		LT = 1	
		$r_p = 1.5$	$r_p = 3.0$	$r_p = 1.5$	$r_p = 3.0$	$r_p = 1.5$	$r_p = 3.0$	$r_p = 1.5$	$r_p = 3.0$
Deployment Velocity Dispersion	0.33%	-0.22	-0.69	-0.22	-0.69	-0.15	-03.9	-0.15	-0.39
In-Plane Pointing	0.5°	-0.20	-0.71	-0.07	-0.57	-0.14	-0.39	-0.06	-0.32
Out-of-Plane Pointing	0.5°	0.00	0.00	0.00	0.00	0.00	0.00	0.00	0.00
In-Plane Position along V_∞	2000km	0.10	0.01	0.01	0.01	0.01	0.01	0.01	0.01
In-Plane Position normal to V_∞	2000km	0.93	0.93	0.93	0.93	0.48	0.48	0.48	0.48
Out-of-plane Position Normal to V_∞	2000km	0.00	0.00	0.00	0.00	0.00	0.00	0.00	0.00
$\Delta\gamma_E$ (deg)		0.98	1.35	0.96	1.29	0.52	0.73	0.50	0.69

TABLE 9-7

1σ ENTRY POSITION DISPERSION ANALYSIS

Contributor	Error Source	$\gamma_E = -15°$ LT=0 r_p=1.5	LT=0 r_p=3.0	LT=1 r_p=1.5	LT=1 r_p=3.0	$\gamma_E = -30°$ LT=0 r_p=1.5	LT=0 r_p=3.0	LT=1 r_p=1.5	LT=1 r_p=3.0
Deployment Velocity Dispersion	0.33%	-0.43	-1.33	-0.43	-1.33	-0.27	-0.73	-0.27	-0.73
In-Plane Pointing	0.5°	-0.39	-1.36	-0.13	-1.09	-0.26	-0.74	-0.12	-0.61
Out-of-Plane Pointing	0.5°	0.00	0.00	0.00	0.00	0.00	0.00	0.00	0.00
In-Plane Position along V_∞	2000km	0.02	0.02	0.02	0.02	0.01	0.01	0.01	0.01
In-Plane Position Normal to V_∞	2000km	1.79	1.78	1.79	1.79	0.90	0.90	0.90	0.90
Out-of-Plane Position Normal to V_{00}	2000km	0.00	0.00	0.00	0.00	0.00	0.00	0.00	0.00
$\Delta\phi_E$(deg)		1.88	2.61	1.84	2.48	0.98	1.37	0.95	1.31

TABLE 9-8

IV ENTRY TIME DISPERSION ANALYSIS

Contributor	Error Source	$\gamma_E = -15°$				$\gamma_E = -30°$			
		LT=0		LT=1		LT=0		LT=1	
		r_p=1.5	r_p=3.0	r_p=1.5	r_p=3.0	r_p=1.5	r_p=3.0	r_p=1.5	r_p=3.0
Deployment Velocity Dispersion	0.33%	-5	-10	-17	-22	2	10	-10	-2
In-Plane Pointing	0.5°	-151	-482	-137	-467	-185	-502	-174	-491
Out-of-plane Pointing	0.5°	0	0	0	0	0	0	0	0
In-plane position along V_∞	2000km	261	262	261	262	261	262	261	262
In-plane position normal to V_∞	2000km	97	97	97	97	71	71	71	71
Out-of-plane Position normal to V_∞	2000km	0	0	0	0	0	0	0	0
Δt_E (sec)		317	557	311	545	328	571	322	561

While upon initial consideration, the entry time dispersion may seem to be a relatively insignificant parameter it can be as important, if not more so, than either the entry angle or entry position dispersion with respect to the design of the relay link telecommunication system in that it directly affects the spacecraft location with respect to the probe at probe entry.

In summary it has been shown that for a spacecraft periapsis radius of 1.5 Jupiter radii: 1) the in-plane position uncertainty along the approach velocity vector is the major contributor to entry time dispersion, and 2) the in-plane position uncertainty normal to the approach velocity is the major contributor to entry angle and entry position uncertainty. Hence the entry dispersions can be significantly reduced with improvements in the space-craft position uncertainty with respect to Jupiter at the time of probe deployment. For a spacecraft periapsis radius of 3.0 the magnitude and direction uncertainty of the deployment velocity in addition to the in-plane position uncertainty normal to the approach velocity all contribute about equally to the entry angle and entry position uncertainty and hence significant improvements in these dispersions cannot be expected unless there are reductions in all three error sources.

9.3 TARGETING REQUIREMENTS TO OPTIMIZE RELAY LINK GEOMETRY

In addition to the science and engineering considerations which constrain the entry location and entry angle respectively, the relay link geometry requirements must also be considered in the specification of the probe deployment conditions and the spacecraft periapsis radius. To establish a relay link with optimum performance it is mandatory to partially, or totally, synchronize the rotation rates of the flyby spacecraft with the rotation rate of the probe in the Jovian atmosphere where the extent of synchronization depends upon the duration of the probe mission. With slight variations in the magnitude and direction of the deployment parameters essentially the same entry angle and entry position can be achieved with varying lead time (the time difference between probe entry and spacecraft periapsis passage). These variations in lead time when coupled with varia-tions in the spacecraft periapsis radius can be employed to synchronize the spacecraft and probe angular rates within relatively tight tolerances. The specific lead time and periapsis altitude is dependent upon the probe entry location with respect to approach asymptote since the spacecraft rotation rate about Jupiter is strongly dependent upon its location with respect to periapsis or the approach asymptote.

The desired probe relay link geometry is defined in Figure 9-1. In order
to maintain the spacecraft in the probe antenna beam width during the descent
portion of the mission it is necessary to synchronize both the probe and
spacecraft rotation rates about Jupiter. This synchronization is accomplished
by the proper selection of the probe lead time and the spacecraft periapsis
radius as a function of the probe entry location. The probe lead time -
spacecraft periapsis radius relationship to achieve angle centering during
probe descent is illustrated in Figure 9-2 as a function of probe entry
location for a ZAP argle of 140 degrees. This relationship was also
established for other ZAP angles, and it was found that basically the curves
shift to the left by 1 degree for each degree decrease in ZAP angle, and the
curves shift to the right by 1 degree for each degree increase in the ZAP
angle. For a ZAP angle of 140 degrees (minimum energy 1978 Type I
transfer trajectory) these results indicate that a periapsis radius of 3 Jupiter
radii is required in combination with a 0.5 hr. lead time to achieve the
desired angle centering synchronization for a probe entry location in the
vicinity of the evening terminator. However, a periapsis radius of 1.5 is
required in combination with a 3 hr. probe lead time to achieve the same
angle centering synchronization for probe entry in the vicinity of the sub-solar
point.

9.4 EFFECTS OF JOVIAN ATMOSPHERE VARIATION OF ENTRY PARAMETERS

Three models of the Jovian atmosphere were used to obtain variations in
entry parameters. Table 9-9 defines the atmospheric properties and con-
stant entry parameters used to run the trajectory cases needed.

Skip boundaries were found for a range of ballistic coefficients using both a
constant mass probe and a variable mass probe. Skip is defined as occurring
when the probe flight path angle goes positive. Variable mass cases were
run simulating a mass loss due to ablation of the heat shield. Table 9-10
indicates the skip boundaries determined. As these results show the skip
boundary is independent of mass loss and has only a .2 degree variation
throughout the range of m/C_DA covered. The largest variation, still only
one degree, covered the three atmosphere models used.

Maximum loads in Earth g's were found as a function of atmosphere model,
m/C_DA, and flight path entry angle for constant and variable probe masses.
Mass variation and m/C_DA variation caused less than a ten percent change
in peak G's during entry. Table 9-11 shows tabulations on peak G encountered

FIGURE 9-1

DESIRED RELAY LINK GEOMETRY

ALLOWABLE S/C
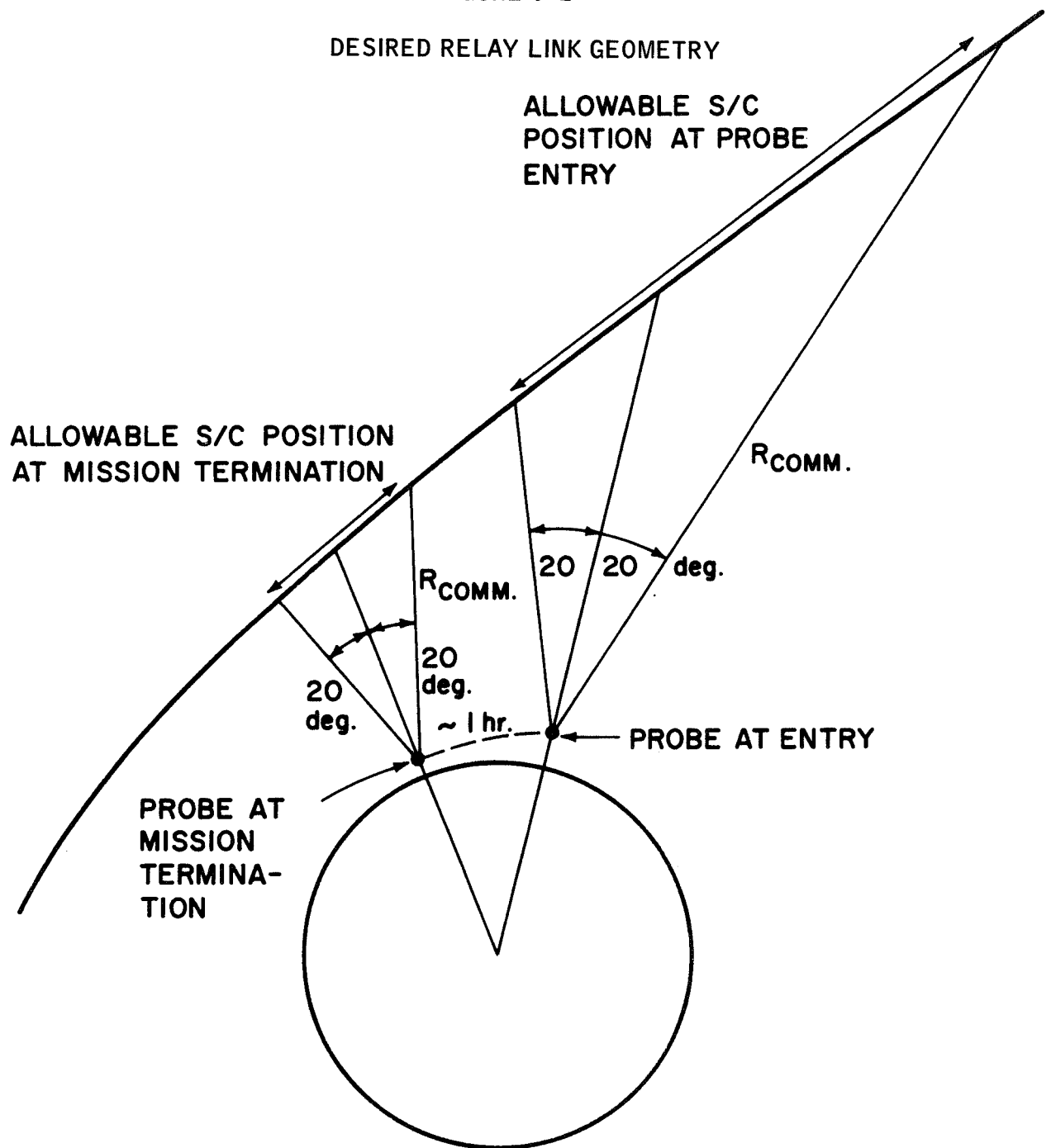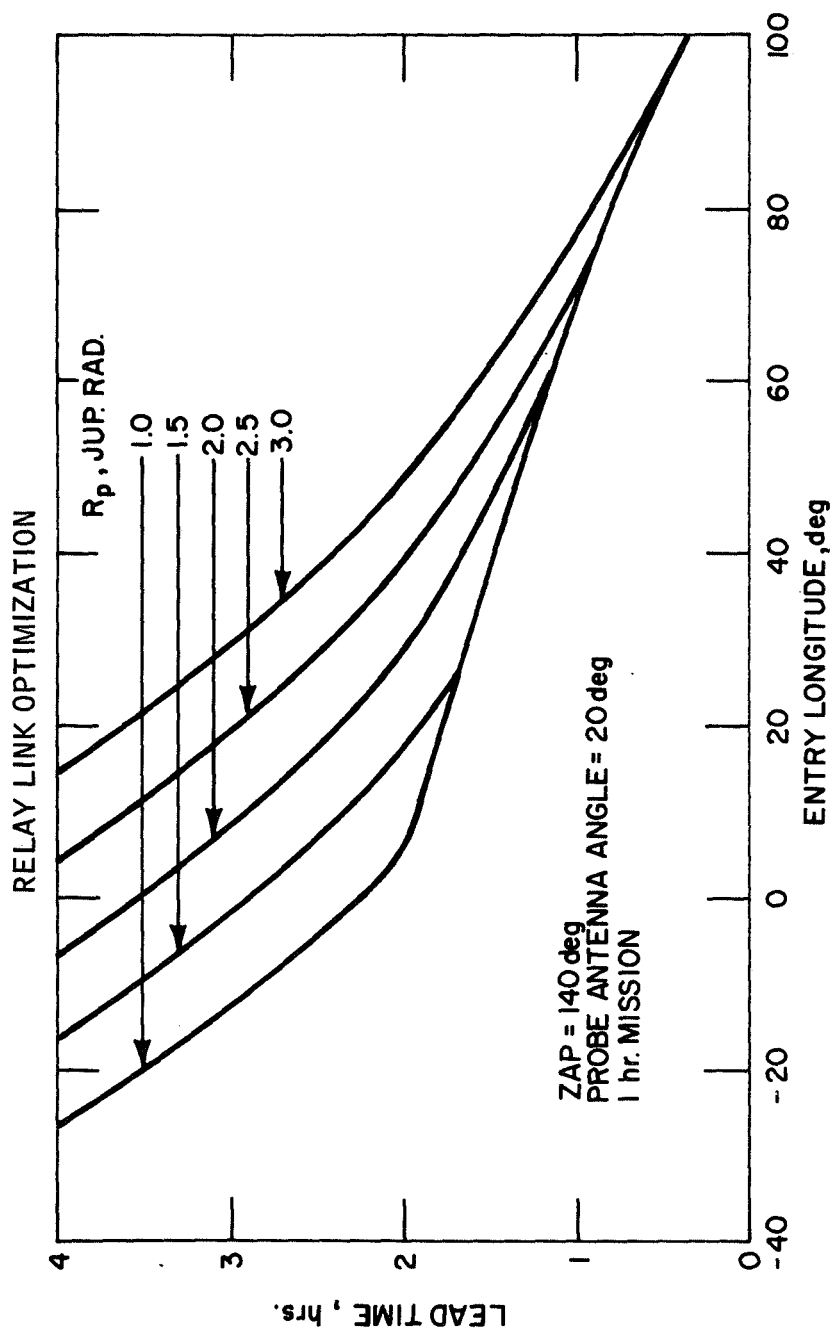POSITION AT PROBE
ENTRY

ALLOWABLE S/C POSITION
AT MISSION TERMINATION

$R_{COMM.}$

$R_{COMM.}$

20 / 20 / deg.

$R_{COMM.}$

20
deg.

20
deg.

~ 1 hr.

PROBE AT ENTRY

PROBE AT
MISSION
TERMINA-
TION

FIGURE 9-2

RELAY LINK OPTIMIZATION

9-15

TABLE 9-9

JOVAIN PHYSICAL PARAMETERS FOR PARTICLE TRAJECTORY ANALYSIS

FROM JPL 131-10

ATM. MODEL	WARM	NOMINAL	COOL
P_o — ATM.	1	1	1
T_o — °K	238	179.4	143.6
ρ_o — g/cm³	1.10×10^{-4}	1.56×10^{-4}	2.29×10^{-4}
Molecular Wt. — g/mole	2.14	2.30	2.70
Troposphere Lapse Rate — °K/KM.	-2.37	-2.07	-1.75
T_{ST} — °K	118	113	108

FROM JPL TR 32-1306

Gravitational Parameter	126707718.8 KM³/SEC²
Planet Radius	71372 KM
Entry Radius	72000 KM
Rotation Rate	1.7734081×10^{-4} RAD/SEC

TABLE 9-10

SKIP BOUNDARY DEFINITION (RELATIVE ENTRY ANGLE)

MASS	INIT M/C_DA	ATMOSPHERE		
		WARM	NOMINAL	COOL
CONSTANT	0.3		-5.8	
"	0.5	-5.4	-6.0	-6.4
"	1.2		-6.0	
VARIABLE	0.3		-5.8	
"	0.5	-5.4	-6.0	-6.4
"	1.2		-6.0	

TABLE 9-11

PEAK ATMOSPHERIC LOADS (EARTH G'S)

$\gamma_{E_{REL}}$ (DEG)	ATMOSPHERE MODEL		
	WARM	NOMINAL	COOL
-15		523	1923
-30	933	1165	
-60		2564	
-90		3734	

9-18

as a function of atmosphere model and $\gamma_{\epsilon rel}$. As shown in the table, higher loads occur during entry into the cool/dense atmosphere and at steeper flight path angles.

It was determined that following deceleration in the upper atmosphere, the entry probe descends at nearly terminal velocity through the Jovian troposphere. An analytical descent time and descent velocity expression was derived based on terminal descent through a constant lapse rate atmosphere. In Figure 9-3 there is shown the variation in descent time for $m/C_D A$ of 1) with pressure. The descent time for any value of ballistic parameters can be obtained by dividing the abscissa by $m/C_D A$. In Figure 9-4 the descent velocity parameter is shown for the three model atmospheres as a function of pressure, and in Figure 9-5 the descent velocity is shown for the three model atmospheres as a function of temperature. Figures 9-6 through 9-10 give pressure, density, and temperatures in the 3 model atmospheres as a function of altitude.

FIGURE 9-3

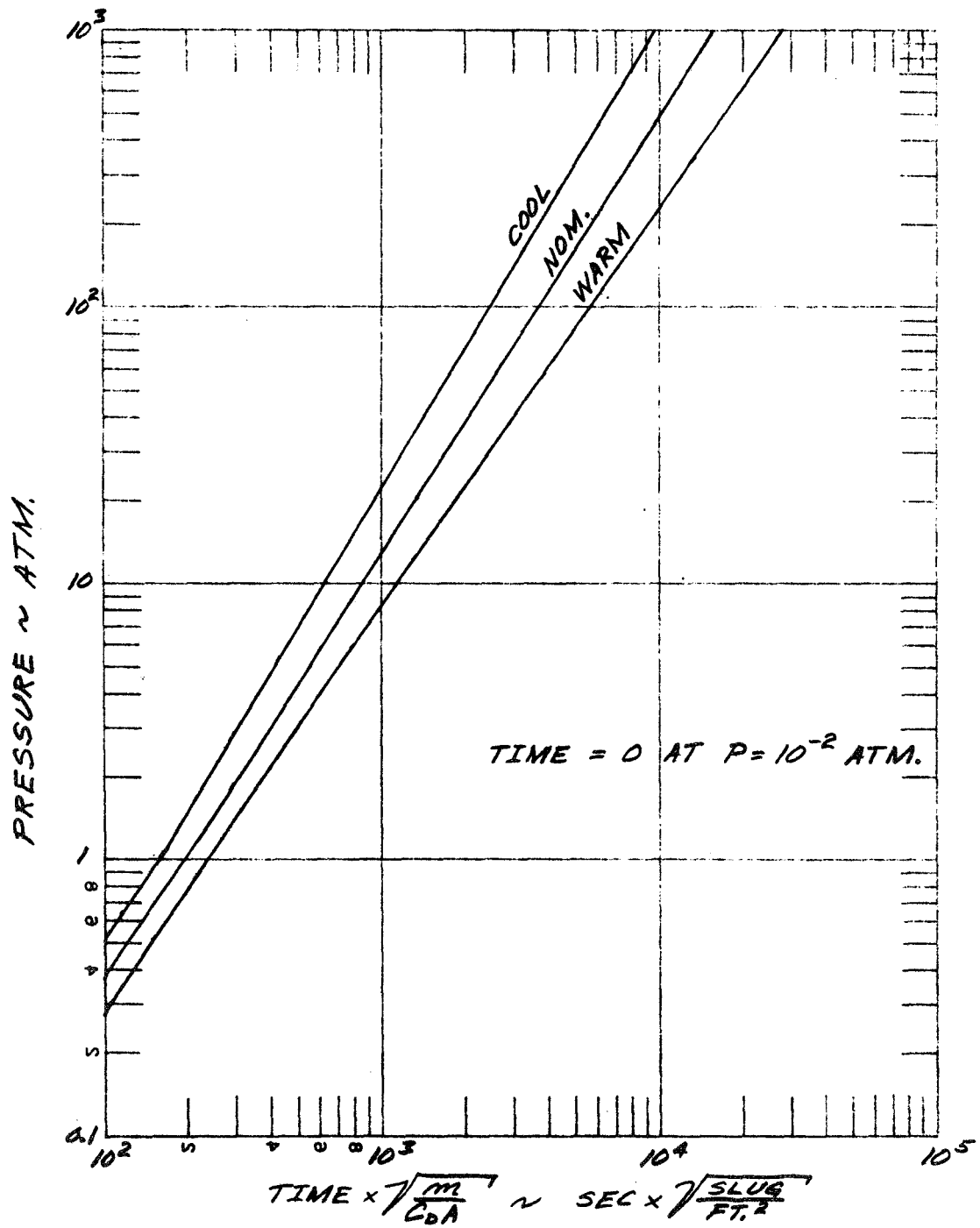## JUPITER DESCENT TIME PARAMETER vs. ATM. PRESSURE

FIGURE 9-4

JUPITER DESCENT VELOCITY PARAMETER vs. PRESSURE
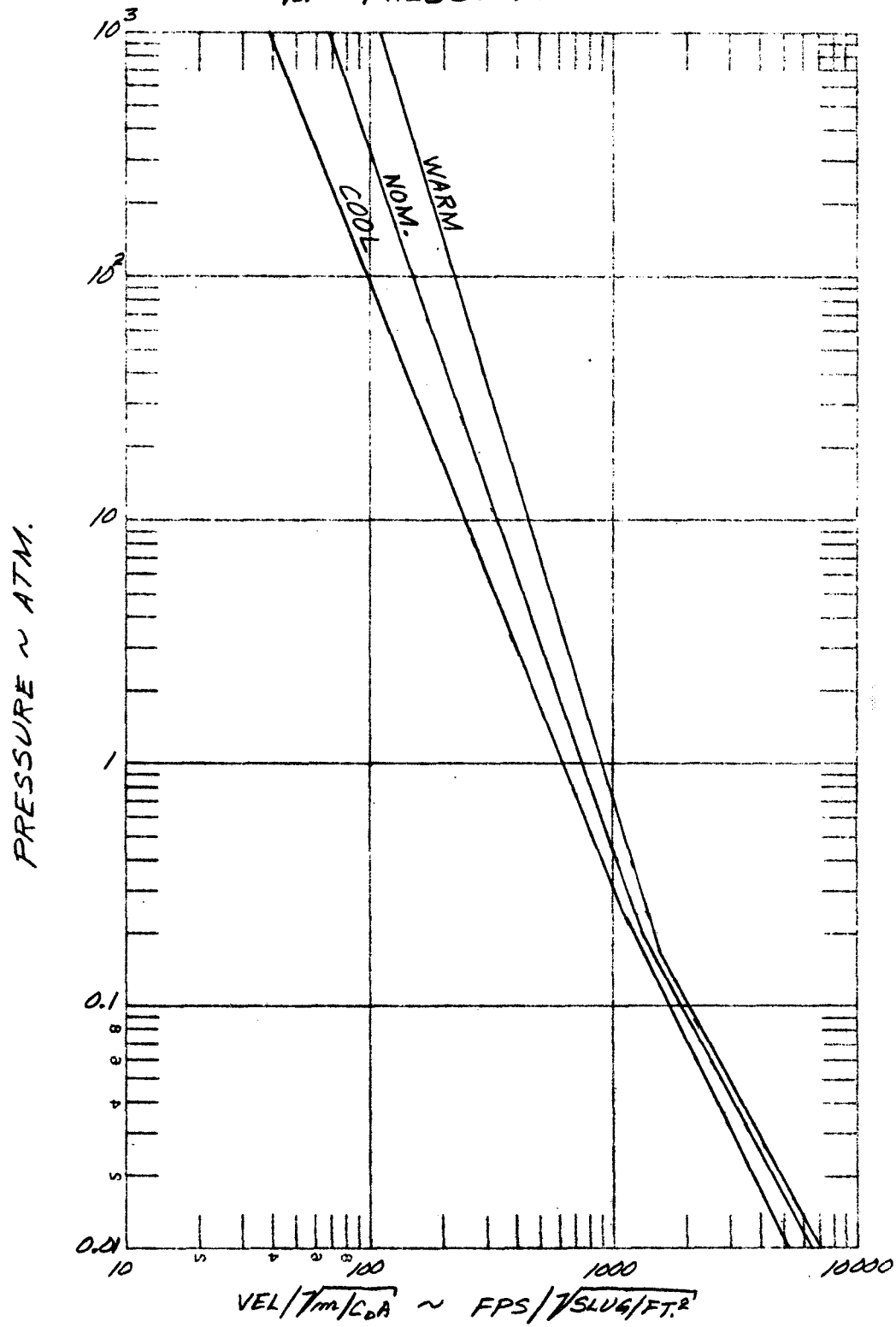
FIGURE 9-5

JUPITER DESCENT TIME PARAMETER vs. TEMPERATURE
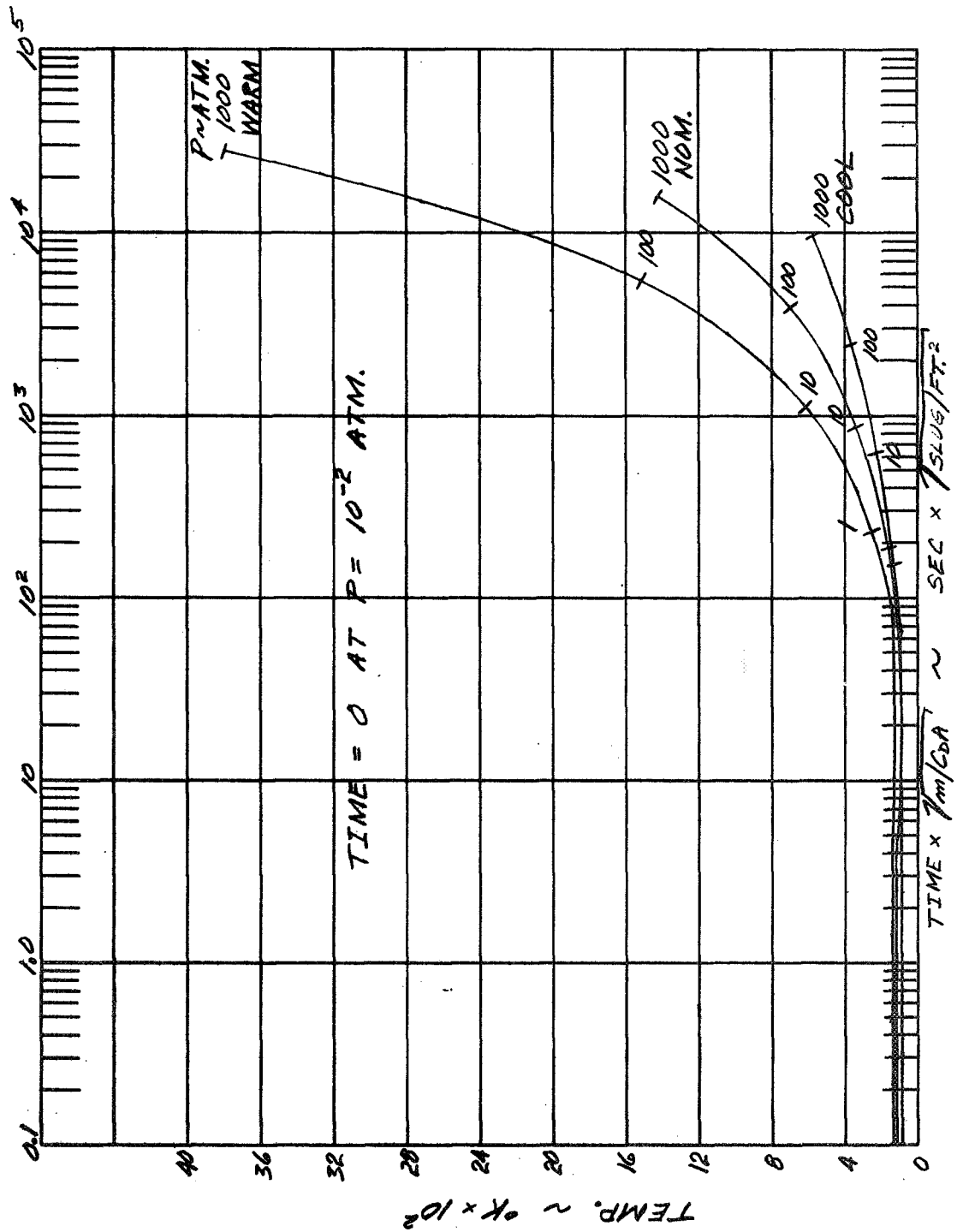
FIGURE 9-6

JUPITER ATMOSPHERE
PRESSURE PROFILE

500,000 TO 2,000,000 FT

COOL   NOM.   WARM
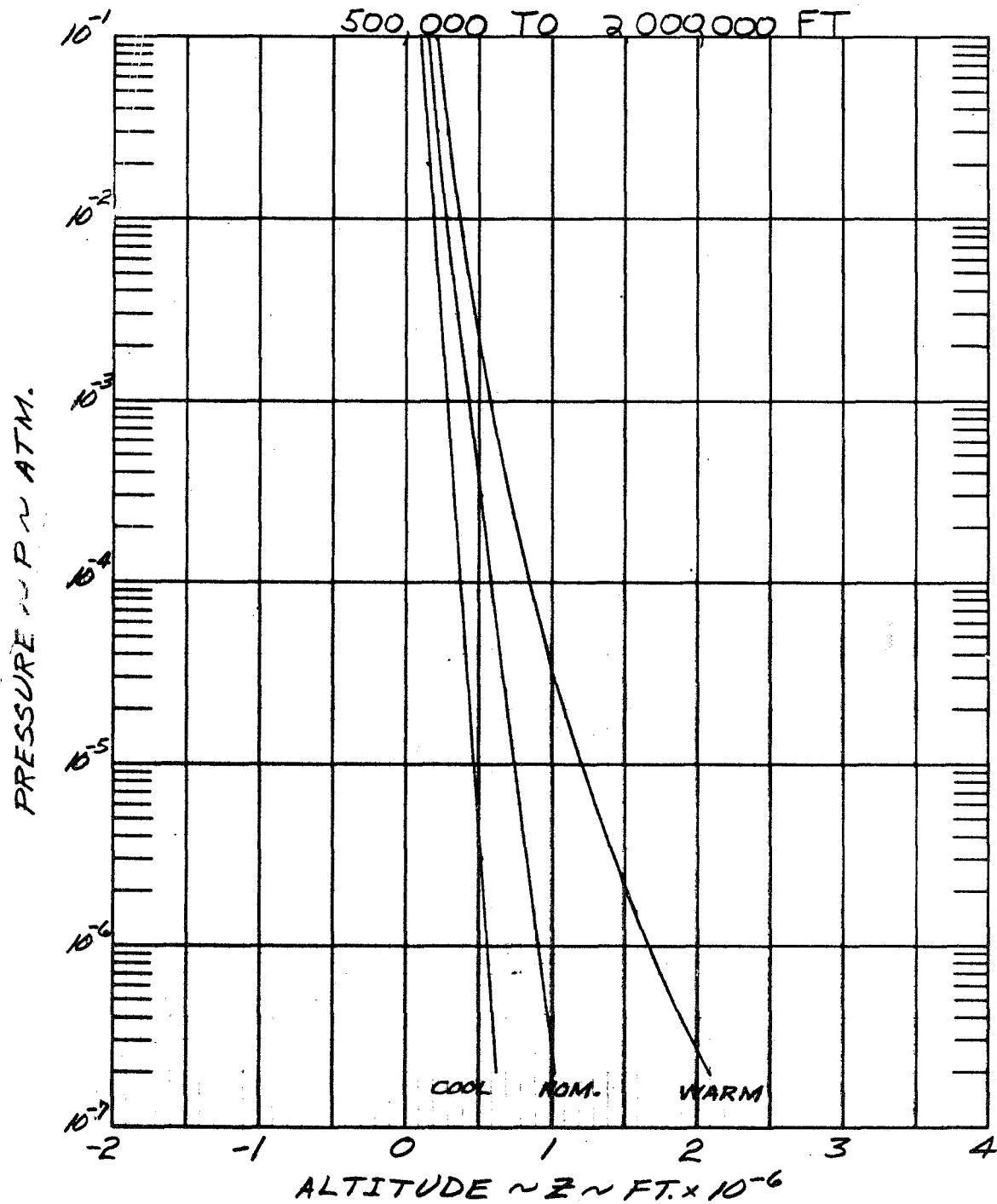
9-23

NOTE: USE TYPE B PENCIL FOR VUGRAPHS AND REPORTS.

FIGURE 9-7

JUPITER ATMOSPHERE
PRESSURE PROFILE
(+ 500,000 TO - 4,000,000 FT)
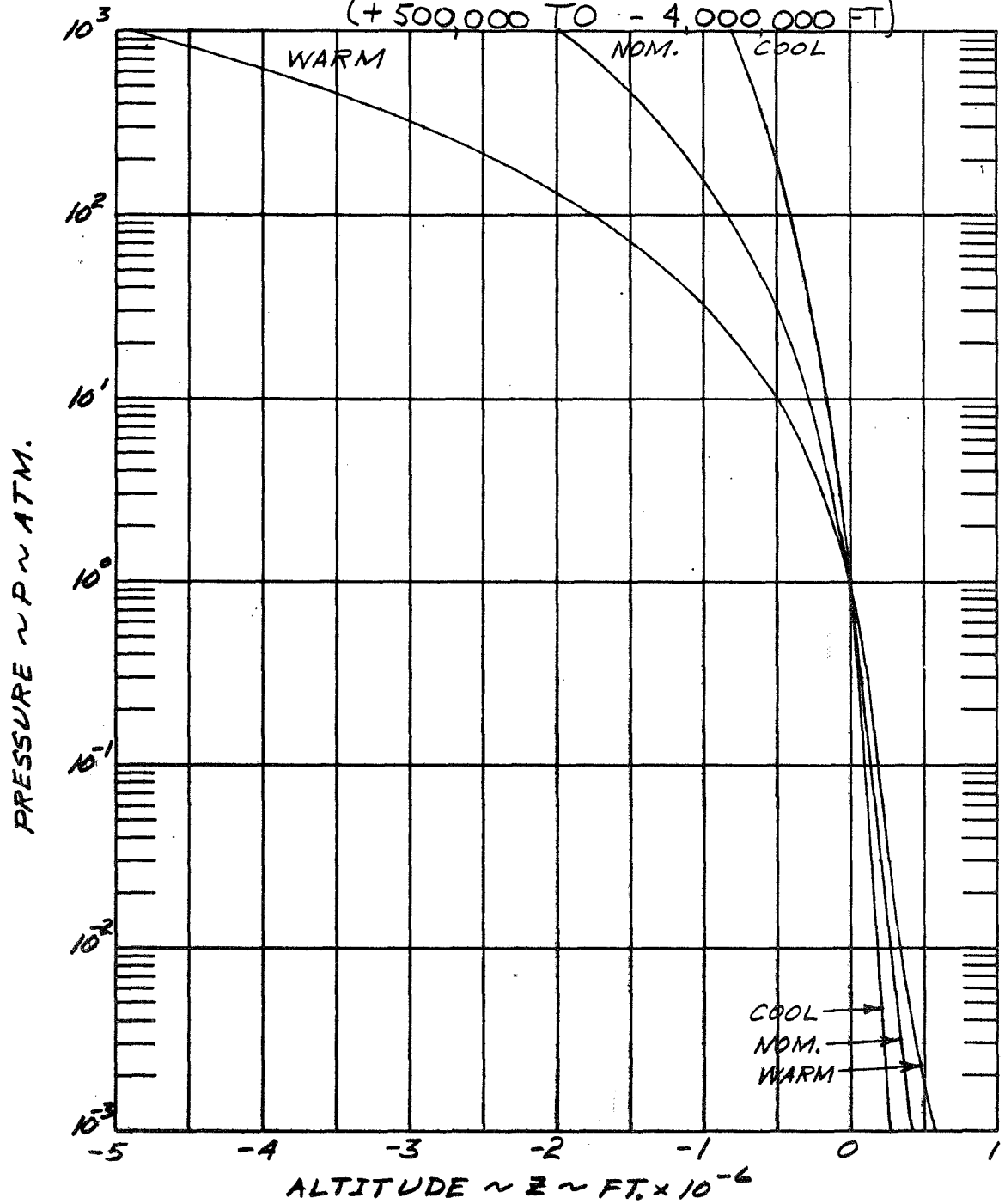
FIGURE 9-8

JUPITER ATMOSPHERE
DENSITY PROFILE
(+2,000,000 TO +500,000 FT)

FIGURE 9-9

JUPITER ATMOSPHERE
DENSITY PROFILE
(+500,000 TO -4,000,000 FT)

FIGURE 9-10

JUPITER ATMOSPHERE
TEMPERATURE PROFILE

9.5 REFERENCES

1. Jovian Encounter Targeting Study, Memo 9-I, Jupiter Atmospheric Entry Probe Study, Section F930, January 1971.

2. Entry Angle Dispersions, Memo 9-II, Jupiter Atmospheric Entry Probe Study, Section F930, January 1971.

10.0 COMMUNICATION SUBSYSTEM TRADEOFFS

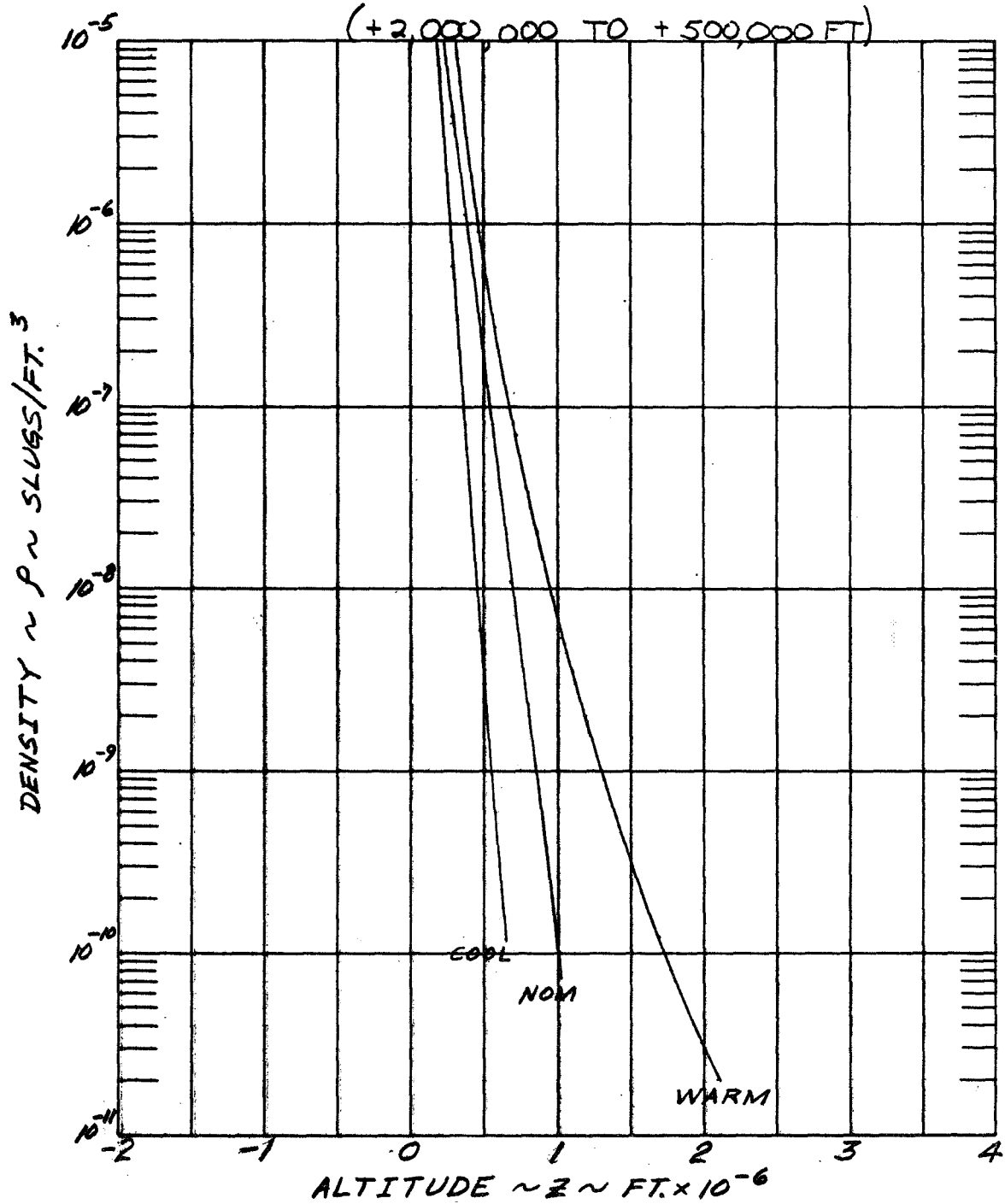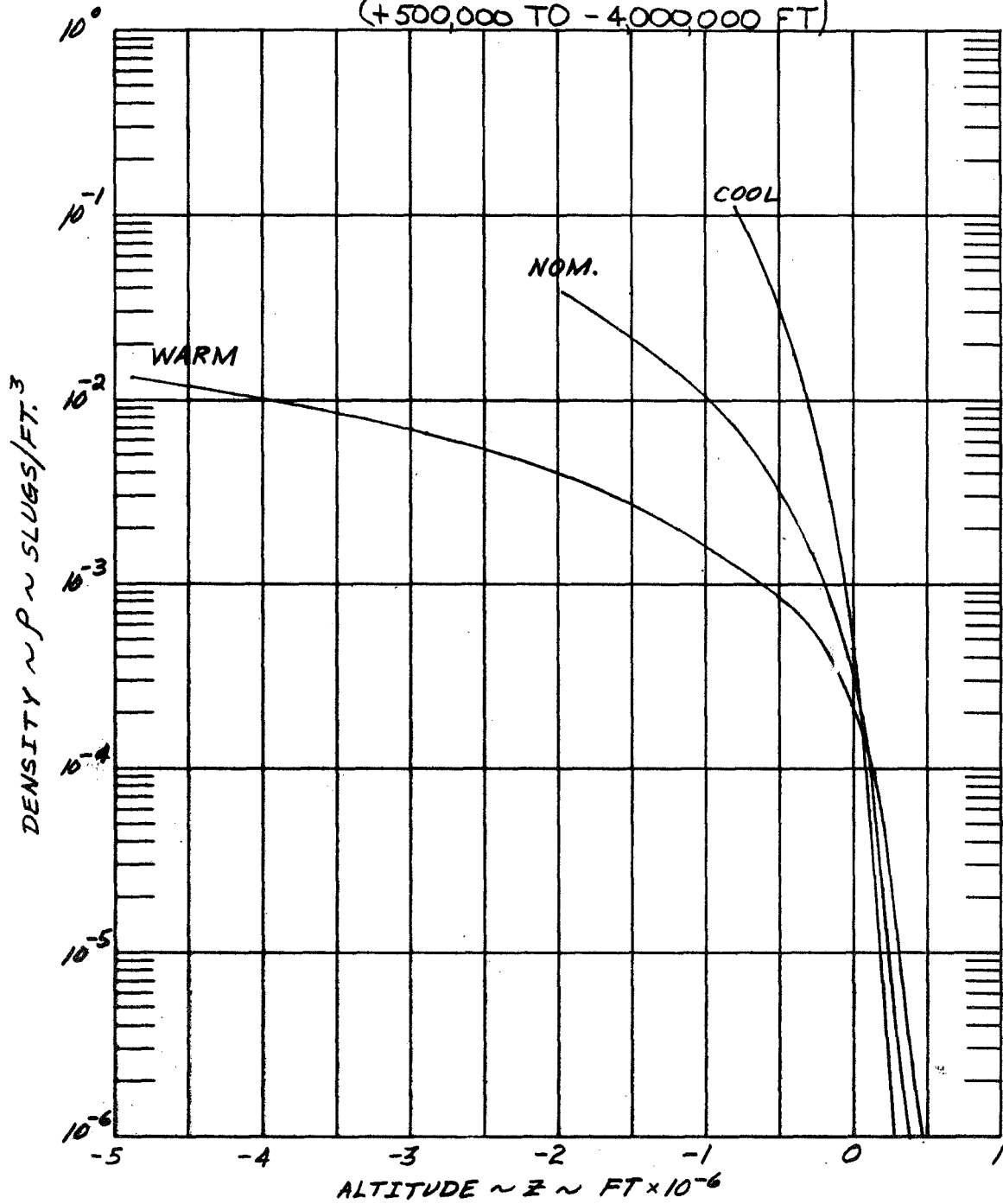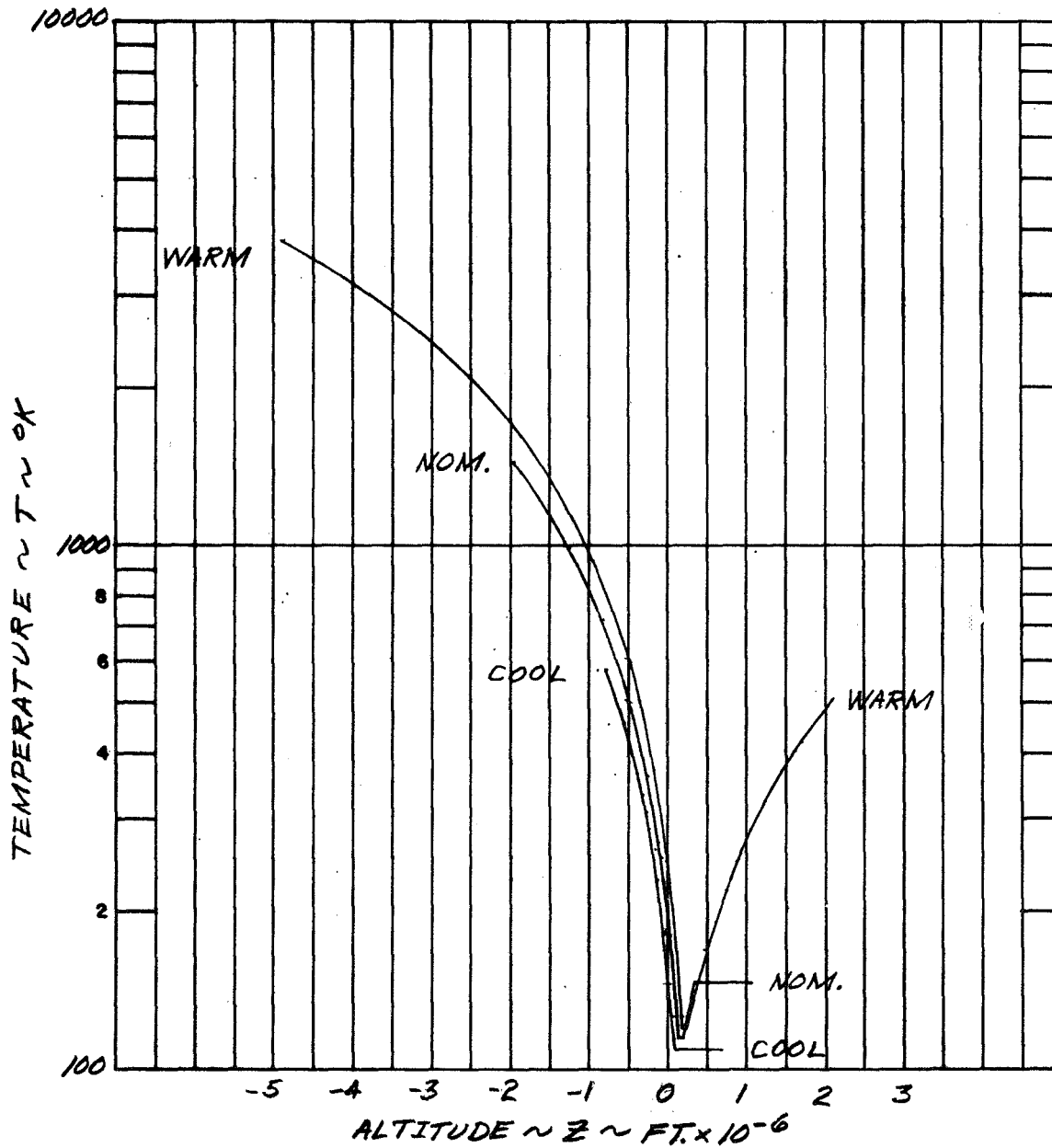This section of the report deals with specific details relative to the communication related subsystem tradeoff studies which were performed in order to arrive at the system performances shown in Section 5.3. Tradeoff and parametric results will be shown only for mission oriented parameters. The various communication link alternatives that are considered include an evaluation of: 1) direct link communication to earth, and 2) relay link communication via either a TOPS or Pioneer F/G spacecraft to earth. Four major study areas will be used to present the details of these two communication link study approaches; the reporting format is broken down into: 1) link assumptions and constraints; 2) link analysis; 3) link performance; and 4) summary and conclusions.

10.1 DIRECT LINK STUDIES

10.1.1 Introduction

The major direct link study elements and their interrelationship is summarized in Figure 10-1. A summary paragraph on each of these items follows

Frequency Selection - The frequency comparison task consists of selecting from the two available DSN frequencies, the more favorable. These results are reported upon in Reference 1.

Contact Analysis - The direct link geometry tradeoffs associated with probe targeting and descent time selection represents a significant tradeoff analysis area. These results will be presented in the following sections of this report.

Antenna Aperture Size/Gain Tradeoffs - A detailed tradeoff study in this area was not conducted. Typically the maximum allowable aperture was assumed for the antenna and for a given operating frequency and beamwidth requirement an antenna concept was selected. Section 8.6.1 reports on these antenna studies.

Link Losses - The link losses represent a summation of all the link dependent performance factors. The output of this task establishes the signal strength available at a particular receiving site. A computer program titled Direct Link Received Power Calculations was written in support of this task and is reported upon in Reference 2.

FIGURE 10-1

DIRECT LINK COMMUNICATION ANALYSIS
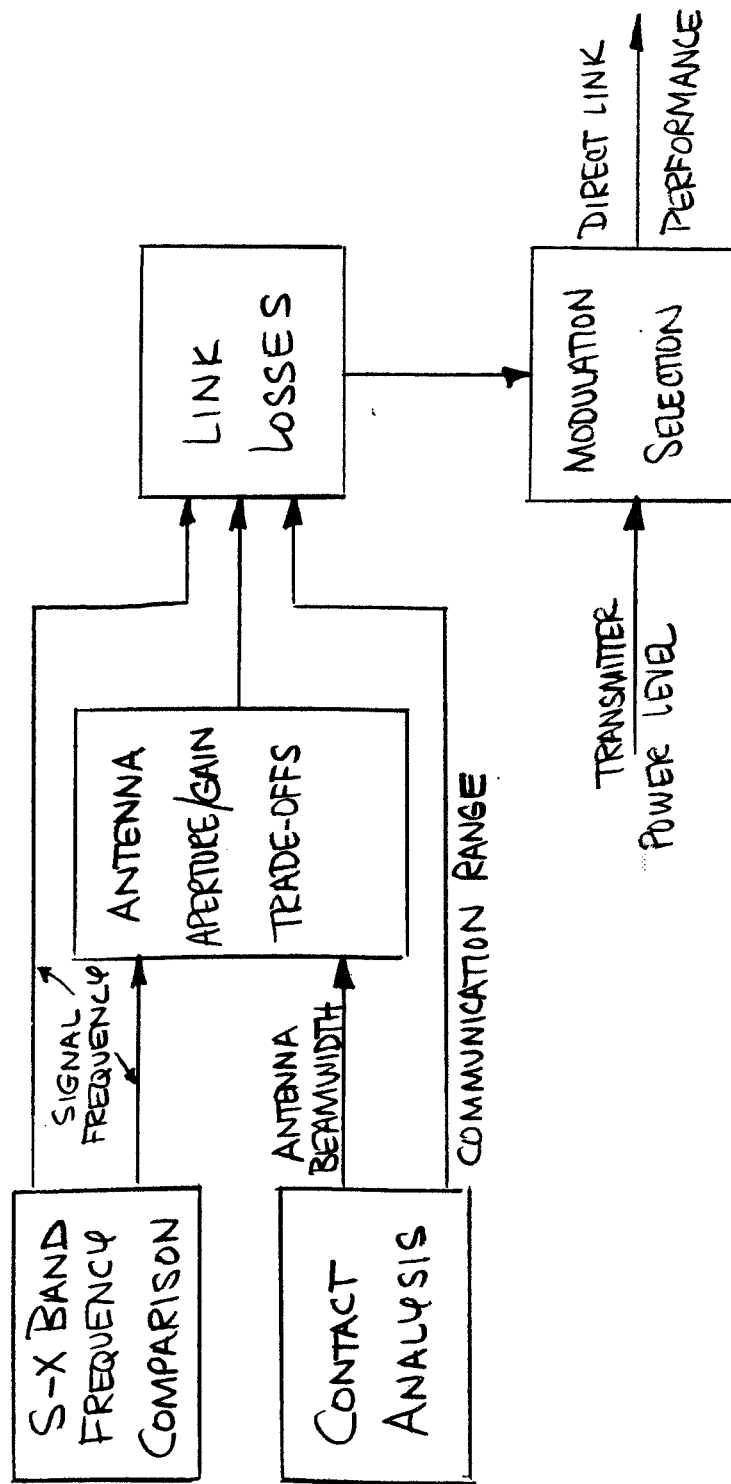
Modulation Selection and Performance Estimates - Selection of the optimum modulation scheme and concomitant link performance is the objective of this task. The modulation tradeoff analysis is included in Reference 3 and the link performance is presented in Section 10. 1. 3.

These five tasks represent the major study elements associated with the analysis of a direct link. This section, however, will be written so as to extract the conclusions from these tasks and apply the results to develop the overall direct link communication capability.

10. 1. 2 Assumptions and Constraints

The major link assumptions and constraints of this analysis can be basically identified as three major elements; the receiving system, the space link, and the probe transmission system.

Receiving System - The assumed ground rules for the Deep Space Network (DSN) are based on three different transmit/receive operating modes. These three operating modes are consistent with both probe and spacecraft up and downlink support requirements from the DSN. These link requirements are: 1) transmit S/receive S and X-band to cover the mission where tracking and T/M from the TOPS spacecraft are required within the same time frame as the probe descent phase; 2) transmit S/receive S to cover the mission where tracking from the Pioneer spacecraft is required; and 3) receive S only for missions where spacecraft link requirements can be suspended during the probe descent phase.

Table 10-1 summarizes for each of the three operating modes the pertinent link characteristics associated with the receiving system aspect of the link. The difference between the receive S only mode and the receive S/X mode amounts to some 2. 1 db. The implication of this factor is considered significant and the impact on link performance will be shown in later sections.

The carrier loop bandwidth assumed in this analysis is 1 Hz which is consistent with 1975 developments. The 9 db threshold SNR for the carrier channel is selected so as to preclude the consideration for radio noise in the data channel. Data rate is a variable in this analysis, however, a minimum value of 6 bps is established in order to be consistent with bit synchronizer requirements. The signal energy/bit/noise spectral density ratio for this modulation scheme is established at 1. 5 db based on results discussed in Reference 3. The value 1. 5 db of other data channel losses shown in

Table 10-1 DSN Operational Characteristics

Characteristic	Transmit → Receive →	DSN Operational Modes		
		S S/X	S S	--- S
Antenna Gain		60.8 dB	61.4 dB	61.4 dB
System Noise Temperature *		31°K	26°K	22°K
Carrier Loop BW		← 1 Hz →		
Carrier SNR		← 9 dB →		
Data Rate		← VARIABLE (MIN. 6bps) →		
Data Channel E/N₀		← 1.5 dB →		
Other Data Channel Losses		← 1.5 dB →		
Net Adverse Tolerance		← 2.2 dB →		

* Includes 4° K for Jupiter Noise ; Antenna Elevation Angle = 45°

Table 10-1 are further broken down in Table 10-2. Tolerance values on each of the receiving system parameters is summarized in Table 10-3; the linear sum of these adverse tolerances is shown to be 2.2 db.

The Space Link - This subsection will assess the impact of those parameters external to both the receiving and transmission system. These space link related items are: 1) the communication range; 2) the sub-earth vector location; and 3) the atmospheric losses.

The communication range between earth and Jupiter varies from 650 MKM to 950 MKM. In the interest of maximizing link performance, it becomes apparent that arrival date selections must be made consistent with minimum communication ranges. This, however, does not represent the sole criterion for arrival date selection since the sub-earth vector locations must also be considered. The effect of the sub-earth vector location manifests itself in the following way.

Based on a requirement to target the probe to a position about the sub-earth vector, the probe entry longitude can vary about 20° (sub-earth vector variation is $\pm$ 10 deg about sub-solar with the positive towards the evening terminator). Since probe entry angles are minimized as entry occurs closer to the evening terminator, it would then be an objective to select an arrival data consistent with a + 10 deg sub-earth vector location.

A combined minimum range and + 10 deg sub-earth vector location mission, however, is not achievable simultaneously and, therefore, a compromise solution must be adopted. For this study an arbitrary compromise between these factors was made; the results of that compromise are indicated in Table 10-4 along with other pertinent mission characteristics.

Another link parameter dependent on position is atmospheric loss. This parameter is dependent on two factors, the depth of penetration into the Jovian atmosphere and the angle at which the transmission propagates through the atmosphere. These RF propagation losses have been calculated as a function of altitude and look angle (azimuth) back to earth. These results are shown tabulated in Table 10-5 for S-band frequencies. The basic components of this loss are: ionospheric attenuation, gaseous absorption (NH_3, H_2O), refractive losses, and cloud absorption and scattering. Complete details on the ground rules and calculation of these losses is included in Reference 4.

TABLE 10-2

DATA CHANNEL LOSSES

PARAMETER	NOMINAL VALUES -dB-
RF LOSSES	0.4
FILTERING & DETECTION LOSSES	0.1
PRE-DETECTION RECORDING LOSSES	1.0
TOTAL LOSSES	1.5

TABLE 10-3

RECEIVING SYSTEM TOLERANCES

PARAMETER	VALUE, dB
RECEIVER NOISE SPECTRAL DENSITY	0.4
E/No	1.0
DATA CHANNEL LOSSES	0.4
ANTENNA GAIN	0.4

TABLE 10-4

DIRECT LINK GEOMETRY FACTORS

ARRIVAL DATE	LAUNCH DATE	APPROACH VELOCITY VECTOR ANGLE	RANGE	SPACE LOSS @ 2295 MHz	EARTH VECTOR LONGITUDE
15 FEB 1981	25 OCT 78	115.9°	701 MKM	276.59 dB	7.5°
23 MAR 1982	5 OCT 78	71.1°	680 MKM	276.32 dB	6.0°
2 MAY 1983	19 DEC 80	115.7°	666 MKM	276.15 dB	6.0°
30 MAY 1984	23 NOV 80	68.9°	650 MKM	275.93 dB	6.0°

TABLE 10-5 RF PROPAGATION LOSSES @ S-BAND

PRESS. (ATM)	LOOK ANGLE, DEGREES								
	0	10	20	30	40	50	60	70	80
1	0.03	0.031	0.033	0.037	0.046	0.06	0.085	0.135	0.3
2	0.1	0.102	0.11	0.12	0.14	0.17	0.235	0.40	1.05
4	0.3	0.31	0.325	0.36	0.41	0.50	0.70	1.12	3.0
6	0.56	0.57	0.60	0.65	0.75	0.91	1.25	2.0	4.6
8	0.88	0.90	0.94	1.02	1.17	1.41	1.91	3.2	7.4
10	1.19	1.20	1.22	1.38	1.60	1.97	2.71	4.4	9.0
12	1.51	1.60	1.70	1.88	2.13	2.60	3.50	5.4	12.0
14	1.85	1.94	2.08	2.25	2.55	3.05	4.0	6.9	18.0
16	2.15	2.20	2.38	2.60	2.95	3.60	4.8	8.3	19.4
17	2.31	2.33	2.50	2.75	3.15	3.75	5.1	9.3	20.0
20	3.0	3.1	3.3	3.6	4.2	5.0	6.7	10.5	23.0

Transmission System: Probe - The probe transmission system characteristics are listed in Table 10-6. A probe transmitter power level of 50 watts is assumed for this study; this power rating is considered consistent with the state of the art technology for 1975 solid state transmitters. A transmitting circuit loss of 0.5 db is considered typical for systems of this type. The S-band downlink frequency is selected for this mission as opposed to X-band based on a frequency tradeoff study that shows that greater performance can be achieved at S-band.

Details of that tradeoff are included in Reference 1. The favored modulation scheme for this link is a coherent coded type. Details of the modulation selection process and the tradeoffs involved are included in Reference 3. Probe antenna systems considered during this study were: 1) a conical reflector, and 2) a turnstyle. Both of these antenna systems are considered simple concepts since no beam switching or adaptive steering techniques are employed. Two antenna concepts were configured in order to satisfy the differing requirements for various mission types. The application of the conical reflector antenna occurred when the link objectives were keyed to maximizing communications capability or performance. The turnstyle antenna, on the other hand, was used for missions where minimum entry angles or reduced interplanetary transit times were the basic requirement. The requirement for the turnstyle antenna was mainly to maximize angular coverage, while the requirement for the conical reflector was based on gain maximization.

The antenna gain patterns factored into the direct link analysis is shown in Figure 10-2 for both antennas. Additional details on the antenna design and performance is included in Section 8.6.1. Also included as part of this analysis is a look angle tolerance of 20 deg. This implies that antenna gain performance factors will be based on a value of look angle which results in the minimum gain over a + 20 deg angular perturbation about the nominal. This tolerance is included to account for probe dynamic and dispersion effects.

10.1.3 Direct Link Analysis Objectives

The objective of the direct link analysis is mainly to synthesize a mission to satisfy the communication requirements (of either 27,000 or 6000 bits) while also minimizing the related engineering requirements. The key factor to minimizing the engineering complexity is in low entry angle missions ($\gamma_E = -20$ deg) which implies probe entry longitudes as close to the evening

TABLE 10-6 PROBE TRANSMISSION CHARACTERISTICS

PARAMETER	VALUE	
TRANSMITTER POWER LEVEL	50 WATTS (MINIMUM)	
TRANSMIT CIRCUIT LOSS	0.5 dB ± 0.2 dB	
LINK FREQUENCY	S-BAND (2295 MHz)	
LINK MODULATION	COHERENT CONVOLUTIONALLY CODED	
CODE RATE	$1/2$	
ANTENNA SYSTEMS	CONICAL REFLECTOR	TURNSTYLE
• ANTENNA GAIN	7.7 dB	4.4 dB
• BEAM PEAK LOCATED	ON AXIS	≈ 40° OFF AXIS
• APERTURE DIMENSION	11"	12"
• GAIN TOLERANCE	± 0.5 dB	± 0.5 dB
LOOK ANGLE TOLERANCE	± 20°	

FIGURE 10-2 PROBE ANTENNA PATTERNS (S-BAND FREQUENCIES)

CONICAL REFLECTOR

TURNSTYLE

GAIN, dB

ASPECT ANGLE, degrees
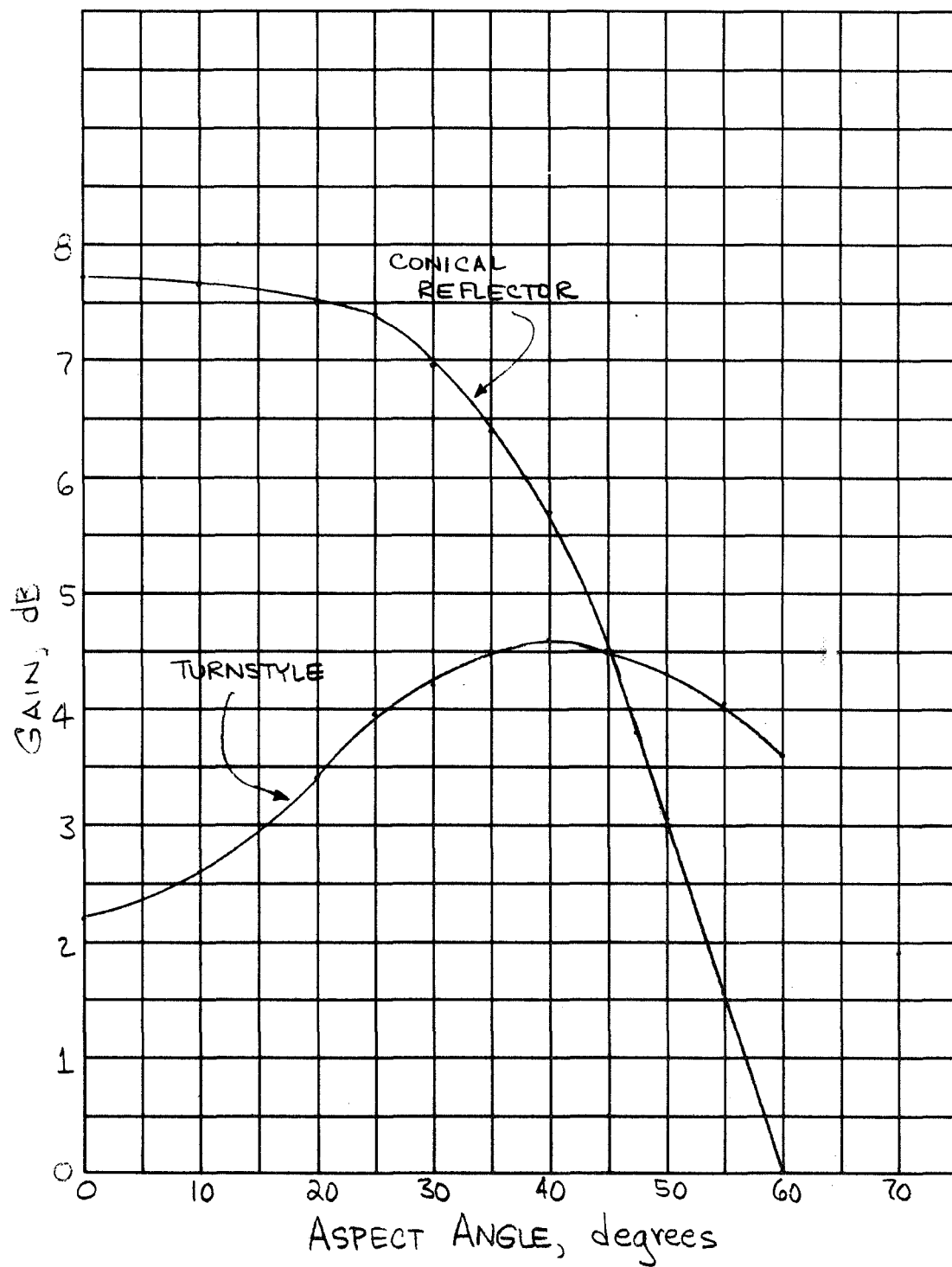
terminator as possible. The sketch in Figure 10-3 shows some of these basic considerations. From this figure, it can be seen that the maximum value of probe to Earth look angle is a function of three items: 1) location of the sub-earth vector; 2) probe entry longitude; and 3) mission descent time.

Since the location of the sub-earth vector has been fixed for this analysis, the only two remaining parameters that can be traded off are probe entry longitude and descent time. And it, therefore, becomes the objective to these link studies to ascertain: 1) the maximum probe entry longitude that satisfies the communication requirements; and 2) the optimum descent time for any given probe entry longitude.

Review of Link Configurations - Ten direct link configurations have been evaluated as part of this study. The characteristics of these links differ according to launch opportunity, trajectory type, DSN operating mode and probe antenna concept. A summary of these missions is presented in Table 10-7.

TABLE 10-7

Direct Link Mission Study Configuration

OPPORTUNITY	ANTENNA TYPE	DSN OPERATING MODE*		
		TRANSMIT S RECEIVE S/X	TRANSMIT S RECEIVE S	RECEIVE S ONLY
78	1	—	—	— TURNSTYLE
78	2	CONICAL REFLECTOR	CONICAL REFLECTOR	CONICAL REFLECTOR TURNSTYLE
80	1	—	—	— TURNSTYLE
80	2	CONICAL REFLECTOR	CONICAL REFLECTOR	CONICAL REFLECTOR TURNSTYLE

* Selection of a particular DSN operating mode is based on the spacecraft link requirements (either T/M or tracking) during the probe descent phase.

FIGURE 10-3

DIRECT LINK GEOMETRY
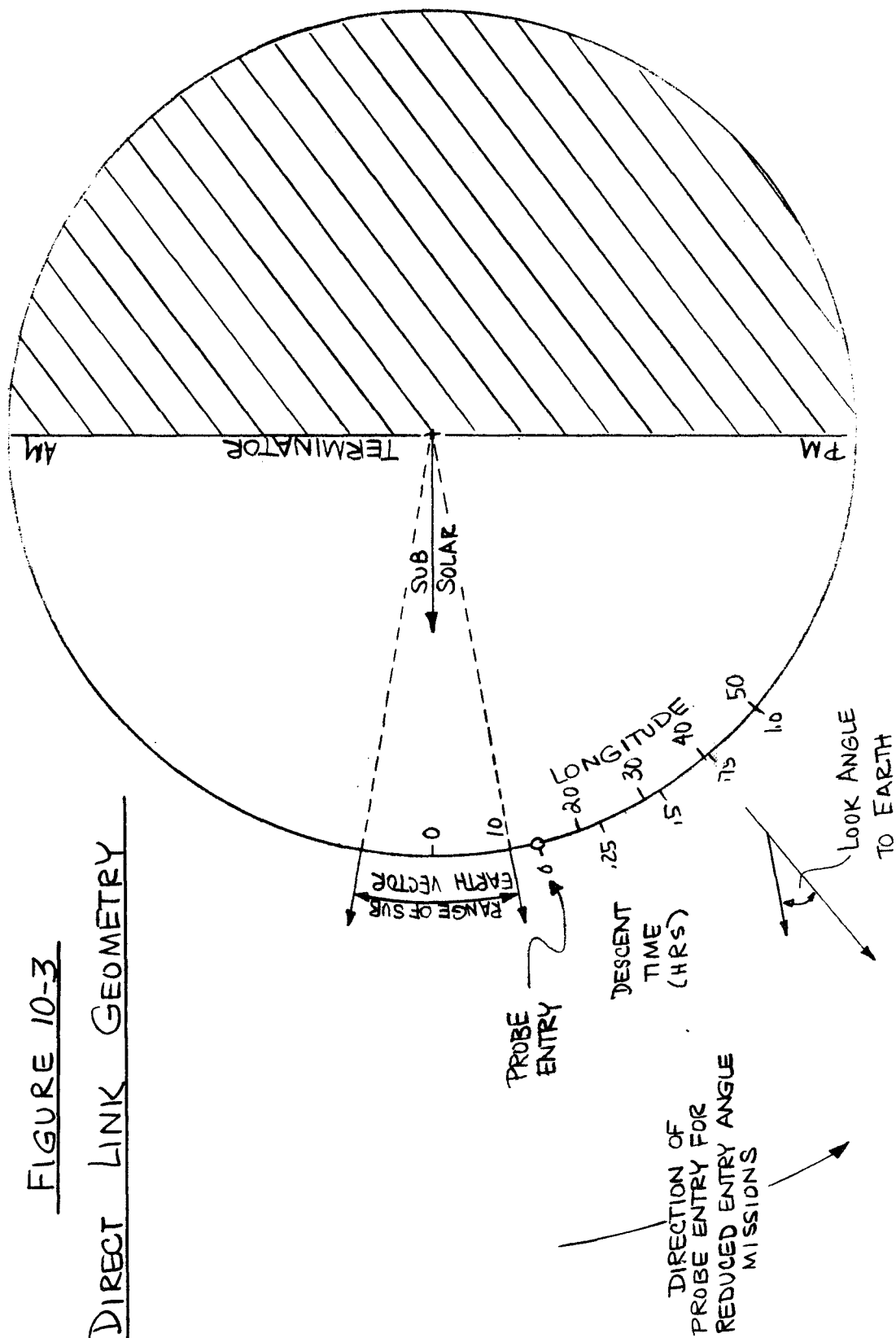
For each of these ten cases, the analyses were conducted such that definition of the shallowest entry angle mission could be made based on the data transfer requirements specified in Section 5.3.2.

Direct Link Data Rate Capability - In considering the achievable data rate capability for any particular mission, a ground rule was established where the data rate during the mission would be held constant; i.e., no mode switching or adaptive data rate scheme would be employed to play out the data. Based on this ground rule, it was determined that the data rate that could be maintained throughout the descent phase of the mission, was sized by the data rate at the bottom of the clouds. The relationship between data rate capability and the probe longitude when at the base of the clouds is shown in Figures 10-4, 10-5, and 10-6. (The link was carried out to 3 atmospheres below the clouds to provide for a finite time to transmit the data obtained below the clouds). The characteristic shape of the profiles shown in these three figures is similar to the probe antenna gain patterns that were used to establish link performance. In Figures 10-4 and 10-5, peak performance occurs for a probe longitude at 6 deg since with the earth directly overhead, the look angle is minimum and the probe antenna gain is at a maximum. For the turnstyle antenna, however, a peak in performance occurs off-axis similar to that of the antenna pattern. Although data rate capability has been established for these various mission configurations, there still exists a requirement to define what combinations of probe entry longitude and descent time can exist to satisfy a given data rate. Sample direct link telecommunication design control charts are presented in Reference 5.

Optimum Descent Time Profiles - Figure 10-7 shows the relationship between probe entry longitude, descent time, and probe position at the base of the clouds. From prior discussions, the stated objective of these studies is to establish the shallowest entry angle mission which, in turn, implies selection of the highest value of probe entry longitude that satisfies the data return requirements. Figure 10-8, 10-9, and 10-10 show these values of descent time that maximize the total data return (product of bit rate and descent time) for a given probe entry longitude. Details relative to the derivation of these results is supplied in Reference 6.

10.1.4 Direct Link Performance

By combining the results of Figure 10-4 through 10-10, it becomes possible to specify direct link data return capability as a function of probe entry longitude. For a given descent time/entry longitude data point from

10-13

FIGURE 10-4

Direct Link Data Rate Capability

1978 Type 2 Trajectory

Conical Reflector Antenna

Receive S

Transmit S Receive S

Transmit S Receive S/X

Includes Linear Sum of Adverse Tolerances

Sub Earth Vector

Probe Longitude at 20 Atmospheres Depth

Achievable Data Rates, Bits/Sec.
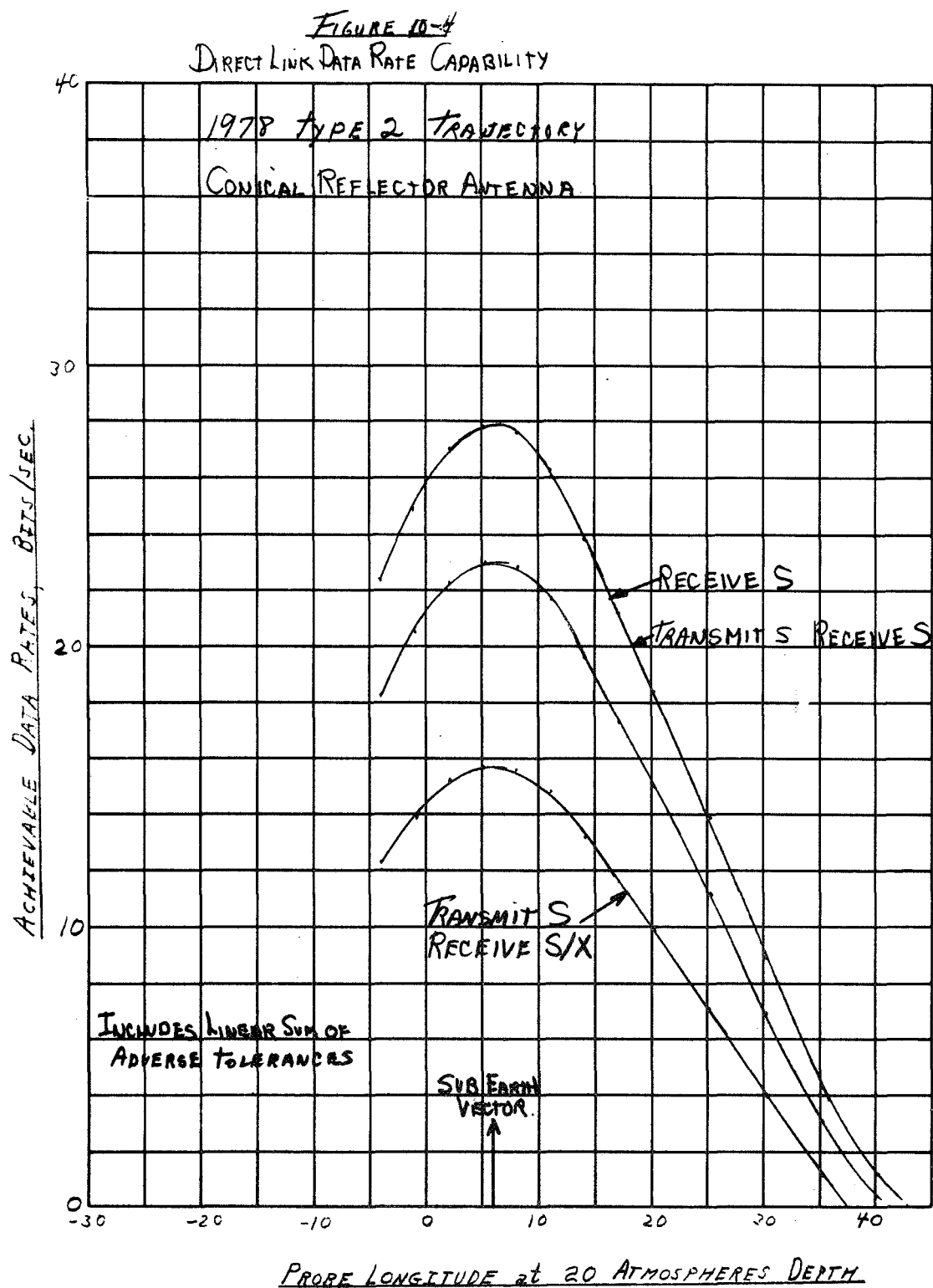
FIGURE 10-5
DIRECT LINK DATA RATE CAPABILITY

1980 TYPE 2 TRAJECTORY
CONICAL REFLECTOR ANTENNA

RECEIVES
TRANSMITS RECEIVES

TRANSMITS
RECEIVE S/X

INCLUDES LINEAR SUM OF
ADVERSE TOLERANCES

SUB EARTH
VECTOR

PROBE LONGITUDE at 20 ATMOSPHERES DEPTH

ACHIEVABLE DATA RATES, BITS/SEC

FIGURE 10-6

DIRECT LINK DATA RATE CAPABILITY

TURNSTYLE ANTENNA

RECEIVE S-BAND ONLY

1980 type II
1980 type I
1978 type II

1978 type I

INCLUDES LINEAR SUM
OF ADVERSE TOLERANCES

SUB EARTH
VECTOR

1980
1978 type I

1978 type II

ACHIEVABLE DATA RATES BITS/SEC

PROBE LONGITUDE AT 20 ATMOSPHERES DEPTH

FIGURE 10-7
PROBE POSITION SUMMARY
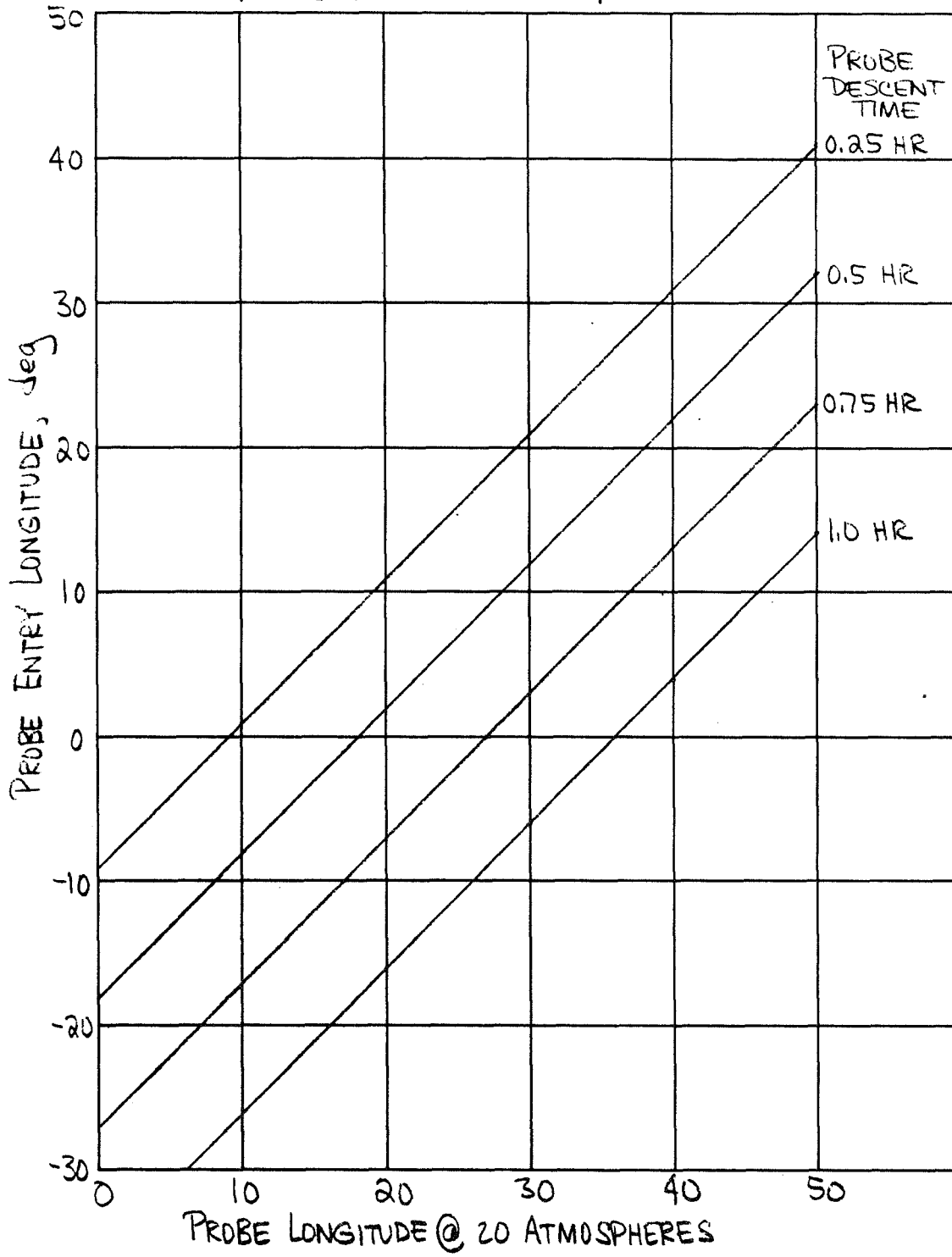
FIGURE 10-8

Optimum Descent Time Profiles

1978 Type 2 Trajectory
Conical Reflector Antenna.

Range of Descent Time for the 3 DSN operating modes.

Descent Time, Seconds

Probe Entry Longitude.

FIGURE 10-9
Optimum Descent Time Profiles
1980 Type 2 Trajectory
Conical Reflector Antenna.

Range of Descent Time for the 3 DSN Operating Modes.

DESCENT TIME SECOND

2500

2000

1500

1000

500

PROBE ENTRY LONGITUDE

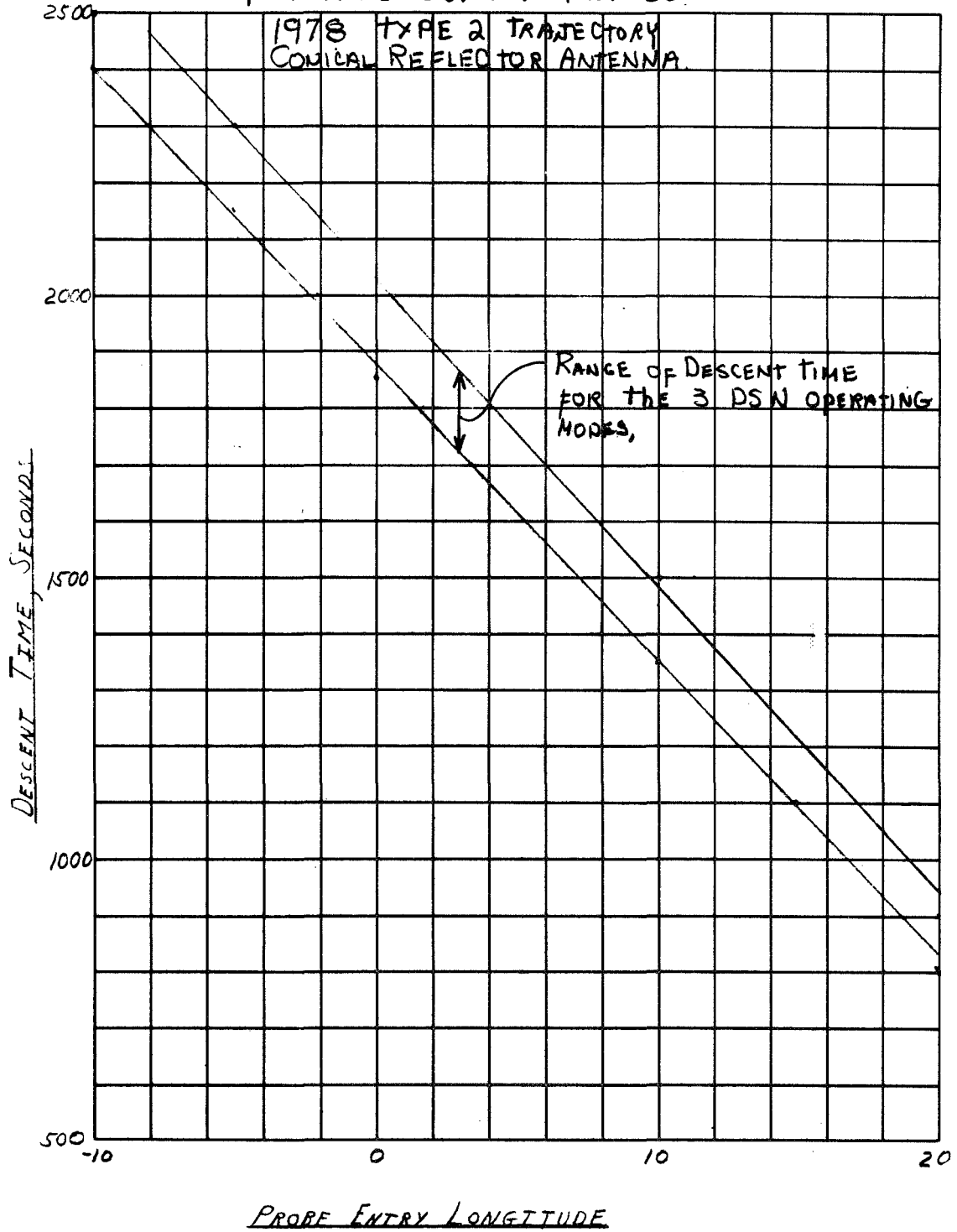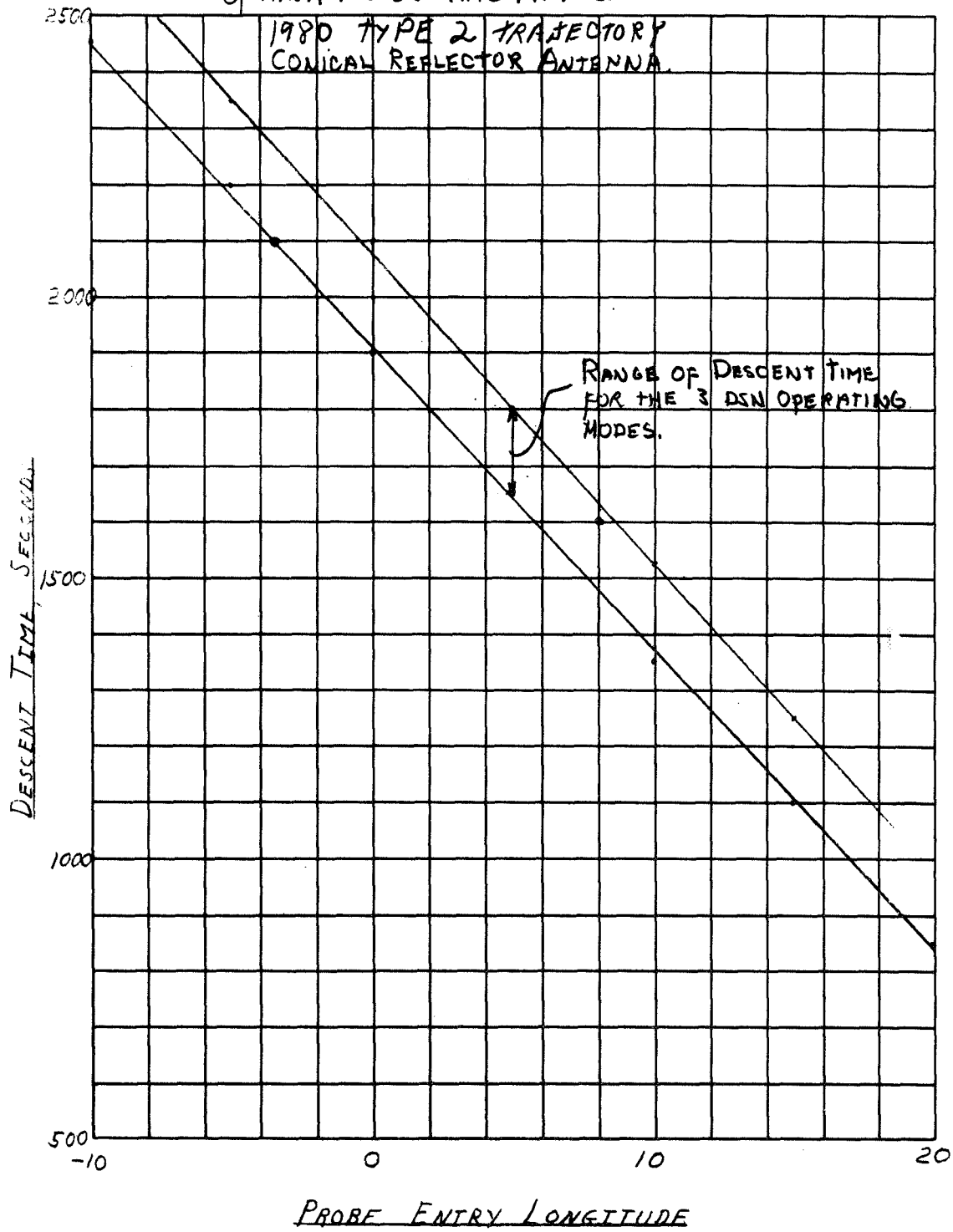-10   0   10   20

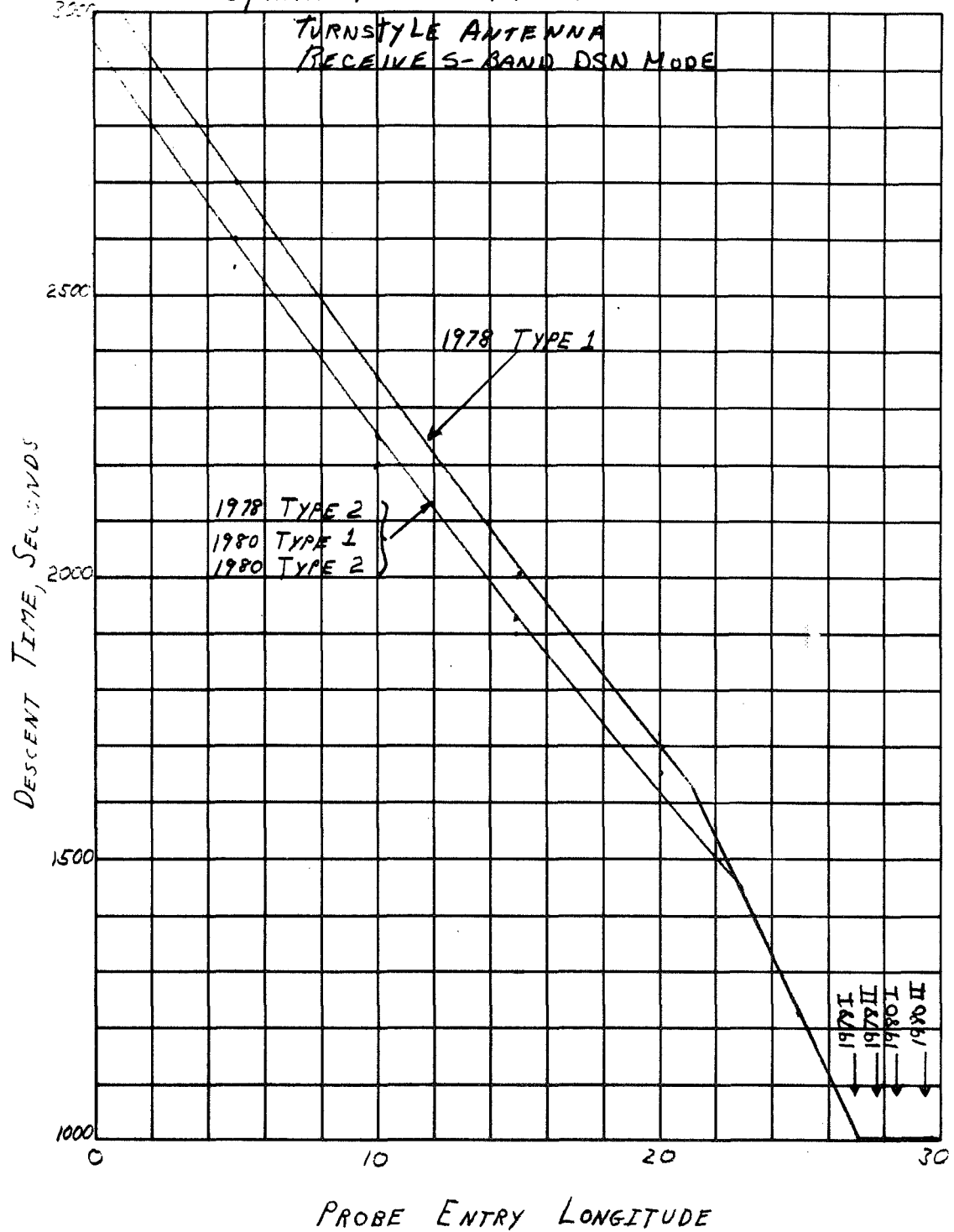Figure 10-10
Optimum Descent Time Profiles

Figure 10-5, the probe position at the 20 atmosphere depth can be ascertained via Figure 10-7; this data can then be used to enter Figure 10-4 to establish the data rate capability. The product of data rate and descent time then establishes the total data return for that probe entry position. A composite plot of these performance factors for the ten mission configurations is shown in Figures 10-11, 10-12, and 10-13. These figures show the achievable data rates and total bit transfer for a given probe entry longitude and DSN operating mode. Each of the three sets of profiles show decreasing data rate capability with increasing probe entry longitude. This occurs because the probe position at the end of the mission (20 atmosphere depth) is further away from the sub-earth vector. In comparing direct links for 1978 and 1980 (Figures 10-10 and 10-11), it can be seen that the latter year results in higher performance. In Figure 10-12, the results for the turnstyle antenna show lower data rate performance, however, the values of probe entry longitudes for which a 6000 bit data return mission can be carried out is extended out by some 5 deg from the conical reflector antenna case.

10.1.5 Summary of Mission Performance

The impact of probe entry longitude and data rate performance on the mission characteristics is typically measured through the entry angle requirement to achieve such a mission. For a given arrival date, the relationship between probe entry longitude and entry angle is fixed. Figure 10-14 shows this relationship for the four combinations of opportunity/trajectory. By combining the results of Figures 10-11 through 10-13 with Figure 10-14, the impact of data rate performance on entry angle requirements can be ascertained. This data is plotted in Figures 10-15 to 10-18. For Figures 10-15 and 10-16, the intersection of the 27,000 bit contour line with the data rate profiles establishes the entry angle requirement for that mission. Figures 10-17 and 10-18 show similar results for a minimum date return mission. For these cases, however, since the 6000 bit contour line is parallel to the 6 bps data rate value, the entry angle requirement is identified by a vertical line for each case. A summary of the characteristics associated with each of these sets of 27,000 bit and 6000 bit missions is presented in Table 5-11.

10.2 RELAY LINK STUDIES

10.2.1 Introduction

The major relay link study elements are similar to those of the direct link presented in Figure 10-1, however, the addition of a moving receiving site

FIGURE 10-11
Direct Link Performance
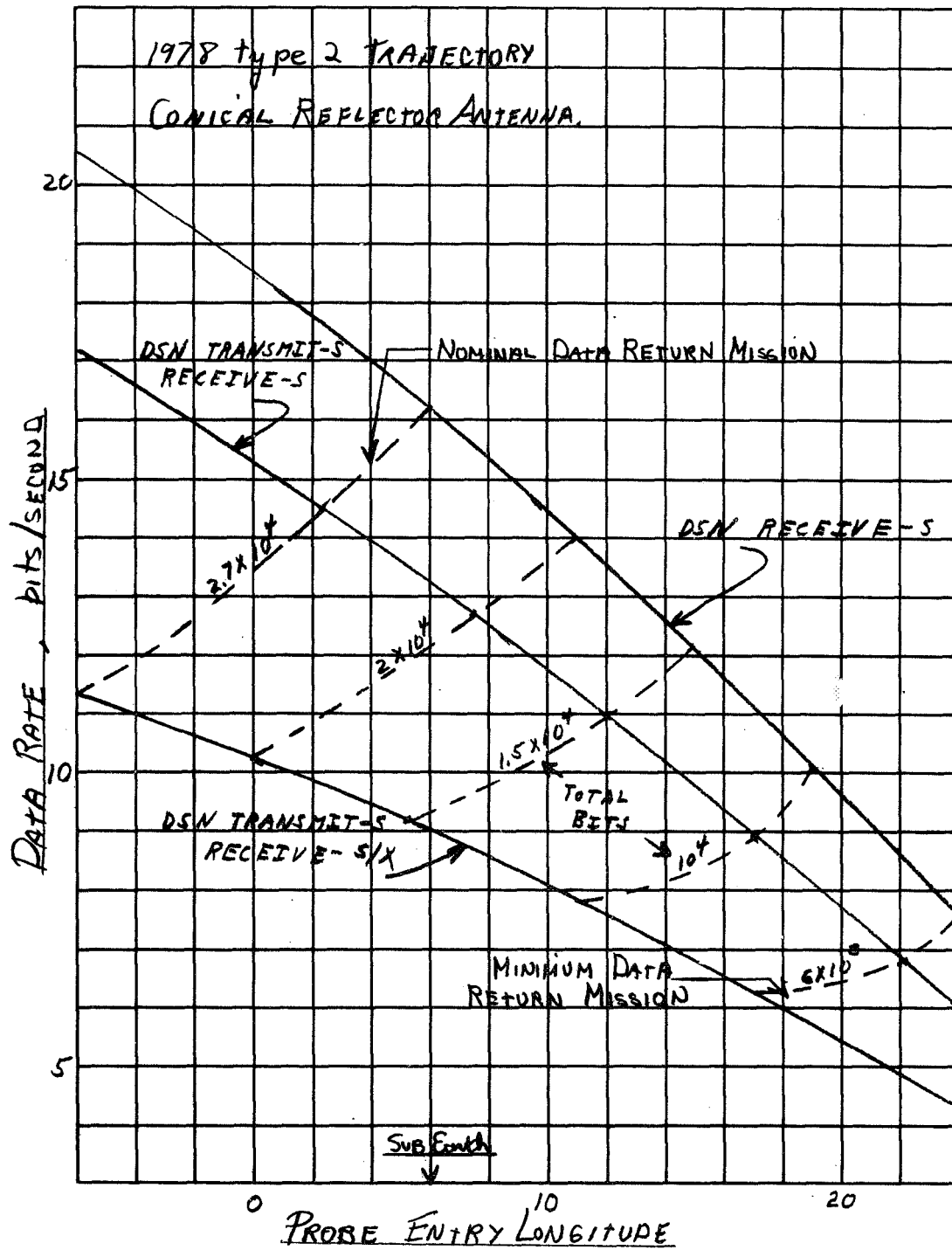
FIGURE 10-12
DIRECT LINK PERFORMANCE
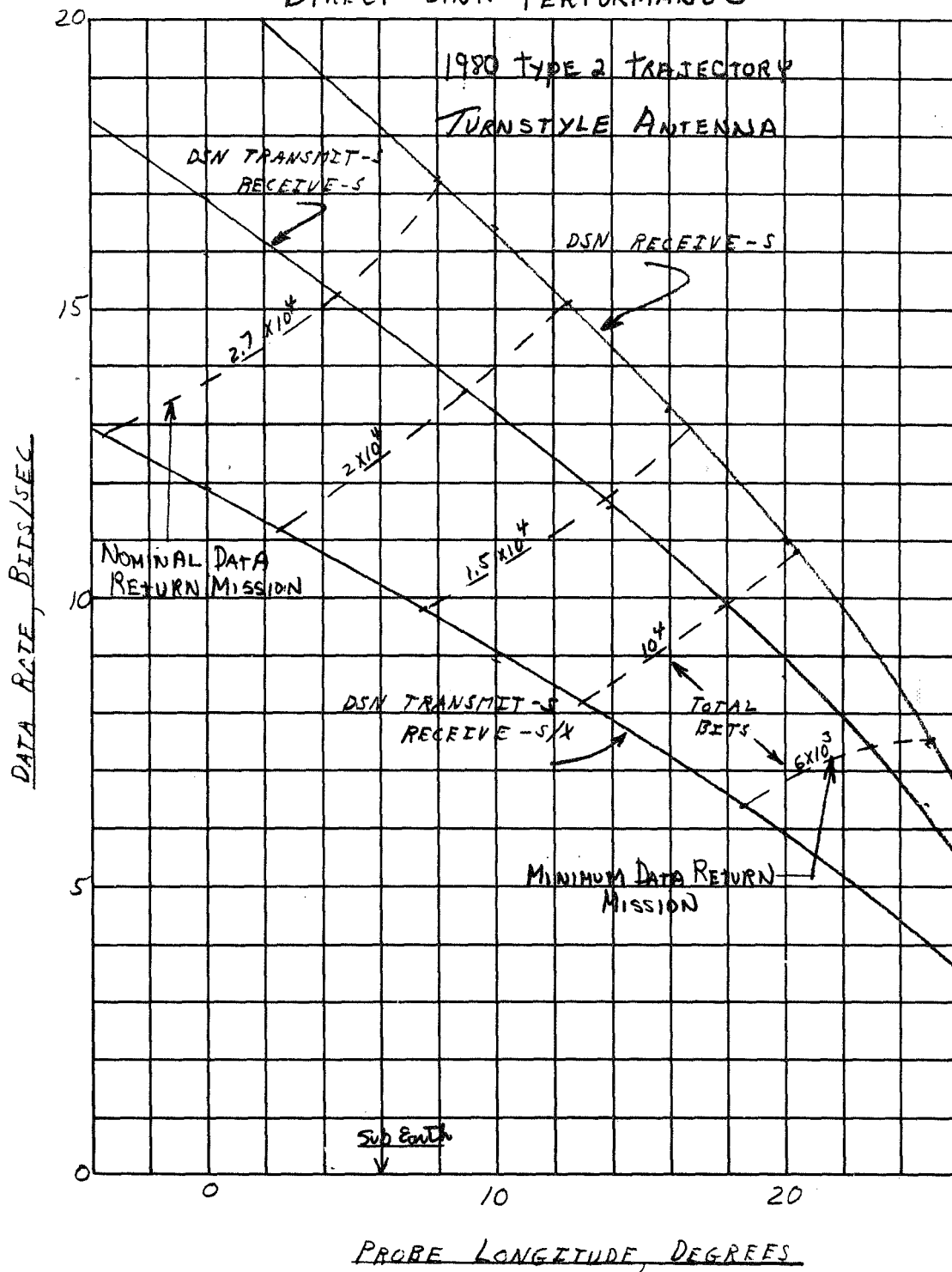
FIGURE 10-13
DIRECT LINK PERFORMANCE
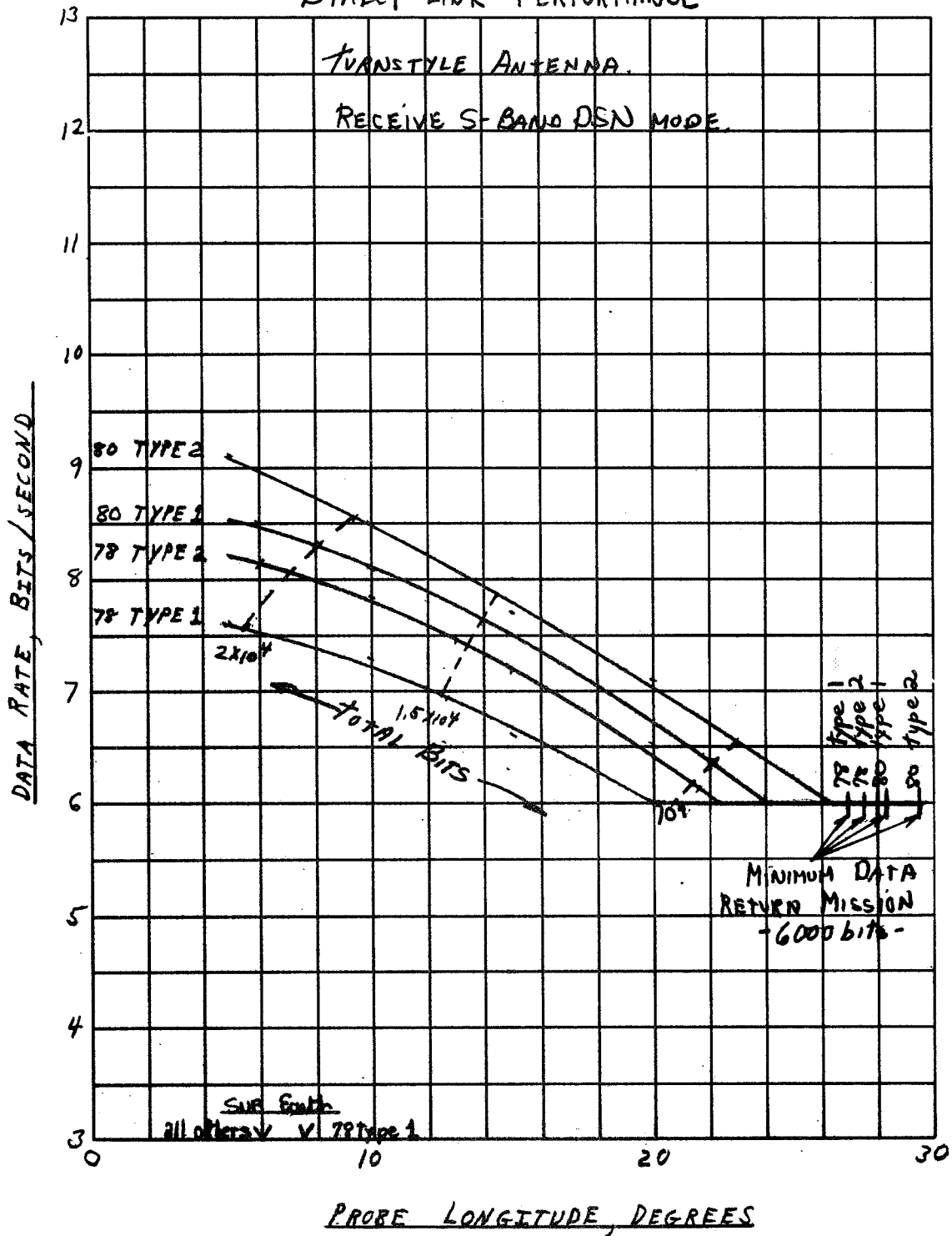
FIGURE 10-14 DIRECT LINK MISSION ENTRY ANGLE PROFILES
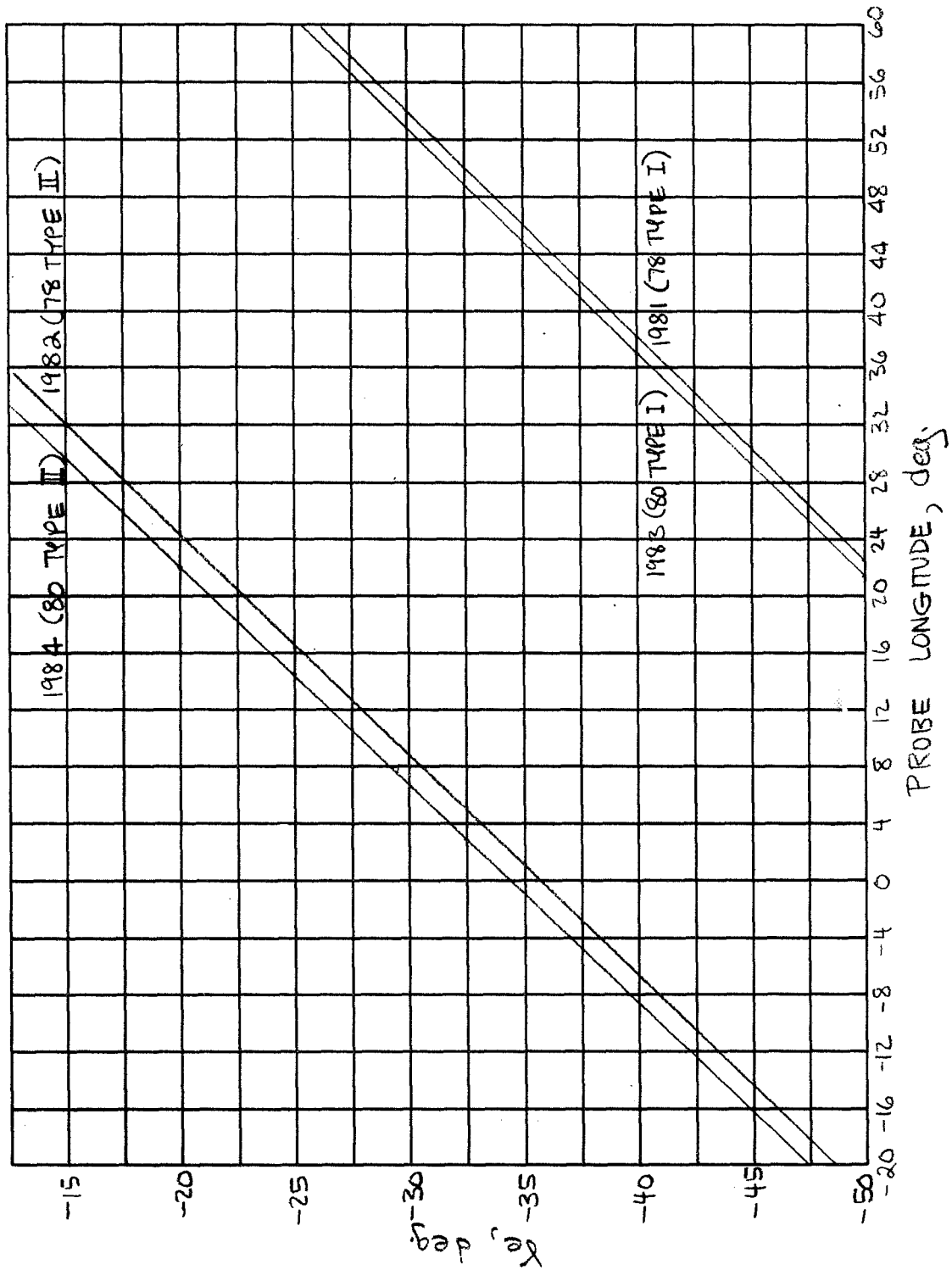
FIGURE 10-15 DIRECT LINK PERFORMANCE

1978 TYPE 2 TRAJECTORY
CONICAL REFLECTOR ANTENNA
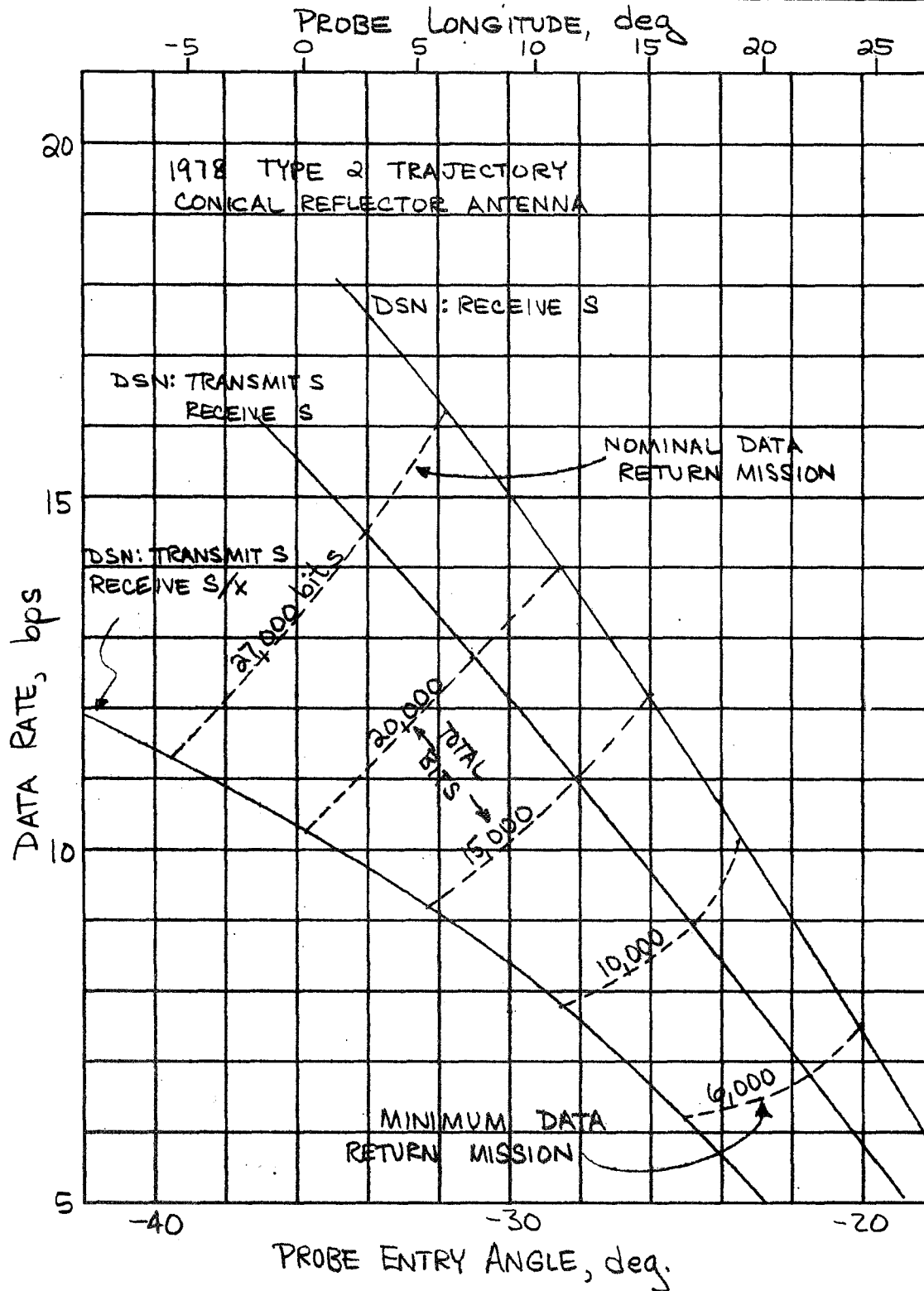
FIGURE 10-16 DIRECT LINK PERFORMANCE

PROBE LONGITUDE, deg

1980 TYPE 2 TRAJECTORY
TURNSTYLE ANTENNA

DSN: RECEIVE S

DSN: TRANSMIT S
RECEIVE S

DSN: TRANSMITS
RECEIVE S/X

27,000 bits

20,000

TOTAL BITS

15,000

10,000

6,000

MINIMUM DATA
RETURN MISSION

PROBE ENTRY ANGLE, deg.

10-27
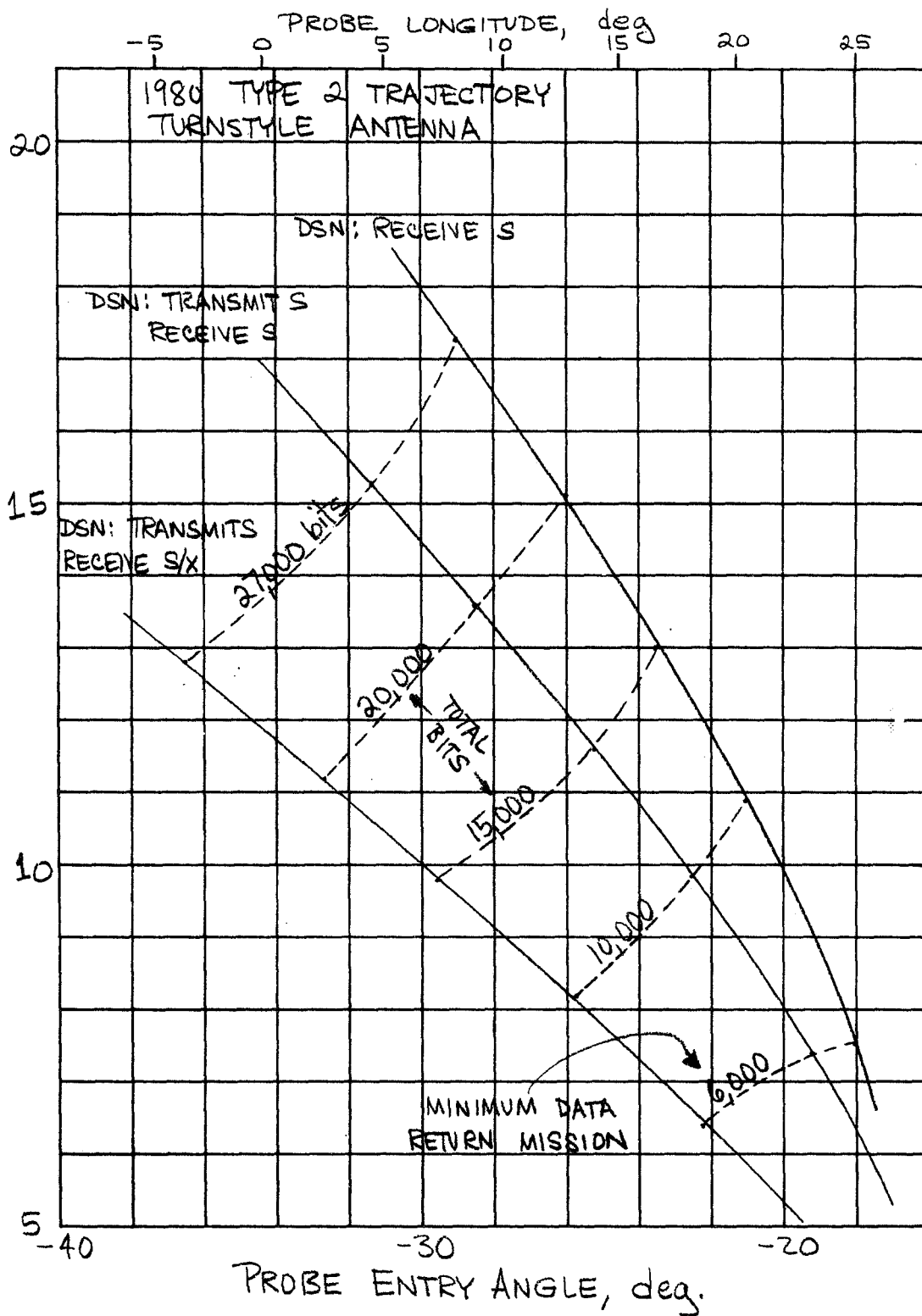
FIGURE 10-17 DIRECT LINK PERFORMANCE

PROBE LONGITUDE, deg.

TURNSTYLE ANTENNA

RECEIVE S-BAND DSN MODE

80 TYPE 1

78 TYPE 1

20,000

TOTAL

BITS

15,000

10,000

78 TYPE 1

80 TYPE 1

MINIMUM DATA RETURN MISSION (6000 BITS)

PROBE ENTRY ANGLE, deg.

DATA RATE, bps

FIGURE 10-18 DIRECT LINK PERFORMANCE

PROBE LONGITUDE, deg

TURNSTYLE ANTENNA

RECEIVE S-BAND DSN MODE

80 TYPE 2

78 TYPE 2

20,000

15,000

TOTAL BITS

10,000

MINIMUM DATA
RETURN MISSION
(6000 BITS)

DATA RATE, bps

PROBE ENTRY ANGLE, deg.

increases the complexity of the contact analysis and frequency selection tradeoffs while adding an additional task identified as S/C antenna tradeoffs. Figure 10-19 shows the interrelationships of these various study elements.

Contact Analysis - The contact analysis is probably the single most important tradeoff of the group since the results of that analysis establishes the performance of both the probe and S/C ante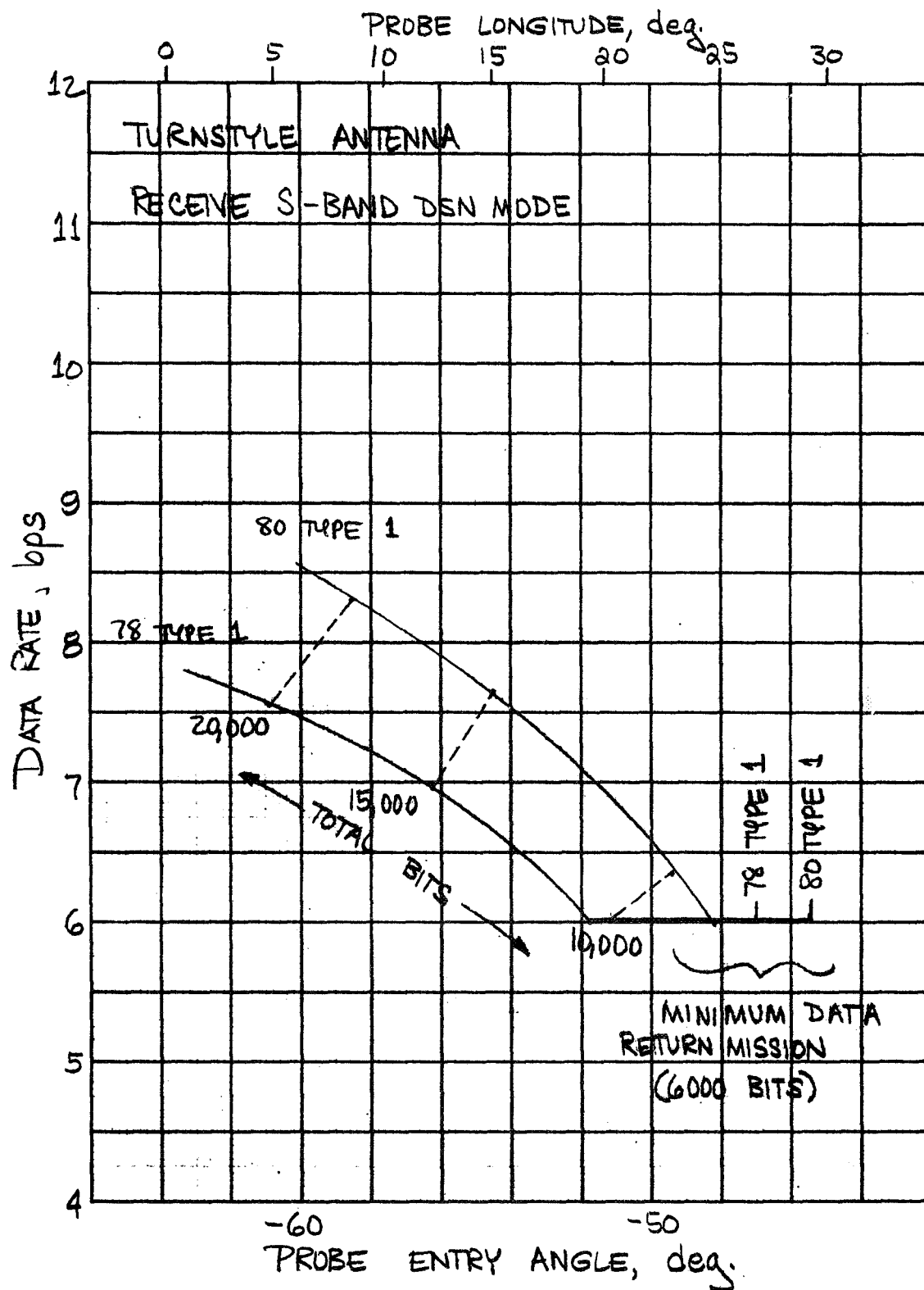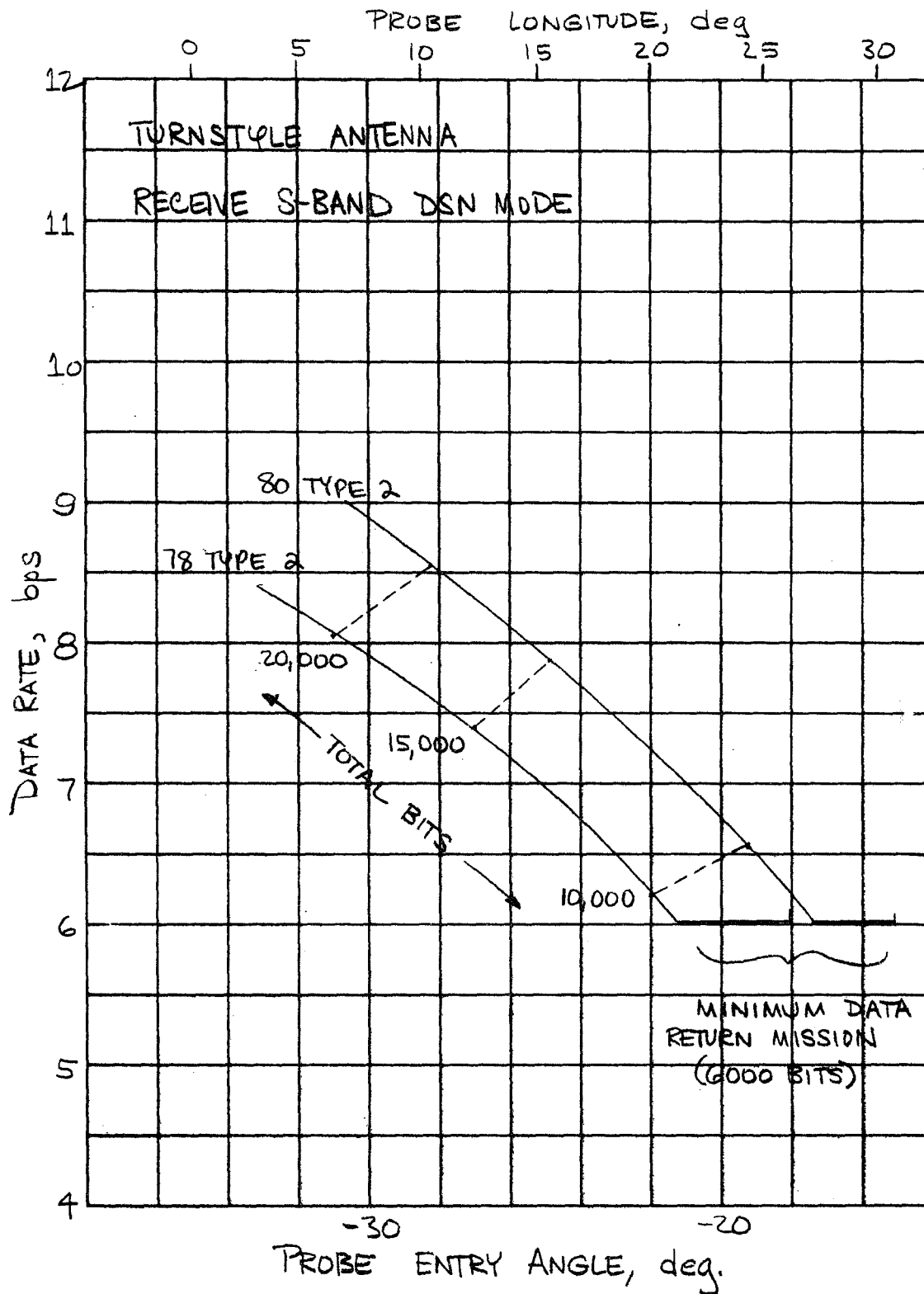nnas and also to some extent plays a role in the relay link frequency selection. The selection of an optimum spacecraft trajectory for a given probe entry condition that maximizes the link signal strength is presented in this section of the report.

Frequency Selection - The relay link frequency is determined by combining the frequency dependent link parameters into a composite profile from which the optimum is selected. Details of this analysis are presented in Reference 1.

Antenna System Tradeoffs - Probe and S/C antenna systems were not considered a parametric study item. Antenna system tradeoffs were conducted only to the extent of satisfying a general set of requirements based on antenna beamwidth requirements and maximum aperture constraints. Details of the antenna system selections are presented in Section 8.6.2.

Link Losses, Modulation Scheme, Relay Link Performance - These tasks are similar to those mentioned for the direct links. Again, as was the case for the direct links, only the results of the individual analyses will be presented.

The relay link analyses conducted for this study include an evaluation of relay link communication to a TOPS or Pioneer F/G flyby spacecraft. The analysis and the resulting performance will be presented in this section.

10.2.2 Assumptions and Constraints

The relay link assumptions and constraints related to the spacecraft receiving system, the probe transmission system and the space link is discussed in the following subsections.

Spacecraft and Receiving System - Table 10-8 lists the pertinent characteristics associated with TOPS and Pioneer F/G spacecraft receiving system.

Four different receiving antenna systems are identified for the various TOPS and Pioneer F/G missions. Although no detail tradeoff analyses were

FIGURE 10-19 RELAY LINK COMMUNICATION ANALYSIS
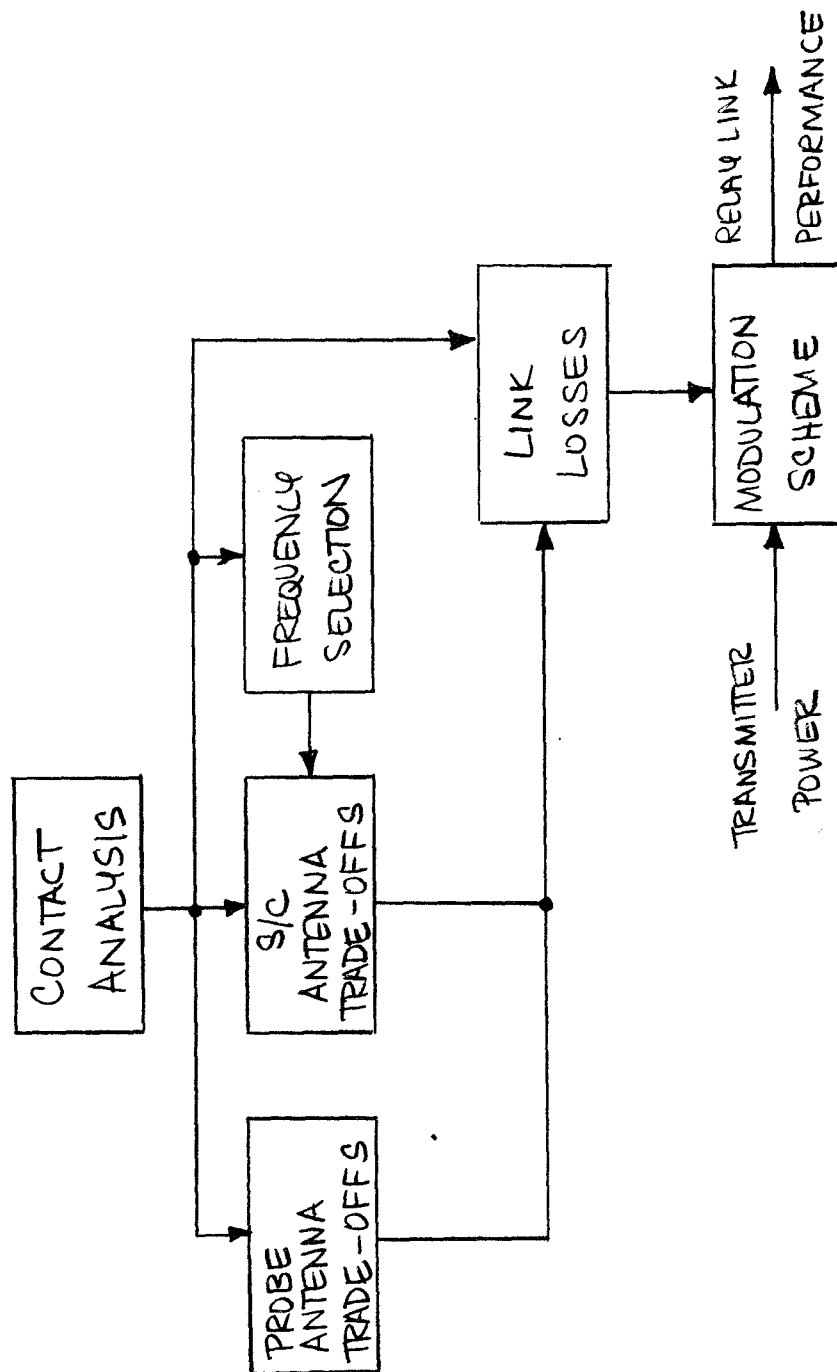
TABLE 10-8 RELAY LINK SPACECRAFT RECEIVING SYSTEM

	SPACE CRAFT			
	TOPS		PIONEER F/G	
	FLYBY	J-U-N	FLYBY	
ANTENNA SYSTEM • TYPE	ELLIPTICAL DISH	CIRCULAR DISH	DESPUN CIRCUMFERENTIAL ARRAY	CIRCULAR DISH
• PEAK GAIN	24.5 dB	27 dB	15 dB	19.7 dB
• 3dB BEAMWIDTH	$10° \times 7°$	$7° \times 7°$	$8° \times 30°$ *	$20° \times 20°$
• FREQUENCY	S-BAND	S-BAND	L-BAND	
• APERTURE (MAX)	41"	41"	48.6"	40"
• TRACKING AID	PLANET TRACKING BOTH PLANES		PLANET TRACKING ROLL PLANE ONLY	NO TRACKING
RECEIVER • CIRCUIT LOSS	← 0.5 dB →			
• NOISE FIGURE	← 5 dB →			
• SYSTEM NOISE FIGURE	← 6.3 →		← 11.1 →	
• CARRIER LOOP BW	← 50 Hz →			
• CARRIER THRESH. SNR	← 9 dB →			
• DATA E/No	← 3 dB →			
• SYSTEM WORD ERROR RATE	← $< 10^{-2}$ →			
• CODING SCHEME	6 BIT BIORTHOGONAL CODED WORD			
• DATA CHANNEL LOSSES	← 1.5 dB →			
RECEIVING SYSTEM TOLERANCES	← ≈ 2.6 dB →			

* 60° BEAMWIDTH IN THE AXIAL PLANE WILL OCCUR FOR A SINGLE BEAM SWITCHOVER.

performed in the selection of these receiving antenna systems, the beam-width requirement was generally constrained by either 1) the maximum aperture available, or 2) the requirement to maintain the probe within the 3 db beamwidth limit including the effects of probe and spacecraft dispersions.

In the case of the TOPS spacecraft, because of three axis attitude control and a planet tracking sensor, the use of a relatively narrow beamwidth high gain antenna is possible. For the J-U-N mission, because of the increased flyby periapsis radius, the beamwidth requirements are less than the TOPS flyby mission and the elevation beamwidth for this mission can be reduced to 7 deg which is the maximum aperture limit value. For the Pioneer F/G spinning spacecraft, tracking in the yaw or elevation plane is not available, therefore, the beamwidth requirements increase, as shown in Table 10-8, to 30 deg. In the roll or circumferential plane, however, with a despun antenna concept, the beamwidth can be maintained at a smaller value. The 30 deg elevation beamwidth associated with the despun circumferential array is still inadequate to cover the range of angular requirements and, therefore, a single beam switch over midway during the descent phase will be incorporated into the system to provide the necessary 60 deg of beamwidth. A second antenna concept that was evaluated for these missions is a simple parabolic dish located on the spin axis of the spacecraft. This concept would be applicable for those missions where the spacecraft to probe line of sight was within 20 deg of the spacecraft spin axis. This restriction on the spacecraft to probe geometry is severe and only those missions where the probe is targeted about the sub-earth vector (Type II) would this antenna apply.

The receiver noise figure and system noise figures used in this analysis to establish the receiver noise spectral density is shown in Table 10-8. The difference in noise figure between the TOPS and Pioneer F/G mission is due to the increased effects of Jovian noise at the lower link frequency for the Pioneer spacecraft. A full account of these calculations is included in Reference 7.

The carrier loop BW of 50 Hz and threshold SNR of 9 db was taken as the reference conditions for satisfactory tracking capabilities. Loop acquisition within 60 seconds and loss of lock probabilities no greater than 1% were the basis for these operating characteristics. Reference 8 presents the details in support of these items.

The characteristics of the data channel show a 3 db signal/energy/bit to noise spectral density (E/N_0) ratio to provide an error rate of less than 1 in 100 for a 6 bit biorthogonal coded modulation shceme. Also included in the list of parameters is a nominal data channel loss of up to 1.5 db to account for coherence, distortion, filtering and decoding losses. The modulation selection process and performance estimates are further described in Reference 3.

The receiving system tolerances included in the link analysis, in order to establish worst case performance, amounts to 2.6 db in addition to pointing loss uncertainties which are mission dependent. A breakdown of these individual component tolerances for these items that are constants in the link is listed in Table 10-9.

Space Link-Probe-To-Spacecraft - Evaluated under this subsection are the space link related parameters. These parameters include the link frequency, communication link geometry, and atmospheric losses.

TABLE 10-9

Relay Receiving System Parameter Tolerances

PARAMETER	VALUE, dB
RECEIVING ANTENNA GAIN	0.5
RECEIVING CIRCUIT LOSS	0.2
RECEIVING SYSTEM NOISE FIGURE	0.5
SNR OR E/N₀	1.0
DATA CHANNEL LOSSES	0.4
TOTAL	2.6

A) Link Frequency

Results of the link frequency tradeoff analyses (Reference 1) indicate S and L-band frequencies as optimum for the respective TOPS and Pioneer F/G spacecraft missions. The frequency dependent factors included in this tradeoff are: 1) Jovian Noise, 2) atmospheric losses, 3) probe antenna directivity, and 4) receiving antenna fixed beamwidth loss. Figure 10-20 shows this relative loss profile as a function of frequency. The basic reason for the difference in frequency selection for the two spacecrafts can be attributed to the fixed antenna beamwidth loss. Since the TOPS spacecraft receiving antenna beamwidth requirements are less than the Pioneer F/G spacecraft, the frequency at which the maximum aperture constraint is reached is higher for TOPS thereby causing the optimum to occur at a higher frequency.

B) Communication Link Geometry

The link geometry parameters that influence the relay communication link performance include: 1) communication range, 2) the entry probe to spacecraft look angles, and 3) the spacecraft to entry probe look angle. A study was conducted to tradeoff the parameters so as to maximize the overall link signal strength. This was accomplished by varying the spacecraft periapsis radius and lead time parameters. Specific details relative to this tradeoff are presented in the following subsection.

C) RF Propagation Losses

The RF propagation losses associated with a communication link operating at the base of the Jovian cloud layers is summarized in Figure 10-21 as a function of frequency. For the two stated relay link frequencies (S-band and L-band) a factor of four difference in this loss value is observed. In carrying out the link studies, this factor of four difference was maintained for other altitudes and look angles. Table 10-5 presents the values of RF propagation losses at S-band as a function of altitude and look angle, and the atmospheric loss values at L-band are those values in Table 10-5 reduced by a factor of four.

Probe Transmission System - A summary of the probe transmission characteristics is presented in Table 10-10 for the three different spacecraft missions.

Probe transmitter power levels of 25, 40 and 50 watts are selected for this analysis. The 40 watt power level at S-band assumed for the J-U-N mission

Figure 10-20 Relay Link Frequency Selection
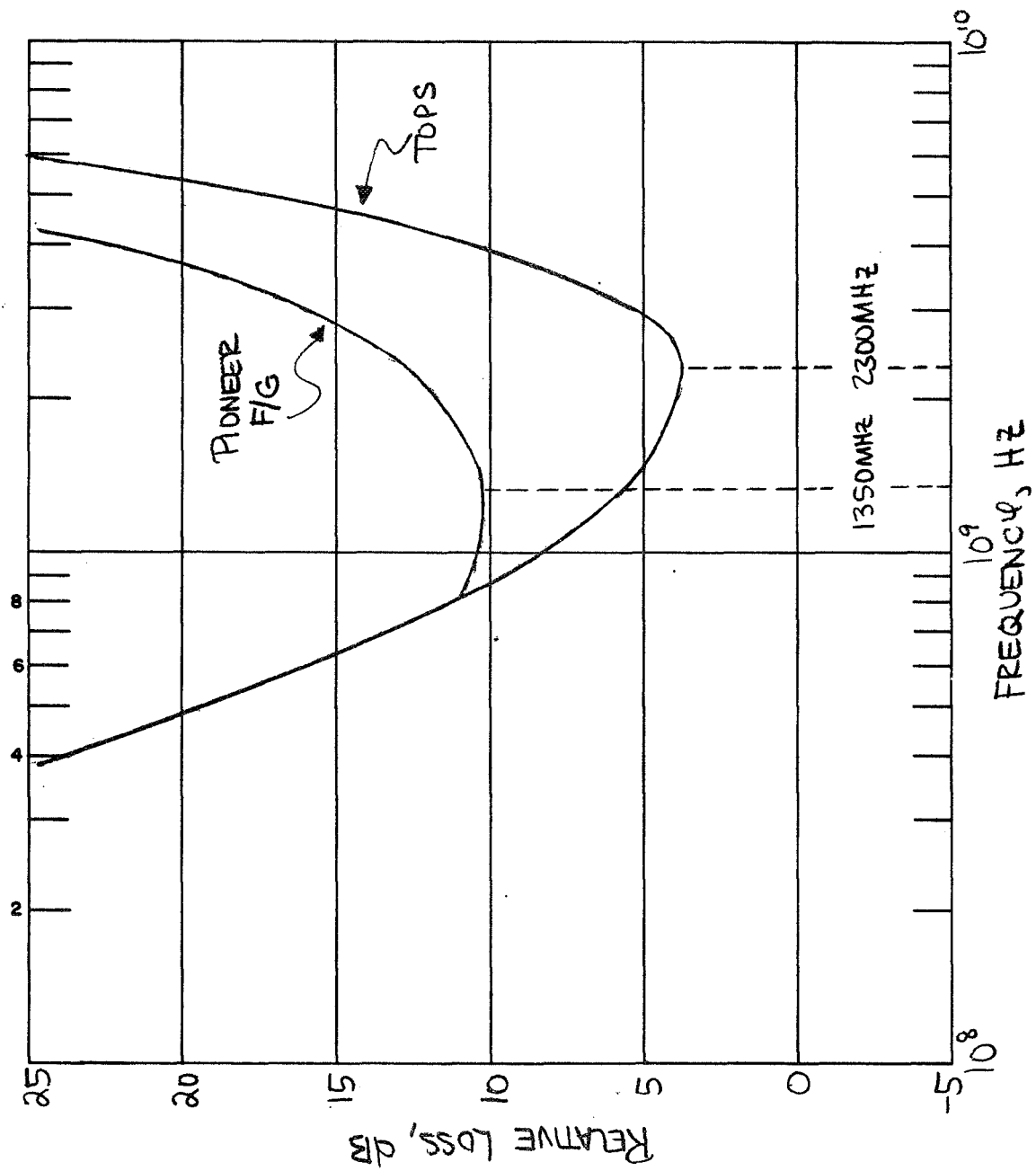
FIGURE 10-21

LOSS PROFILE TO BOTTOM OF CLOUDS

Loss, dB (y-axis) vs. WAVELENGTH, CM (x-axis)

Curves labeled: COOL, DENSE; NOMINAL; WARM, EXTENDED
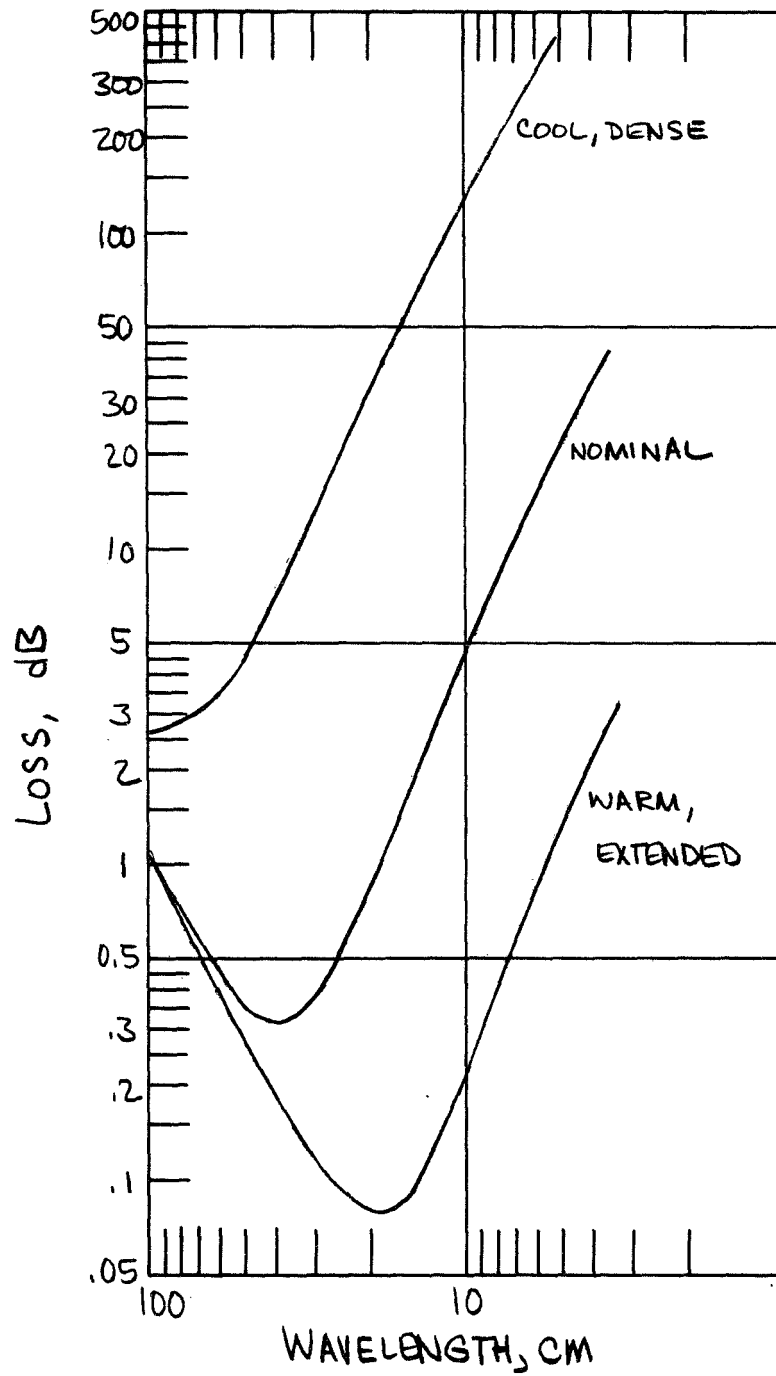
TABLE 10-10 PROBE TRANSMISSION CHARACTERISTICS

MISSION	TOPS	J-U-N	PIONEER F/G
LINK FREQUENCY	S - BAND		L-BAND
TRANSMIT POWER LEVEL (MIN)	25 WATTS	40 WATTS	50 WATTS
TRANSMIT CIRCUIT LOSSES	← 0.5 ± 0.2 dB →		0.5 ± 0.4 dB
TRANSMITTING ANTENNA SYSTEM			
• TYPE	CONICAL REFLECTOR		OPEN-ENDED WAVEGUIDE
• ANTENNA GAIN	← 7.7 dB →		
• BEAM PEAK LOCATION	← ON PROBE AXIS →		
• APERTURE DIM. (MAX)	← 11" →		
• PEAK GAIN TOL.	← 0.5 →		
• LOOK ANGLE TOLERANCE	← ± 1.5° →		

and the 50 watt power level at L-band assumed for the Pioneer F/G missions are considered consistent with the state of the art technology for 1975 solid state transmitters. A .5 db transmitting circuit loss is assumed to be a typical value associated with cabling, insertion and reflected losses in the transmission line network. Two probe antenna systems are considered for relay link communications. One system is designed to accommodate the S-band frequency mission where the second system will apply for the L-band link. Both systems are nearly identical in operating characteristics except the radiation pattern which shows the S-band antenna system to have a slightly larger beamwidth. Figure 10-22 shows the antenna gain pattern for each antenna. A complete description of the probe antenna systems can be found in Section 8. 6. 2.

The look angle tolerance of ± 15 deg shown in Table 10-10 implies that probe antenna gain factor into the link analysis is the lowest value of gain over a ± 15 deg angular perturbation about the nominal; this probe angular tolerance accounts for uncertainties in the probe dynamics. The angular uncertainties resulting from probe and spacecraft dispersions are treated separately and considered as one of the key factors in the relay link geometry tradeoff analysis.

10. 2. 3 Relay Link Analysis Objectives

The objective of the relay link analysis is essentially similar to that of the direct link, however, the approach taken to reach this objective is quite different. Again, as was the case for the direct link, the contact analysis is the key factor in the relay link performance optimization. Figure 10-23 presents a sketch of the parameters involved in the relay link geometry analysis. The factors which play a major role in relative position of probe and spacecraft are: 1) the probe entry longitude; 2) spacecraft lead time; and 3) spacecraft periapsis radius.

In order to optimize communication performance, it is desired to maintain the spacecraft directly over the probe and as close as possible during the descent phase; and therefore, it becomes the objective of this study to: 1) define the periapsis radius and lead time of the spacecraft to provide the optimum probe/spacecraft geometry; and 2) define the shallowest entry angle missions which satisfies the communication requirements.

Review of Link Configurations - A review of link configurations is appropriate at this time in order to isolate the various relay link alternative missions that were considered during the study. Table 10-11 presents such a summary.

FIGURE 10-22 ~ PROBE ANTENNA PATTERNS

FIGURE 10-22 ~ PROBE ANTENNA PATTERNS

Plot of PROBE ANTENNA GAIN, dB (vertical axis, from -10 to 10) versus LOOK ANGLE, deg. (horizontal axis, from 0 to 70), showing two curves labeled 2300 MHZ and 1350 MHZ.
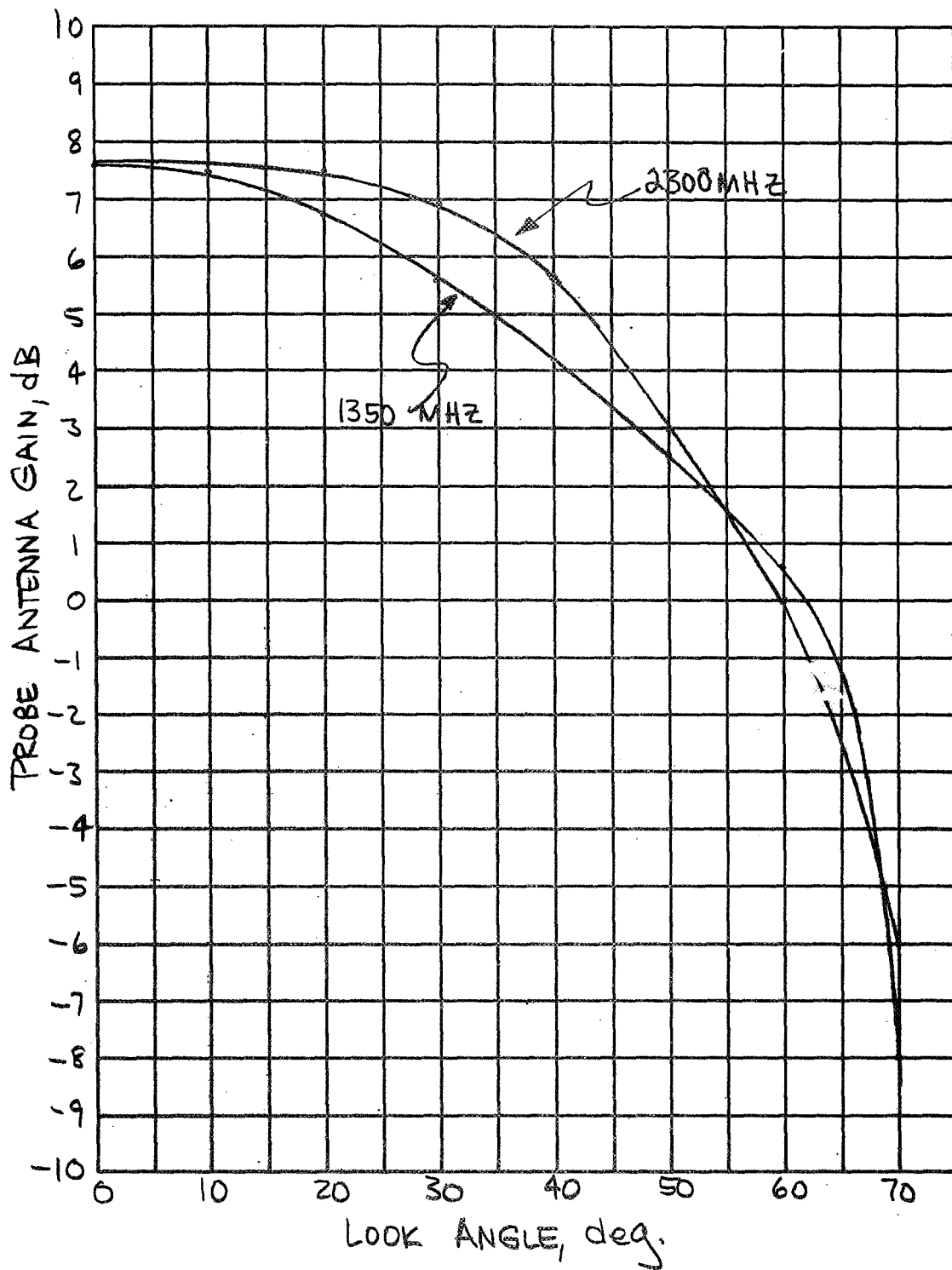
FIGURE 10-23 RELAY LINK GEOMETRY
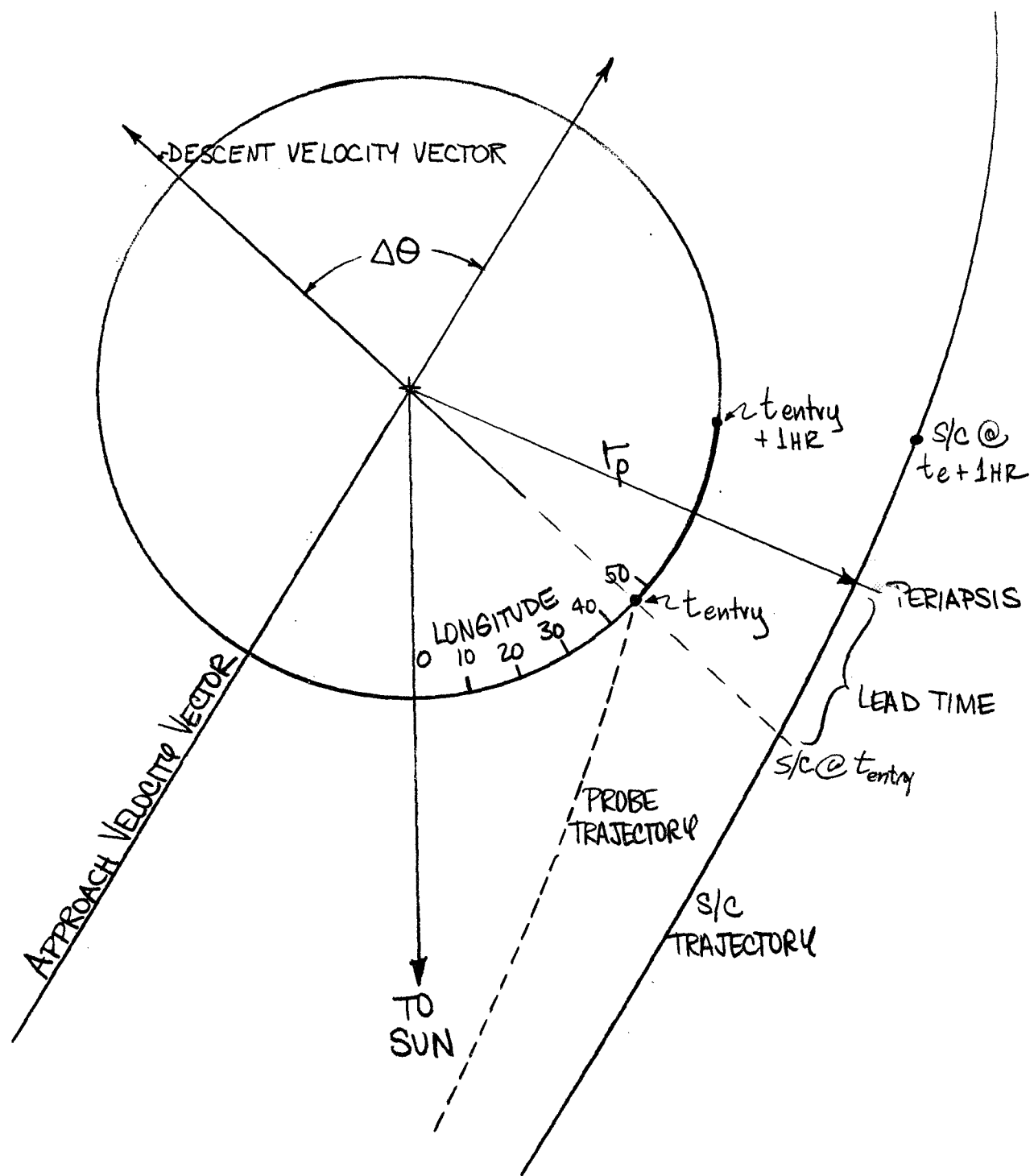
TABLE 10-11   SUMMARY OF RELAY LINK MISSION CONFIGURATIONS

SPACECRAFT MISSION	ANTENNAS		LAUNCH OPPORTUNITY		
	PROBE	S/C	78	79	80
TOPS	CONICAL REFLECTOR	ELLIPTICAL DISH	TYPE 1 TYPE 2		TYPE 1 TYPE 2
J-U-N	"	CIRCULAR DISH		TYPE 1 ONLY	
PIONEER	OPEN-ENDED WAVEGUIDE	CIRCUMFERENTIAL ARRAY	TYPE 1 TYPE 2 FOR PROBE ENTRY LONGITUDES >25°		TYPE 1 TYPE 2 FOR PROBE ENTRY LONGITUDES >25°
		AXIAL ARRAY	TYPE 2 FOR PROBE ENTRY LONGITUDES <15°		TYPE 2 FOR PROBE ENTRY LONGITUDES <15°

As is shown in the table, each spacecraft mission will be evaluated for various combinations of launch opportunity and trajectory type. For the TOPS missions, all combinations of 1978, 1980, and Type I & II launches have been assessed. The J-U-N mission will only be considered for the 1979 Type I due to spacecraft trajectory requirements. And the Pioneer F/G spacecraft will also be evaluated for the 1978, 1980, and Type I & II missions; however, for these cases, consideration must be given as to whether the line of sight between probe and spacecraft is either parallel to or normal to the spin axis of the spacecraft. This results in the configuration of two different spacecraft receiving antennas for various segments of possible Type II dayside entry conditions. The restrictions on these missions for each of the two antenna concepts is shown in Table 10-11. For each of these cases summarized in the table, the studies were conducted such that link performance was evaluated over a range of entry angles/probe longitudes consistent with potential dayside and nightside descent missions.

Relay Link Data Rate Capability - The data rate achievable for a given relay link configuration will be based on a constant value for the duration of the mission which provides for a level of performance margin at least equal to the sum of the adverse link tolerances. Sample relay link telecommunication design control charts are presented in Reference 9. Typically, this value of data rate is sized at the final point in the mission and/or the first point in the mission; and therefore, the link margin will, for all other points in the mission, exceed the value of adverse tolerances.

A) TOPS Flyby Mission

In arriving at an estimate of relay link data rate capability, the relative position of probe and spacecraft during the descent phase is of prime importance. For a given probe entry longitude there is a set spacecraft lead time value which maximizes link performance for a fixed periapsis radius. Figure 10-24 shows these results for a range of probe entry longitudes from 63 deg to 98 deg. The set of contour plots shown in this figure identify the respective peaks in the performance for each value of spacecraft lead time. And for a constant value of probe entry longitude, there is a maximum value of data rate for a certain combination of lead time and periapsis radius. The periapsis radius of 2.8 is noted to be the optimum value for this mission since the data rate peaks at this value. The data rate profile shown at the top of Figure 10-24 present the data rate capability if the probe and spacecraft dispersion effects are not included in the link evaluation, however, it should be noted that all other worst case

FIGURE 10-24
RELAY LINK DATA RATE CAPABILITY.
- TOPS FLYBY MISSION -
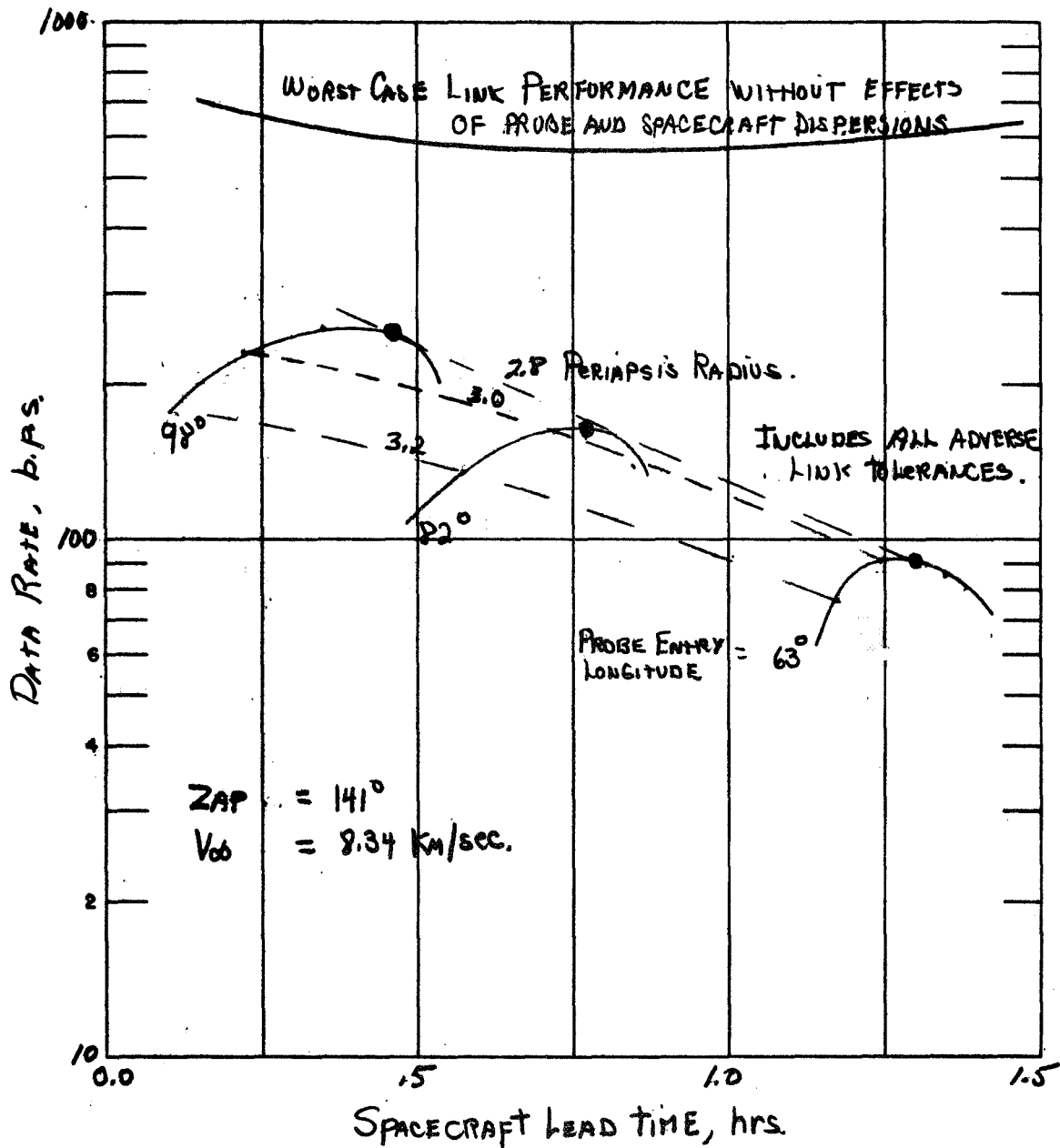
link factors are included in this curve. This upper curve is drawn for those points identified at the peaks of the lower contour curves. Additional details relative to these results are presented in Reference 10.

B) J-U-N Mission

The J-U-N mission data rate capability is shown in Figure 10-25. Since the J-U-N mission is restricted to fly by the planet at a fixed periapsis radius, the data rate contour reduces to a single line. The profile shown for the J-U-N mission differs somewhat from the TOPS mission since the data rate trend is reversed between these cases. The reason for this difference is related to spacecraft lead time dispersions for the TOPS mission and the probe targeting dispersions for the J-U-N mission. In the latter case, this dispersion represents the largest angular uncertainty and it tends to decrease with decreasing probe entry longitude; for the TOPS mission, the spacecraft lead time dispersion is the significant angular uncertainty and its magnitude decreases with increasing probe entry longitude.

C) Pioneer F/G Missions - Circumferential Array

The data rate performance shown for this mission is summarized as a function of the descent time parameter. The profiles, however, are based on an optimized set of lead time and periapsis radius for the one hour mission only. The value of periapsis radius for which these missions optimized at were 3.0 for the 96 deg and 74 deg entry longitude cases and 2.5 for the 53 deg entry longitude case. The uppermost profile again represents the link performance without the effect of probe and spacecraft dispersions for the one hour mission. Figure 10-26 presents these results.

D) Pioneer F/G Missions - Axial Antenna

Although many parametric studies were performed for this configuration, no performance could be achieved for any combination of probe and spacecraft position and, therefore, no results are presented.

Normalized Relay Link Data Rates - It has been said in earlier sections that relay link data rate can be made essentially independent of launch opportunity and trajectory type. This can be achieved if the probe entry conditions are always referenced to the spacecraft approach velocity vector; Figure 10-27 shows the data rate capability for the three spacecraft missions as a function of the angle between the approach velocity vector and the probe entry

FIGURE 10-25
RELAY LINK DATA RATE CAPABILITY
J-U-N MISSION

PERIAPSIS RADIUS = 6.78 rj
ZAP = 156°
V∞ = 12.64 Km/sec.

WORST CASE LINK PERFORMANCE WITHOUT EFFECTS
OF PROBE AND SPACECRAFT DISPERSIONS

PROBE ENTRY LONGITUDE, DEGREES

INCLUDES ALL ADVERSE
LINK TOLERANCES

DATA RATE b.p.s.

SPACECRAFT LEAD TIME, hrs.
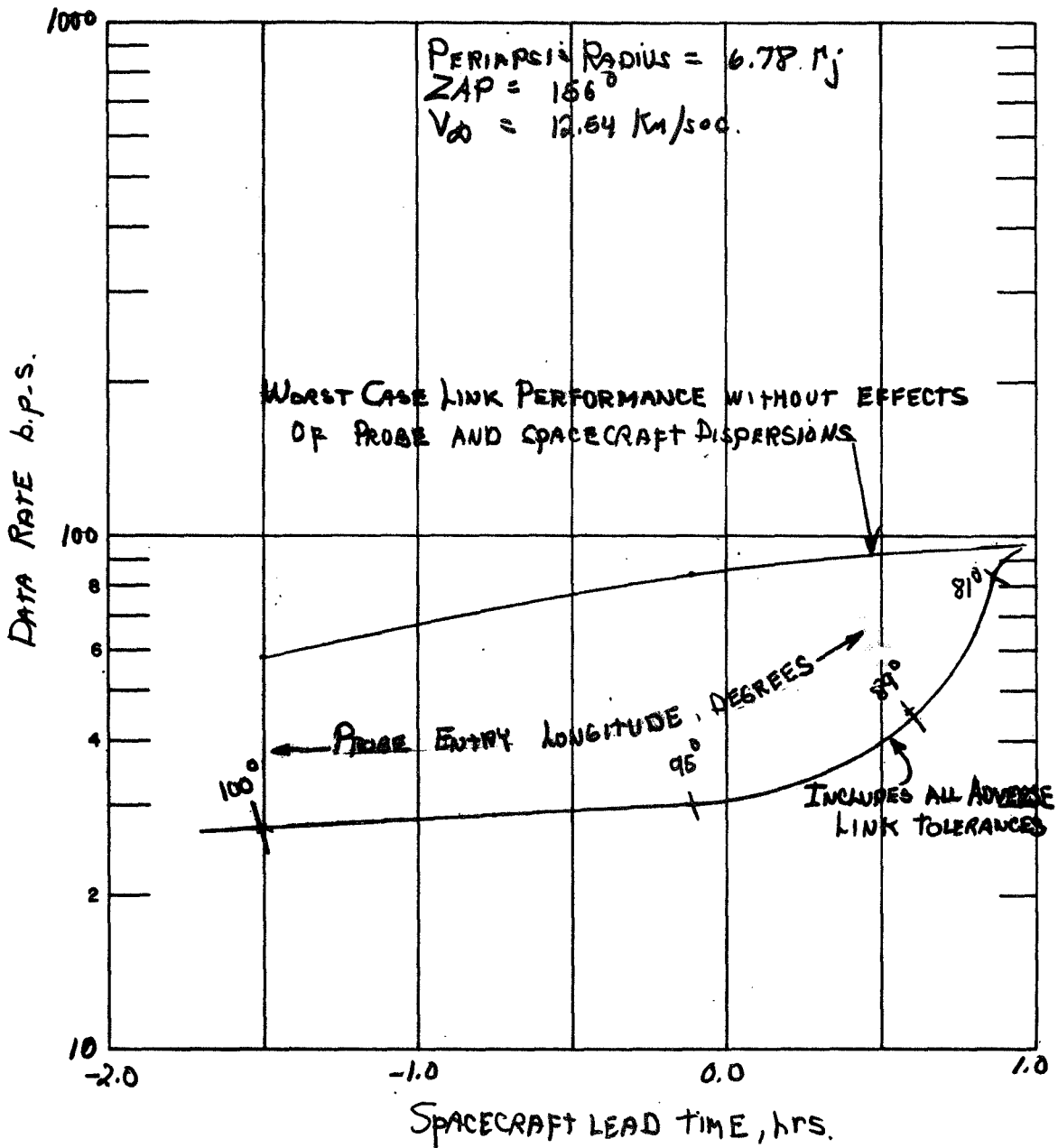
FIGURE 10-26

RELAY LINK DATA RATE CAPABILITY
PIONEER FLYBY MISSION

$Z_{AP} = 141°$

$V_{\infty} = 8.34\ km/sec.$

WORST CASE LINK PERFORMANCE WITHOUT EFFECTS OF PROBE AND SPACECRAFT DISPERSIONS

1 hr.

100

8

6

4

2

10

96°

74°

53°

PROBE ENTRY LONGITUDE

½ hr

¾ hr

MISSION DESCENT TIME = 1 hr.

INCLUDES all ADVERSE TOLERANCE EFFECTS

.5   1.0   1.5

SPACECRAFT LEAD TIME*, hrs.
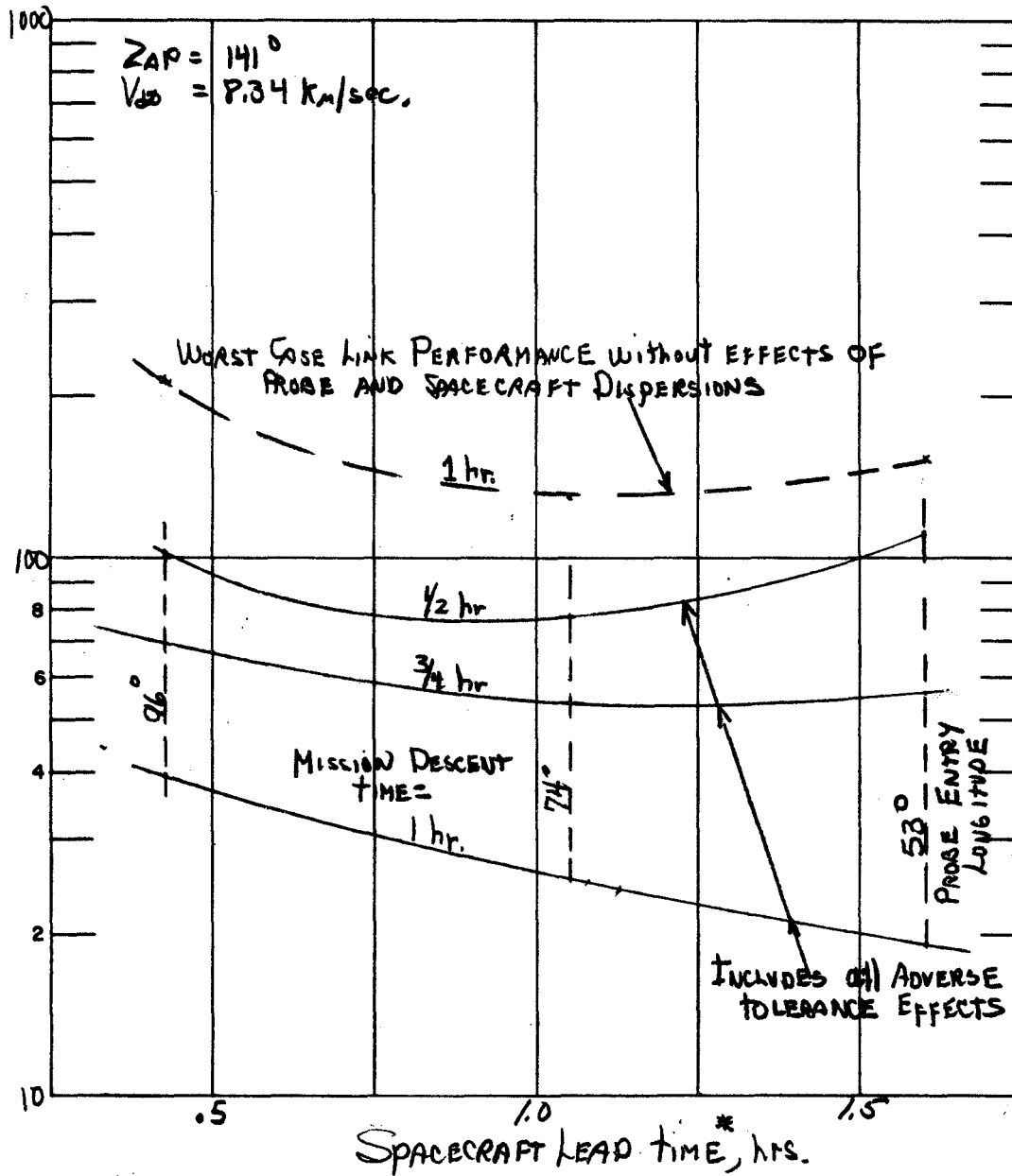
*OPTIMIZED FOR 1 HOUR MISSION ONLY.

FIGURE 10-27.
REFERENCE RELAY LINK DATA RATES

ΔΘ IS THE ANGLE BETWEEN THE ENTRY
PROBE DESCENT LONGITUDE AND THE
APPROACH VELOCITY VECTOR (SEE FIGURE 10-23)

TOPS FLYBY

$V_\infty = 8.34$

J-U-N

$V_\infty = 12.54$

PIONEER F/G
FLYBY
1 hr. mission

$V_\infty = 8.34$

DATA RATE, b.p.s.

ΔΘ - DEG.

10-48
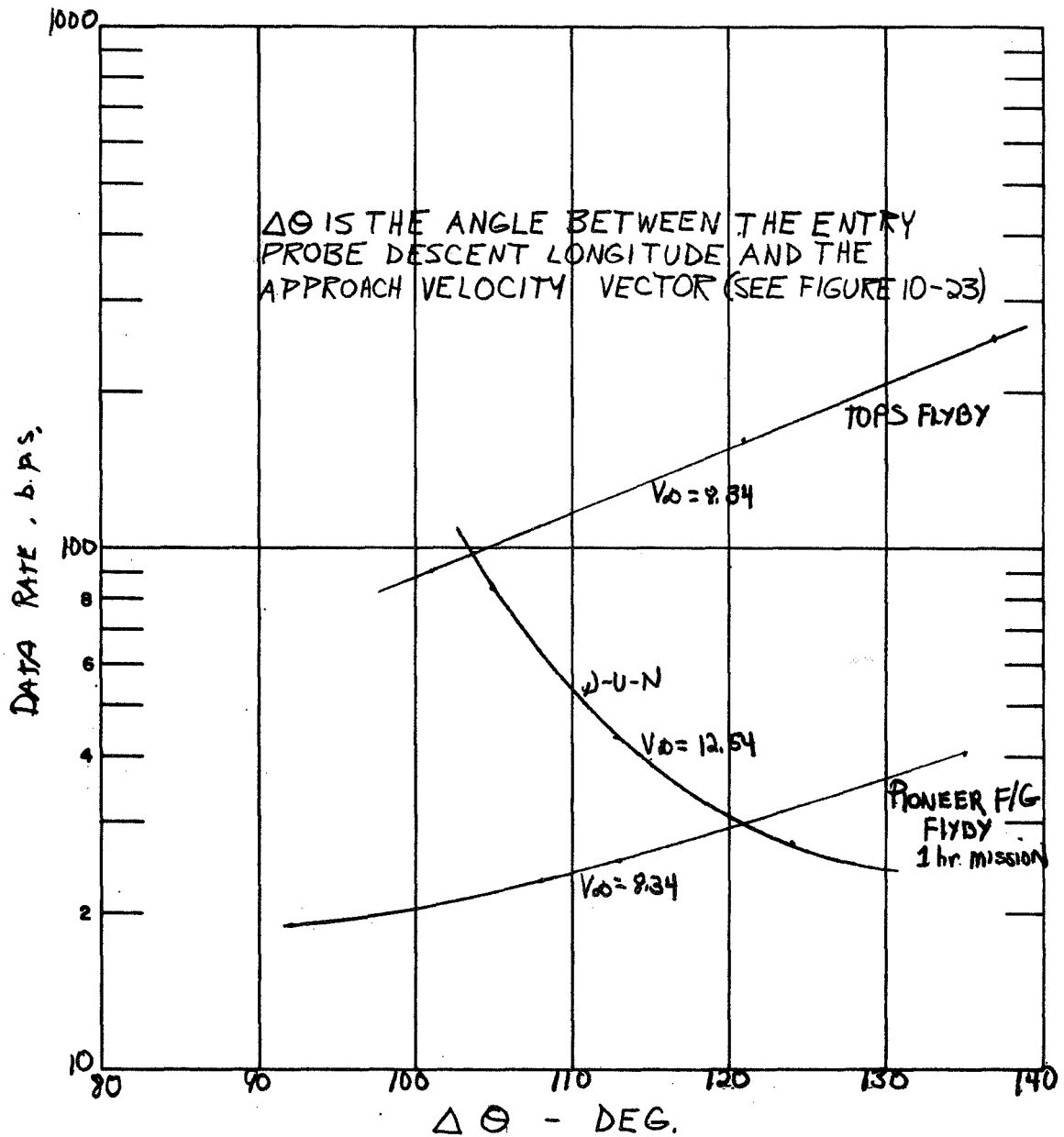
longitude. The worst case data rate (i. e. , includes all adverse link tolerance effects) is shown plotted as a function of this angle. The differing data rate trend between the two flyby missions and the J-U-N mission arises from the effect of spacecraft lead time dispersions and probe position dispersions as described in the earlier section.

The use of Figure 10-27 can be assumed valid for any launch opportunity/ trajectory type mission provided that the approach velocity, the inclination of the spacecraft trajectory, and the latitude of the probe and spacecraft remain unchanged. For this study, these three conditions will be maintained and, therefore, the results of Figure 10-27 establishes the reference relay link data rates for all mission trajectory/targeting combinations evaluated in this study.

10. 2. 4 Relay Link Mission Performance

To establish the tradeoff between relay link data rates and mission engineering requirements, a relationship between the quantity $\Delta \Theta$ (from Figure 10-27) and probe entry angle is developed. This relationship is shown plotted in Figure 10-28 and is considered independent of launch opportunity and trajectory type providing the magnitude of the approach velocity does not vary significantly. From Figure 10-28, the inference is quite clear; i. e. , as the angle $\Delta \Theta$ is reduced, the required entry angle increases until $\Delta \Theta$ is 0 deg and the entry angle reaches 90 deg. The two values of the approach velocity for which this entry angle/probe position relationship is plotted shows that there is roughly a 3. 5 deg decrease in entry angle for a 5 Km/ sec increase in approach velocity. This approximate sensitivity o⁻ -. 875 deg Km/sec can be used to adjust the entry angle for those missior₋ where the approach velocity does not fall on two plotted lines.

If the results of Figure 10-27 and Figure 10-28 are combined, then the resultant will be, as shown in Figures 10-29 through 10-31 for each mission. For each of these missions three performance profiles are shown: 1) the uppermost profile represents the nominal link margin, i. e. , performance based on the nominal values of the link parameters; 2) the next lower profile shows the reduction in performance based on the linear sum of the adverse factors excluding the effects of probe and S/C position uncertainties; and 3) the lowest profile in addition to the adverse tolerances include the dispersion in probe and spacecraft position.

Figure 10-28

Relay Link Entry Angle Requirements

$V_b = 9.34$

$V_b = 12.54$

$\Delta\Theta$, Degrees

Entry Angle, Degrees
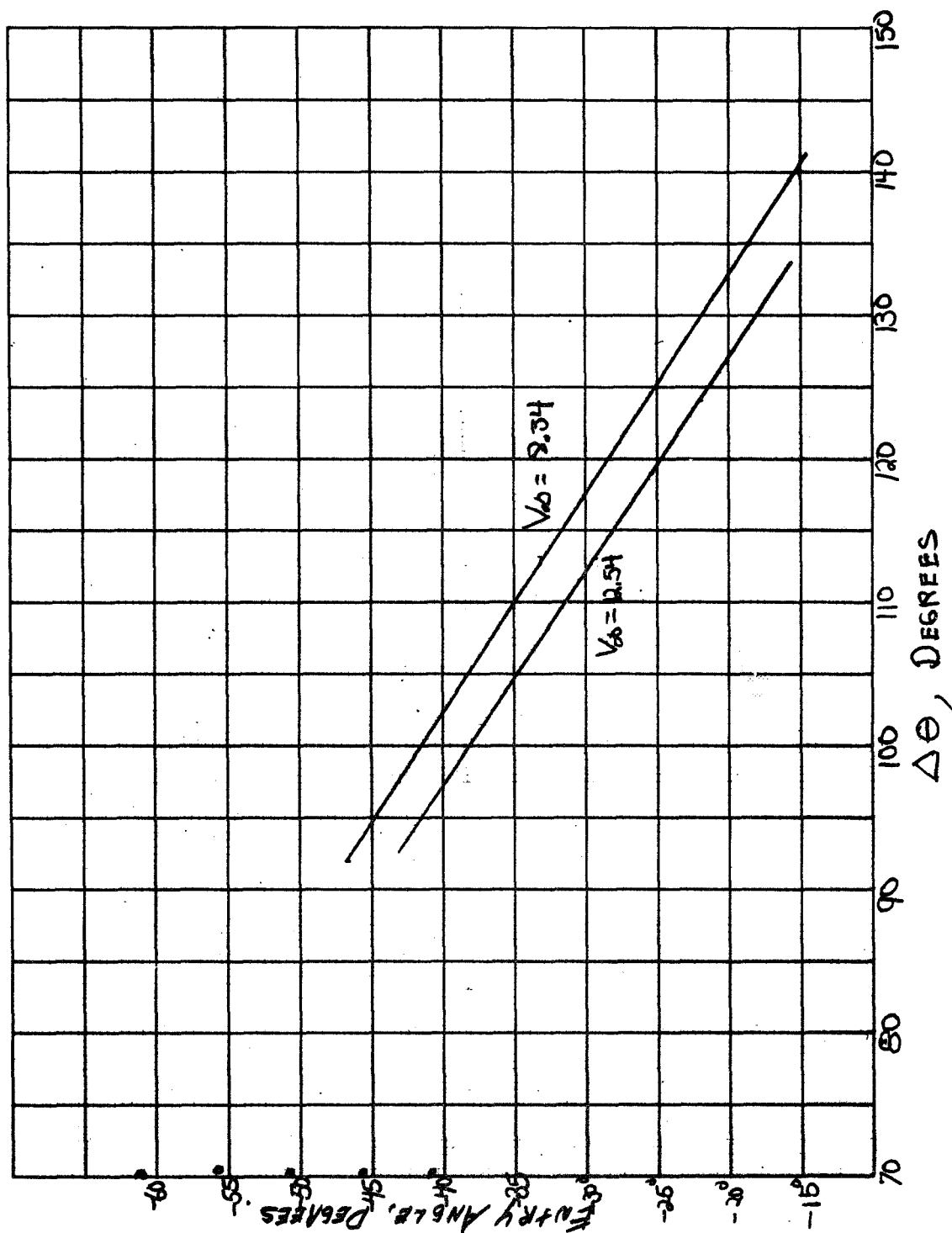
FIGURE 10-29
TOPS FLYBY MISSION RELAY LINK PERFORMANCE

NOMINAL PERFORMANCE

WORST CASE PERFORMANCE
EXCLUDING PROBE AND S/C DISPERSIONS

WORST CASE PERFORMANCE
ALL ADVERSE LINK
FACTORS INCLUDED.

• $V_{\infty} = 8.34$ Km/sec.

DATA RATE, b.p.s.

PROBE ENTRY ANGLE, DEGREES.
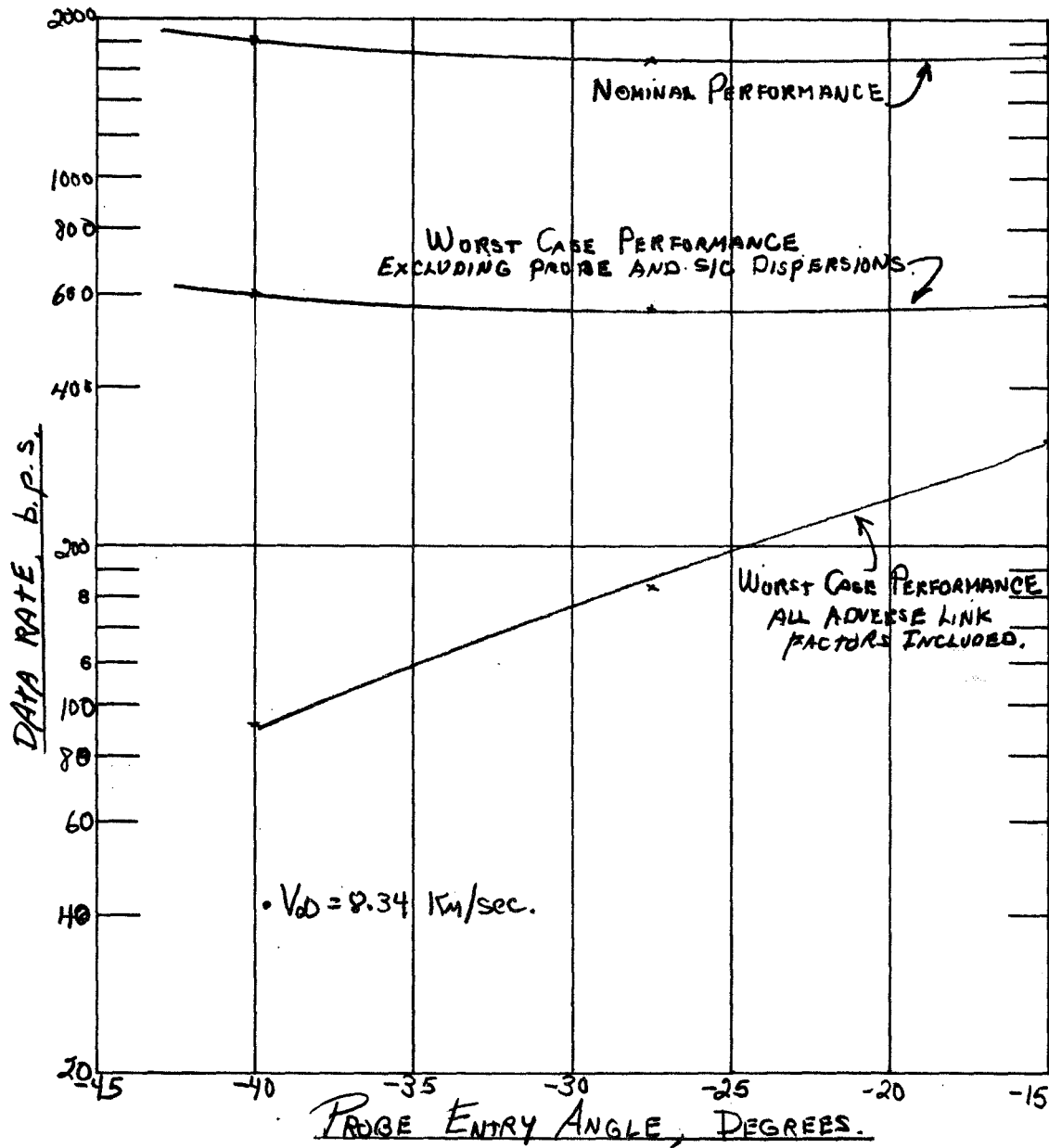
FIGURE 10-30
PIONEER FLYBY MISSION RELAY LINK PERFORMANCE
— CIRCUMFERENTIAL ARRAY —

NOMINAL PERFORMANCE

WORST CASE PERFORMANCE
EXCLUDING PROBE AND S/C DISPERSIONS

WORST CASE PERFORMANCE
ALL ADVERSE LINK FACTORS INCLUDED

$V_\infty = 8.34$ KM/SEC.

DATA RATE, b.p.s.

PROBE ENTRY ANGLE, DEGREES.

10-52

FiGURE 10-31
J-U-N Mission Relay Link Performance

Nominal Performance

Worst Case Performance
Excluding Probe and S/C
Dispersions

Worst Case Performance
All Link Factors Included.

$\circ V_\Phi = 12.54$ km/sec

Probe Entry Angle, Degrees
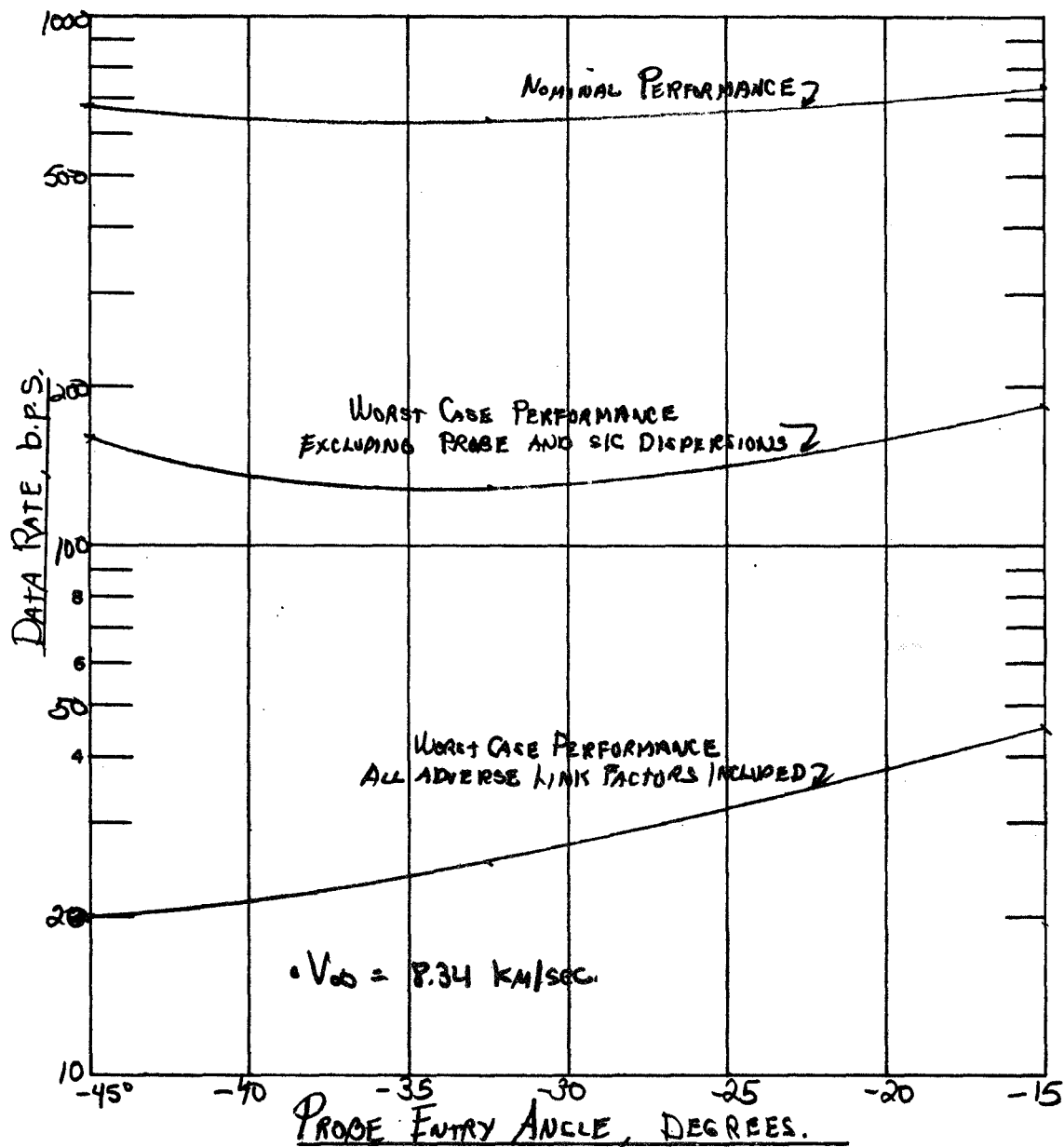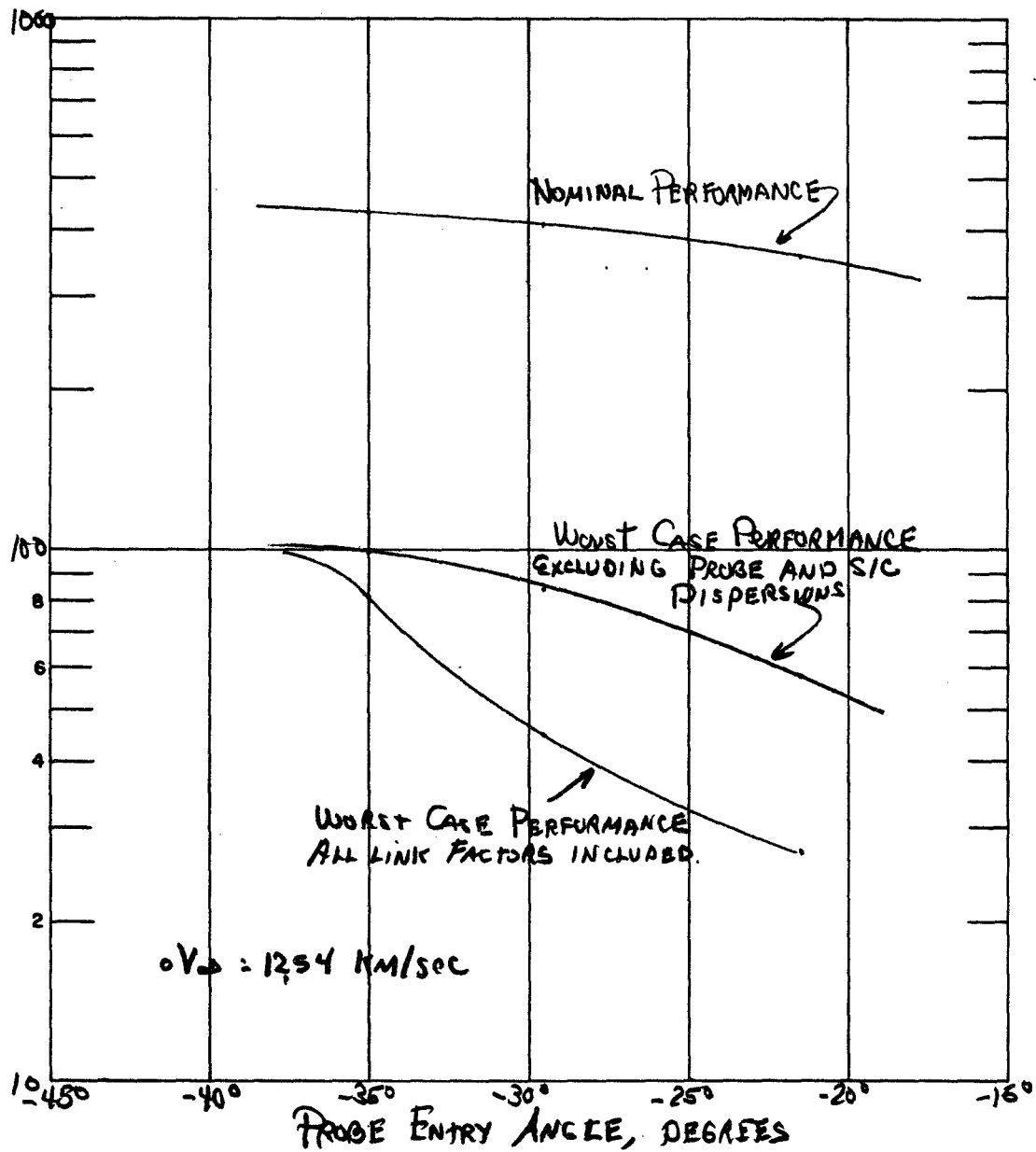
In Figure 10-29, the TOPS flyby link performance shows a relatively constant value except for the case where dispersion effects are included. In comparing the two worst case profiles, it can be noted that the dispersion effects on the link are more severe with increasing entry angle. This is due to the fact that a higher value of ΔV must be applied to enter at a steeper entry angle and for a constant value of the application angle, the in-plane component of ΔV increases, thereby causing increased dispersions in spacecraft lead time. The Pioneer F/G flyby mission results shown in Figure 10-30 exhibit the same characteristics at an overall lower level of performance. For the J-U-N mission profiles shown in Figure 10-31, a somewhat different effect is presented. These results show at increasing trend of performance with steeper entry angles. The difference between this and the previous two cases lies in the fact that the major dispersion contributor is no longer the spacecraft but rather the probe. And for shallower probe entry angle, the probe dispersion effects tend to increase thus giving rise to the decreasing performance. The large periapsis radius of 6. 78 for the J-U-N mission also tends to reduce the effects of dispersion on the link, and at a 40 deg entry angle it can be seen that the dispersion effects become trivial for this mission.

10. 2. 5 Summary of Mission Performance

A summary of the link performance shown in Figures 10-29, 10-30 and 10-31 is presented in Table 10-12 for selected relay link mission configurations. The cases shown in that table are identified according to launch opportunity, trajectory type and descent characteristics. For the given ZAP angle (approach velocity vector angle) and probe entry longitude, the quantity $\Delta \Theta$ can be determined which via Figure 10-28 can lead to the entry angle requirement and from Figures 10-29 through 10-31, the data rate performance can be determined. Further details relative to the relay link tradeoff analysis are summarized in Reference 10. A description of the relay link dispersion effects on the link performance is included in Reference 11.

TABLE 10-13   SUMMARY OF READY-LINK MISSION CONFIGURATIONS

Spacecraft Mission	Trajectory	Day or Night	Zap Angle (deg)	Probe Entry Long. (deg)	Δφ deg	Probe Entry Angle	Spacecraft Lead Time (HRS)	Spacecraft Periapsis Radius	Data Rate bps
TOPS FLYBY	78I	DAY	116	50	114	−33.2°	1.0	2.9	12.5 (½MISSION)
	78I	NIGHT	141	102	141	−14.9	.34	2.8	300
	78II	DAY	60	23	143	−14.8	.34	2.8	300
	80I	DAY	100	50	130	−25.7	.65	2.85	180 (½MISSION)
	80I	NIGHT	140	101	141	−14.9	.34	2.8	300
	80II	DAY	76	34	138	−16.5	.45	2.8	280
J-U-N	79I	NIGHT	156	100	134	−21.5	1.15	6.78	27 (½MISSION)
	78I	DAY	116	50	114	−33.2	1.15	3.0	75 (½MISSION)
PIONEER F/G FLYBY	78I	NIGHT	141	103	142	−14.8	.34	3.0	46
	78II	DAY	66	25	139	−15.0	.34	3.0	45
	80I	DAY	100	34	114	−33.2	1.15	3.0	25
	80I	NIGHT	140	103	142	−14.8	.34	3.0	46
	80II	DAY	64	25	141	−14.9	.34	3.0	45

10.3 REFERENCES

1. Frequency Selection Studies, Memo 10-II, Jupiter Atmospheric Entry Probe Study, Section F450, Avco Systems Division, January 1971.

2. Jupiter Interplanetary Direct Link Communications Program, Memo 10-XI, Jupiter Atmospheric Entry Probe Study, Section F450, Avco Systems Division, January 1971.

3. Modulation Tradeoff Studies, Memo 10-I, Jupiter Atmospheric Entry Probe Study, Section F450, Avco Systems Division, January 1971.

4. R.F. Propagation Studies, Memo 10-III, Jupiter Atmospheric Entry Probe Study, Section F450, Avco Systems Division, January 1971.

5. Direct Link Design Control Charts for Jupiter Atmospheric Probe Study, Memo 10-V, Jupiter Atmospheric Entry Probe Study, Section F450, Avco Systems Division, January 1971.

6. Direct Link Tradeoff Analysis Geometry Considerations, Memo 10-IV, Jupiter Atmospheric Entry Probe Study, Section F450, Avco Systems Division, January 1971.

7. Receiver Noise Figure Analysis, Memo 10-VI, Jupiter Atmospheric Entry Probe Study, Section F450, Avco Systems Division, January 1971.

8. Relay Link Phase Lock Loop Analysis, Memo 10-VII, Jupiter Atmospheric Entry Probe Study, Section F450, Avco Systems Division, January 1971.

9. Relay Link Design Control Charts for Jupiter Atmospheric Probe Study, Memo 10-X, Jupiter Atmospheric Entry Probe Study, Section F450, Avco Systems Division, January 1971.

10. Relay Link Contact Analysis, Memo 10-VIII, Jupiter Atmospheric Entry Probe Study, Section F450, Avco Systems Division, January 1971.

11. Relay Link Error Analysis, Memo 10-IX, Jupiter Atmospheric Entry Probe Study, Section F450, Avco Systems Division, January 1971.